



**HAL**  
open science

# Synthesis of conjugated macromolecules for organic solar cells and organic thermoelectric materials

Malak Qassab

► **To cite this version:**

Malak Qassab. Synthesis of conjugated macromolecules for organic solar cells and organic thermoelectric materials. Organic chemistry. Normandie Université, 2023. English. NNT : 2023NORMC208 . tel-04107506

**HAL Id: tel-04107506**

**<https://theses.hal.science/tel-04107506v1>**

Submitted on 26 May 2023

**HAL** is a multi-disciplinary open access archive for the deposit and dissemination of scientific research documents, whether they are published or not. The documents may come from teaching and research institutions in France or abroad, or from public or private research centers.

L'archive ouverte pluridisciplinaire **HAL**, est destinée au dépôt et à la diffusion de documents scientifiques de niveau recherche, publiés ou non, émanant des établissements d'enseignement et de recherche français ou étrangers, des laboratoires publics ou privés.



Normandie Université

## THÈSE

Pour obtenir le diplôme de doctorat

Spécialité CHIMIE

Préparée au sein de l'Université de Caen Normandie

### Synthesis of Conjugated Macromolecules for Organic Solar Cells and Organic Thermoelectric Materials

Présentée et soutenue par  
**MALAK QASSAB**

Thèse soutenue le 17/03/2023  
devant le jury composé de

M. THANH TUAN BUI	Maître de conférences HDR, Université de Cergy-Pontoise	Rapporteur du jury
MME FRANCOISE SEREIN - SPIRAU	Professeur des universités, ENSCM Montpellier	Rapporteur du jury
M. CYPRIEN LEMOUCHI	Maître de conférences, Université de Caen Normandie	Membre du jury
M. PHILIPPE BLANCHARD	Directeur de recherche au CNRS, Université d'Angers	Président du jury
M. LOIC LE PLUART	Professeur des universités, Université de Caen Normandie	Directeur de thèse

Thèse dirigée par **LOIC LE PLUART (Laboratoire de chimie moléculaire et thio-organique (Caen))**



UNIVERSITÉ  
CAEN  
NORMANDIE



Normande de Chimie





Ce travail a été soutenu et financé par :



*"We cannot solve problems with the kind of thinking we employed when we came up with them."*

*Albert Einstein*

*"Stay away from those people who try to disparage your ambitions. Small minds will always do that, but great minds will give you a feeling that you can become great too."*

*Mark Twain*

*"I never dreamed about success. I worked for it."*

*Estée Lauder*

*"The pessimist sees difficulty in every opportunity. The optimist sees opportunity in every difficulty."*

*Winston Churchill*

*"If you're not positive energy, you're negative energy."*

*Mark Cuban*

*"You cannot plow a field by turning it over in your mind. To begin, begin."*

*Gordon B. Hinckley*

*"Set your goals high, and don't stop till you get there."*

*Bo Jackson*

## Acknowledgments:

Undertaking this PhD has been a truly life-changing experience and it would not have been possible to be carried without the guidance and support that accompanied me during the journey from many people.

To begin with, I would like to sincerely thank the members of my jury: Prof. Françoise SEREIN SPIRAU (reporter), Dr. Thanh Tuan BUI (reporter), Dr. Philippe BLANCHARD (reviewer), Prof. Loïc LE PLUART (thesis director) and Dr. Cyprien LEMOUCHI (reviewer).

Many thanks also to Prof. Thiery LEQUEUX, the director of Laboratoire de Chimie Moléculaire et Thio-organique (LCMT) and Prof. Annie-Claude GAUMONT, the coordinator in the team POHET (Polymer and Heterochemistry).

Foremost, I would like to express by sincere gratitude to my thesis director Prof. Loïc LE PLUART, researcher in polymeric materials at Laboratoire de Chimie Moléculaire et Thio-organique (LCMT) and Dr. Cyprien LEMOUCHI for all the support and encouragement they gave me and for the valuable discussions during these years and for their relevant and efficient corrections of this manuscript.

My thanks also go to the group members in the team of Prof. Loïc LE PLUART LLP: Dr. Isabelle DEZ, Abdel Aziz WAYZANI, Yevhenii PRYKHODKO, Mohammed WAQUARUDDIN SIDDIQUI, Aiguerim BAIMYRZA, Charles JAMBOU, Yougourthen BOUMEKLA, Jean-Nicolas NOEL, Mohammed WEHBI and Romuald HERBINET.

Further on, I want to thank people who participated in some parts of this thesis, basically Victor BOSHEVESKI, who did his Master two internship in the team and Jean-François LOHIER, who joined the team in synthesis of new metallooligomers for organic solar cells.

I would also like to acknowledge with much appreciation the people who contributed in this project: Julie HARDOUIN (PBS, Rouen) for MALDI-TOF, Muriel DURANDETTI (COBRA, Rouen) for carrying the cyclic Voltammetry and Prof. Pierre HARVEY (Sherbrooks University) for photo-physical studies.

Thanks also go to the people who are in charge of the NMR service: Rémi LEGAY and Hussein EL SIBLANI and to Karine JARSALE for mass spectroscopy. I appreciate Guillaume MORCEL for his efficiency in receiving and distributing products and materials.

I acknowledge the kind and efficient secretariat composed of Marie-Cécile HELAINE and Jeannine AMICE.

I would like to thank my referent teacher Prof. Jean-Luc RENAUD through my thesis for his kindness, support and advice.

Thanks to all professors, researchers, lecturers, research engineers and technicians of the LCMT.

I greatly appreciate the support received from my colleagues. Therefore, I thank all my friends in LCMT in particular: Lilia ANANI, Quentin IBERT, Abdel Aziz WAYZANI, Mohammed

WAQUARUDDIN SIDDIQUI, Fatima ALMETWALI and Jawad FAYEK, who made this time joyful but always efficient.

I am extremely grateful to my parents for their love, prayers, caring and sacrifices for educating me and preparing me for my future. A special feeling of gratitude to my loving sisters Ekhlass and Nour. I am very thankful to my fiancé Hussein RAAD for his understanding and continuing support to complete this research work.

## Table of contents :

<b>Acknowledgments:</b> .....	<b>3</b>
<b>Table of contents :</b> .....	<b>5</b>
<b>List of Abbreviations:</b> .....	<b>9</b>
<b>General Introduction</b> .....	<b>15</b>
<b>Chapter I</b> .....	<b>18</b>
<b>I. Conjugated Polymers:</b> .....	<b>19</b>
1. Introduction/general definition: .....	19
2. Electronic structure : .....	21
3. Main properties of Conjugated polymers: .....	24
3.1. Optical properties: .....	25
3.2. Electronic and optoelectronic properties: .....	28
3.2.1. Charge generation: .....	28
3.2.2. Electronic properties:.....	31
3.2.2.1. Charge mobility in semiconductors:.....	31
3.2.2.2. Electrical conductivity of conducting conjugated polymers:.....	33
3.2.3. Optoelectronic properties:.....	33
<b>II. Main strategies to improve the properties of organic conjugated polymers:</b> .....	<b>34</b>
1. The choice of monomer units/P-type and n-type CP: .....	34
2. Decreasing the band gap energy: .....	36
2.1. Using of heterocycle: .....	37
2.2. Increasing the quinoid form stabilization: .....	38
2.3. Increasing the planarity: .....	40
2.3.1. By covalent bond formation : .....	40
2.3.2. Using Non-covalent interactions : .....	43
2.4. New generation conjugated polymer via Donor-Acceptor Approach: .....	47
3. Side chain engineering.....	49
3.1. To Increase Solubility: .....	49
3.1.1. Alkyl side chains: .....	51
3.1.2. Oligoether side chains:.....	56
3.2. To enhance the $\pi$ - $\pi$ aggregation and chain orientation: .....	57
3.3. To increase Stability: .....	59
<b>III. Synthesis of conjugated polymers:</b> .....	<b>62</b>
1. Oxidative polymerization:.....	62
2. Organometallic coupling reactions:.....	63
2.1. Suzuki Coupling: .....	63
2.2. Stille coupling:.....	64
2.3. Sonogashira coupling:.....	64
2.4. Heck coupling:.....	65
2.5. Negishi and Kumada couplings: .....	66
2.6. Direct heteroarylation polymerization: .....	66
3. Synthesis of polymers with a metal center: .....	68
3.1. Copper catalyzed dehydrohalogenation: .....	68
3.3. Oxidative coupling: .....	69
3.4. Alkynyl-ligand exchange: .....	69
<b>IV. Applications of conjugated polymers in materials for energy:</b> .....	<b>71</b>



**Chapter 2..... 72**

**..... 72**

<b>I. Introduction to organic solar cells:.....</b>	<b>73</b>
1. Solar cells:.....	73
2. Organic solar cells:.....	75
3. Architecture of organic Solar Cells: .....	77
4. Active Layer : .....	77
4.1. Single active layer structure:.....	77
4.2. Two layers structure .....	78
5. The mechanism in BHJ OSCs:.....	79
6. How to enhance the PCE: .....	80
6.1. Tuning the electronic structure of D/A:.....	80
6.2. Molecular organization:.....	82
6.3. The choice of the donor and acceptor materials for the blend preparation in bulk heterojunction is very important to the overall performance of the organic solar cells:.....	83
6.3.1. Acceptor material:.....	83
6.3.2. Donor materials: .....	87
6.3.2.1. Small molecule donor materials: .....	88
6.3.2.2. Polymer donor materials: .....	88
7. Metallopolymers: .....	92
7.1. Metal ligand coordination mode : .....	92
7.1.1. Metallopolymer based on N-heterocyclic ligand: .....	93
7.1.2. Metallopolymer based on metal-carbon alkyne conjugated system:.....	93
7.2. Metallooligomers in organic solar cells:.....	94
8. Preliminary results:.....	95
<b>II. New DPP based metallooligomers: .....</b>	<b>99</b>
1. Strategy 1: to increase the molecular mass $M_n$ of DPP based metallooligomers:.....	100
1.1. Improving the reaction conditions of metallooligomer PA:.....	100
1.1.1. Synthesis of LA : .....	101
1.1.2. Synthesis of PA : .....	103
1.1.3. Characterizations of PA .....	103
1.2. Photophysical study of PA: .....	109
1.2.1. Photoreductive electron transfer between PA and electron acceptor:.....	109
1.2.2. Stability test: .....	110
1.3. Functionalizing with solubilizing chain to increase the average molar mass: .....	111
1.3.1. Synthesis of LB .....	112
1.3.2. Optical properties of LB .....	112
1.3.3. Synthesis of PB .....	113
2. Strategy 2: Narrow band gap metallooligomers:.....	115
2.1. Synthesis of PC: .....	116
2.1.1. Preparation of Ligand LC:.....	116
2.1.2. Synthesis of PC:.....	117
2.1.3. Characterizations of PC .....	118
2.2. Synthesis of functionalized EDOT containing metallooligomers PD:.....	121
2.2.1. Preparation of the generic Synthon ( <i>R</i> )-EDOT-MeOR-OP.....	124
2.2.1.1. Synthesis of ( <i>R/S</i> )-EDOT-MeOH:.....	124
2.2.1.2. Synthesis of ( <i>R</i> )-EDOT-MeOH .....	125
2.2.1.3. Synthesis of ( <i>R</i> )-EDOT-MeO-ROP:.....	126
2.2.2. Example of pre- functionalization with the direct functionalization of ( <i>R</i> )-EDOT-R-OP with alkyl chains:.....	127
2.2.2.1. Synthesis of branched alkyl chain: .....	128

2.2.2.2. Synthesis of <b>EDOT-R-OR'</b> .....	129
2.2.3. Example of post- functionalization with the insertion of ( <i>R</i> )-EDOT-R-OP in the DPP containing ligand: .....	129
2.2.4. Synthesis of the generic ligand L' with the preparation of the EDOT and DPP containing intermediate 26: .....	131
3. Conclusion and Perspectives: .....	132
<b>Chapter 3</b> .....	<b>134</b>
.....	<b>134</b>
<b>I. Introduction:</b> .....	<b>135</b>
1. Thermoelectric materials: .....	135
1.1. Principle of thermoelectric devices: .....	136
1.2. Performance of thermoelectric devices: .....	137
1.3. P-type conjugated polymers for OTHes: .....	139
1.4. N-type conjugated polymers for OTHes: .....	141
1.5. Doping:.....	144
1.6. Increase the charge carrier transport:.....	145
1.6.1. Planarity .....	146
1.6.2. Molecular morphology:.....	146
1.6.3. Average molar mass:.....	148
1.7. Enhance the device stability: .....	148
1.8. Side chain engineering:.....	149
1.8.1. Alkyl side chains:.....	149
1.8.2. Perfluoroalkyl side chains: .....	153
1.8.3. Ethylene Glycol polar group:.....	156
2. Organic field effect transistors: .....	156
2.1. Principle of OFET:.....	157
2.2. Organic semiconductors OSC:.....	158
3. Preliminary results:.....	159
<b>II. New n-type Conjugated Polymers:</b> .....	<b>165</b>
1. Synthesis of new n-type conjugated polymer T1: .....	167
1.1. Synthesis of the acceptor unit .....	168
1.2. Synthesis of the acceptor of D-A-D unit BDTD-2TR1 (Synthon A-Synthon B) (32).....	169
1.3. Synthesis of EDOT-containing units (Synthon C): .....	172
1.3.1. Synthesis of Distannic EDOT.....	173
1.3.2. Synthesis of Functionalized EDOT Synthon C2 (41) .....	173
1.3.3. Synthesis of Synthon C3: Functionalization of ( <i>R</i> )-EDOT-MeOH and ( <i>R</i> )-EDOT-MeCl with perfluoroalkylchain.....	174
1.3.3.1. Direct Functionalization of ( <b>R</b> )-EDOT-MeOH and ( <b>R</b> )-EDOT-MeCl with perfluoroalkylchain .....	175
1.3.3.2. Synthesis of ( <b>R</b> )-EDOT-R-OC <sub>10</sub> F <sub>21</sub> with spacer: .....	178
1.4. Synthesis of the polymer T1: .....	179
1.5. Characterization of T1.....	180
<b>III. Conclusion and Perspectives</b> .....	<b>182</b>
<b>General Conclusion:</b> .....	<b>185</b>
<b>Supporting Information</b> .....	<b>190</b>
<b>Materials and Methods</b> .....	<b>191</b>
<b>Experimental part of chapter 2</b> .....	<b>194</b>

Experimental part of chapter 3.....	215
-------------------------------------	-----

## List of Abbreviations:

### A

A: Acceptor

AP: Affinity potential

### B

BDTD: Benzo[1,2-b:4,5-b']dithiophene-2,6-dione

BDT: Benzodithiophene

BTz : Benzo(2,1,3)thiadiazole

BT: Bithiophene

BBT: Bibenzothiophene

BHJ: Bulk heterojunction

BTI: Bithiophene imide

BDFD: Benzodifurandione

BDD: 1,3-bis(4-(2-ethylhexyl)thiophen-2-yl)-5,7-bis (2-alkyl)benzo[1,2-c:4,5-c']dithiophene-4,8-dione

BN-Py: B-N bridged bipyridine

### C

CsCO<sub>3</sub>: Cesium carbonate

c: Speed of light

CDT: Cyclopentene dithiophene

### D

D: Donor

D/A: Donor/ Acceptor

DPP: Diketopyrrolopyrrole

DIAD: Diisopropyl azodicarboxylate

DMF: N,N-dimethylformamide

DMSP: Dimethylsulfoniopropionate

DMAc: Dimethylacetamide

DCM: Dichloro methane

DMSO: Dimethyl sulfoxide

DCTB: 2-[(2E)-3-(4-tert-butylphenyl)-2-methylprop-2-enylidene]malononitrile

DIPA: Diisopropanolamine

DMBI-H: 4-(1,3-dimethyl-2,3-dihydro-1H-benzoimidazol-2-yl)phenyl)dimethyl amine

### E

E<sub>g</sub><sup>opt</sup>: Optical band gap

E<sub>g</sub><sup>elec</sup>: Electric band gap

ETL: Electron transporting layers

E: Charge carrier  
Et<sub>3</sub>N: Triethylamine  
eq.: Equivalent(s)  
EA: Electron affinity

## **F**

F4TCNQ: 2,3,5,6-tetrafluoro-7,7,8,8-tetracyanoquinodimethane  
FF: Fill factor

## **G**

GPC: Gel permeation Chromatography  
GIWAXS: Grazing incident wide-angle X-ray scattering

## **H**

HTL: Hole transporting layer  
HOMO: Highest occupied molecular orbital  
H<sub>2</sub>SO<sub>4</sub>: Sulfuric acid  
h: Planck constant

## **I**

IP: Ionization potential  
I<sub>sc</sub>: Short-circuit current density  
ICL: interconnecting layer

## **K**

K<sub>2</sub>CO<sub>3</sub>: Sodium carbonate

## **L**

LDA: Lithium diisopropylamide  
LUMO: Highest occupied molecular orbital

## **M**

MO: Molecular orbital  
MALDI-Tof: Matrix Assisted Laser Desorption Ionization - Time of Flight  
m-CPBA: meta-chloroperoxybenzoic acid  
Me<sub>2</sub>S<sub>2</sub>: Dimethyl disulfide  
MeOH: Methanol  
M<sub>n</sub>: Number averaged molecular weight  
MgSO<sub>4</sub>: Magnesium sulfate

## N

NMR: Nuclear magnetic resonance spectroscopy  
NDI: Naphthalenedicarboximide  
Nu: Nucleophile  
NFAs: Non-Fullerene acceptors  
NBS: N-Bromosuccinimide  
NaOAc: Sodium acetate

## O

OFET: Organic Field-Effect Transistor  
OTHE: Organic thermoelectrics  
OLED: Organic light emitting diode  
OSC: Organic solar cell  
OPV: Organic photovoltaic  
-OR: Alkoxide

## P

PA: Polyacetylene  
PEDOT: Poly(3,4-ethylenedioxythiophene)  
PPY: Polyparaphenylene  
PPV: poly(phenylene vinylene)  
PT: polythiophene  
PTbT: Polythieno[3,4-b]thiophene  
PITN: Polyisothianaphthene  
PTs : Polythiophenes  
P3ATs: Poly(3-alkylthiophene)s  
PTP: Poly-(thieno(3,4-b) pyrazine)  
PC: Polycyclic  
Ppv: Poly(phenylenes)  
PEDOT: Poly(3,4-ethylenedioxythiophene)  
PDQT: DPP quaterthiophene polymer  
Pd: Palladium  
Pd(OAc)<sub>2</sub>: Palladium acetate  
PtBu<sub>2</sub>Me-HBF<sub>4</sub>: Di-tert-butyl(methyl)phosphonium tetrafluoroborate  
PCE: Power conversion efficiency  
P<sub>max</sub>: Maximum power  
P<sub>in</sub>: Incident power  
P3HT: Poly (3-hexylthiophene)  
PC<sub>61</sub>BM: (6,6)-phenyl-C61-butyric acid methyl ester  
PHJ: Planar heterojunction  
PDI: Perylene diimide  
P-TSA: *p*-Toluenesulfonic acid  
PSS: Polystyrene sulphonic acid

Pd(dba<sub>2</sub>)<sub>3</sub>: Tris(dibenzylideneacetone)dipalladium(0)

P(o-tolyl)<sub>3</sub>: Tri(o-tolyl)phosphine

Pd(PPh<sub>3</sub>)<sub>2</sub>Cl<sub>2</sub>: Bis(triphenylphosphine)palladium

## Q

QA: Quinacridone

## R

R.T: Room temperature

R<sub>f</sub>: Retention value

## S

S: Seebeck coefficient

## T

TAM: Trisaminomethane

TP: Thieno(3,4-b)pyrazine

TTz: Thieno(3,4-b)(1,2,5)thiadiazole

TID: Thienoisindole-dione

TbT: Thieno(3,4-b)thiophene

T: Thiophene

TT: Thiophenethiophene

TVT: Thiophene Vinylthiophene

TPD: Thieno[3,4-c]pyrrole-4,6-dione

TBA-Cl: Tetrabutylammonium chloride

THF: Tetrahydrofuran

TCO: Transparent oxide

T<sub>d</sub>: Decomposition temperature

TLC: Thin Layer Chromatography

TMS: Tetramethylsilane

TBAF: Tetra-n-butylammonium fluoride

TPBT: Dithienothiophen[3,2-b]-pyrrolobenzothiadiazole

## U

UV-Vis: ultraviolet-visible

## V

V<sub>oc</sub>: Open-circuit voltage

V<sub>max</sub>: Maximum voltage

V<sub>G</sub>: Gate voltage

V<sub>T</sub>: Threshold voltage

$V_{DS}$ : Source/ drain voltage

### **Symbols:**

$\lambda_{abs}^{(onset)}$ : Onset absorption wavelength  
 $\lambda_{abs}^{(max)}$ : Maximum absorption wavelength  
 $\lambda_{exc}$ : Excitation wavelength  
 $\epsilon_{\lambda}$ : Absorption capacity  
 $\mathfrak{D}$ : Dispersity  
 $\mu_e$ : Electron carrier mobility  
 $\mu_h$ : Hole carrier mobility  
 $\sigma$ : Electrical conductivity  
 $\rho$ : Electrical resistance.  
K: Electrical resistance  
 $\delta$ : Chemical shift  
 $\Psi$ : Phi

### **Units**

$^{\circ}\text{C}$ : Celsius degree  
g: Gram  
h: Hour  
Hz: Hertz  
Mg: Milligram  
Min.: Minute  
mL: Milliliter  
mmol: Millimole  
ppm: parts per million



# General Introduction

## General Introduction

Most of the energy produced is derived from finite resources, which not enough to keep up as the consumption speed is increasing. Demand for energy is growing as populations increase. Global energy consumption is increasing in an average of 1 % to 2 % per year. The main source of energy we use comes from non-renewable resources for most countries. Most non-renewable energy comes from fossil fuels such as petroleum, crude oil, coal, natural gas, and nuclear fuel since there is a finite uranium supply in the world. Currently, there is a depletion of non-renewable resources that may let them nonexistent in future generations. However, many European countries still depend heavily on fossil fuel. Hence, it was possible to estimate that by 2050, only 14 % of oil proven reserve, 18 % of gas proven reserve and 72 % of coal proven reserve will remain.<sup>1</sup>

Fossil fuels are not only limited but also, they are harmful at the same time. They release carbon dioxide when heated, which disrupt the balance of gases on earth and making them responsible for global warming and other environmental problems such as air pollution. Therefore, the transition to renewable and clean energy is required to avoid the complete depletion of fossil fuels and to minimize the environmental and health impacts.

Renewable energy is derived from natural sources that are recharged in higher speed that they are consumed. Sunlight and wind are examples of renewable sources. Generating renewable energy releases lowers emissions that non-renewable sources. Hence, green growth of energy has become a famous term among researchers.

Solar energy is the most profuse of all energy resources, where sun provides the most abundant energy to earth. Solar technologies can create heat, cooling, lightening and electricity from sunlight. Solar cell is one of the solar technologies that have attracted the attention as a key device to convert light energy into electrical energy by electrochemical reaction (photovoltaic effect).<sup>2</sup> Another attractive green renewable energy is thermal energy or thermoelectricity. Converting thermal energy into electricity occurs using thermoelectric generator.<sup>3</sup> Thermoelectric device employs waste heat to produce power. Thus, it can be considered as eco-friendly energy source. From economic side, sunlight is free and waste heat is a free source generated by human body, automobile engines and industries, which makes them suitable techniques through the energy and environmental crises.

Since the creation of solar cells and thermoelectric materials, they can be classified into two generations: inorganic that is the traditional one and organic generation. Traditional devices are based on their manufacturing on inorganic materials as semiconductors for creating electricity.

---

<sup>1</sup> F. Martins, C. Felgueiras, M. Smitkova, N. Caetano, *Energies*, **2019**, 12, 964

<sup>2</sup> Chemistry of Nanomaterials Fundamentals and Applications, Book • **2020**, <https://doi.org/10.1016/C2018-0-04648-4>

<sup>3</sup>H. Mamur, Ö.F. Dilmaç, J. Begum, M.R.A. Bhuiyan, *Cleaner Materials*, **2021**, 100030

The highest solar cell efficiency is approaching 29-30% based on undoped crystalline silicon<sup>4</sup> and it reached 32.5% using a combination of multiple perovskite with multiples of silicon.<sup>5</sup> However, the best thermoelectric performance were noticed for devices based on inorganic materials.<sup>6,7</sup> On the other hand, devices based on inorganic materials require high power consumption and require complicated processing technique and expensive materials, that make them limited for application in sensing devices. Moreover, inorganic materials are expensive and toxic specially for bio-used applications. The undesirable in most inorganic compounds cannot be removed by oxidation or thermal decomposition. Therefore, replacing inorganic semiconductors with organic counterpart is a need.

Organic semiconductors are made up of polymers and  $\pi$ -bonded molecules based on carbon and hydrogen atoms and may include heteroatoms such as nitrogen, sulfur and oxygen. In principle, they are insulators but conduct when charge carriers are injected by certain methods such as doping and photoexcitation. One of the main advantages of organic semiconductors is flexibility. They are generally synthesized via chemical methods with easier conditions allowing them to be with higher potential applications for flexible electronic systems. In addition, they are of low weight and low cost, which make them economically attractive. Solubility of organic semiconductors is another interesting parameter, which could be controlled by incorporation of functional groups to facilitate the film processing in devices manufacturing. Moreover, organic semiconductors as conjugated polymers are with unique properties as the possibility of having high average molar mass, better flexibility through the molecular chain and mechanical flexibility that is suitable for large-area industrial applications.<sup>8</sup> A remarkable progress has been made in their different applications since their first report in 1940s.<sup>9</sup> Conjugated polymers are used in light-emitting field-effect transistors OLED, organic field-effect transistor OFET, organic thermoelectric OTHE, and organic solar Cells OSCs.

The enhancement of the properties of conjugated polymers can be performed by varying the electronic structure. Small modifications of the chemical structure can have a large effect on the electrical and optical properties of the organic semiconductor.<sup>10</sup> Applying functionalization strategies is a strategy to increase the solubility and the charge carrier mobility. In addition, molecular organization is one of the methods to increase aggregation and specify the chain orientation.

Therefore, the aim of this PhD project is to develop new conjugated polymers as organic semiconductors to be used in solar cells and thermoelectric materials for enhanced performance. To maintain this objective, we will have a literature review followed by applying practical strategies such as functionalization strategies to improve the current properties.

---

<sup>4</sup>A. Richter, M. Hermle, and S.W. Glunz, *IEEE Journal of Photovoltaics*, **2013**, 1184–1191.

<sup>5</sup><https://newatlas.com/energy/perovskite-silicon-tandem-solar-cell-efficiency-record-32-5-percent/>

<sup>6</sup>T. Ghosh, M. Dutta, D. Sarkar, and K. Biswas, *J. Am. Chem. Soc.* **2022**, 144, 23, 10099-10118

<sup>7</sup>A. Kandemir, A. Ozden, T. Cagin, C. Sevik, *Science and Technology of Advanced Materials*, **2017**, 18:1, 187-19

<sup>8</sup> Y. Yao, H. Dong, W. Hu, *Polym. Chem.*, **2013**, 4, 5197-5205

<sup>9</sup> P. Martin and E. S. Charles, *Electronic Processes in Organic Crystals and Polymers*, Oxford University Press, Oxford, 2<sup>nd</sup> edn, **1999**

<sup>10</sup> M.C. Scharber, N.S. Sariciftci, *Adv. Mater. Technol.*, **2021**, 6, 2000857

This manuscript is composed of three chapters. The first chapter is an introduction to conjugated polymers and their electric and optoelectronic properties. The second chapter focuses on organic solar cells and the development of new metallooligomers based on diketopyrrolopyrroles **DPP** as donor materials for achieving high power conversion efficiencies. The third chapter is introducing thermoelectric materials and developing new n-type conjugated polymers to be used as conducting polymer after doping in thermoelectric materials or to be integrated in organic field effect transistors without doping. Then, the main results will be presented in general conclusion of the manuscript.

# Chapter 1

## I. Conjugated Polymers:

### 1. Introduction/general definition:

In 2000, Heeger, MacDiarmid, and Shirakawa were awarded a Nobel Prize granted the discovery of conducting polymers after their work on polyacetylene **PA** (Figure 2), which is a long carbon chain, and each carbon is bound to two neighboring different carbons and one hydrogen atom. This polymer was first synthesized in 1958 within the group of Giulio Natta, but its semiconducting properties were not studied at this stage.<sup>11</sup> In 1970 more studies were carried by the group of Heidi Shirakawa to study the polymerization and the polymer shape by making films for spectroscopic studies.<sup>12</sup> They demonstrated that the electrical conductivity of **Trans-PA** could reach  $105 \text{ S cm}^{-1}$  which started the interest for using organic materials in electronic devices.<sup>13</sup>

The ability of **PA** to be conductive is related to the fact that it is a conjugated polymer. Conjugated polymers are characterized by a carbon backbone made up of alternative single and double bonds. Conjugated polymers have delocalized  $\pi$ -electrons due to the overlapping p-orbitals.<sup>14</sup>

For better understanding of conjugation ( $\text{C}=\text{C}$ ), ethylene is the simplest organic molecule with a double bond to be explained. Each carbon in the ethylene molecule has three  $\text{sp}^2$  orbitals and one  $p_z$  orbital. The overlapping of the two  $\text{sp}^2$  orbitals form the  $\sigma$  bond, while the overlapping of  $p_z$  can be overlapped in-phase (similar lobes of  $p_z$  orbital overlap) or out of phase. The two different types of overlapping lead to the formation of bonding and anti-bonding molecular orbitals (MOs), where the bonding molecular bonding ( $\pi$ ) is highly stable compared to the anti-bonding molecular orbitals ( $\pi^*$ ) (Figure 1). Upon energy supply, electrons can jump from  $\pi$  to  $\pi^*$ .

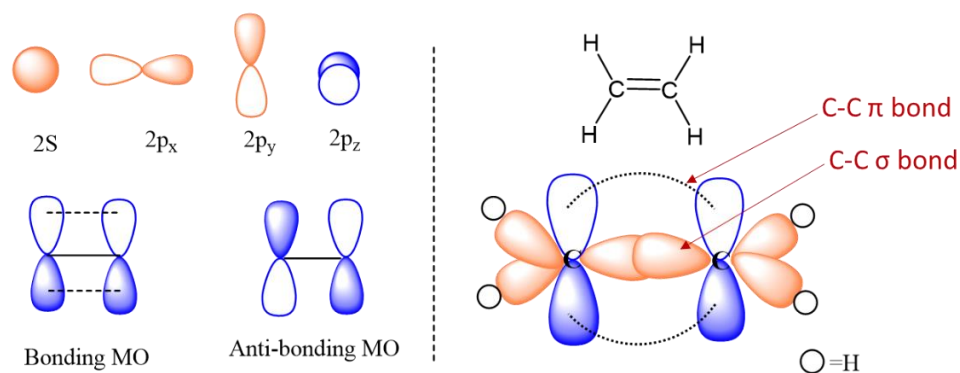


Figure 1: The different structures of molecular orbitals in ethylene

<sup>11</sup>G. Natta, G. Mazzanti, P. Corradini, *Atti Accad. naz. Lincei, Cl. Sci. Fis. Mat. Nat. r.*, **1958**, 25, 3

<sup>12</sup>H. Shirakawa, S. Ikeda, *Polymer Journal*, **1971**, 2, 231-244

<sup>13</sup>H. Shirakawa, S. Ikeda, *Polym. Z.*, **1977**

<sup>14</sup> Polymer-Based Advanced Functional Composites for Optoelectronic and Energy Applications, Book **2021**, 31-49

For organic molecules with more than two carbons, such as butadiene there is an alternation of double and single bonds. A molecule with separation of double bonds by a single bond is called “conjugated” molecule.<sup>15</sup>

The mechanism of electron transfer in conjugated polymers has been explained based on polyacetylene. The single and double bonds existed in the conjugated system contain a localized sigma bond that favors the strong chemical bond. Besides, the double bond carries a delocalized  $\pi$ -bond that is weaker than that of the sigma bond.<sup>16,17</sup> The overlap between the  $p_z$ -orbitals of  $\pi$  bonds allow their electrons to move freely through the system.

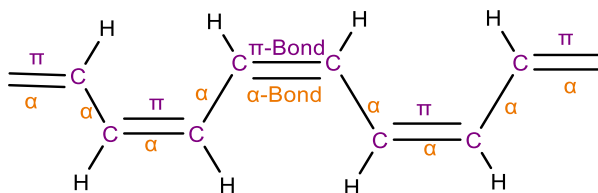


Figure 2: The conjugated  $\pi$ -system in *cis*-polyacetylene

Conjugated compounds can be linear or cyclic. At the beginning of 1980s, aromatic molecules were still used as conducting materials due to the instability of polyacetylene **PA**. It is related to the sensitivity towards oxygen. Due to the fact that oxidative attack on the polymer backbone happens simultaneously and with long term exposure or upon high temperature, the concentration of oxygen as dopant decreases through intramolecular regrouping of hydrogen atoms leading to the formation of hydroxyl groups and more polymer degradation.<sup>18</sup> Polyparaphenylene **PPy** is another well studied conjugated polymer that shows a better thermal stability.<sup>19,20</sup> However, due to the low solubility and difficulties in the reproducibility of **PPy**, alkyl substituents **PPy-1** was introduced to enhance the solubility<sup>21</sup> but it led to more rotation than polymers without alkyl substituents and then it affected the conjugation. Other well-known conjugated polymers are poly(phenylene vinylene) **PPV**, and polythiophene **PT** (Figure 3).

<sup>15</sup> J. Clayden, N. Greeves, S. Warren, P. Wothers, In *Organic Chemistry*; Oxford University Press, **2001**; pp. 151–180

<sup>16</sup> R. Ravichandran, S. Sundarajan, J. R. Venugopal, S. Mukherjee, S. Ramakrishna, *J. R. Soc. Inter-face*, **2010**, 7, S559–S579.

<sup>17</sup> D.L. Wise, G.E. Wnek, D.J. Trantolo, T.M. Cooper, J.D. Gresser (**1998**). *Electrical and Optical Polymer Systems: Fundamentals, Methods, and Applications*, Boca Raton, FL: CRC Press.

<sup>18</sup> F.G. WILL and D.W. McKEE, *General Electric Corporate Research and Development*, **1983**, 21(12), 3479–3492.

<sup>19</sup> M. Akiyama, Y. Iwakura, S. Shiraishi, YJ. Imai, *Polym Sci Part B Polym Lett.*, **1966**, 4, 305-8.

<sup>20</sup> G. Grem, G. Leditzky, B. Ullrich, G. Leising, *Adv Mater.*, **1992**; 4, 36

<sup>21</sup> T. Vahlenkamp, G. Wegner, *Macromol Chem Phys.*, **1994**, 195, 1933.

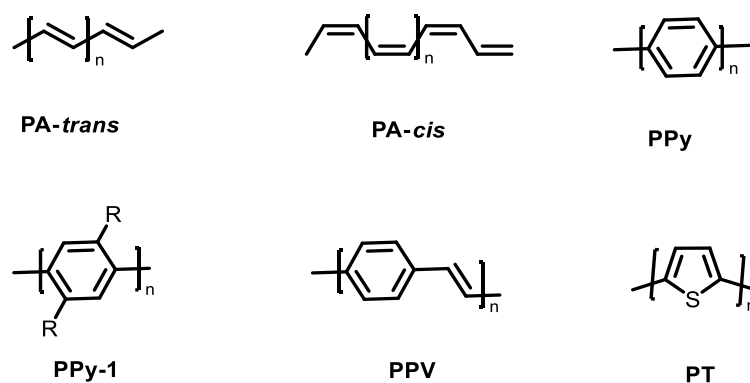


Figure 3: The main families of studied conjugated polymers<sup>11,13,19,20,21</sup>

## 2. Electronic structure :

Electronic structure of atoms and molecules is the series of energy levels that it is possible for a bound electron to occupy that is not allowed to leave its orbit.

In conjugated molecules, there are more than one bonding and one anti-bonding molecular orbitals leading to different orbitals termed by  $\psi$ . Upon energy supply the electron transfer from the bonding molecular orbital that is less stable, which is termed as highest energy occupied molecular level (HOMO) to the most stable anti-bonding molecular orbital that is termed as lowest energy unoccupied molecular orbital (LUMO) (Figure 4).

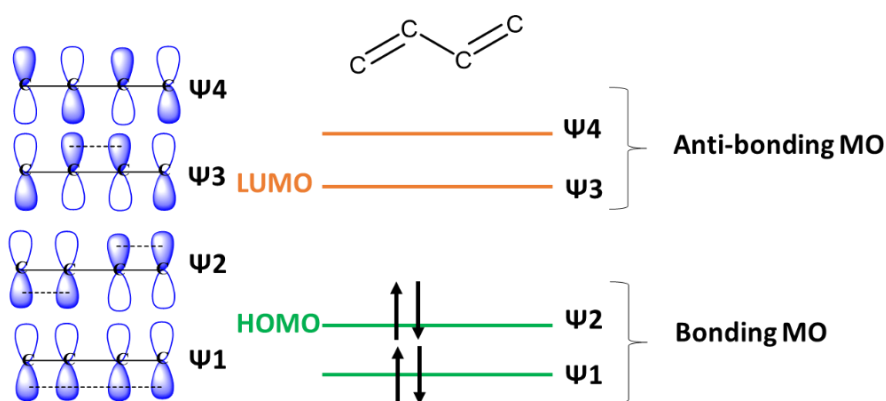


Figure 4: The different bonding and anti-bonding molecular orbitals in butadiene

The length of a molecule can be increased by joining another similar molecule to it. For example, 1,3-butadiene can be formed by joining two ethylene. Hence, the butadiene has two  $\pi$ - $\pi^*$  pairs, which the identical copies are degenerated, and the two levels are split into four.

By increasing the length of the conjugated molecule, more  $\pi$  and  $\pi^*$  are added. This allows a decrease in the gap between the highest  $\pi$  and the lowest  $\pi^*$  level. These frontier orbitals correspond to the valence and conduction bands in conjugated polymers.



Indeed, the increase in the conjugation length not only transform levels into bands, but also progressively decreases the band gap between the HOMO and LUMO levels allowing conjugated polymers to have a suitable low energy gap to be used as semi-conducting materials. It is noted in the literature that there is an impact of the extension of the  $\pi$ -conjugation length either in the bond length or in the length in the polymer chain on the value of the band gap (Figure 5). As the number of monomer units increases, the number of  $\pi$ -electrons increases which leads to a greater number of overlapped atomic orbitals. The number of bonding and anti-bonding molecular orbitals increases along the width of the energy band consequently a smaller gap between the HOMO and LUMO levels.<sup>22</sup>

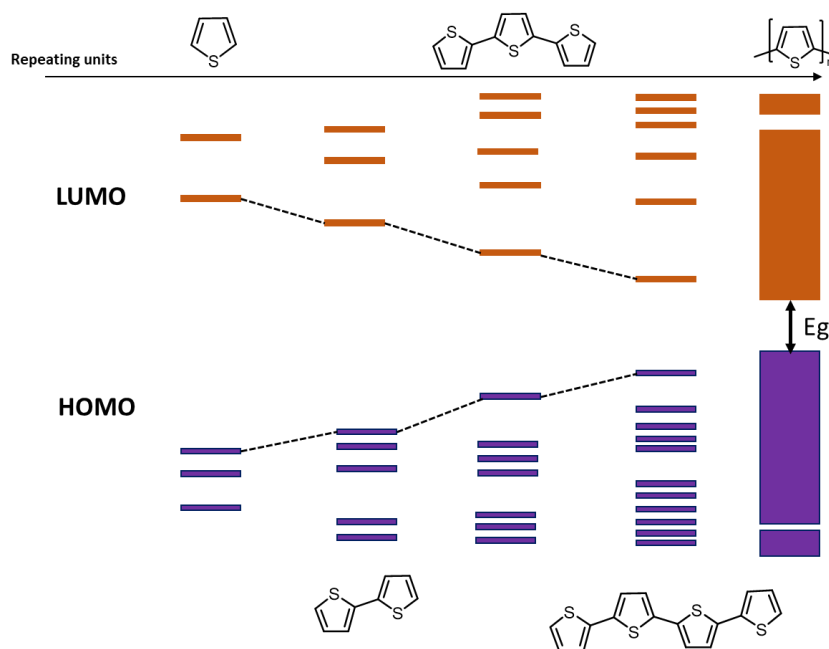


Figure 5: Development of the band gap as the number of repeating units of the thiophene monomer<sup>23</sup>

Energy band theory allows explaining the differences between insulators, semiconductors and conductors. The band gap in a highly conjugated system is the energy difference between the valence and the conduction band in the material. This formation of bands is a feature of valence electron in the atom, with high conjugation length, the energy levels of the atoms which contain the valence electrons is called the valence band. Conduction band is the band of electron orbitals that electrons can jump up into from the valence band when excited. The energy band gap corresponds to the energy required to promote a valence electron to become a conduction electron. The band gap can be calculated by the energy difference between them.

<sup>22</sup> Conjugated Polymer Nanostructures for Energy Conversion and Storage Applications, First Edition. Edited by Srabanti Ghosh. © 2021 WILEY-VCH GmbH.

<sup>23</sup> U. Salzner, J.B. Lagowski, P.G. Pickup, R.A. Poirier, *Synthetic Metals*, **1998**, 96, 177-189.

It corresponds to the difference between the ionization potential (IP) and the affinity potential (AP). IP is the minimum energy required to remove the most loosely bound electron of the molecule, whereas AP is the minimum energy to capture an electron (Figure 6).

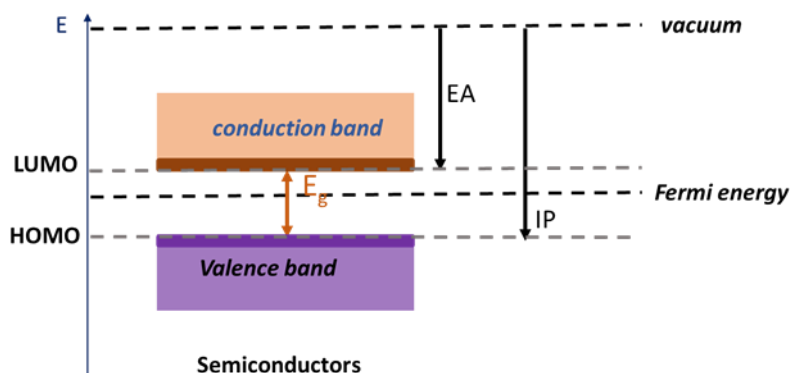


Figure 6: The electron affinity and ionization potential in organic semiconductors

Moreover, the HOMO and LUMO levels depend on the composition of the aromatic units of the monomer not only the length of the conjugated system. The presence of strong donor group leads to increase in the HOMO energy level and consequently an increase in the ionization potential. Hence, the conjugated polymer is considered as donor material that is easily can be oxidized. On the other hand, the presence of strong acceptors leads to decrease in the LUMO energy level and then increase in the electron affinity and then the conjugated polymer will be considered as acceptor material, which can easily be reduced.

In order to evaluate the  $E_{\text{HOMO}}$  and  $E_{\text{LUMO}}$  we use the cyclic voltammetry diagram. It is a very suitable method for a range of applications. It is a standard technique for characterizations. HOMO represents the energy needed to extract an electron that is an oxidation process, and LUMO represents the energy needed to inject an electron to the molecule that is a reduction process. Cyclic voltammetry measures these processes through measuring the redox potential  $E_{\text{red}}$  and  $E_{\text{ox}}$ . Ferrocene is utilized as a reference to calculate the HOMO and LUMO energies according the following equations with -4.4 eV the ferrocene value.<sup>24</sup>

$$E_{\text{HOMO}} = -e [E_{\text{ox}}^{\text{onset}} + 4.4] \quad (1)$$

$$E_{\text{LUMO}} = -e [E_{\text{red}}^{\text{onset}} + 4.4] \quad (2)$$

Wherefore, two types of conjugated polymers can be differentiated according to the composition of the monomer unit. Polymer with monomer of donor nature is considered as p-type conjugated polymer with hole mobility semiconductor after oxidation of the polymer through p-doping process. While monomer with acceptor nature is considered as n-type

<sup>24</sup> L. Leonat, G. Sbarcea, I.V. Branzoi, *U.P.B. Sci. Bull., Series B*, Vol. 75, Iss. 3, 2013

conjugated polymer with electron mobility semiconductor after the reduction of the polymer through n-doping process.

For a very large band gap (more than 2 eV) the material is classified as an insulator. When the conduction band overlaps the valence band then the band gap is zero the materials are classified as conductors (Figure 7). In this thesis, we are more interested in semiconductor materials that can conduct electricity upon excitation due to the presence of a small band gap (non-zero less than 2 eV).<sup>25</sup> Organic conjugated polymers aren't well explained via the energy band theory. Hence, their charge transport mechanism is studied from theoretical and experimental views by a number of researchers.<sup>26,27</sup>

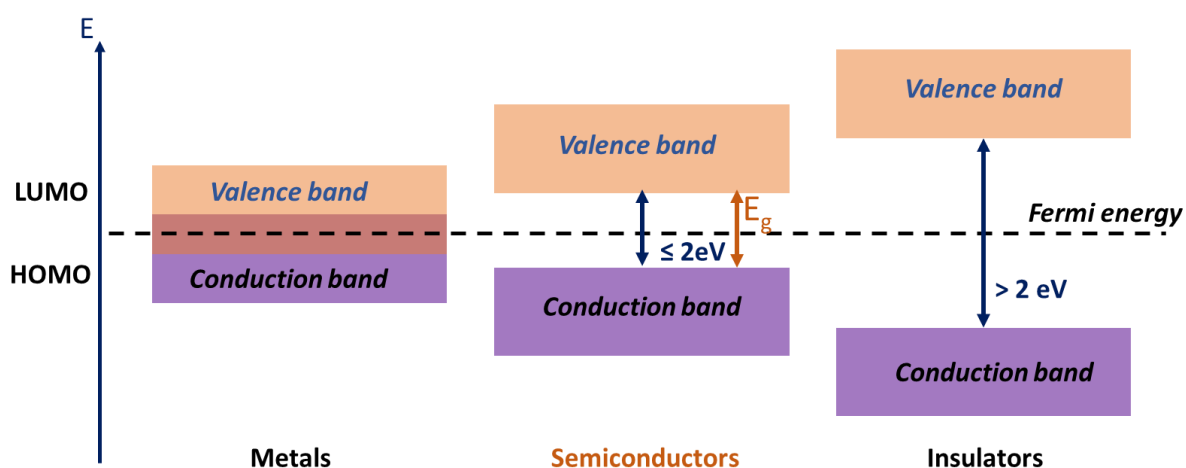


Figure 7: Difference of energy levels among metals, semiconductors and insulators

Therefore, the band gap is strongly related and affected to the chemical structure and the morphology of polymer. Hence, there are a variety of parameters affecting the properties of conjugated polymer as the optical, electronic and optoelectronic properties.

### 3. Main properties of Conjugated polymers:

Since the discovery of conjugated polymers, they have received increasing attention owing to their properties: optical, electronic and optoelectronic properties.

<sup>25</sup> André-Jean Attias, *Technique de l'ingénieur*, E1862 V2, **2017**.

<sup>26</sup> S. Stafström, K.A. Chao, *Phys. Rev. B*, **1984**, 30, 2098–2103

<sup>27</sup> J.L. Bredas, G.B. Street, *Acc. Chem. Res.*, **1985**, 18: 309–315

### 3.1. Optical properties:

These properties are more related to the optical excitations and transitions between HOMO and LUMO levels based on the mechanical effect of light on electronic materials, especially organic semiconductors in organic solar cells.

Optical properties such absorption, transmittance and dispersion represent the behavior of the conjugated polymer with light. The particular optical absorption of a conjugated polymer is critical to the performance of the optoelectronic device.<sup>28</sup> The absorption represents the phenomenon by which the energy of a photon is converted to internal energy taken by another particle, for example an electron.

The amount of energy carried by photon depends on its wavelength. The shorter the wavelength of light, the higher the energy.

Absorption spectroscopy is a way to study the energy levels of atoms, molecules and polymers. The spectrum of a molecule or a polymer depends on its energy-level structure. The minimum energy difference allowing a photon to be absorbed is called optical band gap  $E_g^{\text{opt}}$ .

Conjugated polymers owe similar electronic band gap as conventional semiconductors with electron-electron and electron-hole coupling.<sup>29</sup> The  $\pi$  electron from the ground state (HOMO) after excitation can absorb a photon and jump to the excited state  $\pi^*$  (LUMO), forming a positive charge behind. These holes formed are bonded to electrons by Coulomb interaction forming an exciton (neutral quasiparticle) and then this attraction allow the formation of exciton band below the conduction band threshold. The difference between the HOMO level and exciton band is named optical band ( $E_{\text{opt}}$ ) with exciton binding energy ( $E_b = E_g - E_{\text{opt}}$ ) with average range 0.5-1.0 eV for many conjugated polymers (Figure 8).<sup>30</sup>

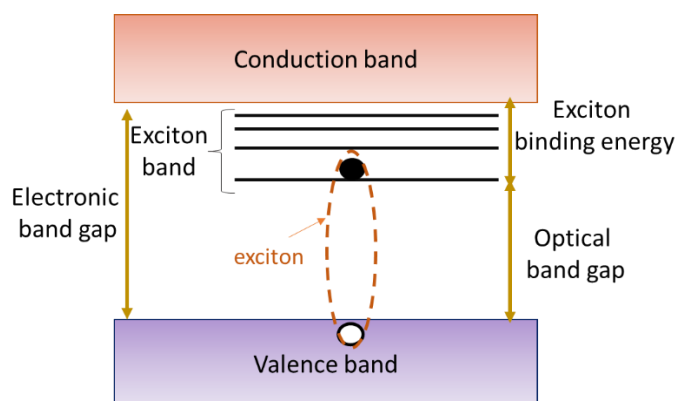


Figure 8: Electronic band gap and exciton band formed in conjugated polymers.

<sup>28</sup> M.S. Vezie, S. Few, I. Meager, G. Pieridou, B. Dörfling, R.S. Ashraf, A.R. Goñi, H. Bronstein, I. McCulloch, S.C. Hayes, M. Campoy-Quiles, J. Nelson, *Nature Mater*, **15**, 746–753 (2016).

<sup>29</sup> W. Barford, *J. Phys. Chem. A*, **2013**, 117: 2665–2671

<sup>30</sup> G.D. Scholes, G. Rumbles, *Nat. Mater.*, **2006**, 5: 683–696.

The  $E_g^{\text{opt}}$  can be calculated from a UV-Vis spectroscopy absorption spectrum, according to the following equation:

$$E_g^{\text{opt}} = \frac{hc}{\lambda_{\text{abs}}^{\text{(onset)}}}$$

Where,  $h$  is the Planck constant,  $c$  is the speed of light in vacuum, and  $\lambda_{\text{abs}}^{\text{(onset)}}$  is the wavelength of the less energetic photon absorbed from the absorption spectrum (Figure 9).

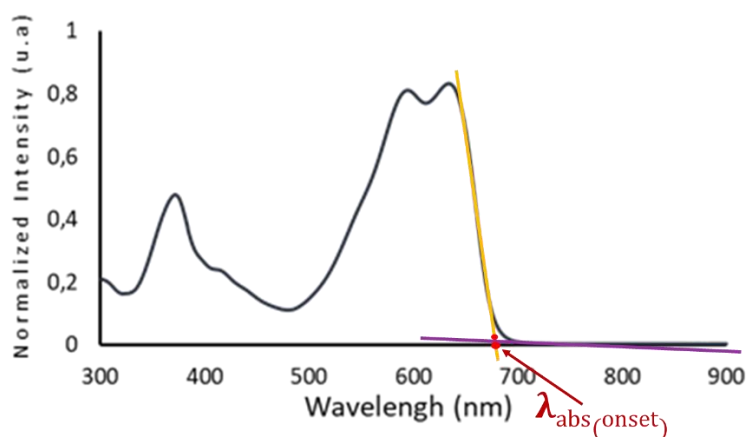


Figure 9: Calculating the  $\lambda_{\text{abs}}^{\text{(onset)}}$  from the UV-Vis spectroscopy absorption spectrum

Perrin-Jablonski diagram is widely used in fluorescence spectroscopy to illustrate the excited states of a molecule and the radiative and non-radiative transitions that can occur between them. It is a molecule energy level diagram to illustrate the absorption and emission of light. The fundamental state is the energetic level of an electron in the HOMO. This electron can reach the LUMO or higher energetic level upon the absorption of photons. This diagram explains five transitions: Absorption, internal conversion, fluorescence, intersystem conversion and phosphorescence (Figure 10).<sup>31</sup>

<sup>31</sup> M. Pope, C.E. Swenberg, *Electronic Processes in Organic Crystals and Polymers*, 2nd ed., Oxford Science Publications, Oxford, 1999.

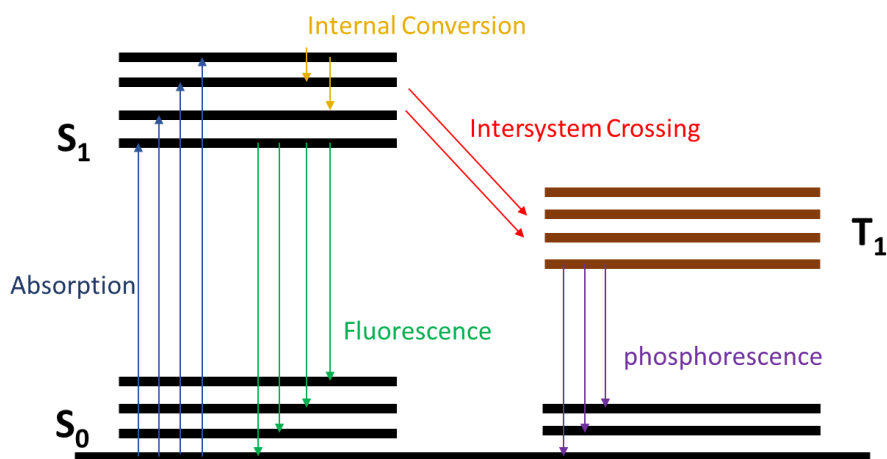


Figure 10: Jablonski diagram for a photoluminescent system

The first mechanism is absorption ( $10^{-15}$  s) of photons by a molecule. It causes electrons from the fundamental state ( $S_0$  on figure 10) to reach higher energetic states ( $S_1$  on figure 10). Then, there are two possible radiative pathways for electron to go back to its fundamental state: Fluorescence and Phosphorescence and two non-radiative pathways: intersystem crossing and internal conversion.

Fluorescence ( $10^{-9}$  s to  $10^{-7}$ s) is the emission of photons with radiative transition from  $S_1$  to  $S_0$ . Internal conversion is non-radiative transition between two electronic states of the same spin multiplicity. It proceeds rapidly on a timescale ( $10^{-11}$  s to  $10^{-9}$ s) between two singlet excited states.

An alternative transition to fluorescence and internal conversion is intersystem crossing from  $S_1$  to the  $T_1$  state. It is a non-radiative transition between two isoenergetic vibrational levels belonging to electronic state of different spin multiplicity. After intersystem crossing the molecule directly undergo vibrational relaxation toward the ground vibrational level  $T_1$ . This non-radiative decay mechanism from  $S_1$  to  $T_1$  reduces the luminescence.

Phosphorescence ( $10^2$  to  $10^{-4}$  s) is the second radiative pathway for electron between two electronic states of different spin multiplicity. It is the transition from  $T_1$  to  $S_0$ .

Conjugated polymers with optical properties could be used in two main fields: light generation and light harvesting. In light generation field, there are important applications includes polymer light emitting diodes and lasers. As light harvesting materials, they are mainly used in solar cells, where electrons need to be collected before returning to their fundamental state.<sup>32</sup>

<sup>32</sup> E. Perzon, F. Zhang, M. Andersson, W. Mammo, O. Inganäs, M. R. Andersson, *Adv. Mater.*, **2007**, 19, 3308–3311

## 3.2. Electronic and optoelectronic properties:

In this paragraph we will explain the methods of charge creation in a conjugated polymer and their electronic and optoelectronic properties, which are a set of parameters that describe the state and the behavior of electrons in the material.

### 3.2.1. Charge generation:

The charge generation can be created by different mechanisms depending on the type of excitation. First, it can be the formation of exciton (dissociated electron/hole pair) under light as previously described. After the absorption of a photon, and the formation of exciton, an electron can reach the conduction band if recombination is hindered. This property is utilized in organic solar cells based on conjugated polymers as explained in the optoelectronic properties paragraph.

Second, the charge carrier creation also can be through the formation of a polaron. Polarons form due to the coupling of excess electrons or holes with a local polarization field. A polaron can be radical cation or radical anion in the case of p- or n- chemical doping, respectively. These polarons are responsible for conductivity (Figure 11) that is explained in the next paragraph.

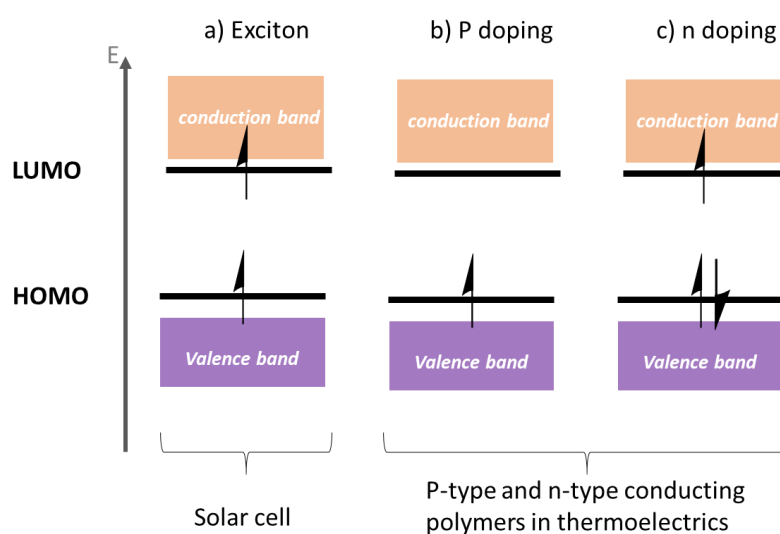


Figure 11: The different ways of charge generation in conducting polymers

Doping represents the oxidation and reduction reactions in conjugated polymers that induce conductivity. Molecular doping is applied in the field of organic electronics.<sup>33</sup> The performance of a doped conjugated polymer strongly influenced by the type of dopant and its distribution. In organic electronics, the most dopants for conjugated polymers are

<sup>33</sup> Y. Lu, J.-Y. Wang, J. Pei, *Acc. Chem. Res.* **2021**, 54, 13, 2871–2883

molecules with different energy levels from the host polymers. It is classified as p-doping and n-doping (Figure 12).

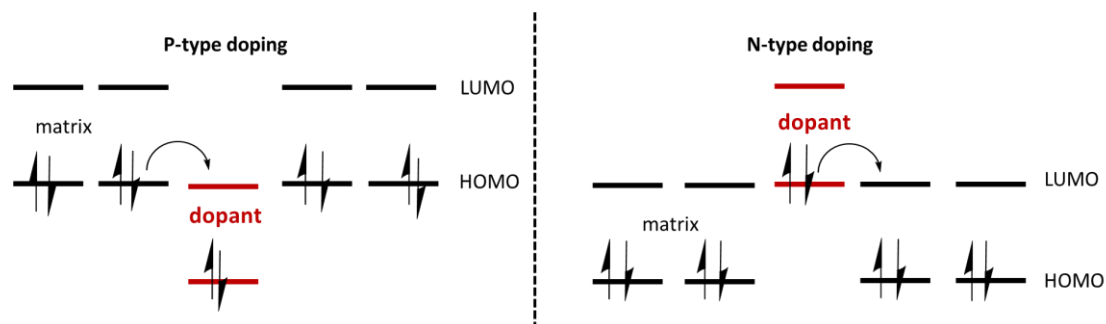


Figure 12: The different mechanisms in p-type and n-type doping<sup>34</sup>

P-doping is a way to introduce charges to the semiconducting polymer. This process involves an electron transfer between the semiconducting polymer and a small molecule. There are a broad variety of p-type dopant, such as 2,3,5,6-tetrafluoro-7,7,8,8-tetracyanoquinodimethane (**F4TCNQ**), which has electron affinity (EA= 5.2 eV) to easily oxidize polymers like poly(3-hexyl thiophene). 1,3,4,5,7,8-hexafluoro-tetracyano-naphthoquinodimethane (**F6TCNNQ**) with EA= 5.3 eV and hexacyano-tri-methylene-cyclopropane with EA= 5.9 eV are other examples of p-dopants with high electron affinity (Figure 13).<sup>35</sup>

We are more interested in n-doping for n-type conjugated polymers, where the conductivities are mainly below  $10 \text{ S cm}^{-1}$  and the thermoelectric power factor not more than  $10 \mu\text{Wm}^{-1}\text{K}^{-2}$ .<sup>36</sup>

N-doping of conjugated polymers is when the dopant plays the role of donor, so it donates electron to the LUMO level of the n-type conjugated polymer. As examples of dopants are the small atoms as alkali metals such as Lithium, cesium and Lewis acids. However, small molecule are dopants able to diffuse and then lead to device instability. Therefore, using large and aromatic molecules as donor is more efficient in preparation of stable device to not diffuse in the thin film, but the size must not be too large to not act as a trap, where they have to be allowed to inject an electron to the LUMO level of the conjugated polymer. Hence, the HOMO level must lie above the LUMO of the matrix.<sup>37</sup> This type of doping is still complicated due to the limited molecules combining the stability with appropriate high LUMO state compared to the organic conjugated polymers because the stability of the dopant against oxidation decreases as the HOMO level increases. As examples of n-type doping molecules, there are

<sup>34</sup> C. Heiliger, B.K. Meyer, *Phys. Status Solidi A* 210, **2013**, No. 1, 67-68

<sup>35</sup> A.I. Hofmann, R. Kroon, S. Zokaei, E. Järsvall, C. Malacrida, S. Ludwigs, T. Biskup, C. Müller, *Adv. Electron. Mater.*, **2020**, 6, 2000249

<sup>36</sup> Y. Lu, J.-Y. Wang, J. Pei, *Chem. Mater.*, **2019**, 31, 6412-6423.

<sup>37</sup> C. Heiliger, B.K. Meyer, *Phys. Status Solidi A* 210, **2013**, No. 1, 67-68



(4-(1,3-dimethyl-2,3-dihydro-1H-benzimidazol-2-yl)phenyl)dimethyl amine (**N-DMBI-H**) and trisaminomethane (**TAM**) (Figure 13).<sup>38</sup>

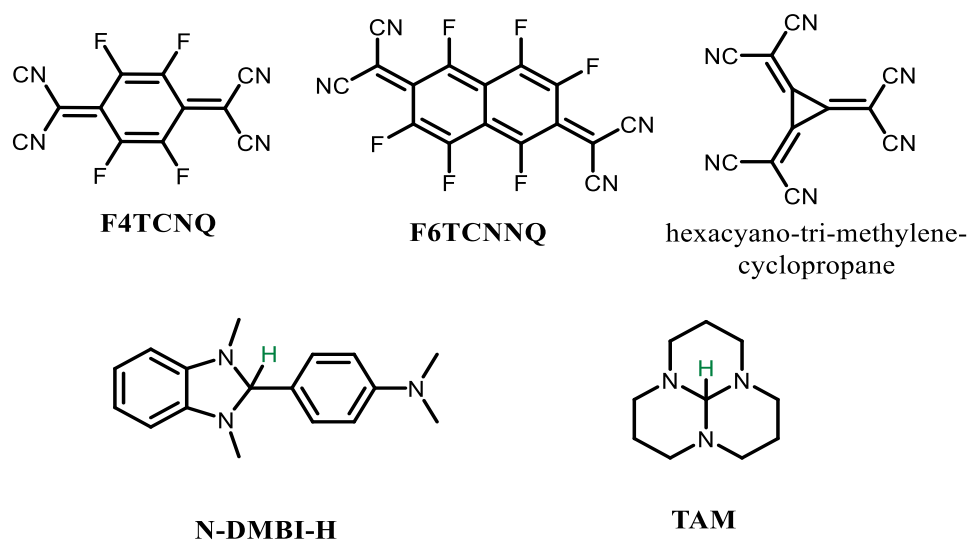


Figure 13: Some examples of p-type and n-type dopants

Both doping processes are required for organic thermoelectric devices, which need both n-type and p-type conjugated polymers.

The increased doping level is coherent with enhanced electrical conductivity. For example, the conductivity of Polythieno[3,4-b]thiophene **PTbT** (Figure 14) homo polymer is increased from  $10^{-5} \text{ S cm}^{-1}$  in the neutral state to  $0.2 < \text{ S cm}^{-1}$  in the doped state. In the same study, it has been demonstrated that morphological features and aggregation could impose an impact on the electrical conductivity.<sup>39</sup>

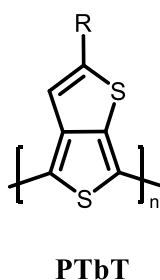


Figure 14: Structure of **PTbT** homo polymer

<sup>38</sup> Y. Lu, Z-D. Yu, Y. Liu, Y-F. Ding, C-Y. Yang, Z-F. Yao, Z-Y. Wang, H-Y. You, X-F. Cheng, B. Tang, J-Y. Wang, J. Pei, *J. Am. Chem. Soc.*, **2020**, 142, 15340–15348

<sup>39</sup> D. Yuan, L. Liu, X. Jiao, Y. Zou, C. R. McNeill, W. Xu, X. Zhu, D. Zhu, *Adv. Sci.*, **2018**, 1800947

### 3.2.2. Electronic properties:

There are two main electronic properties which determine the behavior of conjugated polymers: the charge mobility and the electrical conductivity.

#### 3.2.2.1. Charge mobility in semiconductors:

The charge mobility refers to how quickly electrons and holes (in n-type and p-type materials, respectively) can be displaced under the application of an electric field. It is influenced by various structural parameters such as the chemical structure or the molecular arrangement of the conjugated polymer but also by its average molar mass.

Charge mobility can be explained by polaron delocalization. There are two types of polaron delocalization after its generation: intrachain and interchain (Figure 15). The interchain polaron propagation arises from two different polymer chains or one folded single chain.<sup>40</sup> The intramolecular mobility is highly sensitive to the chemical structure of polymer chain.<sup>41</sup> It is related to the charge movement within a polymer chain. Intermolecular mobility is when charges are able to delocalize and move along chains. The arrangement of the transport path plays an important role in governing mobility, where charges are confined to the ordered region compared to the amorphous polymer.<sup>42</sup> Note that ordered or crystalline-like regions are polymer chains arranged in a regular manner. In polymers, crystalline regions are based upon long-chain molecules and usually they are entangled with amorphous regions.<sup>43</sup> Interchain hopping is another term that explains the charge mobility in molecular solids in an electric field period within disordered regions.

---

<sup>40</sup> J.Cornil, D. Beljonne, J-P. Calbert, J-L. Brédas, *Adv. Mater.*, **2001**, 13, 1053–1067

<sup>41</sup> Y.V. Anufriyeva, N.P. Kuznetsova, M.G. Krakovyak, R.N. Mishayeva, V.D. Pautov, G.V. Semisotnov, T.V. Sheveleva, *Vysokomol. Soyed*, **1977**,19(1), 119–125

<sup>42</sup> M. Statz, D. Venkateshvaran, X. Jiao, S. Schott, C.R. McNeill, D. Emin, H. Sirringhaus, R. Di Pietro, *Commun. Phys.*, **2018**, 1, 16

<sup>43</sup> Modern Physical Metallurgy and Materials Engineering Science, process, applications Book • Sixth Edition • **1999**

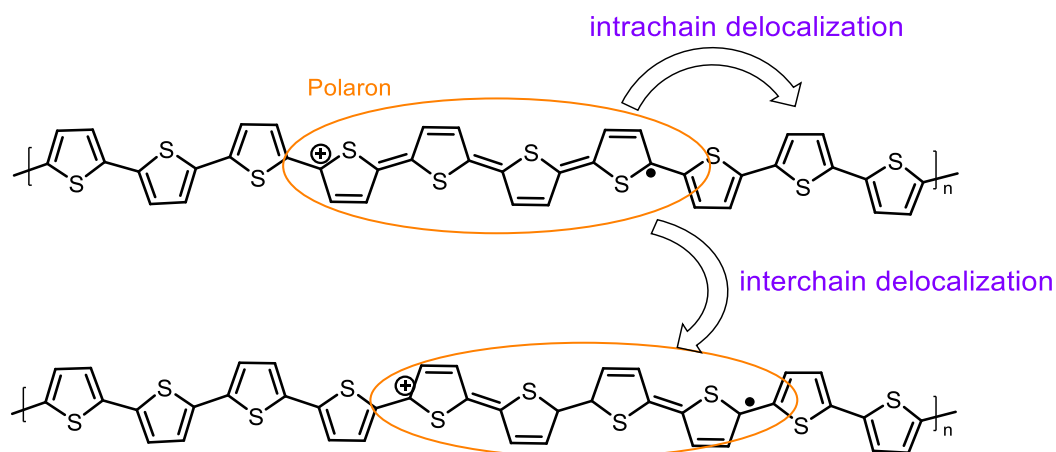


Figure 15: Mechanism of intra chain and interchain delocalization of a polaron

Indeed, it has been shown that high average molar mass polymers lead to larger mobilities. The average hole mobility for example, is improved by two orders of magnitude from  $2 \times 10^{-3}$  to  $0.15 \text{ cm}^{-2} \text{ V}^{-1} \text{ s}^{-1}$ , when the average molar mass is doubled from 30.1 to 61.8 kg/mol.<sup>44</sup> In the case of one of DPP based polymer (**DPP-DTT**), (Figure 16) extremely high average molar mass of  $110 \text{ kg} \cdot \text{mol}^{-1}$  led to very high mobility around  $8 \text{ cm}^{-2} \text{ V}^{-1} \text{ s}^{-1}$  with maximum of  $10.5 \text{ cm}^{-2} \text{ V}^{-1} \text{ s}^{-1}$ , while with average molar mass of  $29 \text{ kg} \cdot \text{mol}^{-1}$  the mobility is around  $1 \text{ cm}^{-2} \text{ V}^{-1} \text{ s}^{-1}$ .<sup>45</sup>

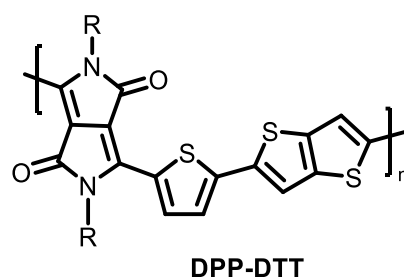


Figure 16: The structure of DPP-DTT polymer

An explanation for the relation between high molecular weight and mobility is that the ordered regions are more interconnected by longer chains with a higher degree of molecular ordering. This improves the interchain charge hopping resulting with facilitated charge carrier transport in disordered regions.<sup>46</sup>

<sup>44</sup> J. J. Intemann, K. Yao, H.-L. Yip, Y.-X. Xu, Y.-X. Li, P.-W. Liang, F.-Z. Ding, X. Li and A. K. Y. Jen, *Chem. Mater.*, **2013**, 25, 3188–3195

<sup>45</sup> J. Li, Y. Zhao, H. S. Tan, Y. Guo, C. A. Di, G. Yu, Y. Liu, M. Lin, S. H. Lim, Y. Zhou, H. Su and B. S. Ong, *Sci. Rep.*, **2012**, 2, 754.

<sup>46</sup> B. Fu, J. Baltazar, Z. Hu, A.-T. Chien, S. Kumar, C. L. Henderson, D. M. Collard and E. Reichmanis, *Chem. Mater.*, **2012**, 24, 4123–4133

However, in a study by Takimiya et al there is no impact of increasing the average molar mass on the carrier mobility with increasing the average molar mass from 12 to 46 Kg.mol<sup>-1</sup>.<sup>47</sup> N-type conjugated polymers can even exhibit higher electron mobility due to the higher crystallinity obtained with lower average molar mass.<sup>48</sup> Hence, increasing the average molar mass of conjugated polymers increases charge mobility in both n-type and p-type conjugated polymers.

Semiconducting conjugated polymers with high charge mobility are widely used in organic field effect transistors (OFETs). OFET is a voltage-controlled three terminal device. One of its basic components is semiconductor layer. Inorganic semiconductors are replaced by conjugated polymers. Both p- and n- type OFETs are required for organic electronics. Thus, p- or n-type conjugated polymers are used depending on the type of OFET device. They are promising candidates for OFETs since they offer unique advantages compared with traditional silicon electronics, including mechanical flexibility, solution processability and tunable optoelectronic properties.<sup>49</sup>

### 3.2.2.2. Electrical conductivity of conducting conjugated polymers:

The conductivity of a material depends on the concentration of free electrons in it. It is determined by the carrier mobility ( $\mu$ ) and the doping level ( $n$ ) with  $\sigma = n e \mu$ , where  $n$  is the density of charge carrier and  $\mu$  is the carrier mobility and  $e$  is the carrier charge that is constant. Therefore, the electrical conductivity is affected by the charge transport and the doping process.<sup>50</sup>

### 3.2.3. Optoelectronic properties:

In organic solar cells (OSCs) the recombination of photogenerated charge carriers is the most important loss mechanism. Thus, limiting the recombination losses is considered as a key strategy to enhance efficiencies. In OSCs recombination can occur at different stages during photocurrent generation. After absorption, organic semiconductors strongly bound exciton. This exciton can move through diffusion and split at the Donor-Acceptor interface by charge transfer. But, if exciton does not reach the interface during its lifetime, exciton recombination occurs.<sup>51</sup>

---

<sup>47</sup> I. Osaka, M. Akita, T. Koganezawa and K. Takimiya, *Chem. Mater.*, **2012**, 24, 1235–1243

<sup>48</sup> Y. Karpov, W. Zhao, I. Raguzin, T. Beryozkina, V. Bakulev, M. Al-Hussein, L. Häußler, M. Stamm, B. Voit, A. Facchetti, R. Tkachov and A. Kiriy, *ACS Appl. Mater. Interfaces*, **2015**, 7, 12478–12487

<sup>49</sup> J. Yang, Z. Zhao, S. Wang, Y. Guo, Y. Liu, *Chem* 4, 2748–2785, December 13, **2018**

<sup>50</sup> D. Yuan, L. Liu, X. Jiao, Y. Zou, C. R. McNeill, W. Xu, X. Zhu, D. Zhu, *Adv. Sci.* **2018**, 1800947

<sup>51</sup> S. Wilken, "Charge Recombination in Organic Solar Cells," in *Soft-Matter Thin Film Solar Cells: Physical Processes and Device Simulation* [AIP Publishing, Melville, New York, **2020**]

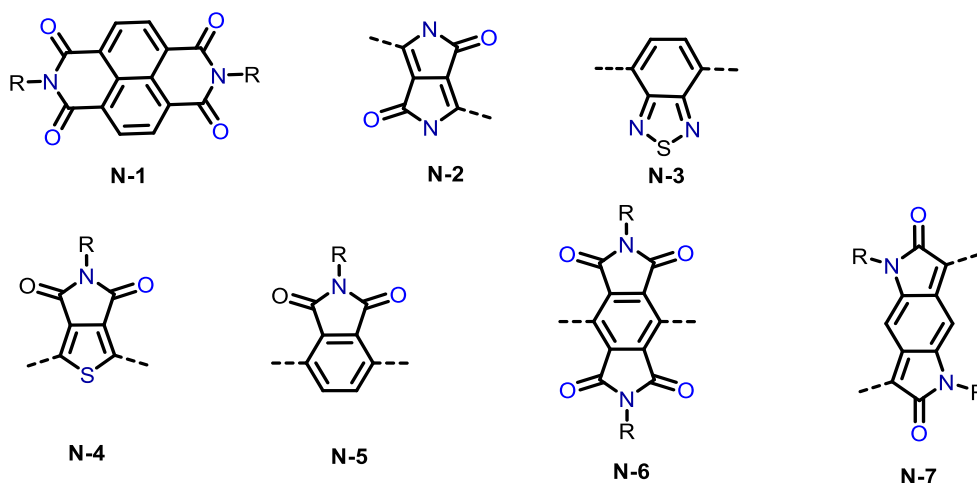
## II. Main strategies to improve the properties of organic conjugated polymers:

Conjugated polymers have attracted the attention due to the ability to tune the band gap and the position of HOMO and LUMO levels by designing the molecule structure. Small modification of the chemical structure can have a large effect on the properties of these organic semiconductors.<sup>52</sup>

Several strategies can be applied to enhance the physical properties of conjugated polymers for improved efficiencies of organic electronic devices, starting with the choice of the type of the conjugated polymers destined. Then, looking to decrease the band gap mostly for organic solar cells. Then, to improve the solubility of the synthesized conjugated polymer and finally to increase the  $\pi$ - $\pi$  aggregation and to control the chain orientation depending on the application.

### 1. The choice of monomer units/P-type and n-type CP:

The choice of the conjugated polymer backbone depends on the targeted application of the desired conjugated material. For the synthesis of n-type conjugated polymer, it is crucial to decrease the affinity potential (AP) to obtain a high HOMO level. Hence, it is crucial to use acceptors blocks in the monomer unit. Therefore, creating strong acceptor units is essential in the synthesis of low-band gap conjugated polymers. Nowadays, a big number of strong acceptor units have been reported in the literature, such as naphthalenedicarboximide (**NDI**) **N-1**,<sup>53</sup> diketopyrrolopyrrole (**DPP**) **N-2**,<sup>54</sup> and benzothiadiazole (**BTz**)**N-3**<sup>55,56</sup> and many other nitrogen-based acceptor units depicted in figure 17.



<sup>52</sup> M.C. Scharber, N.S. Sariciftci, *Adv. Mater. Technol.*, **2021**, 6, 2000857

<sup>53</sup> X. Guo, A. Facchetti, T. J. Marks, *Chem. Rev.* **2014**, 114, 8943–9021

<sup>54</sup> Q. Liu, S E. Bottle, P. Sonar, *Adv. Mater.* **2019**, 1903882

<sup>55</sup> P. Cheng, Y. Yang, *Acc. Chem. Res.* **2020**, 53, 1218– 1228.

<sup>56</sup> Y. Wang, T. Michinobu, *J. Mater. Chem. C*, **2016**, 4, 6200–6214

Figure 17: Chemical structures of electron-deficient nitrogen-based units

Polyisothianaphthene (**PITN**) (Figure 23) was the first polymer with a small band gap. The repeating unit of this polymer consists of bicyclic quinoid structure of high electron-donating ability. This makes the polymer with high HOMO level (around -4.88 eV), which makes them suffer from oxidation under ambient conditions. Analogues of **ITN** with high electron deficiency have been developed such as thieno(3,4-b)pyrazine (**TP**), thieno(3,4-b)(1,2,5)thiadiazole (**TTz**), Thienoisindole-dione (**TID**), thieno(3,4-b)thiophene with ester group (**TbT**) and benzo(2,1,3)thiadiazole (**BTz**),<sup>57</sup> simple bithiazole and thiazolothiazole.<sup>58</sup> And benzodithiophenedione **BDTD**<sup>59</sup> (Figure 18).

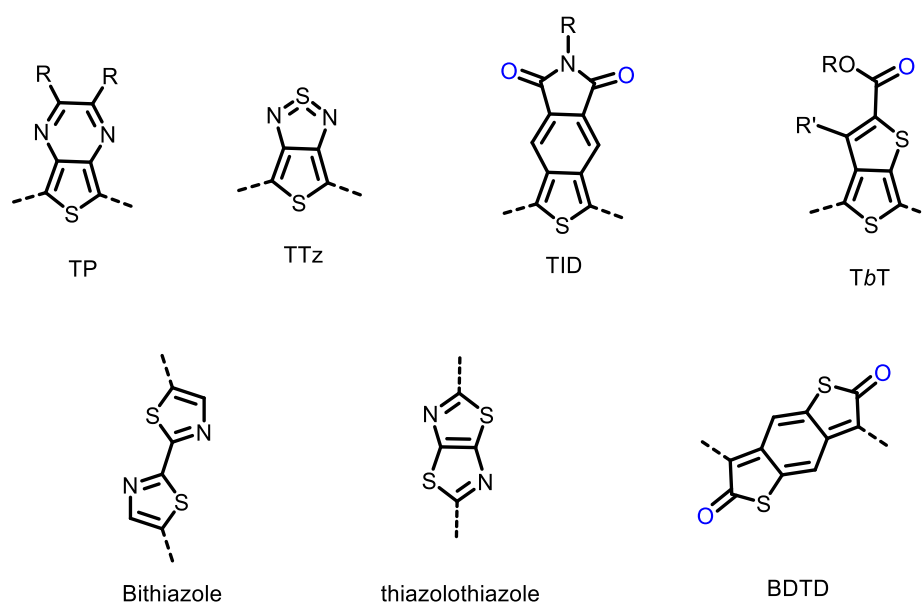


Figure 18: Chemical structures of electron-deficient thiophene based units (A)

All these units have been incorporated into  $\pi$ -conjugated polymers to obtain small band gap with oxidative stability, where careful selection of donor and acceptor units allows modulation of the band gap as well as the HOMO and LUMO energy levels.

Concerning the synthesis of p-type conjugated polymers, it is required to have high ionization potential (IP). Therefore, it is required to use donor blocks in the monomer structure to decrease the LUMO level.

Various donor units have also been used in the formation of D-A conjugated polymers, such as thiophene **T**, selenophene **S**, bithiophene **BT**, bibenzothiophene **BBT**, thiophenethiophene **TT**, thiophene Vinylthiophene **TVT**, cyclopentene dithiophene **CDT**,<sup>60</sup>

<sup>57</sup> T. Mikie, I. Osaka, *J. Mater. Chem. C* **2020**, 8, 14262–14288.

<sup>58</sup> Y. Lin, H. Fan, Y. Li, X. Zhan, *Adv. Mater.* **2012**, 24, 3087.

<sup>59</sup> K. Kawabata, M. Saito, I. Osaka, K. Takimiya, *J. Am. Chem. Soc.* **2016**, 138, 7725–7732.

<sup>60</sup> M. Kim, S U Ryu, S A. Park, K. Choi, T. Kim, D. Chung, T. Park, *Adv. Funct. Mater.*, **2019**, 1904545

phenyl Fluorene derivatives **F-1**, **F-2** and carbazole derivatives **C-1** and **C-2** with the structures depicted on Figure 19.<sup>61,62</sup>

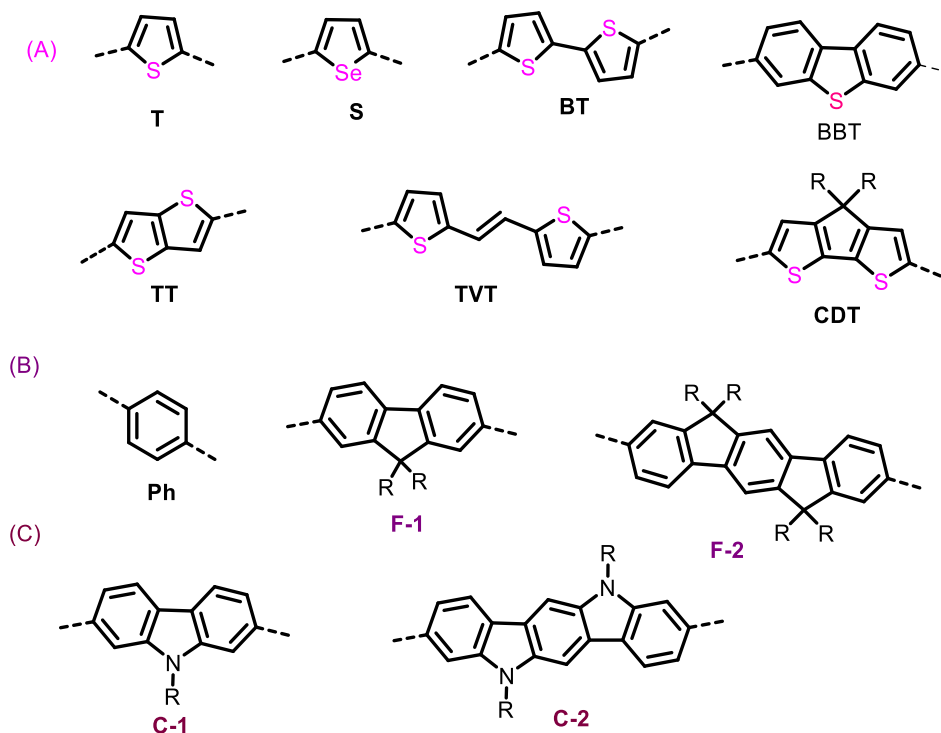


Figure 19: Structure of common donor units

These donor units are used in building p-type conjugated polymers. The performance of p-type semiconducting polymers has achieved much progress. There still exist several challenges for n-type semiconducting polymers. Obtaining conjugated polymer with a small band gap is one of the effective approaches to enhance their performance.

## 2. Decreasing the band gap energy:

Decreasing the band gap energy in the absorption range is required for organic solar cells applications since with smaller band gap more photons can be absorbed, less energetic photons will be able to generate excitons. Another advantage of a small band gap is the reduction of the energy loss. The energy loss in organic solar cells is attributed to the charge transfer, separation and transport. Small band gap could reduce the energy loss by enhancing the diffusion of exciton and reducing its recombination during charge diverse pathways.

Various strategies have been developed to obtain a narrower band gap, such as using heterocycle, increasing the planarity, stabilizing the aromatic resonance or applying the donor-acceptor approach.

<sup>61</sup> J. Yang, Z. Zhao, S. Wang, Y. Guo, Y. Liu, *Chem* 4, 2748–2785, December 13, 2018

<sup>62</sup> X. Guo, M. Baumgarten, K. Müllen, *Progress in Polymer Science*, 2013, 38,1832

## 2.1. Using of heterocycle:

Introducing heteroatoms by using heterocycles in the monomer units leads to less aromatic structures due to the electronegativity of the heteroatom. These cycles are energetically less stable as the resonance energy decreases, which favors smaller band gap (Figure 20).<sup>63</sup>

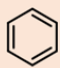
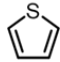


The aromatic unit	Resonance energy	
	KJ/mol	eV
Benzene 	138-151	1.43-1.56
thiophene 	121	1.25
Pyrorole 	89-92	0.92-0.95
Furane 	67	0.69

Figure 20: Resonance energy of benzene and heterocycles

Among the number of  $\pi$ -conjugated polymers, polythiophenes (**PTs**) are widely studied and they have reached industrial utilization in light emitting diodes and organic transistors.<sup>64</sup> It has been confirmed that the increase in the number of thiophene repeating units leads to a smaller band gap.<sup>65</sup>

It was found that the 2,5-coupled polythiophene **PT** is highly conductive with thermal stability but insoluble. Flexible side chains were added to enhance the solubility. Poly(3-alkylthiophene)s (**P3ATs**) were synthesized with the same method as 2,5-coupled polythiophenes in the late 1980.<sup>66,67</sup> However, random couplings in **P3AT** were created using chemical and electrochemical couplings. Regio isomeric, regioregular and regioirregular couplings were obtained with only 50-80 % head-tail (HT) couplings, hence not enough rigidity of the conjugated polymer backbone. This led to an increased band gap energy (Figure 21).<sup>44</sup>

<sup>63</sup>Y.J Cheng, S.H Yang, C.H Hsu, *Chem. Rev.*, **2009**, 109, 5868

<sup>64</sup>R.D. McCullough, *Adv. Mater.*, **1998**, 10, 93–116

<sup>65</sup>C.L. Chochos, S.A. Choulis, *Progress in Polymer Science* 36, **2011**, 1326–1414

<sup>66</sup>R.L. Elsenbaumer, K.Y. Jen, R. Oboodi, *Synth. Met.***1986**,15, 169–174

<sup>67</sup>R. Sugimoto, S. Takeda, H.B. Gu, K. Yoshino, *Chem. Express*, **1986**,1, 635–638



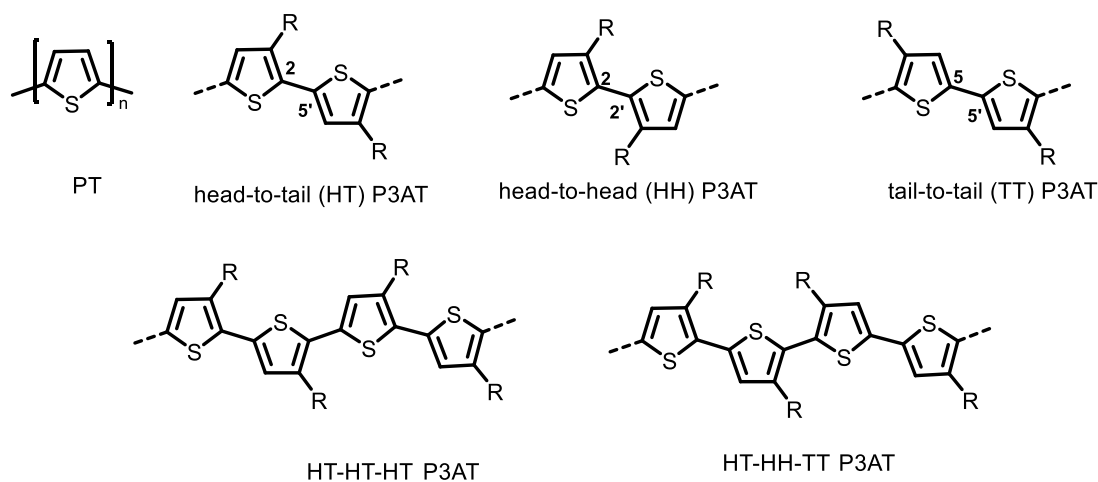


Figure 21: Chemical structures of unsubstituted 2,5-coupled PT, regioregular P3AT (top) and regioirregular P3AT (bottom)

## 2.2. Increasing the quinoid form stabilization:

One of the most important parameters to consider is the stability of the resonance structures to maintain a small band gap. In this field, there are two main forms: the aromatic form and the quinoid form (Figure 22), which is obtained by the delocalization of  $\pi$ -electrons. Normally, due to the delocalization of  $\pi$ -electrons and the breakdown of aromaticity the quinoid form is energetically less stable than the aromatic form but it allows obtaining polymers of smaller band gap.<sup>68</sup>

<sup>68</sup> J.L. Bredas, *J.chem.phys.*, **1985**, 42, 3808

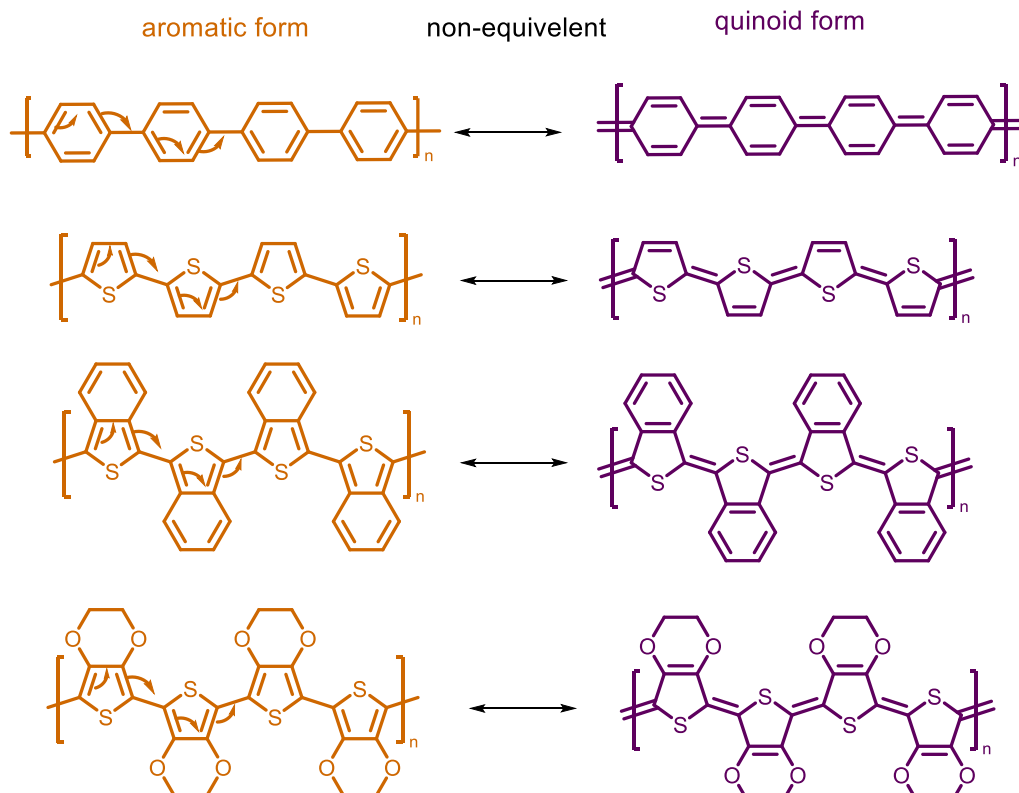


Figure 22: Aromatic and quinoid forms of some conjugated polymers<sup>10</sup>

Polypyrrole and polythiophene were synthesized with band gaps of 3.2 eV and 2.0 eV, respectively.<sup>69,70</sup> More work was done for polythiophene to obtain a smaller band gap. The addition of one benzene ring is one of the methods, which is followed for a further decrease of the band gap. Polyisothianaphthene **PITN** is a result of this strategy that shows a decrease in the band gap to 1 eV with a favored quinoid form (Figure 23). More benzene units were added to study the effect of the number of benzene units on the band gap value so **PITN-1** and **PITN-2** were synthesized. However, these supplementary units didn't allow a smaller band gap due to the disfavored quinoid form.<sup>71</sup>

More polythiophene derivatives were synthesized in the last decades with quinoid form since one of the most efficient approaches is to tailor the monomer structure to increase the quinoid structure. Poly-(thieno(3,4-b) pyrazine) **PTP** has been synthesized with one of the lowest band gaps of 0.95 eV because of the planar quinoid form (Figure 23).<sup>72</sup>

<sup>69</sup> U. Salzner, J.B. Lagowski, P.G. Pickup, R.A. Poirier, *Synthetic Metals*, 96, **1998**, 177-189.

<sup>70</sup> E. Bundgaard, F.C. Krebs, *Solar Energy Materials & Solar Cells*, **2007**, 91, 954.

<sup>71</sup> P. Otto, J. Ladik, *Synth. Metal*, **1990**, 36, 327

<sup>72</sup> M. Pomerantz, B. Chaloner-Gill, L.O. Harding, J.J. Tseng, W.J. Pomerantz, *J. Chem. Soc. Chem. Commun.*, **1992**, 1672.

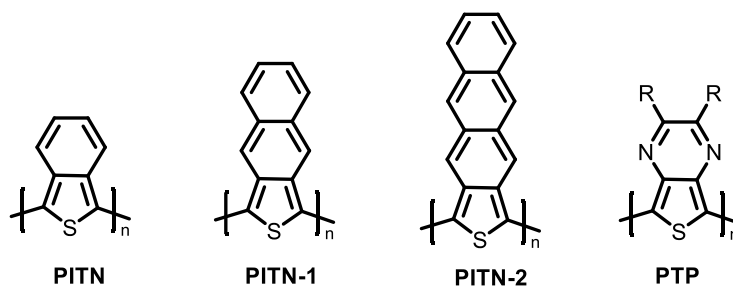


Figure 23: Structure of polymers with the low band gap

### 2.3. Increasing the planarity:

It is crucial to keep a good planarity of the conjugated polymer backbone to maintain the conjugation with no disruption due to the bond rotation and steric hindrance. Developing highly planar semiconducting polymers is a basic property for achieving a good mobility. Planar conformation extends the  $\pi$ -conjugation length and  $\pi$ -electron delocalization. Moreover, it leads to strong solid-state  $\pi$ - $\pi$  stacking between chains and then a narrow band gap.<sup>73,74</sup>

#### 2.3.1. By covalent bond formation :

Planarity with covalent bond formation can be in a form of double bonds or in ladder structure as in figure 24.

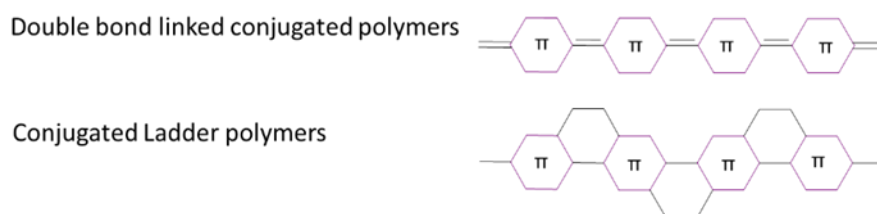


Figure 24: The two forms of covalent bond for achieving planarity in conjugated polymers.

Ladder conjugated polymers are conjugated polymers with good planarity due to the presence of an uninterrupted sequence of adjacent rings sharing two or more atoms.<sup>75</sup> In this type of polymers, the restricted torsional motion of the backbone extends the carrier delocalization and prevents the conformation disorder. This will encourage the charge transfer, interchain interactions and thermal stability.<sup>76</sup>

<sup>73</sup> F.A. Arroyave, C.A. Richard, J.R. Reynolds, *Org Lett.*, **2012**, 14, 6138–41

<sup>74</sup> J. Ren, W. Chen, Y. Zhang, M. Qiu, J. Ren, T. Zhu, F. Liua, M. Suna, R. Yang, *J Mater Chem C*, **2016**, 4, 11088–95

<sup>75</sup> V. Metanomski, R. E. Bareiss, J. Kahovec, K. L. Loening, L. Shi, V. P. Shibaev, *Pure Appl. Chem.* **1993**, 65, 1561–1580.

<sup>76</sup> L. Yu, M. Chen, L. R. Dalton, *Chem. Mater.*, **1990**, 2, 649 – 659.

Hence, the synthesis of polycyclic **PC** compound of fluorene type (standard backbone in figure 25) has been widely studied. Using alkyl or alkoxy substituents to position 9 is one of the promising strategies to improve both the solubility and the rigidity of the polymer.<sup>77</sup>

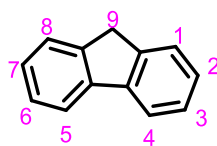


Figure 25: Standard backbone of fluorene

There are a variety of polycyclic compounds of fluorene with different length of the repeating unit that affect the rigidity and the electronic band gap with a strong bathochromic shift between **PC-1** and **PC-2** (Figure 26).<sup>78</sup>

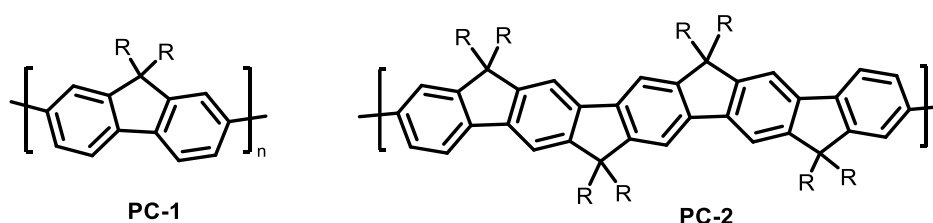


Figure 26: Structure of polyfluorene derivatives

Another way to obtain a rigid conformation is the utilization of polycyclic hydrocarbons **PAHs**. These hydrocarbons include phenanthrene, the triphenylene and Pyrene with benzoic positions, which permit easy functionalization (Figure 27).

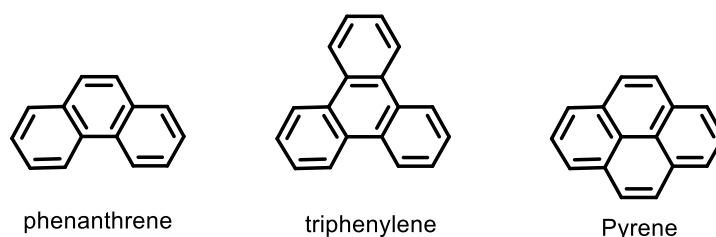


Figure 27: Structure of some polycyclic hydrocarbon

As a method to obtain a rigid and planar confirmation was the insertion of methyl bridge between thiophene units. Synthesis of **PT-1** (Figure 28) clearly demonstrates that rigidification constitutes is an efficient strategy to reduce the HOMO-LUMO gap. The resulting band gap is 1.65 eV.<sup>79</sup> Other modifications were carried on position 3 and 4 of thiophene

<sup>77</sup> X. Guo, M. Baumgarten, K. Müllen, *Progress in Polymer Science*, **2013**, 38,1832.

<sup>78</sup> A.C. Grimsdale, K. Müllen, *Macromol Rapid Commun.*, **2007**, 28, 1676

<sup>79</sup> J. Roncali, C. Thobie-Gautier, *Adv. Mater.*, **1994**, 6, 846.

molecule to form poly(2-decylthieno(3,4-b)thiophene)). **PT-2** with an alkyl group for processability. The resulted band gap is 1.2 eV.<sup>80</sup>

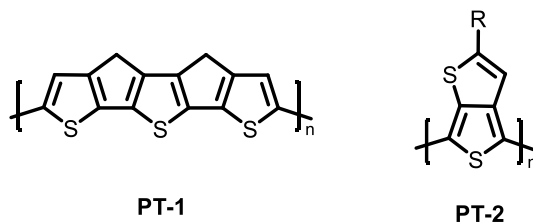


Figure 28: Structure of polythiophene derivatives with the low band gap

While focusing on achieving a coplanar conformation, the  $\pi$ -interactions among the aromatic units lead to a decrease in the solubility of the conjugated polymers. Therefore, some modifications were carried, such as the addition of alkyl groups to phenanthrene **PAH-1** and Pyrene **PAH-2** and phenyl groups to triphenylene **PAH-3** (Figure 29). Number of derivatives were obtained using different R substituents followed by the study of their effects on the optical properties of the obtained polymers. However, the UV-Vis spectrum of **PAH-2** is blue shifted due to the alkoxy groups on poly(arylene) backbone that increase the dihedral angle of consecutive aromatic rings and lead to less electronic conjugation. It is concluded that higher number of aryl units is favored since the polymer is of less capability to aggregate and the extra arylene units between triphenylene repeating unit reduce the twist in the polymer backbone and hence obtaining a well-organized structure.<sup>81,82</sup>

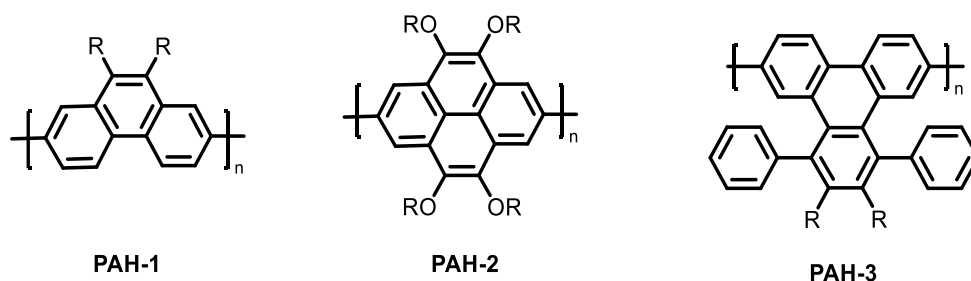


Figure 29: Polycyclic hydrocarbon derivatives

Taking fluorene molecule as standard, the introduction of a heteroatom to rigid backbone is interesting to be explored as a combination of the presence of planarity and a heteroatom for obtaining a smaller band gap. The introduction of nitrogen atom allows the synthesis of carbazole aromatic character due to the lone pair of the nitrogen atom (Figure 30).<sup>83</sup> Moreover, the presence of a heteroatom facilitates the functionalization of the monomer unit and consequently the modification of the chemical and physical properties.

<sup>80</sup> M. Pomerantz, G. Xiaomin, *Synthetic Metals*, **1997**, 84, 243.

<sup>81</sup> M. Saleh, M. Baumgarten, A. Mavrinskiy, T. Schafer, K. Müllen, *Macromolecules*, **2010**, 43, 137.

<sup>82</sup> M. Saleh, Y.S. Park, M. Baumgarten, J.J. Kim, K. Müllen, *Macromol Rapid Commun.*, **2009**, 30, 1279.

<sup>83</sup> J.F. Morin, M. Leclerc, D. Adès, A. Siove, *Macromol. Rapid. Commun*, **2005**, 26, 761.

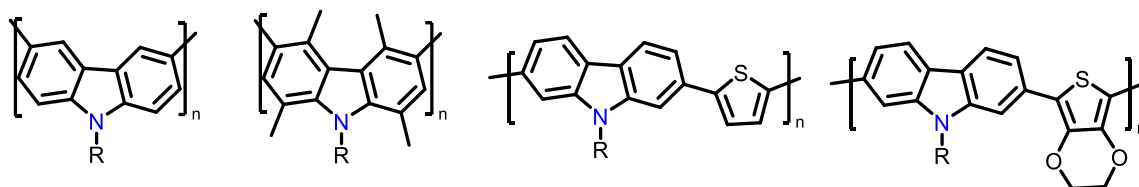


Figure 30: Some examples of poly(2,7-carbazole)s

Benzosilols are compounds with silicon as hetero atom. The first synthesis of 9,9-diphenylsilafluorene (Figure 31) was done in 1955.<sup>84</sup> The utilization of silafluorene derivatives has gained much attention in the synthesis of copolymer and a series of copolymers were synthesized.<sup>85</sup> This family of conjugated polymers is of interesting optoelectronic properties of organic solar cells and as blue emitters in polymer light emitting diodes.

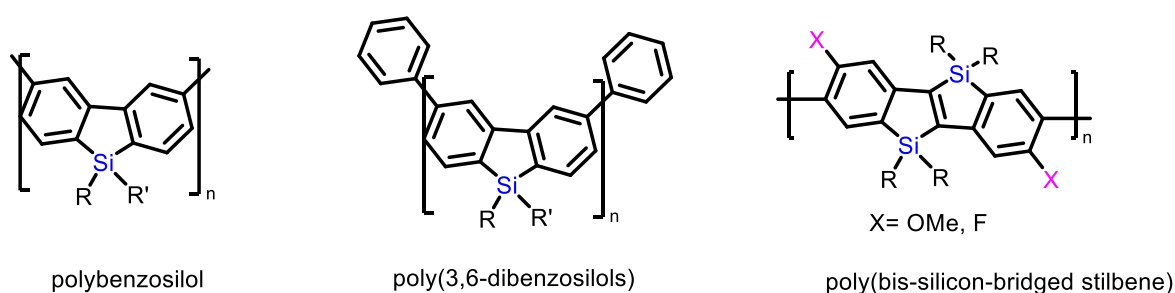


Figure 31: Examples of polysilol derivatives

### 2.3.2. Using Non-covalent interactions :

The rigidity of the synthesized polymer can also be controlled by the presence of intramolecular interactions through utilization of heteroatoms. Some features of conjugated polymers are shown in figure 32.

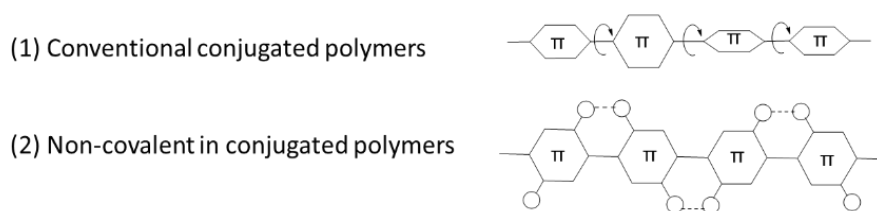


Figure 32: Types of conjugation system in conjugated polymers

Introducing noncovalent interactions into the backbone of conjugated polymers is one of the frequently used methods to achieve planarity. Non-covalent bonds are non-covalent interactions that do not involve the sharing of electrons. There are a wide variety of examples in different fields as supramolecular chemistry.<sup>86</sup> Non-covalent bonds include hydrogen

<sup>84</sup> H. Gilman, R.D. Gorsich, *J. Am. Chem. Soc.*, **1955**, 77, 6380–6381

<sup>85</sup> T.T. Dang, H.M.T. Nguyen, H. Nguyen, T.N. Dung, M.T. Nguyen, W. Dehaen, *Molecules*, **2020**, 25, 548

<sup>86</sup> J. Bernstein, R.E. Davis, L. Shimoni, N-L. Chang, *Angew.chem.Int.Ed.Engl.*, **1995**, 34, 1555-1573

bonds, coordinative interactions and sulfur bonds. Normally, non-covalent bonds are weaker than covalent bonds by one or more in magnitude order.<sup>87</sup>

The binding energies of noncovalent interactions cannot be neglected since they reach 4 KJ.mol<sup>-1</sup> in certain molecules. Therefore, binding energies play an obvious role in serving extra binding energy that lock the coplanar conformation of conjugated polymers through minimizing its energy and increasing the torsional barrier of the conjugated polymer backbone (Figure 33).<sup>88</sup>

Non-covalent interactions	Binding energy KJ/mol
Traditional hydrogen bond Y-H...X	8.36 -41.84
Coordinative interactions N→B	71
Non-traditional hydrogen bond C—H...N C—H...O C—H...F	9.20 7.78 3.93
Sulfur bonds O--S N--S F--S	2.13 1.92 1.84

Figure 33: Binding energies of noncovalent interactions in conjugated polymers

Hydrogen bonds are the most known non-covalent interactions. They are attractive forces between two permanent dipoles described as a special dipole-dipole forces. H-bonding has been represented by structural formulas A:H: B-type bonding elements, and it has been concluded that the H-bonding is largely ionic in character.

In 1997, a new family of poly(phenylenes) (**pPYs**) has been synthesized by the group of Moigne. Amino and esters groups were preinstalled on the same monomer to achieve planarity of the conjugated polymer backbone through hydrogen bonding as depicted in figure 33.<sup>89</sup> In 2013, a new n-type conjugated polymer benzodifurandione-based oligo(*p*-phenyl vinylene) (**BDOPV**) was synthesized. It contains nontraditional hydrogen bonds via electronegative carbonyl oxygen and aromatic unit.<sup>90</sup> In 2014, two new derivatives of poly(*p*-phenylene vinylene) **PPV**, **BDPPV** and **FBDPPV** were synthesized which differ by the presence of fluorine atoms. Fluorine atoms can lower the LUMO level and lock the conformation of the conjugated polymer with nontraditional hydrogen bonds. Hence, these polymers show

<sup>87</sup> P. Hobza, K. Meller-Dethlefs, *Royal Society of Chemistry*, **2009**

<sup>88</sup> C. Zhu, L. Fang, *Macromol. Rapid Commun.*, **2018**, 39, 1700241

<sup>89</sup> M. Moroni, J. Le Moigne, T. A. Pham, J. Y. Bigot, *Macromolecules* **1997**, 30, 1964 – 1972.

<sup>90</sup> T. Lei, J. Dou, X. Cao, J. Wang, J. Pei, *J. Am. Chem. Soc.*, **2013**, 135, 12168 – 12171

shorter  $\pi$ - $\pi$  stacking distance and enhanced rigidity, coplanarity and order of interchain packing (Figure 34).<sup>91</sup>

Introducing intramolecular interactions results in a decrease of the band gap and in an increase in the charge transfer rate upon impacting the HOMO and LUMO levels. Therefore, high planarity of conjugated polymer backbone facilitates electron delocalization and  $\pi$ - $\pi$  intermolecular interactions, which lead to a small band gap and fast charge transfer.<sup>92</sup>

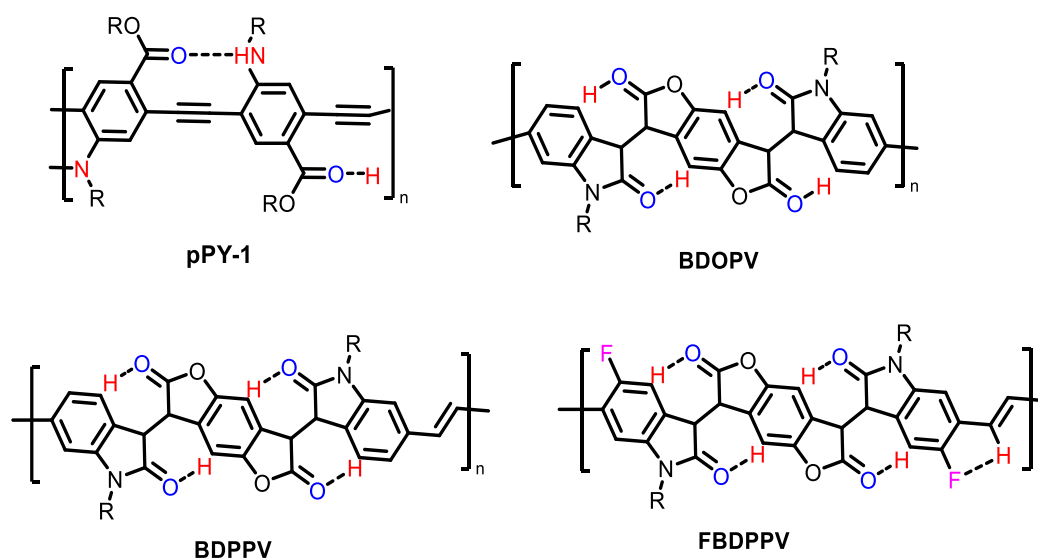


Figure 34: Conjugated polymers with noncovalent bonds

Due to the importance of conformation control, more investigations have been carried. Group of Thelakkat applied this strategy in diketopyrrolopyrroles (**DPP**) based polymers by altering the phenyl ring with five membered thiophene ring. It favored less steric congestion and then formation of a hydrogen bond resulting with more planar and rigid **DPP-T2** (Figure 35).<sup>93</sup>

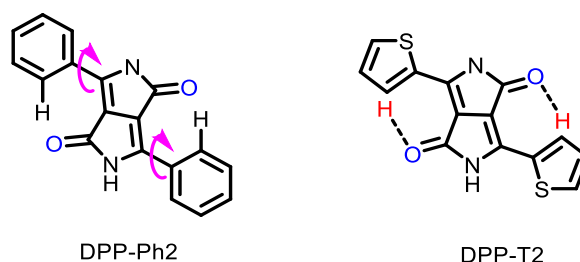


Figure 35: Conformation of **DPP** derivatives using different aryl flanking units

<sup>91</sup> T. Lei, X. Xia, J. Wang, C. Liu, J. Pei, *J. Am. Chem. Soc.*, **2014**, 136, 2135–2141.

<sup>92</sup> B. Liu, D. Rocca, H. Yan, D. Pan, *JACS Au.*, **2021**, 1, 2182–2187

<sup>93</sup> C. J. Mueller, E. Gann, C. R. Singh, M. Thelakkat, C. R. McNeill, *Chem. Mater.*, **2016**, 28, 7088–7097



Among noncovalent interactions are coordinative interactions related to nitrogen-boron interactions such as the classic chromophore boro-dipyrromethane (**BODIPY**).<sup>94</sup> Usually, conjugated polymers with this type of interactions have low LUMO level and small optical band gap.<sup>95</sup> In 2015, the group of Pammer worked on the synthesis of locked conjugated polymers starting from regioregular poly(pyridine) (**PPY**) equipped with 6-(1-alkenyl) side chain following post functionalization strategy.<sup>96</sup> In 2016, group of Liu synthesized a new electron deficient conjugated polymer **BNBP** with fixed coplanar conformation due to N-B coordinative interactions.<sup>97</sup> Therefore, the planarity is maintained (Figure 36).

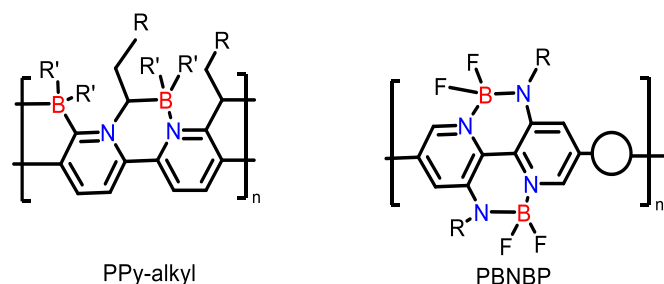


Figure 36: Locked conformation Conjugated polymers with N-B interactions

Due to the highly recommended properties of polythiophene derivatives and the usage of thiophene unit in a great variety of building blocks for polymer backbone, sulfur atoms play an obvious role not only as heteroatom but also in the conformation control of the conjugated polymers (Figure 37).<sup>98</sup> There are a wide number of non-covalent interactions between a sulfur atom and an electronegative atom as nitrogen, oxygen and fluorine, due to the partial donation of a lone pair of an electronegative atom to the 3d empty orbital of the sulfur atom.<sup>99</sup>

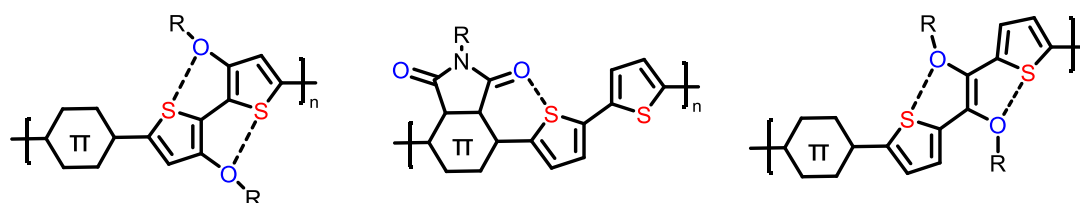


Figure 37: Structures of planar conjugated polymers via Sulfur-Oxygen bonds

One of the most important examples of polythiophene derivatives with non-covalent interactions is poly(3,4-ethylenedioxythiophene) (**PEDOT**) (Figure 38), where 3,4 position of

<sup>94</sup> A. Loudet, K. Burgess, *Chem. Rev.*, **2007**, 107, 4891 – 4932.

<sup>95</sup> H. Shimogawa, O. Yoshikawa, Y. Aramaki, M. Murata, A. Wakamiya, Y. Murata, *Chem. Eur. J.*, **2017**, 23, 3784 – 3791

<sup>96</sup> M. Grandl, F. Pammer, *Macromol. Chem. Phys.*, **2015**, 216, 2249– 2262

<sup>97</sup> C. Dou, X. Long, Z. Ding, Z. Xie, J. Liu, L. Wang, *Angew. Chem. Int. Ed.*, **2016**, 55, 1436 – 1440

<sup>98</sup> N. E. Jackson, B. M. Savoie, K. L. Kohlstedt, M. Olvera de laCruz, G. C. Schatz, L. X. Chen, M. A. Ratner, *J. Am. Chem. Soc.*, **2013**, 135, 10475 – 10483.

<sup>99</sup> A. S. zen, C. Atilgan, G. Sonmez, *J. Phys. Chem. C.*, **2007**, 111, 16362 – 16371.

thiophene is bridged with an oxyalkane unit. Its structure favors sulfur-oxygen interaction, which leads to a self-rigidification of the conjugated structure.<sup>100,101</sup>

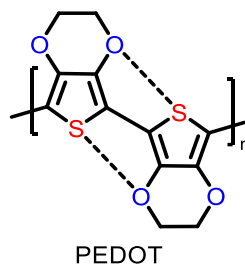


Figure 38: Sulfur-oxygen interaction in **PEDOT**

Rigidification can lead to conjugated polymers with smaller band gap than poly(3-alkylthiophenes).<sup>102</sup>

#### 2.4. New generation conjugated polymer via Donor-Acceptor Approach:

Insertion of electron withdrawing groups has a dominant effect that is the shift of LUMO away from the vacuum Level. However, the insertion of electron donating groups shifts the HOMO toward the vacuum level allowing high-lying highest occupied molecular orbitals (HOMO). This shift in HOMO level leads to easier oxidation of the polymer and then poor ambient stability.

More efficient way is to reduce the lowest unoccupied molecular orbital (LUMO) and obtain a smaller band gap via incorporating strong acceptor unit.<sup>102</sup>

Therefore, one of the most successful routes to decrease the band gap is to apply the donor-acceptor D-A approach. It was first carried by the group of Havinga.<sup>103</sup> It is based on a regular alternation of two units: electron rich donor (D) and electron poor acceptor (A) along the conjugation backbone. The band gap of the resulted polymer is calculated by the hybridization of the corresponding frontier orbitals of each of the donor and acceptor units. Due to the presence of a resonance form between the donor and acceptor units, the double bond character of the single covalent bonds increases. Hence, a reduction in bond length and then generation of new energy levels with increased HOMO level and decreased LUMO level with a smaller band gap (Figure 39).

<sup>100</sup> J. Kim, M. Rémond, D. Kim, H. Jang, E. Kim, *Adv. Mater. Technol.*, **2020**, 1900890

<sup>101</sup> G. Heywang, F. Jonas, *Adv. Mater.*, **1992**, 4, 116.

<sup>102</sup> J. Roncali, *Macromol. Rapid Commun.*, **2007**, 28, 1761–1775

<sup>103</sup> E. E. Havinga, W. T. Hoeve, H. Wynberg, *Polym. Bull.*, **1992**, 29, 119.

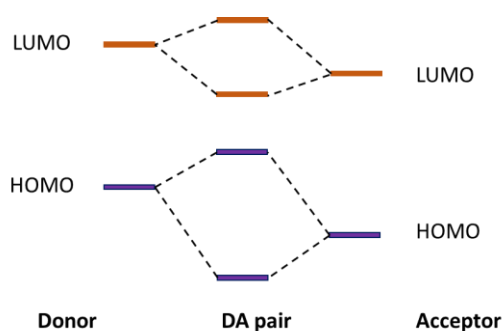


Figure 39: HOMO-LUMO splitting in covalently bound donor-acceptor pairs<sup>104</sup>

Introducing of an acceptor unit with different donor units give rise to a wide number of D-A conjugated polymers, the choice of the donor and acceptor units depends on the physical properties required of the desired polymer. We can distinguish three types of conjugated polymers: p-type, n-type and ambipolar conjugated polymers.

The **PTB** family synthesized by the group of Luping Yu.<sup>105</sup> It consists of alternating benzodithiophene (**BDT**) units as donor and TT as acceptor units (Figure 40), where a variety of substituents of donor and acceptor units were studied to optimize the properties of the polymer taking into consideration that the extension of the conjugation structure reduces the band gap.

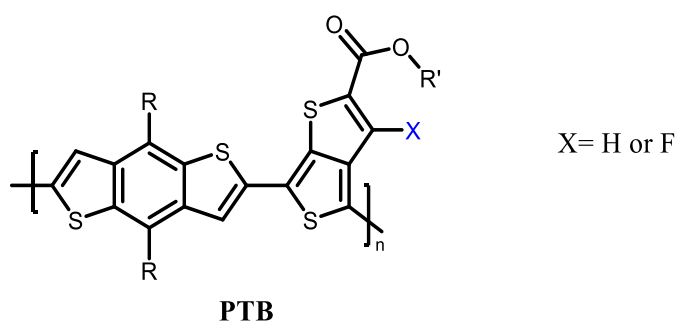


Figure 40: Structure of **PTB** polymers

Obtaining a small band gap energy is essential in the synthesis of organic semiconductors. However, small band gap energy is not enough for better performance. Tuning the morphology of the conjugated polymer is a method to control the physical properties.

In this thesis, we are more interested in the donor-acceptor conjugated polymers due to their low band gap. As we demonstrated, achieving conjugated polymer with high electron mobility is not only related to low band gap and planarity of the system, but also to the molecular orientation and the average molar mass of the D-A polymers. The next paragraph

<sup>104</sup> M.C. Scharber, N.S. Sariciftci, *Adv.Mater. Technol.*, **2021**, 6, 2000857

<sup>105</sup> L. Lu, T. Zheng, Q. Wu, A. M. Schneider, D. Zhao, L. Yu, *Chem. Rev.*, **2015**, 115, 12666.

will demonstrate how the morphology of the conjugated polymer and consequently the physical properties can be tuned by applying functionalization strategies such as side chain engineering.

### 3. Side chain engineering

Side chain engineering consists in making chemical modifications on the molecular structure of conjugated polymer. The role of the used side chain mostly for enhancing the solubility, increasing the  $\pi$ - $\pi$  aggregation, controlling the chain orientation and improving the stability of the obtained polymer under ambient conditions.

#### 3.1. To Increase Solubility:

As previously explained the charge carrier mobility is related to the average molar mass of the polymer. In most cases, the charge mobility increases as the average molar mass increase. The average molar mass of conjugated polymers depends on the chemical structure of the monomer, and the synthetic pathway. It is generally improved when the solubility of the monomers and of the growing polymer chain are good.

Side chain engineering is an efficient method to improve the solubility. In order to control the solubility of the polymer and for better processability, the side chains are introduced on the backbone. According to their chemical nature, the interactions with the solvents can be tuned, but they can also play a role on the polymer planarity and self-organization. Various flexible chains have been used as side chains for conjugated polymers such as: alkyl side chains, hybrid side chains, ionic side chains, oligoether side chains, fluoroalkyl side chains and latent reactive side chains (Figure 41).<sup>106</sup>

---

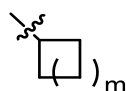
<sup>106</sup> J. Mei, Z. Bao, *Chem. Mater.*, **2014**, 26, 604–615

1) alkyl side chains:

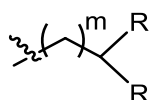
linear



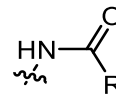
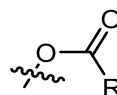
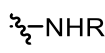
cyclic



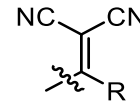
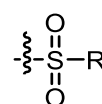
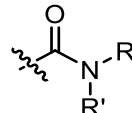
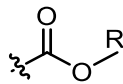
branched



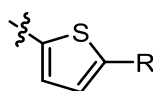
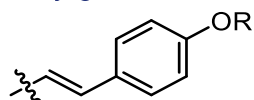
2) hybrid side chains: electron donating



electron accepting



conjugated molecules

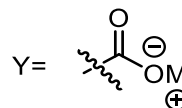
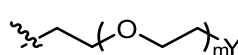
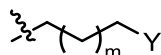


alkyl chain with functional moiety

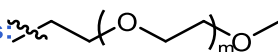


Y = electron donating/accepting side chains

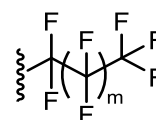
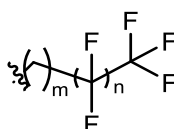
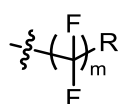
3) ionic side chains:



4) Oligoether side chains:



5) Fluoroalkyl side chains:



6) Latent reactive chains:

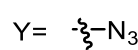
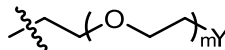


Figure 41: Some examples of different types of side chains<sup>106</sup>

For the conjugated polymers in this thesis in order to improve the solubility, we will focus on three types of side chains: alkyl side chains, oligoether side chains, and fluoroalkyl side chains.

### 3.1.1. Alkyl side chains:

Alkyl side chains have been proven to play an effective role in intermolecular interactions and supramolecular self-assembly. They are directly attached to the conjugated polymers as solubilizing groups to enhance the solubility of the polymers in organic solvents.<sup>107</sup>

The common types of used alkyl chains in conjugated polymers are linear and branched chains. Linear chains could be of different length as hexyl, octyl and dodecyl chains.<sup>108</sup> Linear chains with an even number of carbons are more familiar in conjugated polymers. It has been noticed that linear chain can favor interchain interdigitation.<sup>109</sup>

The branched alkyl chains (Figure 42) reduce the interchain interdigitation and lower the polymer interactions due to their higher steric hindrance that can decrease the polymer planarity and then rise the  $\pi$ -stacking distance in the structure layer.<sup>110</sup> However, branched alkyl chains have a positive impact on the solubility of the conjugated polymer.<sup>107</sup>

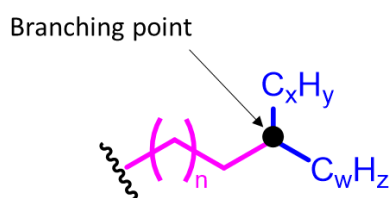


Figure 42: General chemical Structure of branched alkyl side chain

**P3AT** samples were synthesized with different linear alkyl side chains to study the impact of the alkyl chain on the solubility and consequently the average molar mass (Figure 43). As the length of the alkyl side chain increased from four (**P3AT-R1**) to twelve carbons (**P3AT-R3**), the average molar mass has been increased from 6.3 Kg.mol<sup>-1</sup> to 22 Kg.mol<sup>-1</sup>. But polymer with eight carbons alkyl chain (**P3AT-R2**) shows higher average molar mass of 35 kg.mol<sup>-1</sup> due to higher degree of polymerization. The conjugated polymer with the higher average molar mass (**P3AT-R2**) exhibits average mobilities of 0.19 cm<sup>2</sup> V<sup>-1</sup> s<sup>-1</sup> that is almost double of **P3AT-R1** (0.10 cm<sup>2</sup> V<sup>-1</sup> s<sup>-1</sup>).<sup>111</sup>

<sup>107</sup> T. Lei, J-H. Dou, J. Pei, *Adv. Mater.*, **2012**, 24, 6457–6461

<sup>108</sup> J.R. Matthews, W. Niu, A. Tandia, A.L. Wallace, J. Hu, W-Y. Lee, G. Giri, S.C.B. Mannsfeld, Y. Xie, S. Cai, H.H. Fong, Z. Bao, M. He, *Chem. Mater.*, **2013**, 25, 782–789

<sup>109</sup> I. McCulloch, M. Heeney, C. Bailey, K. Genevicius, I. MacDonald, M. Shkunov, D. Sparrowe, S. Tierney, R. Wagner, W. Zhang, M.L. Chabinyc, R.J. Kline, M.D. McGehee, M.F. Toney, *Nat. Mater.*, **2006**, 5, 328–333.

<sup>110</sup> I. Osaka, R. Zhang, G. Sauvé, D.-M. Smilgies, T. Kowalewski, R. D. McCullough, *J. Am. Chem. Soc.*, **2009**, 131, 2521–2529.

<sup>111</sup> G. Sauvé, A. E. Javier, R. Zhang, J. Liu, S. A. Sydlík, T. Kowalewski, R. D. McCullough, *J. Mater. Chem.*, **2010**, 20, 3195–3201

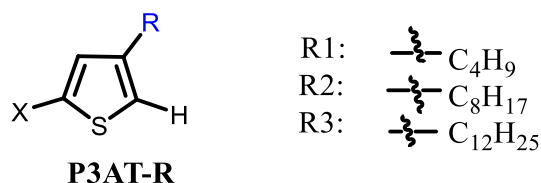


Figure 43: Structure of **P3AT-R** polymers

A family of five copolymers of terthiophene-*alt*-isoindigo with different alkyl chains **P[T3(R)-il]** have been synthesized (Figure 44), in order to study the influence of alkyl and branched alkyl side chains on solubility.

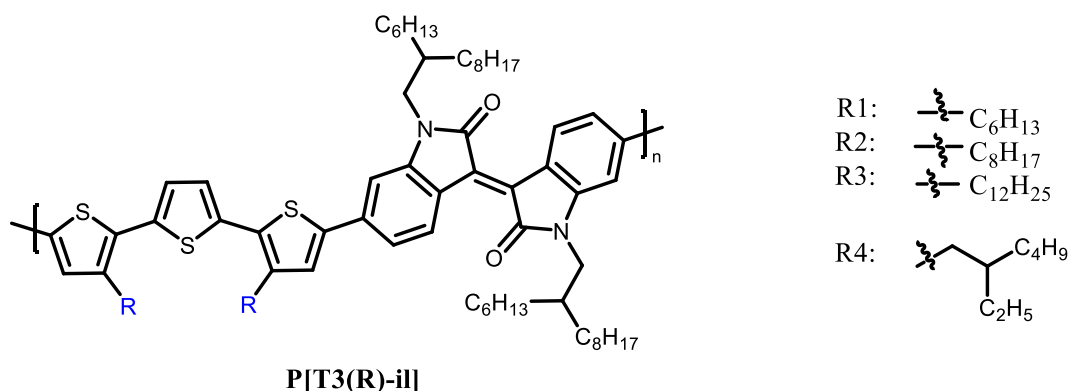


Figure 44: Structure of **P[T3(R)-il]** polymers

The solubility of these polymers was measured. It is found to be around 2 mg/mL for the conjugated polymer with R1 linear chain. Better solubility was observed when the length of the alkyl chain increased to 12 carbon (R3) with 21 mg/mL. But, replacing the linear alkyl chain with branched chain (R4) results in the best solubility of 27 mg/mL. Hence, the solubility can be tuned by changing the length and the branching of the alkyl side chain.<sup>112</sup>

Moreover, replacing linear alkyl chains by branched side chains does not only affect the solubility but also it can increase the  $\pi$ -stacking distance up to 0.5 Å and consequently reduces the hopping rate of the charge carrier along the packing direction.<sup>113</sup> However, a better crystallinity can be obtained when short branched chains are replaced with longer chains.

In the example of figure 45, the  $\pi$ -stacking distance of **CDT-BTZ**<sup>114</sup> with R1 is about 3.5Å, it increased to 4.0 Å with **R3** due to the steric hindrance.

<sup>112</sup> C. Grand, W. Zajackowski, N. Deb, C. K. Lo, J. L. Hernandez, D. G. Bucknall, K. Mü llen, W. Pisula, J. R. Reynolds, *ACS Appl. Mater. Interfaces*, **2017**, 9, 15, 13357–13368

<sup>113</sup> V. Coropceanu, J. Cornil, D. A. da Silva Filho, Y. Olivier, R. Silbey, J.-L. Brédas, *Chem. Rev.*, **2007**, 107, 926–952

<sup>114</sup> W. Pisula, H. Tsao, D. Dudenko, D. Cho, S. Puniredd, Y. Zhao, A. Mavrinskiy, J. Shu, M. Hansen, M. Baumgarten, K. Mullen, *Polymers*, **2013**, 5, 833

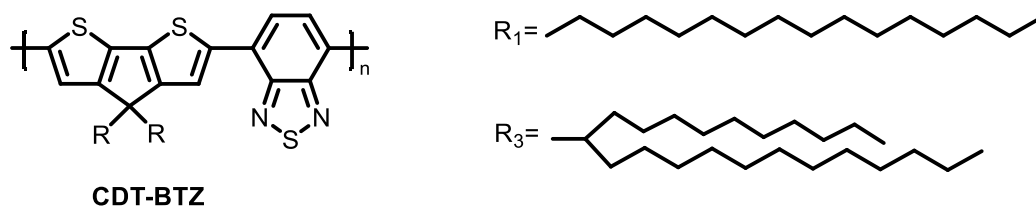


Figure 45: **CDT-BTZ** conjugated polymer with different type of alkyl side chains

To study the effect of the change of the length and the type of the chain not only on the  $\pi$ -stacking distance but also on the molecular orientation of the conjugated polymers, a series of polymers (Figure 46) have been synthesized with different alkyl side chains.

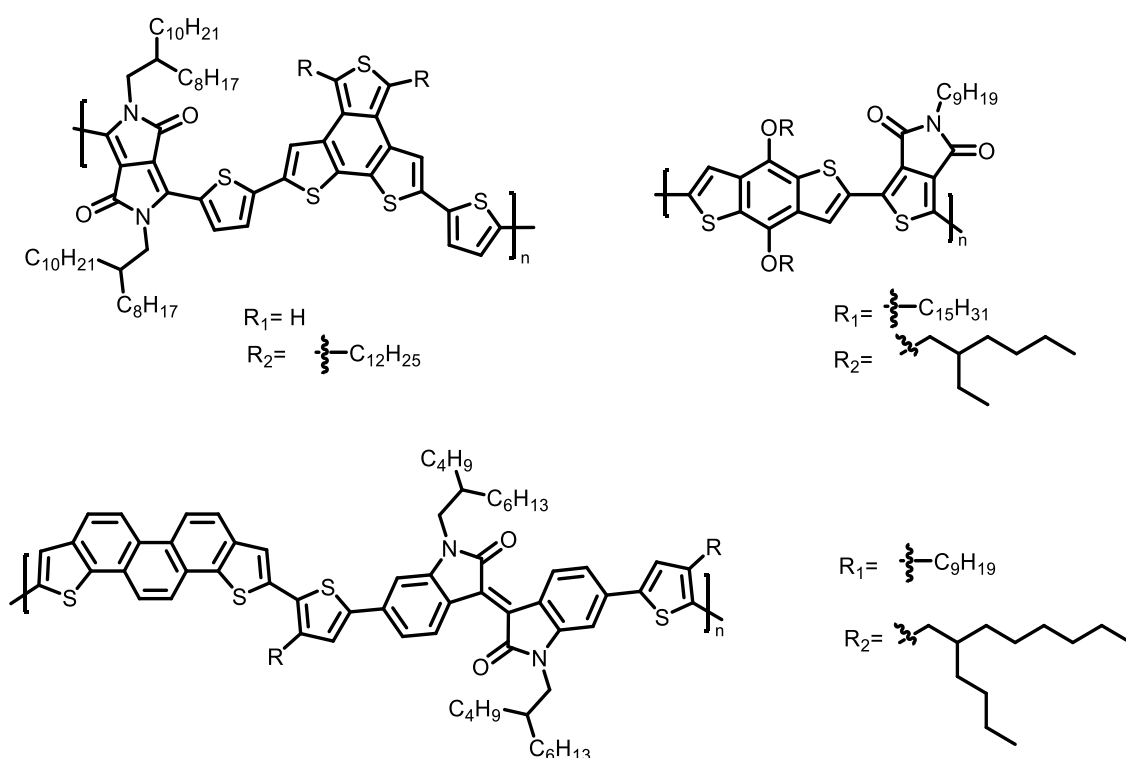


Figure 46: Chemical structures of **D-A** conjugated polymers with different alkyl side chains<sup>115,116,117</sup>

In the presence of branched alkyl side chains, the aggregation of single polymer chains is poor, so they are more flexible and capable to interact with the surface by non-covalent bond (Van der Waals interactions) and then the polymer chains are ordered in face-on orientation. While, the edge-on orientation with linear alkyl side chains can be explained by the strong aggregation of the conjugated polymer prior to the polymer/ surface interactions.

<sup>115</sup> X. Guo, S. R. Puniredd, M. Baumgarten, W. Pisula and K. Mullen, *Adv. Mater.*, **2013**, 25, 5467–5472.

<sup>116</sup> C. Cabanetos, A. El Labban, J. A. Bartelt, J. D. Douglas, W. R. Mateker, J. M. Frechet, M. D. McGehee, P. M. Beaujuge, *J. Am. Chem. Soc.*, **2013**, 135, 4656–4659.

<sup>117</sup> S. Nishinaga, H. Mori, Y. Nishihara, *Macromolecules*, **2015**, 48, 2875–2885



To overwhelm the disadvantage of branched alkyl side chain on the polymer packing and to keep the solubility, researchers are applying a new strategy to shift the branching point away from the polymer backbone with more than one carbon.

This concept was applied to **CDT-BTZ** conjugated polymers. Using 5-ethylnonyl side chain **R4**, it showed an improved supramolecular organization with respect to the conjugated polymer using 2-ethylhexyl side chain **R2**.<sup>118</sup>

The  $\pi$ -stacking decreases from 3.75 Å for two carbon spacers to 3.57 Å for four and five carbon spacers between the branching point and the conjugated polymer backbone.

The same chemical modifications were carried on **DPP** derivatives to study the impact of shifting the branched point and the effect of the chain length. Three DPP derivatives **PDQT**: using **R1** with two carbon spacer and C10 and C8 chains, **R2**: two carbon spacers with C10 and C12 chains and **R3** with four carbon spacer and C10 and C12 chains. **PDQT-1** and **PDQT-2** display similar crystallinity while using longer size chains showed much better mobility 3.37  $\text{cm}^2\text{V}^{-1}\text{s}^{-1}$  instead of 2.10  $\text{cm}^2\text{V}^{-1}\text{s}^{-1}$  in **PDQT-1**. The  $\pi$ -stacking slightly increased from 3.79 Å to 3.86 Å but with no benefit on the mobility. Therefore, the better performance was explained by smoother surface morphology and better interconnected networks and then efficient charge transport. Using longer side chain with shifting the branching point **PDQT-R3** showed a further increase in mobility up to 6.9  $\text{cm}^2\text{V}^{-1}\text{s}^{-1}$  with lower crystallinity but much shorter  $\pi$ -stacking distance (3.68 Å) which is the reason behind the high mobility (Figure 47).<sup>119</sup>

Therefore, shifting the branching point in the alkyl side chain reduces the crystallinity but can induce shorter  $\pi$ -stacking distance and planarity.

---

<sup>118</sup> J. Lee, T. Marszalek, K. C. Lee, J. Kim, W. Pisula, C. Yang, *Macromol. Chem. Phys.*, **2015**, 216, 1244–1250

<sup>119</sup> S. Chen, B. Sun, W. Hong, H. Aziz, Y. Meng and Y. Li, *J. Mater. Chem. C*, **2014**, 2, 2183

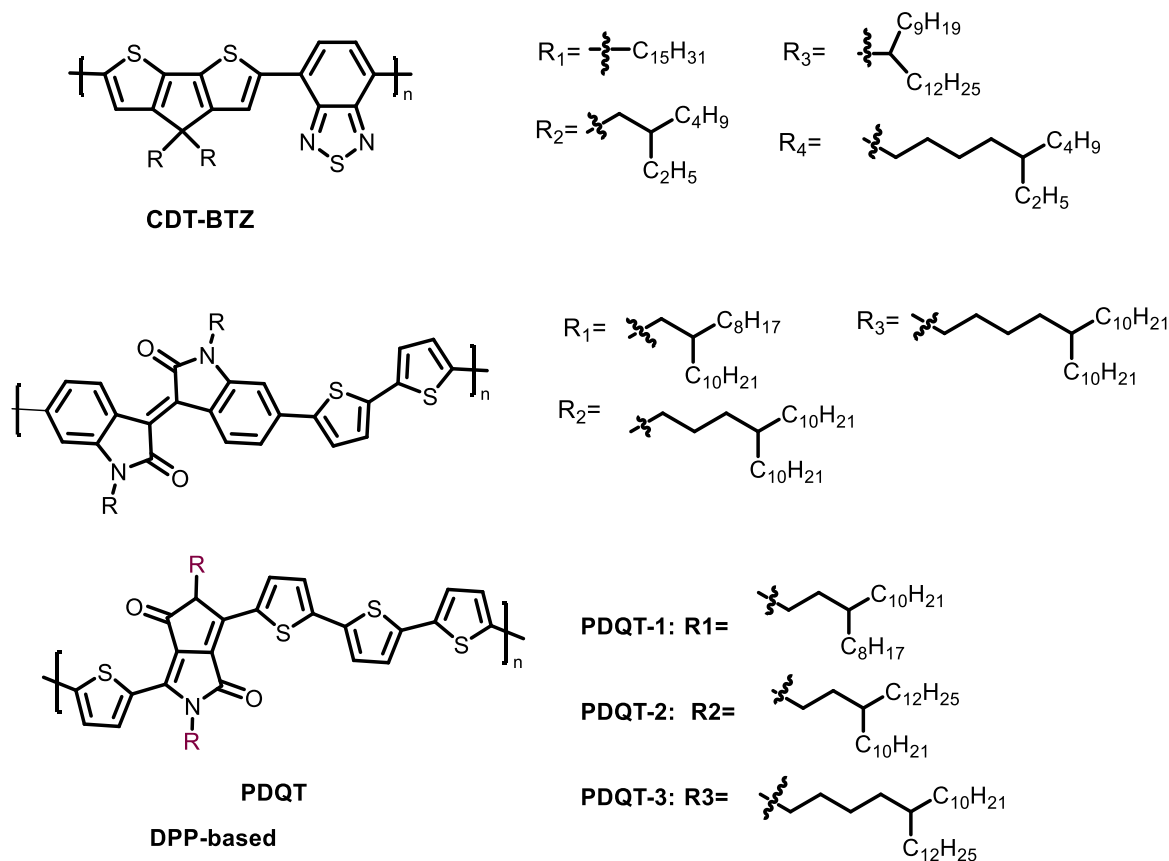


Figure 47: Some conjugated polymers functionalized with alkyl side chains

Similarly, the branching position effect was investigated by introducing a range of branched alkyl side chains with different carbon spacer length from one up to four carbons into the N-position of Quinacridone (QA) copolymerized with unsubstituted bithiophene unit (**PQA2T-R**) represented in figure 48.

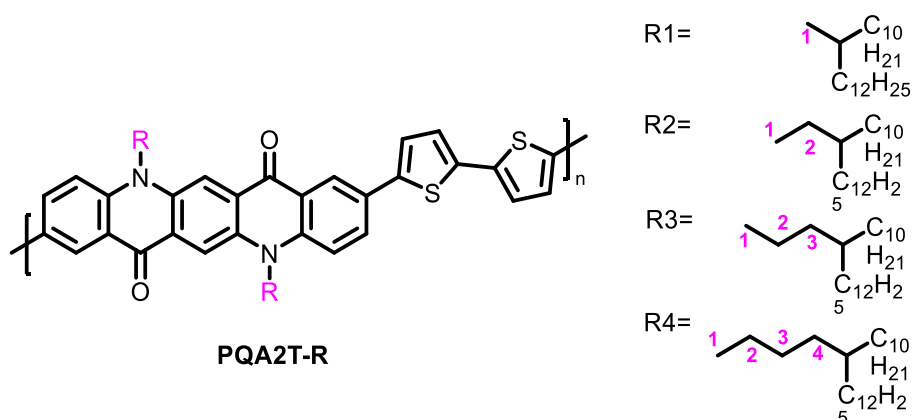


Figure 48: **PQA2T** chemical structure functionalized with different branched alkyl chain with different spacer length

The increase in the carbon spacer length leads to a slight decrease in the solubility of the conjugated polymers synthesized, which decreases the average  $M_w$  from 13 kDa to 9 kDa. However, it also results in a red shift absorption and consequently smaller band gap, which means better intermolecular interaction or better ordering in the solid state. The increased intermolecular interactions are explained by a decrease in  $\pi$ - $\pi$  stacking that could be due to the reduced steric hindrance. These polymers were studied with atomic force microscopy, which suggested the polymers formed lamellar structures with edge-on orientation.<sup>120</sup>

Other than the type of alkyl side chain and the branching point position, the position of the attached side chain “substituent position” has a huge impact on the charge carrier mobility.

Thieno[3,4-c]pyrrole-4,6-dione (TPD) based copolymers with thiophene and bithiophene as donor units were investigated. **PTPD-1** and **PTPD-3** showed better intermolecular interactions. **PTPD-3** displayed one of the highest reported mobility. The big difference in carrier mobility was not related to average molar mass, where **PTPD-1** owes the largest average molar mass and both polymers are with same type of alkyl chain. Therefore, it is more linked to the position of the alkyl side chain (Figure 49).<sup>121</sup>

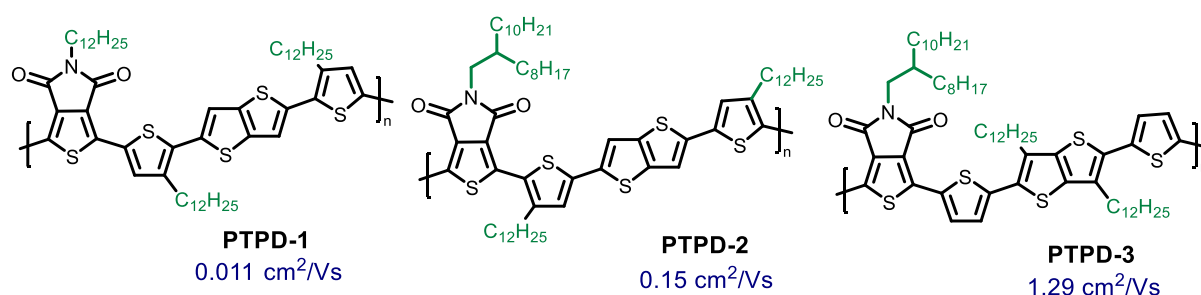


Figure 49: Conjugated polymers with different functionalization position with their charge mobility

### 3.1.2. Oligoether side chains:

Recently, water-soluble conjugated polymers have attained exceptional interest for high sensitivity bio and chemo sensor applications. To increase the water solubility of conjugated polymers oligoether side chains are beneficial due to their hydrophilicity, their potential to offer solubility in polar solvents with no need of ionic groups as well as their propensity to complex with metal ions if it is required.

Regioregular poly(3-hexylthiophene) is a conjugated polymer with a high mobility and a good chemical stability, therefore, several groups worked to synthesize water-soluble polythiophene derivatives, but most of these polymers were with charged ionic groups. To

<sup>120</sup> K. Kawabata, M. Saito, N. Takemura, I. Osaka, K. Takimiya., *Polymer Journal*, **2017**, 49, 169–176

<sup>121</sup> Q. Wu, M. Wang, X. Qiao, Y. Xiong, Y. Huang, X. Gao, H. Li, *Macromolecules*, **2013**, 46, 3887–3894

overcome this ionic character, hydrophilic  $-(2-(2-(2\text{-methoxyethoxy})\text{ethoxy})\text{ethoxy})\text{methyl}$  side chain has been used. This type of chains allows the formation of a conjugated polymer with well-defined ordered crystalline structure by self-assembly through strong  $\pi\text{-}\pi$  intermolecular interaction of backbones.<sup>122</sup> Other examples of using oligoether side chains are copolymer based on **DPP** synthesized by Patil and co-workers<sup>123</sup> and polymers based on bithiophene-thienothiophene backbone, poly(2-(3,3-bis(2-(2-(2-methoxyethoxy)ethoxy)ethoxy)-[2,20-bithiophen]-5-yl)thieno[3,2-b]thiophene)s **P(g2T-TT)** with propylene glycol (Figure 50).<sup>124</sup>

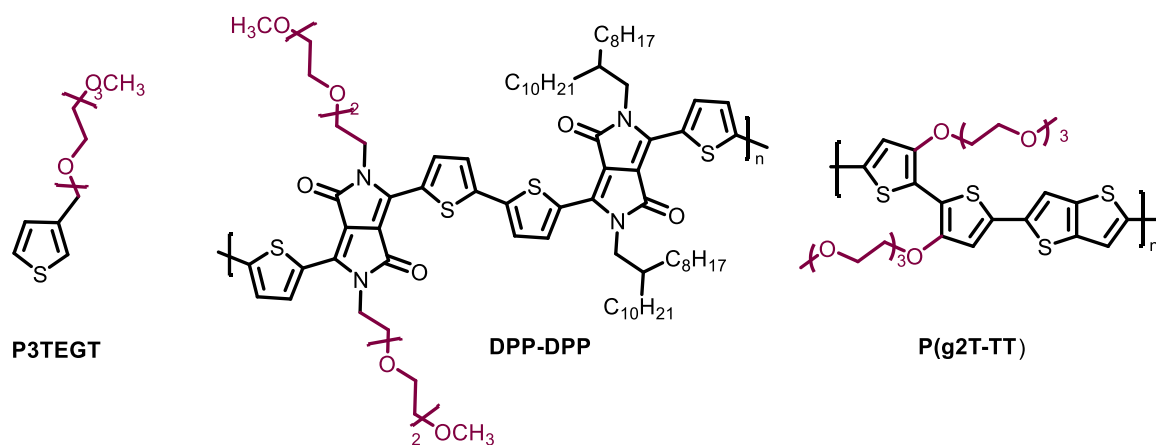


Figure 50: Conjugated polymers with oligoether side chain

Indeed, oligoether side chains not only improve the solubility of conjugated polymers in water but also in polar aprotic solvents due to the presence of ether and flexible alkyl chain.<sup>125</sup> Hence, they are interesting to be applied to increase the solubility of conjugated polymers.

### 3.2. To enhance the $\pi\text{-}\pi$ aggregation and chain orientation:

The properties of conjugated polymers in devices such as solar cells are strongly affected by their morphology and self-organization ability. The type of side chain such as alkyl or alkoxy chains and their position strongly impacts the molecular orientation of the conjugated polymer.<sup>126</sup> However, self-organization is more linked to the use of fluoroalkyl side chains. Semi-fluoroalkyl side chains are famous type of side chains for inducing rigid backbone and molecular organization. The insertion of these side chains in conjugated polymers results

<sup>122</sup> M. Shao, Y. He, K. Hong, C.M. Rouleau, D.B. Geohegan, K. Xiao, *Polym. Chem.*, **2013**, 4, 5270–5274.

<sup>123</sup> H. Yan, Z. Chen, Y. Zheng, C. Newman, J.R. Quinn, F. Dotz, M. Kastler, A. Facchetti, *Nature*, **2009**, 457, 679–686

<sup>124</sup> M. Moser, Y. Wang, T. C. Hidalgo, H. Liao, Y. Yu, J. Chen, J. Duan, F. Moruzzi, S. Griggs, A. Marks, N. Gasparini, A. Wadsworth, S. Inal, I. McCulloch, W. Yue, *Mater. Horiz.*, **2022**, 9, 973–980

<sup>125</sup> S. Mehdipour-Ataei, F. Zigeimat, *European Polymer Journal*, **2007**, 43, 1020–1026

<sup>126</sup> S. Bölke, D. Batchelor, A. Früh, B. Lassalle-Kaiser, T. Keller, F. Trilling, M. Forster, U. Scherf, T. Chassé, H. Peisert, *ACS Appl. Energy Mater.*, **2022**, 5, 12, 15290–15301

in polymers exhibiting high electron mobility values of up to  $6.50 \text{ cm}^2 \text{ V}^{-1} \text{ s}^{-1}$  for **PNDIF-TVT** that is naphthalene diimide (**NDI**) unit alternated with bithiophene **T2** donating unit (Figure 51).<sup>127</sup>

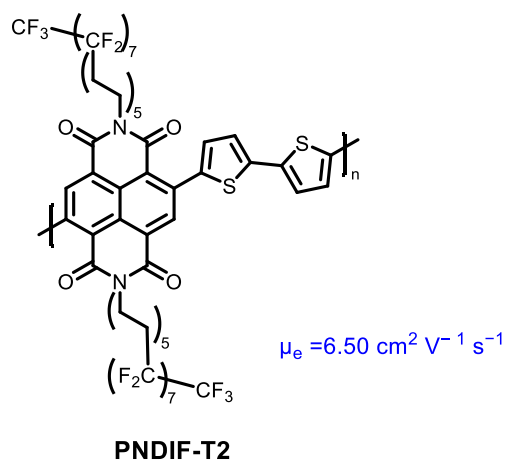


Figure 51: Structure of **PNDIF-TVT** conjugated polymer

Not only self-organization but also small  $\pi$ - $\pi$  spacing is preferred in conjugated polymers. Small  $\pi$ - $\pi$  spacing reduces the energy barrier for interchain charge hopping, which is a crucial charge transport mechanism in conjugated polymers. Organization of  $\pi$ - $\pi$  stacking is essential to increase the aggregation. The increase in aggregation leads to enhanced solid-state order and better field effect mobility. Polymers aggregation is a strategy used to favor crystallinity and then better performance for applications as organic photovoltaic and OFETs.<sup>128</sup>

The structure of the side chains controls the aggregation in the synthesized polymer through the interchain interactions of semiconducting polymers.<sup>129</sup> Another factor that can enhance the aggregation is the planarity of the polymer.

Polaron propagation that has been previously described is related to the chain orientation of the conjugated polymer. For better understanding, two types of packing can occur when a conjugated polymer is applied on a surface: lamellae face-to-face packing model (face on orientation), in this type the aromatic plane of the backbone lies flat on the surface of the substrate and the  $\pi$ -stacking is perpendicular to the substrate. The second type is along  $\pi$ - $\pi$  stacking direction (edge on orientation), the  $\pi$ -stacking is oriented parallel to the substrate and in the same plane of the charge transport (Figure 52).<sup>130</sup>

<sup>127</sup> B. Kang, R. Kim, S. B. Lee, S-K. Kwon, Y-H. Kim, K. Cho, *J. Am. Chem. Soc.*, **2016**, 138, 11, 3679–3686

<sup>128</sup> M. S. Chen, O. P. Lee, J. R. Niskala, A. T. Yiu, C. J. Tassone, K. Schmidt, P. M. Beaujuge, S. S. Onishi, M. F. Toney, A. Zettl, J. M. J. Fréchet, *J. Am. Chem. Soc.*, **2013**, 135, 19229–19236

<sup>129</sup> B. McDearmon, E. Lim, I-H. Lee, L. M. Kozycz, K. O'Hara, P. I. Robledo, N. R. Venkatesan, M. L. Chabiny, C. J. Hawker, *Macromolecules*, **2018**, 51, 7, 2580–2590

<sup>130</sup> C. Mattheus, G. A. de Wijs, R. A. de Groot, T. T. M. Palstra, *J. Am. Chem. Soc.*, **2003**, 125, 6323–6330.

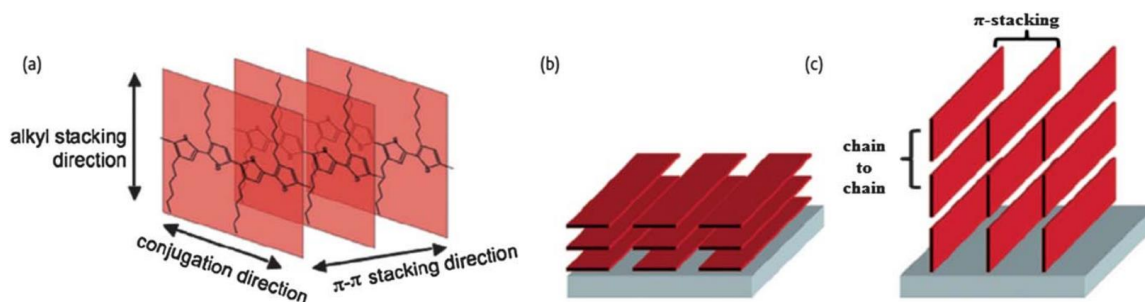


Figure 52: (a) Schematic presentation of charge transport model in lamellae stacking conjugated polymers; (b) face-on orientation; (c) edge-on orientation<sup>131</sup>

The face-on arrangement was showed to be promoted by the utilization of branched alkyl side chains due to the bulky and steric hindered chains. Edge-on orientation is obtained by the utilization of linear alkyl chain in some D-A conjugated polymers based on diketopyrroloopyrrole, thienopyrroledione and phenanthrodithiophene.<sup>132</sup>

The two kinds of crystalline structure are applicable to different device configurations according to the direction of the charge carrier transport. As an example, in field effect transistors, the molecules are preferred to be with edge-on orientation for better device performance because of the efficient two-dimensional charge transport along the conjugated system and the  $\pi$ - $\pi$  stacking.<sup>133</sup> However, polymers with well-ordered face-on orientation are the best for organic solar cells.<sup>134</sup> Then controlling the molecular ordering is essential for achieving high charge carrier transport. A series of **DPP** quaterthiophene polymer **PDQTs** have been investigated with three different side chain modifications (Figure 47). The use of branched alkyl side chains with the **DPP** backbone results in edge-on orientation in the three polymers.<sup>135</sup>

The chemical morphology is with tight relation to the molecular orientation of the conjugated polymer. Researchers have found some common properties and functionalization strategies to favor the formation of the desired orientation of molecules of the conjugated polymers according to the fabricated device system.

### 3.3. To increase Stability:

Fluoroalkyl side chains are characterized by their unique characteristics, such as hydrophobicity, thermal stability, chemical and oxidative resistance and self-organization

<sup>131</sup> A. Salleo, *Mater. Today*, **2007**, 10, 38–45

<sup>132</sup> S. Nishinaga, H. Mori, Y. Nishihara, *Macromolecules*, **2015**, 48, 2875–2885

<sup>133</sup> R. J. Kline, M. D. McGehee, M. F. Toney, *Nat. Mater.*, **2006**, 5, 222–228

<sup>134</sup> I. Osaka, M. Saito, T. Koganezawa, K. Takimiya, *Adv. Mater.*, **2014**, 26, 331–338

<sup>135</sup> S. Chen, B. Sun, W. Hong, H. Aziz, Y. Meng, Y. Li, *J. Mater. Chem. C*, **2014**, 2, 2183–2190

ability, which make them good candidates as side chains for increasing the stability of conjugated polymers.

Synthesis of conjugated polymers such as polythiophene with electron-withdrawing substituents is still limited due to their high oxidation potential of monomers, their substituents reactivity and the steric hindrance among substituents which disrupts the conjugation within the system. A type of side chains that has recently attracted the researcher's attention is the fluoroalkyl side chain due to their amphiphilicity that can have an impact on the thermochromism, liquid crystallinity and solid-state assembly with short alkyl spacer to serve a separation of the conjugated polymer backbone from the electron-withdrawing substituents.

Perfluoroalkyl side chains with direct attachment to the polymer backbone supply the electronic structure of the  $\pi$ -system, but they're still limited to doping procedures for thermoelectric applications. Fluoroalkyl side chains form a helical low energy conformation.<sup>136</sup>

With fluoroalkyl side chains, both backbone and side chain are hydrophobic and they are of sufficient difference in size to cause twisting of the conjugated backbone, taking into consideration that the van der Waals radius of fluorine is 1.35 Å that is higher by 12.5% that of hydrogen atoms (1.20 Å). Hence, number of conjugated polymers have been developed with semi fluoroalkyl groups with unique properties such as rigidity, thermal stability, chemical and oxidative resistance, and self-organization of the chains due to their hydrophobicity (Figure 53).

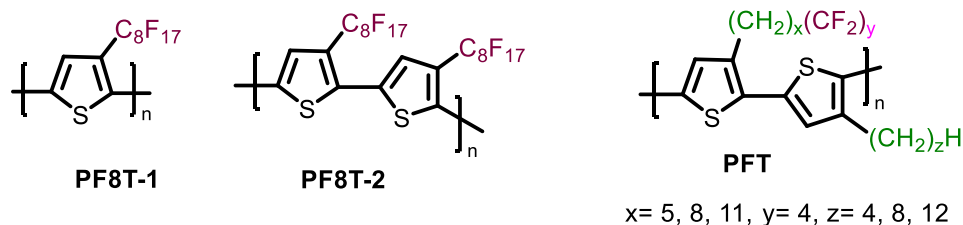


Figure 53: Conjugated polymers with fluorinated side chains

Series of poly(3-alkylthiophene), **PFT** have been prepared by Collard and co-workers with the general structure depicted in figure 47 to investigate the self-assembly and charge transport properties.<sup>137</sup>

Introducing fluoroalkyl side chains to the donor-acceptor system permits the synthesis of high electron mobility and air-stable semiconducting conjugate polymers. Naphthalene (**NDI**) acceptor functionalized with semi fluoroalkyl chain  $(\text{CH}_2)_{10}(\text{CF}_2)_7\text{CF}_3$  by Kilwon Cho et al

<sup>136</sup> M. Collard, *Adv.Mater.*, **2004**, 16, No.2, january 16

<sup>137</sup> B. Wang, S. Watt, M. Hong, B. Domercq, R. Sun, B. Kippelen, D.M. Collard, *Macromolecules*, **2008**, 41, 5156–5165.

was coupled into two types of donor units: bithiophene (**T2**) or thienylene-vinylene-thienylene(**TVT**) to form **PNDIF-T2** and **PNDIF-TVT**, respectively (Figure 54).

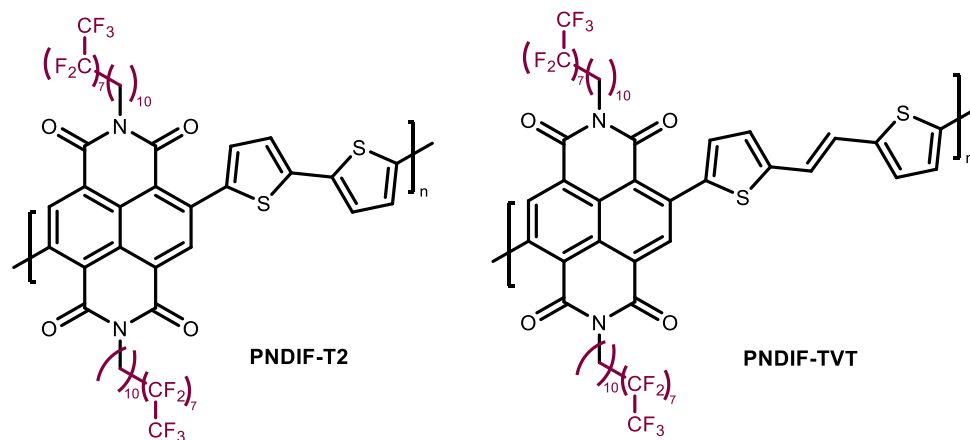


Figure 54: Conjugated polymers with fluoroalkyl side chains

These two polymers exhibit good solubility in common solvents due to the flexibility of the semi fluoroalkyl side chain with average molar masses of 28 and 33 KDa. The band gaps were found to be 1.61 eV and 1.39 eV for **PNDIF-T2** and **PNDIF-TVT**, respectively. This difference comes from the HOMO level of **PNDIF-TVT** (-5.38eV) that is higher than that of **PNDIF-T2** (-5.62 eV) due to the extended  $\pi$ -conjugation. Moreover, the presence of fluorine provokes low LUMO level of both polymers around -4.0 eV. And it was proved that this type of chains enhances the thermal stability, which might be a consequence of the strong organizational properties of semi fluorinated alkyl chains.<sup>127</sup> In particular, the introduction of this side chain results in high electron mobility of  $6.50 \text{ cm}^2 \text{ V}^{-1} \text{ s}^{-1}$  for **PNDIF-T2**.

Side chain engineering is a promising method to apply via chemical modification strategies on the conjugated polymer at the stage of monomer synthesis. It is widely applied in organic synthesis of conjugated polymers for enhanced physical properties through controlling chemical morphology.



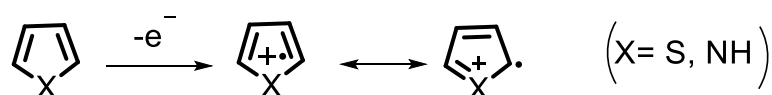
### III. Synthesis of conjugated polymers:

The three main methodologies that have been developed to synthesize  $\pi$ -conjugated polymers are: oxidative polymerization, organometallic coupling reactions, and synthesis of conjugated polymers with a metal center.

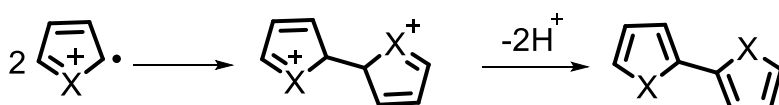
#### 1. Oxidative polymerization:

Chemical oxidative polymerization COP is a well-known method from aromatic compounds like aniline, pyrrole, phenols, thiophenols, diphenylsulfide and thiophene. The oxidation of the monomer is performed using an inorganic or organic oxidizing agent or by applying a potential (electrochemical oxidative polymerization). In this type of polymerization, cation or cation radical sites are formed in the conjugated molecule (monomer or polymer), in order to do the initiation step.<sup>138</sup> The next step is the formation of dimer, followed by oxidation, coupling and rearomatization and then the chain propagation (Figure 55).

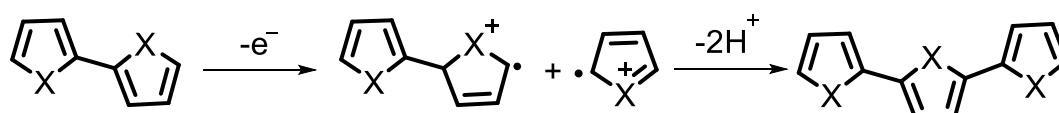
##### 1- Oxidation:



##### 2- Formation of dimer:



##### 3- Oxidation, coupling and rearomatization:



##### 4- Chain propagation:

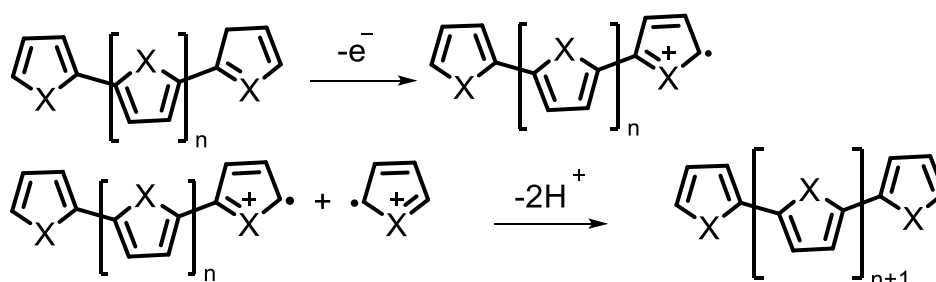


Figure 55: The mechanism of oxidative polymerization for thiophene and pyrrole based conjugated polymers

<sup>138</sup> N.Y. Abu-Thabit, *J. Chem. Educ.*, **2016**, 93, 1606–1611

However, this type of polymerization lacks selectivity and results in a decrease of the efficiency of the obtained polymer. Therefore, looking for other methods is required such as organometallic coupling reactions.

## 2. Organometallic coupling reactions:

Organometallic coupling reactions allow the formation of C-C bonds between aromatic units. It is a powerful tool to synthesize a wide range of macromolecules and conjugated polymers. Different types of coupling reaction have been developed. They are performed in the presence of a catalyst (organometallic compound) in three main steps: oxidative addition, transmetallation and reductive elimination. The oxidative addition is between the organometallic catalyst (zero oxidation state) and a halogen derivative R-X such as iodine and bromine. After the transmetallation, which is the metal exchange step to have an R group instead of the halogen. For the reductive elimination, it allows the formation of the desired C-C bond for the final compound R-R' (Figure 56).

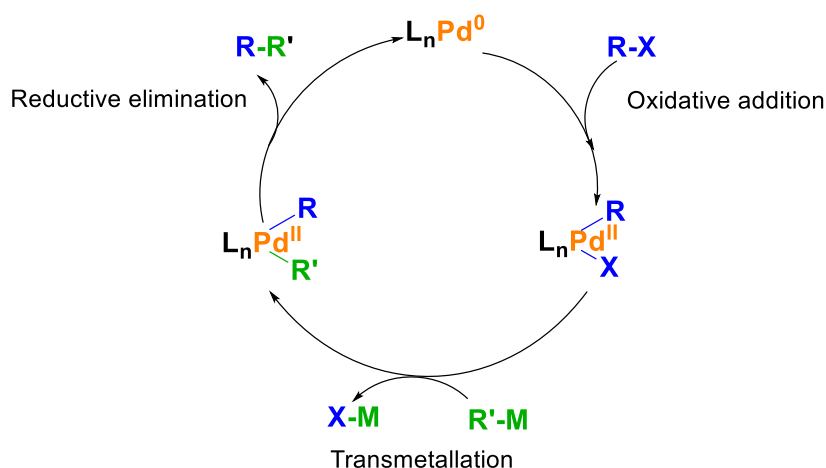


Figure 56: General mechanism of organometallic coupling reactions

According to the type of the catalyst used and the halogen atom, we can classify different types of coupling reactions.

### 2.1. Suzuki Coupling:

It is an organic reaction in the presence of palladium (0) complex as a catalyst and the boronic acid as organohalide partner. This reaction requires the presence of a base, the most common base is alkoxide ( $OR^-$ ) to substitute the halogen with the nucleophile ( $R-Pd-Nu$ ) at the stage of oxidative addition and to form the borate intermediate ( $R'-BY_2-Nu$ ) to accelerate the reductive elimination (Figure 57).

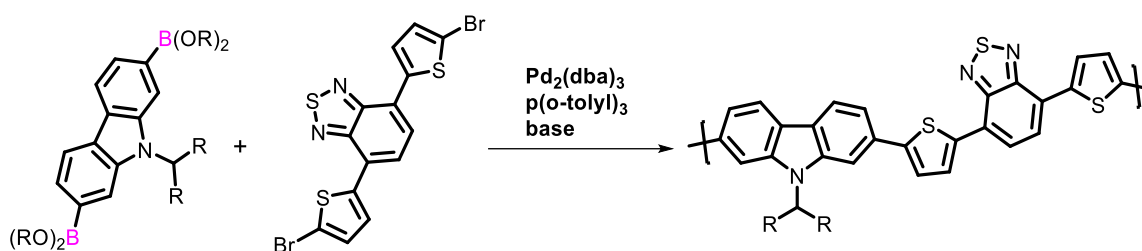


Figure 57: Typical polymerization reaction for D-A polymerization using Suzuki coupling<sup>139</sup>

## 2.2. Stille coupling:

It is a coupling in the presence of palladium (0) catalyst and organohalide, triflate or carbonylchloride. The organic groups are aryl, heterocyclic or vinyl and the metal included in the transmetalation step is tin (stannic reagent). Knowing that the reaction shows tolerance to many functional groups like amines, aldehydes, esters, ethers and nitrogen groups, and usually the reaction yield is high.<sup>140</sup> However, tin derivatives are toxic. Photoactive benzothiophene **BDT** D-A based conjugated polymer is an example on Stille coupling polymerization (Figure 58).<sup>141</sup>

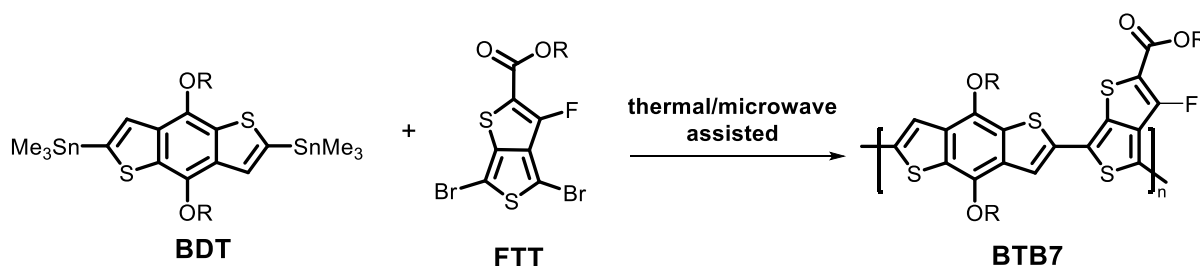


Figure 58: Polymerization example with Stille coupling

## 2.3. Sonogashira coupling:

Homogenous Pd catalysts such as  $\text{Pd}(\text{PPh}_3)_2\text{Cl}_2$ ,  $\text{Pd}(\text{PPh}_3)_4$  and their derivatives are also used for this kind of coupling reactions in the presence of CuI and inert atmosphere. It was developed by Sonogashira et al in 1975 between vinyl or aryl halides and terminal alkyne.<sup>142</sup> The synthesis of poly(porphyrindithianothiophene) is an example where porphyrine unit is the electron deficient unit and dithianothiophene is the electron rich unit were polymerized in the

<sup>139</sup> P. Morin, T. Bura, M. Leclerc, *Mater. Horiz.*, **2016**, 3, 11-20

<sup>140</sup> Z. Bao, W. K. Chan, L. Yu, *J. Am. Chem. Soc.*, **1995**, 117, 50, 12426–12435

<sup>141</sup> M. Atzori, F. Artizzu, E. Sessini, L. Marchiò, D. Loche, A. Serpe, P. Deplano, G. Concas, F. Pop, N. Avarvari, M. Laura Mercuri†, *J. Name.*, **2013**, 00, 1-3

<sup>142</sup> M. Nasrollahzadeh, N. Motahharifar, F. Ghorbannezhad, N. S. S. Bidgoli, T. Baran, R. S. Varma, *Molecular Catalysis*, 480 (2020) 110645

presence of Pd(0), CuI, triethylamine as a base and toluene as solvent under inert and dry atmosphere (Figure 59).<sup>143</sup>

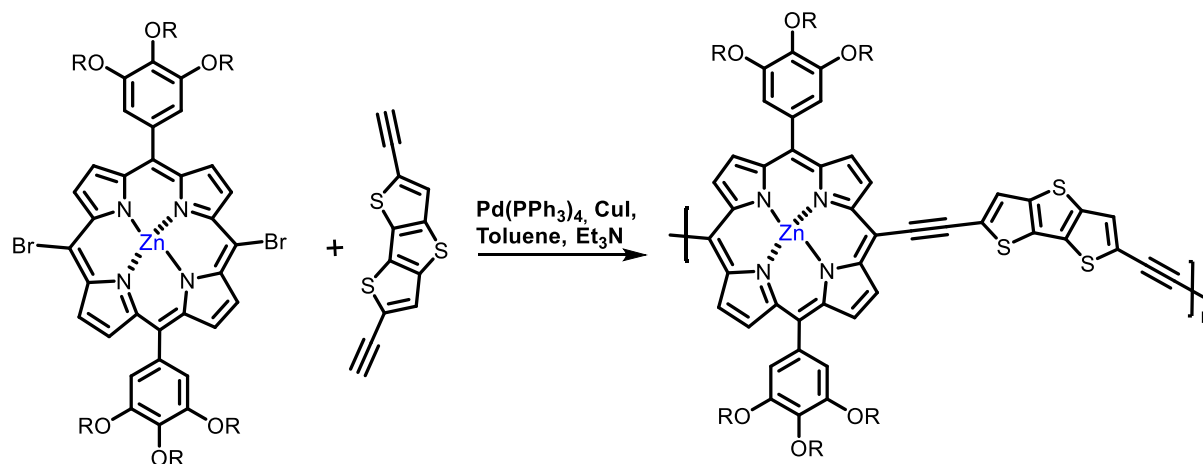


Figure 59: Polymerization via Sonogashira coupling reactions

#### 2.4. Heck coupling:

It's a palladium catalyzed coupling between aryl or vinyl halides and activated alkenes in the presence of a base. From the mechanistic side, this reaction starts with oxidative addition then, insertion step followed by beta H-elimination instead of transmetalation and reductive elimination to obtain the desired molecule (Figure 60).

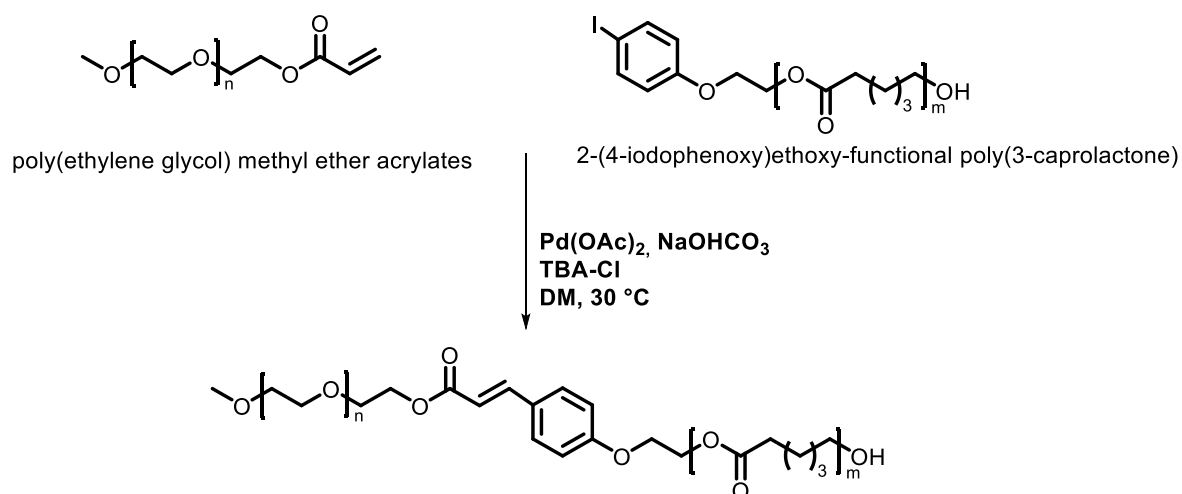


Figure 60: Heck coupling for polymer-polymer conjugation method<sup>144</sup>(TBA: tetrabutylammonium chloride)

<sup>143</sup> X. Huang, C. Zhu, S. Zhang, W. Li, Y. Guo, X. Zhan, Y. Liu, Z. Bo, *Macromolecules*, **2008**, 41, 19, 6895–6902

<sup>144</sup> M. Winkler, L. M. de Espinosa, C. Barner-Kowollik, M. A. R. Meier, *Chem. Sci.*, **2012**, 3, 2607–2615

## 2.5. Negishi and Kumada couplings:

These reactions couple organic halides or triflates and organozinc compounds for C-C bond formation. In general, palladium (0) is used but also a variety of Ni(0) and Ni(II) can be integrated in Negishi cross coupling. What is important in these reactions in the presence of deactivated alkyl electrophiles, transmetalation could occur before the oxidative addition, alkyl zinc would first transmetalate with the nickel catalyst where nickel takes the halide from the alkyl halide to form an alkyl radical and result in the oxidation of the catalyst. The reductive elimination from Ni(II) or Ni(III) if the used catalyst was Ni(I) (Figure 61).

Kumada coupling is similar to that of Negishi by the reaction of Grignard reagent instead of alkyl zinc and an organic halide. It is about four steps, oxidative addition, transmetalation, trans-cis isomerization and then the reductive elimination (Figure 61).

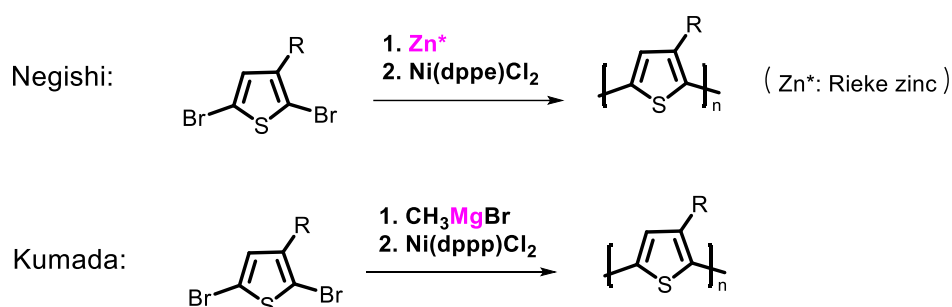


Figure 61: Negishi and Kumada coupling for the synthesis of poly(3-alkylthiophene)s<sup>139</sup>

## 2.6. Direct heteroarylation polymerization:

Direct heteroarylation (DHAP) is a recent method for organic conjugated polymer synthesis with less waste and using simpler monomers<sup>145</sup>. It was investigated by Lemaire group for poly(alkylthiophene) synthesis.<sup>146</sup> DHAP is a metal-catalyzed coupling reaction between an arene and an aryl halide (Figure 62). The main advantage of this polymerization is that it can be performed on easily accessible monomers (arenes and arylhalides). It is performed using catalysts based on rhodium or palladium.<sup>147</sup> DHAP allows the synthesis of polymers hardly obtained via the traditional coupling (Figure 62).

<sup>145</sup> L. G. Mercier and M. Leclerc, *Acc. Chem. Res.*, **2013**, 46, 1597–1605.

<sup>146</sup> M. Sévignon, J. Papillon, E. Schulz, M. Lemaire, *Tetrahedron Lett.*, **1999**, 40, 5873–5876.

<sup>147</sup> B. Biswas, M. Sugimoto, S. Sakaki, *Organometallics*, **2000**, 19, 3895–3908.

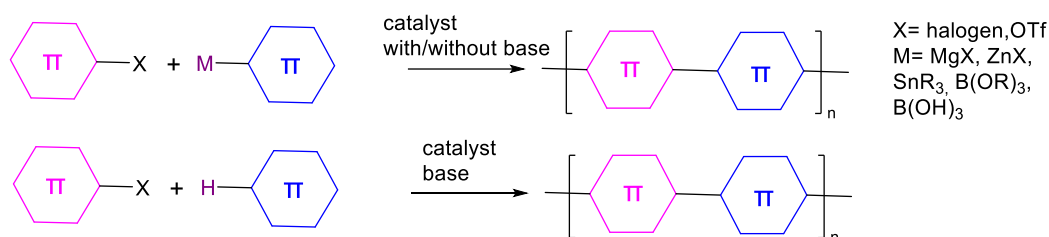


Figure 62: General reaction scheme of DHAP polymerization compared to classical coupling reactions

In this type of reaction, the precatalyst used and its amount play an important role in the polymerization in obtaining high molecular weight materials and an excess of this reagent leads to high reactivity (Figure 63).

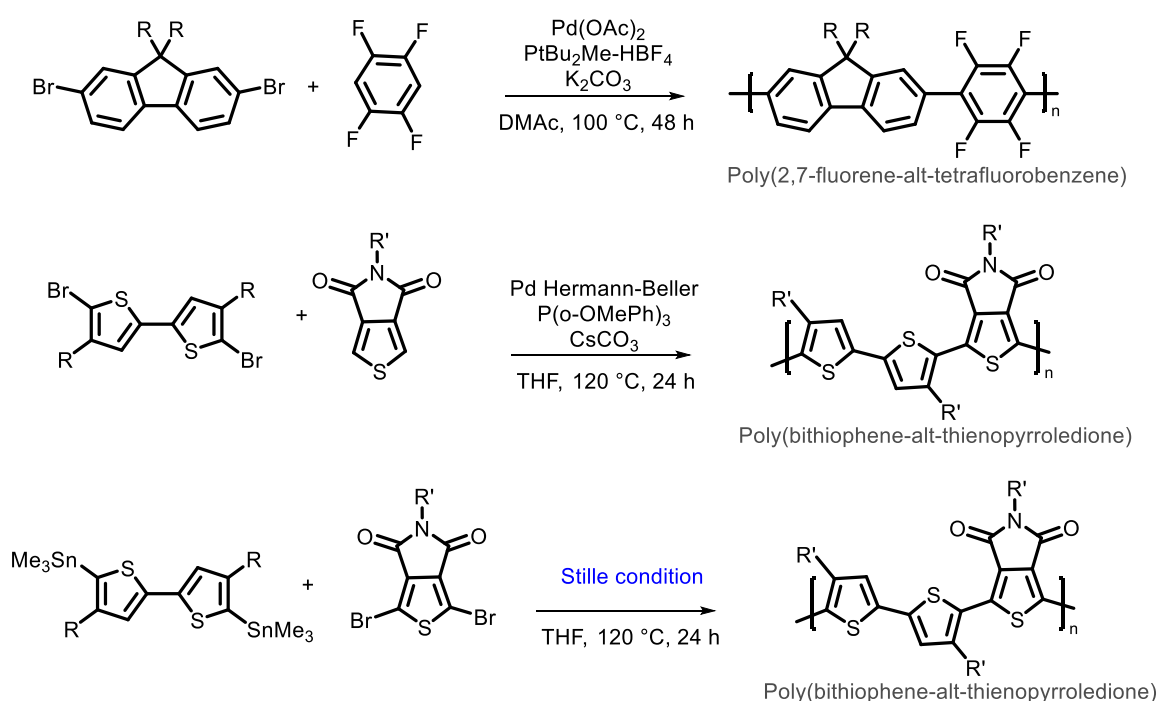


Figure 63: Polymers obtained by DHAP in the literature<sup>148,149,150</sup>

These methodologies using organometallic reactions have advantages in the synthesis of conjugated oligomers and polymers. They allow building regio- and stereo-regular conjugated polymers with a wide variety of functional groups and in general they require mild conditions. The available options appear enough with the increasing demand for structures with optical and electrical properties.<sup>151</sup>

<sup>148</sup> W. Lu, J. Kuwabara and T. Kanbara, *Macromolecules*, **2011**, 44, 1252–1255

<sup>149</sup> P. Berrouard, A. Najari, A. Pron, D. Gendron, P.-O. Morin, J.-R. Pouliot, J. Veilleux, M. Leclerc, *Angew. Chem., Int. Ed.*, **2012**, 51, 2068–2071.

<sup>150</sup> F. Grenier, K. Goudreau, M. Leclerc, *J. Am. Chem. Soc.*, **2017**, 139, 2816.

<sup>151</sup> F. Babudri, G. M. Farinola, F. Naso, *J. Mater. Chem.*, **2004**, 14, 11–34

### 3. Synthesis of polymers with a metal center:

The utilization of semiconductor conjugated polymers has spread in a various area and recently thanks to the transition metals that could form complexes with the monomer units. These polymers which contain metal atoms in their backbone are named as metallopolymer.

The incorporation of a transition metal element is an attractive platform to combine the electronic, optical, magnetic and chemical properties of those complexes with the organic conjugated polymers. This transition metal insertion to the  $\pi$ -conjugated system allow the tunability of the physical properties of the resulted materials through a strong interaction between the metal and the organic component to provoke a distinctive photophysical, electrochemical and photochemical properties.

The introduction of a metallocene unit into the conjugated chain may affect a range of properties as redox, magnetic, optical, and electronic properties, where alkynyl ligand can bridge multiple metal center. These polymers prepared by the interaction of alkaline metal or alkaline earth metal alkynyl complex with transition metal halide MX (M=Pt, Pd or Ni as transition metal and X= Cl, Br, I) using copper-catalyzed dehydrohalogenation, oxidative coupling and Alkynyl ligand exchange.<sup>152</sup>

#### 3.1. Copper catalyzed dehydrohalogenation:

In this type of polymerization, the cupreous halide plays the role of a catalyst between diterminal alkynes and transition metal halides (Figure 64).<sup>153</sup>

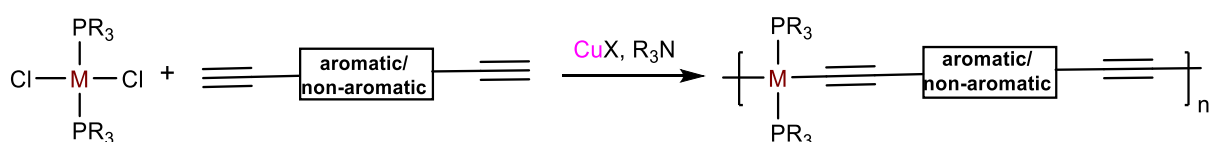


Figure 64: Copper catalyzed dehydrohalogenation

For preparation of oligomers and polymers using this method, the number of equivalents must be not in much excess to avoid the formation of small compounds. Therefore, there is stoichiometric restriction on reactant. However, this type of polymerization proceeds smoothly at room temperature and under reflux.

<sup>152</sup> N.J. Long, C.K. Williams, *Angew. Chem. Int. Ed.*, **2003**, 42, 2586-2617

<sup>153</sup> K. Sonogashira, S. Kataoka, S. Takahashi, N. Hagihara, *J. Organomet. Chem.*, **1978**, 160, 319.

### 3.3. Oxidative coupling:

In this reaction, a catalytic amount of a cuprous halide and oxygen is used to have coupling with two terminal alkynyl groups (Figure 65).<sup>154</sup>

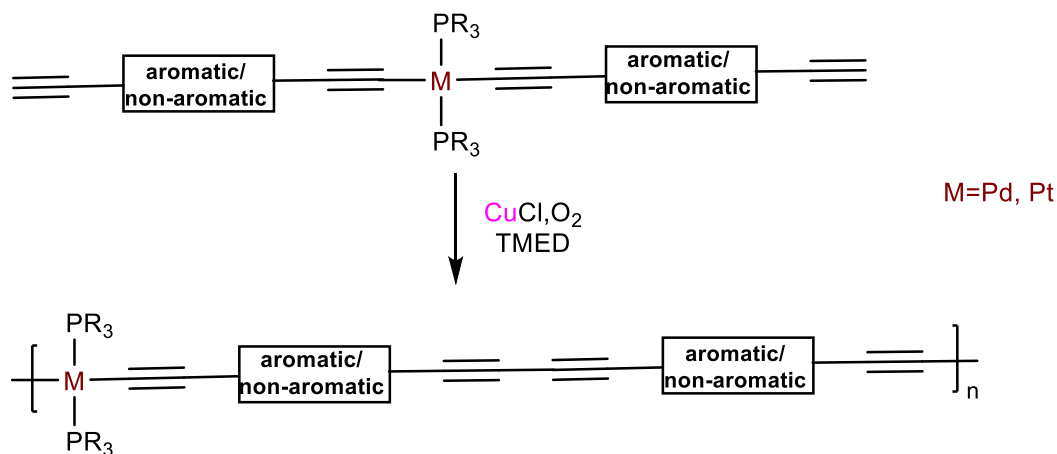


Figure 65: Homocoupling of terminal alkynes

Oxidative coupling is a convenient preparative method, where no stoichiometric restriction. Consequently, the degree of polymerization is usually high.

### 3.4. Alkynyl-ligand exchange:

This type of reaction was carried for metallopolymer with Ni. It is also a copper catalyzed reaction that involves alkynyl ligand in the presence of amine solvents with an addition of  $\text{PR}_3$  to suppress the phosphine dissociation from the metallic center (Figure 66).<sup>155</sup>

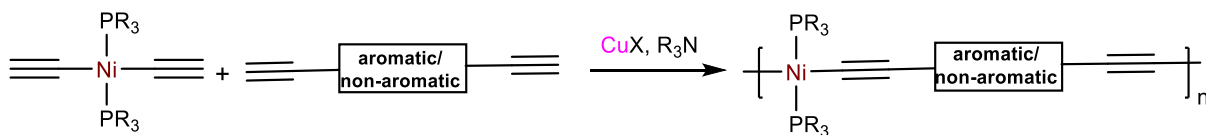


Figure 66: Copper-catalyzed alkynyl ligand exchange

Alkynyl-ligand exchange works well with Ni contained polymer, where their preparation is limited using the previous methods.

<sup>154</sup> S. Takahashi, E. Murata, K. Sonogashira, N. Hagihara, *J. Polym. Sci. Polym. Chem. Ed.*, **1980**, 18, 661.

<sup>155</sup> K. Sonogashira, K. Ohga, S. Takahashi, N. Hagihara, *J. Organomet. Chem.*, **1980**, 188, 237



Alkynyl polymers are well-studied type of organometallic polymers since these polymers have unique properties such as liquid crystalline properties and electrooptic behavior. Involving Pt as transition metal in these polymers has attracted attention over the past decades. A lot of studies were carried to provide better understanding of the metal center influence and spacer group on the electronic excitations and the concept of triplet state in these complexes. This will be more explained in chapter two of this manuscript.

## IV. Applications of conjugated polymers in materials for energy:

Conjugated polymers have received attention in various electronic devices due to their solution processability, light weight, flexibility and low thermal conductivity. Both n-type and p-type conjugated polymers have been investigated for high performance devices.<sup>156</sup>

Conjugated polymers and recently metallooligomers are widely studied and explored in the field of organic photovoltaics as organic semiconductors in the active layer of organic solar cell. Conjugated polymers can be used as hole transfer materials, electron transfer materials and an interface layer for better charge transfer.<sup>157</sup> Metallooligomers and metallopolymers will be studied in chapter two for solar cells application.

Currently, conjugated polymers are also hailed as promising organic thermoelectric since their constituents are more abundant than inorganic counterparts, they can be scaled up for mass production and because of their flexibility, they can harvest wasted heat from a variety of shapes.<sup>158</sup> The use of conjugated polymers in thermoelectrics will be more explained in chapter three of this manuscript. N-type conjugated polymers are still suffering from poor stability and low electrical conductivity. Therefore, in this thesis we are more interested in synthesis new n-type conjugated polymers. However, the synthesized polymers will be also used before doping process in n-type organic field effect transistors (OFETs) as organic semiconductors.

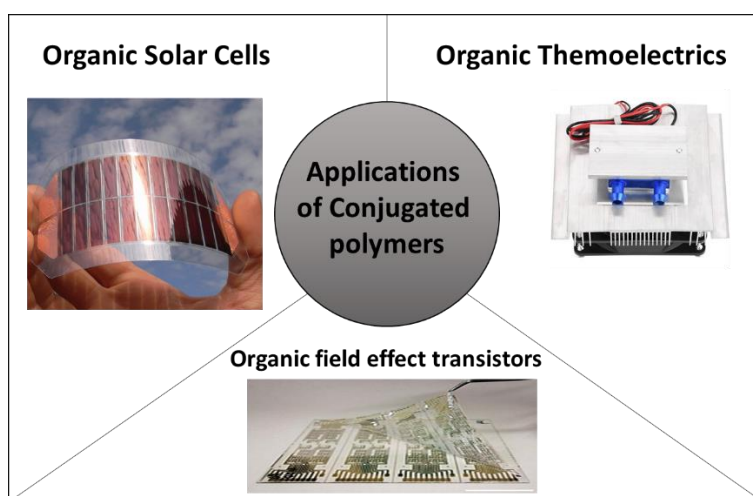


Figure 67: Some applications of conjugated polymers

<sup>156</sup> B. Meng, J.Liu, L. Wang, *Nano Materials Science*, **2021**, 3, 113-123

<sup>157</sup> W. Hou, Y. Xiao, G. Han, J-Y. Lin, *Polymers*, **2019**, 11, 143

<sup>158</sup> S. Wang, G. Zuo, J. Kim, H. Sirringhaus, *Progress in Polymer Science*, **2022**, 129, 101548

# Chapter 2

## I. Introduction to organic solar cells:

### 1. Solar cells:

The history of solar cells started in 1876 when Grylls with Richard Day, who is one of his students discovered that electricity can be produced when selenium was exposed to light.<sup>159</sup> In 1953, Calvin Fuller, Gerald Pearson and Daryl Chapin discovered the silicon based solar cells, which can give an efficient amount of energy for some small electrical devices to work.<sup>160</sup> In 1956, commercially the first solar cell was available then a lower cost solar cell was discovered at the beginning of 1970.<sup>161</sup>



Figure 68: First satellite solar cell<sup>162</sup>

The efficiency of solar cell is evaluated by the power conversion efficiency PCE. This value is determined by the figure of merit:

$$\text{PCE} = \frac{P_{\max}}{P_{\text{in}}} = \frac{FF V_{\text{oc}} I_{\text{sc}}}{P_{\text{in}}}$$

$V_{\text{oc}}$  is the open-circuit voltage, when there is no current running through the device,

$I_{\text{sc}}$  is short-circuit current density at  $V = 0$ , which is the maximum photocurrent generation value.

$FF$  is the fill factor and  $P_{\text{in}}$  the incident light power (Figure 69).

Where  $FF$  is the ratio of the maximum power divided by  $V_{\text{oc}} \cdot I_{\text{sc}}$ . For  $FF$  over 60 %, it is considered benchmark for solar cells.<sup>163</sup>

$$\text{FF} = \frac{P_{\max}}{V_{\text{oc}} I_{\text{sc}}} = \frac{V_{\max} I_{\max}}{P_{\text{in}}}$$

<sup>159</sup> S.S. Rais, N.I.M. Enzai, N. Ahmad, N. Ahmed, R. Darus, Z. Jusoh, N.N.S.N. Dzulkefli, S.A.C. Kar, S. Mohamed, N.N. Mahzan, K.S.S.K.M. Noh, H. Husni, *Journal of Fundamental and Applied Sciences*, **2017** - ajol.info

<sup>160</sup> D.A. Kleinman, *US Patent*, **1965**, 3, 175, 929

<sup>161</sup> M.A. Green, K. Emery, Y. Hishikawa, W. Warta, *Progress in Photovoltaics*, **2009**

<sup>162</sup> Le photovoltaïque pour satellite, **2013**-Solarpedia, <http://fr.solarpedia.net/wiki/index.php>

<sup>163</sup> G. Li, W.-H. Chang, Y. Yang, *Nat. Rev. Mater.* **2017**, 2, 17043.

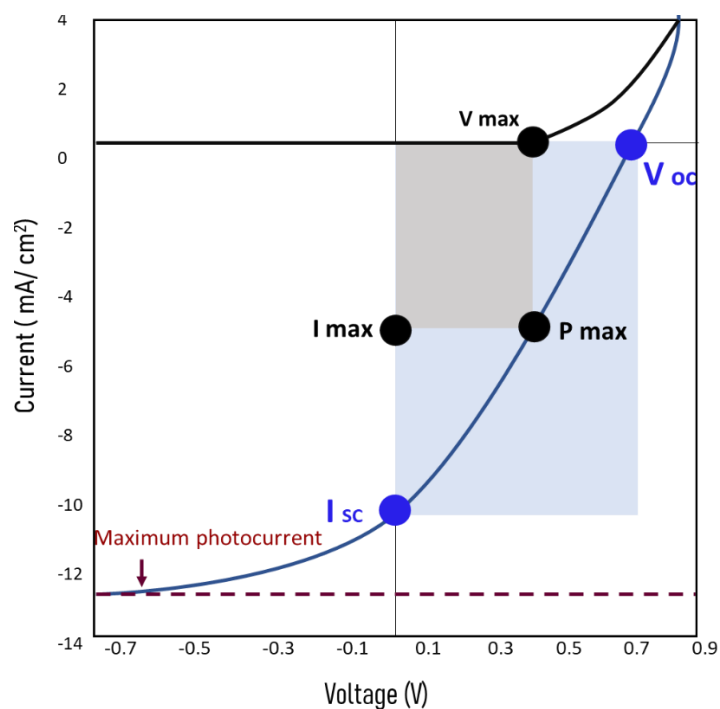


Figure 69: Current-tension graph of solar cells

The first and second generations of solar cells are made up of silicon and cadmium telluride (CdTe) or copper indium gallium selenide/sulfide (CIGS) as absorbers. The PCE of inorganic solar cells reaches 47 %. They are efficient, but they need high requirements during their production, such as typical thin film deposition techniques of CdTe, vapor-transport deposition and close-spaced sublimation.<sup>164</sup>



Figure 70: The first silicon solar cell<sup>165</sup>

Recycling technologies to reuse silicon from the solar cells are still not commercially available. To overcome the recycling problems of silicon scientists developed the organic or hybrid solar cells combined with dyes to replace the inorganic materials in the traditional solar cells. Recently, perovskite solar cells are of researchers interest. Technical advances provoke a jump in conversion efficiency to reach 25 %.<sup>166</sup>

<sup>164</sup> F. Ullah, H. Chen, CZ. Li - *Chinese Chemical Letters*, **2017** - Elsevier

<sup>165</sup> <https://www.pinterest.com/pin/838302918135943684/>

<sup>166</sup> G.H. Kim, D.S. Kim, *Joule*, **2021**, 5, 1033-1035

Nevertheless, the utilization of organic materials is gaining much interest in the preparation of solar cells. Indeed, organic materials can hold up the potential to develop environmentally safe materials for long-term technologies such as organic solar cells.

## 2. Organic solar cells:

Organic solar cells have important properties starting from the low cost of materials, less toxic components, and high throughput roll-to-roll production to the mechanical flexibility and light weight.<sup>167</sup>



Figure 71: Sample of organic solar cells<sup>168</sup>

In this area polymer solar cells have attracted a great attention in the research field because of the worthy advantages related to polymer solar cells over the previous generation of inorganic solar cells. The power conversion efficiency (PCE) has increased from 1 % to over 8 % during 1990's.<sup>169</sup> The PCE value is calculated by the same method used for inorganic solar cells, which is the use of figure of merit.

$$\text{PCE} = \frac{P_{max}}{P_{in}} = \frac{FF V_{oc} I_{sc}}{P_{in}}$$

The parameters used for calculating the power conversion efficiency depend on the energy levels of donor and acceptor used in preparing the organic solar cell, for example  $V_{oc}$  depends on the energy levels of HOMO<sup>D</sup> of the donor and LUMO<sup>A</sup> of the acceptor in particular to the offset of a proportional relation  $E_{HOMO}^D - E_{LUMO}^A$ .

And FF has positive depending on  $\Delta HOMO$  energy levels of the donor and acceptor in the blend. Changing the HOMO-HOMO offsets provokes change in the FF value.

The most well studied system in the field of organic photovoltaics OPV consists of a blend of **P3HT** and (6,6)-phenyl-C<sub>61</sub>-butyric acid methyl ester **PC<sub>61</sub>BM**<sup>170</sup> with maximum power conversion efficiency reaching 4.24 %.<sup>171</sup> In the last fifteen years, a significant progress has been made to enhance the power conversion efficiency (PCE) of polymer bulk solar cells and the achieved efficiencies have increased from less than 1 % in the poly (phenylenevinylene)

<sup>167</sup> D. Neher, J. Kniepert, A. Elimelech, L.J.A. Koster, *Sci Rep*, **2016**, 6, 24861

<sup>168</sup> *Organic Solar Cells: Power from Plastic Photovoltaics*, **2011**, 89, 51

<sup>169</sup> B.W. Carney, *Bulletin of the American Astronomical Society*, **1989**, 347, 266-281

<sup>170</sup> D.J. Lipomi, B.C.K. Tee, M. Vosgueritchian, Z. Bao, *Advanced Materials*, **2011**, 23, 1771-1775

<sup>171</sup> D. Chi, S. Qu, Z. Wang, J. Wang *J. Mater. Chem. C*, **2014**, 2, 4383

(PPV) system in 1995 to 4–5 % in solar cells based on poly (3-hexylthiophene) (P3HT) system in 2005, to achieve a yield of more than 11 % in 2016.

After around thirty years of progress, the PCE of organic solar cells has been increased to reach 20 % to approach the traditional counterparts. However, the efficiency of the polymer solar cell is still lower than that of the silicon solar cells that is of PCE 29.1 %<sup>172</sup> and that of Perovskite solar cells which is approaching 26 %.<sup>173</sup> Stability is considered as limitation for organic solar cells, since under illumination and simultaneous exposure to water vapor or oxygen, degradation of the active layer occurs.<sup>174</sup> The progress of different solar cells is illustrated in the chart of figure 72.

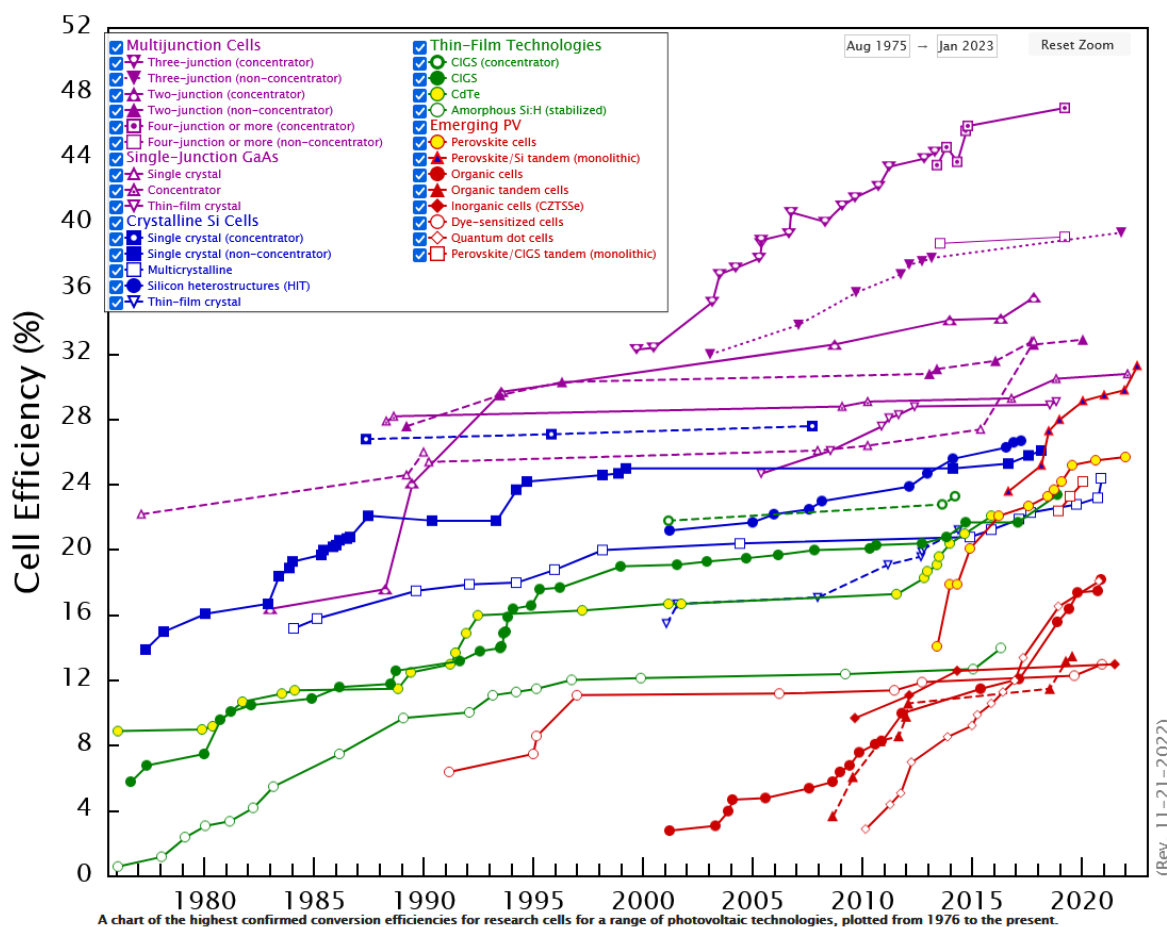


Figure 72: Chart illustrating the performance of solar cells from 1975 to 2020<sup>175</sup>

The performance of BHJOSCs could be enhanced by three main strategies. First, to vary the architecture of the organic solar cells. Second, to develop new p-type and n-type semiconductors. Third, to control the morphology of acceptor/donor blend in the active layer of BHJOSCs.

<sup>172</sup> S. B. Mdluli, M. E. Ramoroka, S. T. Yussuf, K. D. Modibane, V. S. John-Denk, E. I. Iwuoha, *Polymers*, **2022**, 14, 716

<sup>173</sup> Z. Guo, A. K. Jena, G. M. Kim, T. Miyasaka, *Energy Environ. Sci.*, **2022**, 15, 3171-3222

<sup>174</sup> S. Günes, H. Neugebauer, N.S. Sariciftci, *Chemical reviews*, **2007**, 107, 4, 1324-1338

<sup>175</sup> NREL updates interactive chart of solar cell efficiency, November 21, 2022

### 3. Architecture of organic Solar Cells:

Organic Solar cells are classified into three configurations: regular, inverted and tandem depending on the arrangement of the layers in the solar cell (Figure 73), where organic solar cells are made-up of five main layers. Most of organic solar cells are with an organic layer inserted in between two different electrodes. One of the electrodes should be (semi-) transparent anode electrode as transparent oxide (TCO) as indium-tin oxide (ITO), also thin metal layer can be used. The second electrode is the cathode. It is usually aluminum (calcium, magnesium, gold and others are also used)<sup>176</sup> and two layers inserted between the electrodes and the active layer as electron transporting layers (ETL), which extract the electrons from the active layer to the electrode and hole transporting layer (HTL), which extracts and transports the holes in the active layer to the electrode and acts as energy barrier to prevent the electron transfer to the anode electrode. In tandem solar cell we can define the interconnecting layer (ICL) that is electrically connects two sub cells and has a role in determining the performance of the organic solar cell.

The inverted device architecture gained research attention due to the device stability. The polarity of charge collection is opposite to the regular configuration.<sup>177</sup> In my project, the donor polymer will be evaluated with the regular architecture.

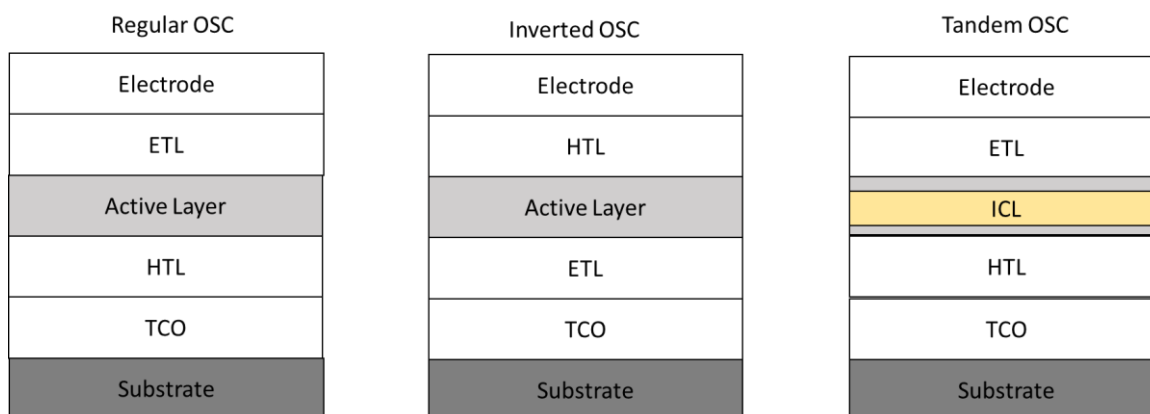


Figure 73: The different configurations of organic solar cells

### 4. Active Layer :

Moreover, these cells also classified according to the type of their active layer architecture: single and double.

#### 4.1. Single active layer structure:

Single active layer structure organic solar cells consist of an active layer made up of one type of semiconductors (Figure 74). The major limitation of this type of organic layer is

<sup>176</sup> M. Helgesen, S.A. Gevorgyan, F.C. Krebs, *ACS Publications*, **2009**

<sup>177</sup> S. K. Hau, H.L. Yip, A. K.-Y. Jen, *Polymer Reviews*, **2010**, 50, 474–510



that the electric field generated from the difference between two conductive electrodes is not always efficient to split the excitons.

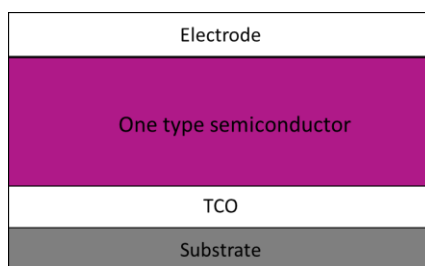


Figure 74: Single active layer OSCs configuration

## 4.2. Two layers structure

It consists of two components, a p-type material (donor= D) and n-type material (acceptor= A). Two types of heterojunction solar cells have been developed: planar heterojunction (PHJ) (Figure 75-a) and bulk heterojunction (BHJ) (Figure 75-b). PHJ is formed by two distinct layers, donor and acceptor. It has the advantages to have an efficient charge extraction, but the limitation is the small donor-acceptor interface. So, the BHJ is more used because of mixing the donor and acceptor layers, resulting in an increase of the D/A interface required for exciton dissociation to produce more free charge.<sup>178</sup>

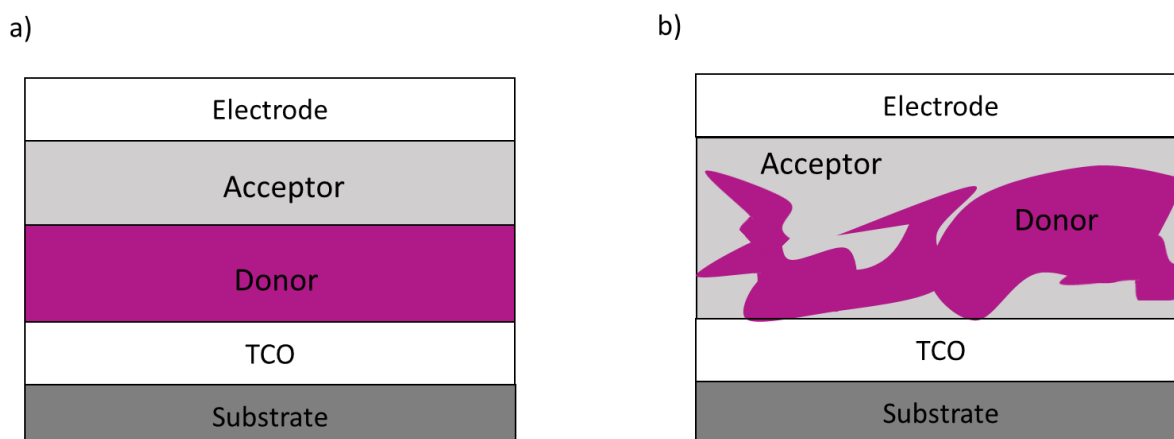


Figure 75: The different bilayer active layer, (a) PHJ OSCs and (b) BHJ OSCs

Therefore, Bulk heterojunction is the most utilized p-n junction organic solar cells.<sup>179</sup> It shows a relevant morphology to favor efficient charge separation and transport. Also, it provides continuous network for charge transport. Nevertheless, because of the different chemical nature of the donor and acceptor, it is usually complicated to control the active layer morphology for better device performance.<sup>180</sup> The performance could be enhanced by controlling the morphology of active layer via increasing the D/A interface and to lead to

<sup>178</sup> L. Hong, H. Yao, Y. Cui, P. Bi, T. Zhang, Y. Cheng, Y. Zu, J. Qin, R. Yu, Z. Ge, J. Hou, *Adv. Mater.*, **2021**, 2103091

<sup>179</sup> G. Yu, J. Gao, J. C. Hummelen, F. Wudl and A. J. Heeger, *Science*, **1995**, 270, 1789–1791.

<sup>180</sup> G. J. Hedley, A. Ruseckas and I. D. W. Samuel, *Chem. Rev.*, **2017**, 117, 796–837.

vertical segregation. The ideal morphology is interpenetrated donor and acceptor as illustrated in figure 76. This morphology increases exciton dissociation, charge generation and collection to the electrode. Hence, improving vertical segregation is a key step to enhance the physical properties in organic solar cells.

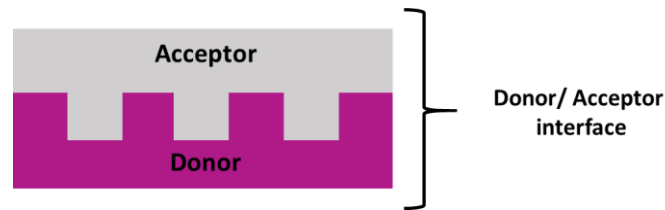


Figure 76: D/A interface using vertical segregation

## 5. The mechanism in BHJ OSCs:

The conversion, of incident photons into electric current in bulk heterojunction involves four fundamental steps (Figure 77):

1. Absorption of light and the generation of exciton
2. Exciton diffusion to the D-A interface (length around 10-15 nm)
3. Exciton dissociation at D-A interface to free charge (hole as positive charge and electron as negative charge)
4. Then, transport of the charges to the respective electrodes

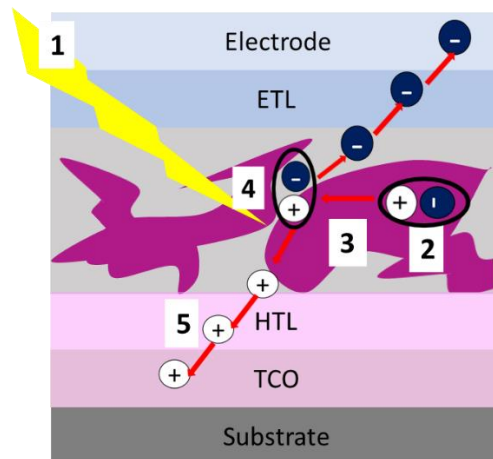


Figure 77: The mechanism of incident photon into current generation BHJ OSCs

After the photon absorption there are two possible pathways for the excitation as shown in figure 78. In channel one, the excitation occurs in the donor part and then the electron is transferred from the donor to the acceptor. In the second pathway, the excitation occurs in the acceptor part and then followed by electron transfer from the acceptor to the donor. The nature of the acceptor is the main parameter in the determination of the mechanism. Generally, channel one dominates the photocurrent generation when fullerene-

based acceptors are used, while the two excitation pathways occur in non-fullerene organic solar cells.<sup>181</sup> In this thesis, we are interested in the mechanism of channel I.

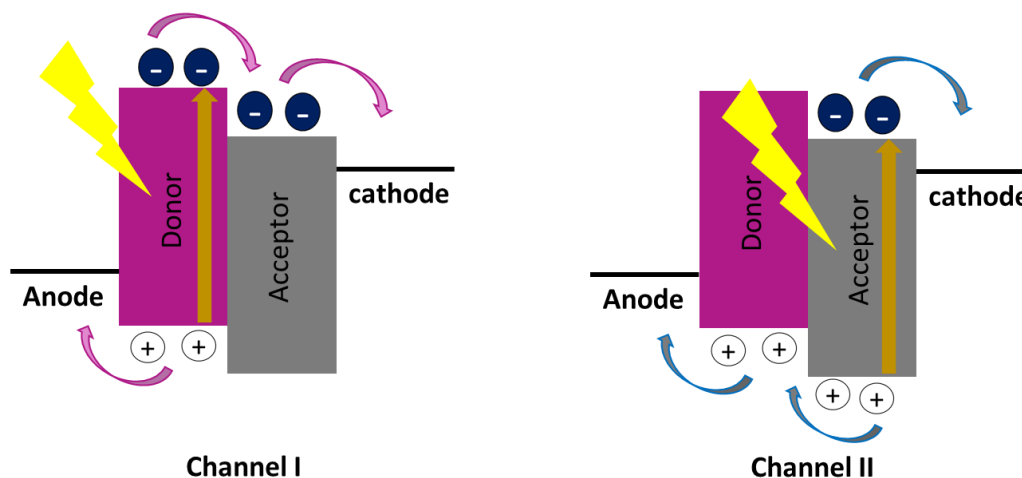


Figure 78: The photon absorption possible pathways represented in two channels (I, II)

The performance of the solar cells depends on the nature of the donor and acceptor used in the blend of the active layer. Enhancing optical properties, suitable electronic band's structure, charge transport with an appropriate molecular organization are promising strategies to increase solar cell performance. This could be achieved by modifying the molecular design of the donor and working on its functionalization. Therefore, tuning the optical, electronic and optoelectronic properties relies on the structure of the polymer used. The donor-acceptor materials in BHJ OSCs must have key properties:<sup>182</sup>

1. Complementary absorption spectrum between donor and acceptor to broaden the absorption wavelength to absorb the maximum of solar light (to approach sunlight spectrum with air mass coefficient AM 1.5). Therefore, allowing less energetic photons to produce excitons.
2. Suitable electronic structure with appropriate band levels for effective electronic transfer.
3. High charge carrier mobility and well-balanced electron and hole mobilities to prevent recombination.
4. Nanoscale phase separation of donor/acceptor blend in the active layer.
5. Donor/acceptor vertical segregation.

## 6. How to enhance the PCE:

### 6.1. Tuning the electronic structure of D/A:

In order to enhance the PCE, the material must show high absorption capacity with the determination of the molar extinction coefficient ( $\epsilon_\lambda$ ) and broad absorption wavelength range

<sup>181</sup> X. Xu, G. Zhang, Y. Li, Peng, Q. Chin, *Chem. Lett.* **2019**, 30, 809–825

<sup>182</sup> R. Xue, J. Zhang, Y. Li, Y. Li, *Small*, **2018**, 14, 1801793.

close to that of sunlight spectrum with air mass coefficient 1.5 AM. One of the efficient ways to broaden the absorption range of the polymer is by narrowing down the optical band gap.<sup>183</sup> There are several strategies to decrease the band gap as explained in chapter one of the manuscript:

1. Increase the effective conjugation length.
2. Increase the planarity.
3. Allow an increase in the alternating donor-acceptor  $\pi$ -conjugation.
4. Increase the stability of quinoid form.

Therefore, looking for a coplanar main chain of the conjugated polymers allows the extension of the conjugated polymer, increases in the intermolecular  $\pi$ - $\pi$  stacking; hence, it improves the charge transport properties.

In organic solar cells, there are two important parameters  $\Delta E1$  and  $\Delta E2$  (Figure 79).  $\Delta E1$  is the energy difference between the LUMO level of the donor and the LUMO level of the acceptor. It should be around 0.3 eV or less depending on the type of the acceptor used to allow the dissociation of the exciton.  $\Delta E2$  is the energy difference between the LUMO level of the acceptor and the HOMO level of the donor polymer.  $\Delta E2$  is proportional to  $V_{oc}$ , where  $V_{oc}$  is the value of the maximum voltage that the solar cell can extract for an external circuit, and it is originated from the energy offset between the HOMO of the donor and the LUMO of the acceptor such as **PCBM**.  $V_{oc}$  is expressed in the following equation:<sup>184</sup>

$$V_{oc} = (1/e) |E_{HOMO \text{ of donor}}| - |E_{LUMO \text{ of acceptor}}| - 0.3$$

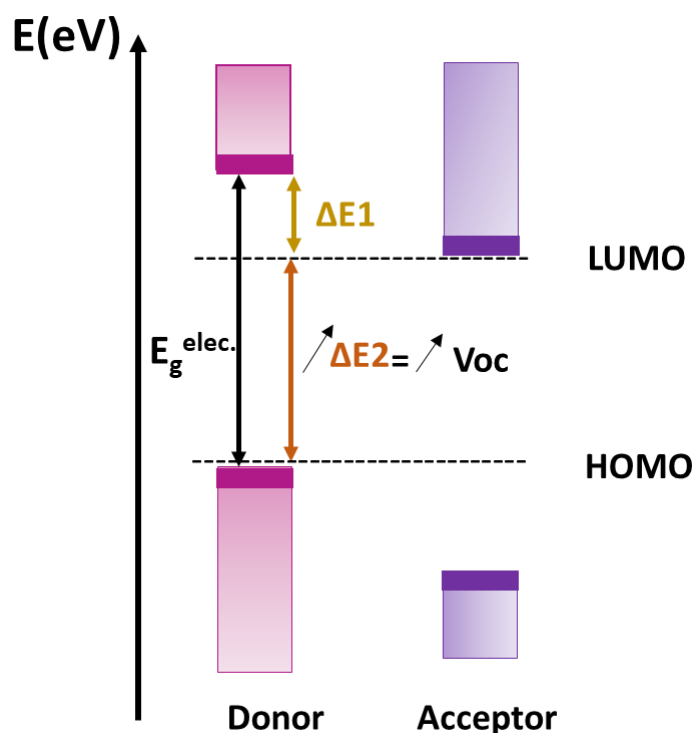


Figure 79: Electronic structures of donor and acceptor with some key parameters in organic solar cells

<sup>183</sup> J. Chin., *Chem. Soc.*, **2014**, 61, 115-126

<sup>184</sup> S. Garg, N. Goel, *J. Phys. Chem. C*, **2022**, 126, 9313-9323

HOMO and LUMO levels have a remarkable influence for obtaining high PCE, since they are strongly related to the  $V_{oc}$  and the charge separation efficiency of OSCs. For designing efficient p-type materials, it is important to downshift the HOMO level and keep the LUMO level above that of the n-type material.<sup>185</sup> Good solubility in common organic solvents, good film, rigidity, self-assembly, high molecular weight, and ambient stability are required parameters to be taken into consideration during the synthesis of p-type materials.

According to Scharber and co-workers, the ideal polymer for fullerene acceptor as **PCBM**, must have a LUMO level between -3.7 and -4.0 eV and small band gap of 1.5 to 1.8 eV.<sup>186</sup> High average molar mass is not less important parameter. Studies on the influence of the average molar mass on electronic properties of the polymer showed that the performance of BHJ solar cell is improved as the average molar mass of the conjugated polymer is increased. As an example on this property, BHJ solar cell based on poly[(4,4-didodecyldithieno[3,2-b:2',3'-d]silole)-2,6-diyl-alt-(2,1,3-benzothiadiazole)-4,7-diyl] active layer has increased short-circuit current density from 4.2 to 17.3 mA cm<sup>-2</sup> and increased fill factor FF from 0.35 to 0.61 with the increase in the average molar mass from 7 to 34 Kg.mol<sup>-1</sup>, which results in increased PCE value from 1.2 % to 5.9 %.<sup>187</sup>

## 6.2. Molecular organization:

The major issue surrounding polymer solar cells and more precisely the polymer solar cells is the low power conversion efficiency. Recent advances in their performance are through narrowing the band gap to enhance the short circuit current, while keeping low the HOMO level to increase the open circuit voltage  $V_{oc}$ . Another problem that organic solar cells are facing is the low stability under ambient conditions or the low stability of organic materials within the device and during the cell manufacturing.

Therefore, the main goal in this field is to obtain high charger carrier mobility in the donor materials in the active layer blend. Such property is achieved for materials with three-dimensional order with semi-crystalline film morphology. Structural and molecular parameters are crucial ingredients for high PCE in polymer solar cells.<sup>188</sup> Favoring the face-on orientation is also necessary for building an organic solar cell (Figure 80).

---

<sup>185</sup> L. Dou, J. You, Z. Hong, Z. Xu, G. Li, R. A. Street, Y. Yang, *Adv. Mater.*, **2013**, 25, 6642–6671

<sup>186</sup> S. Wakim, S. Beaupré, N. Blouin, B.-R. Aich, S. Rodman, R. Gaudiana, Y. Tao, M. Leclerc, *J. Mater. Chem.*, **2009**, 19, 5351-5358

<sup>187</sup> Z. Xiao, K. Sun, J. Subbiah, T. Qin, S. Lu, B. Purushothaman, D. J. Jone, A. B. Holmes, W. W. H. Wong, *Polym. Chem.*, **2015**, 6, 2312-231

<sup>188</sup> Z. B. Henson, K. Müllen, G. C. Bazan, *Nat. Chem.* **2012**, 4, 699

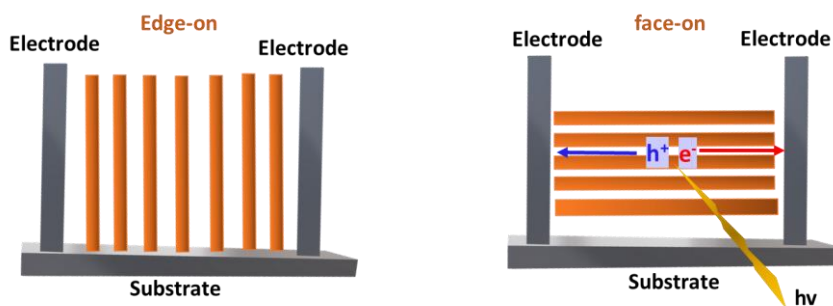


Figure 80: The favored face-on orientation and unfavored edge-on orientation of conjugated polymers in a solar cell

Besides, side chain engineering is a method, which is used to enhance these properties and to improve the solubility.<sup>189</sup> Another interesting property is creating a rigid conjugated backbone to enhance the crystallinity and to promote charge transport.<sup>190</sup> Since, increasing the planarity is required to increase the intramolecular interactions.

Designing the appropriate donor and acceptor materials for organic solar cells must be taken into consideration as a key step in obtaining an enhanced performance.

6.3. The choice of the donor and acceptor materials for the blend preparation in bulk heterojunction is very important to the overall performance of the organic solar cells:

#### 6.3.1. Acceptor material:

The history of acceptor materials has been started when Sariciftci and *al* have discovered that the photo-induced electrons can transfer from the polymer to a fullerene molecule.<sup>191</sup>

**PC<sub>61</sub>BM** is one of the common fullerene acceptors used in OSCs, it is composed of a **C<sub>60</sub>** fullerene cage, aryl group, alkyl chain and end group, thus serving four possible variables to enhance the efficiency of fullerene based solar cells by modifying these four terms. It was widely used because of its better performance compared to that of pristine **C<sub>60</sub>** (Figure 81).

<sup>189</sup> R. L. Uy, S. C. Price, W. You, *Macromol. Rapid. Comm.*, **2012**, 33, 1162

<sup>190</sup> W. W. Li, K. H. Hendriks, W. S. C. Roelofs, Y. Kim, M. M. Wienk, R. A. J. Janssen, *Adv. Mater.*, **2013**, 25, 3182

<sup>191</sup> N.S. Sariciftci, L. Smilowitz, A.J. Heeger, F. Wudl, *Science*, **1992**, 258, 1474

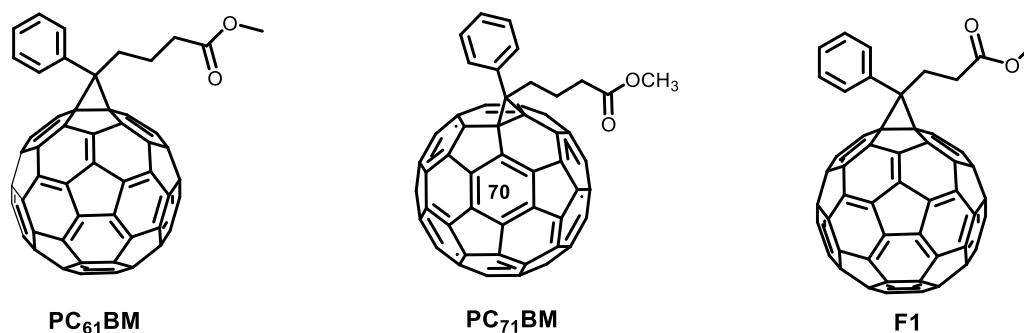


Figure 81: Some examples of fullerene derivatives.<sup>192</sup>

Although fullerene acceptors are widely used in the field of BHJ, they have their intrinsic limitations: restricted tunability of electronic structure and then no variation of the energy levels, weak absorption potential in the visible and near infrared ranges, morphological instability and expensive synthetic procedures.<sup>193</sup> **PCBM** based blend in **PffBT4T**-based polymer yield PCE around 12 % that is among the highest values in fullerene based OSCs.<sup>194</sup>

By 2015, Lin and co-workers reported the non-Fullerene acceptors NFAs, which showed better absorption than the fullerene in the visible region. Hence, NFA-based OSCs have attracted much attention and recently their performances have made a significant progress with an increase in the PCE from 12 % to around 20 % in bulk heterojunction solar cells.<sup>195</sup>

NFAs possess definite advantages in the absorption spectrum complementary with donor material in binary and ternary systems. NFAs are more flexible to vary the HOMO and LUMO energy levels in electronic structure. They have tunability of the band gap with higher LUMO level and then higher  $V_{oc}$  and  $I_{sc}$ .<sup>196</sup> Hence, NFAs have less energy loss and better exciton dissociation with the possibility to alter the optoelectronic properties. Moreover, they have better molecular organization with increased donor /acceptor interface and face-on orientation. NFAs can be classified into small molecules and polymeric NFAs.

Small molecules include imide-based NFAs and A-D-A type NFAs. A-D-A are conjugated Push-Pull structures, where **A** represents electron withdrawing moieties and **D** represents electron-rich moieties, such combination aims a decrease in the band gap. **ITIC** (Figure 82) has been reported in 2015 in Zhan's group, which is based on indacenodithienol [3,2-b]thiophene (**IDTT**) as the core and 2-(3-oxo-2,3-dihydroinden-1-ylidene)malononitrile (**INCN**) group with 4-hexyl groups substituted on it. These carbonyl and cyano groups down-shift the LUMO energy level and the push-pull structure induces an intramolecular charge transfer with extension of the absorption range, while the hexylphenyl group restricts the aggregation. This type of acceptors shows an intense absorption in 500-800 nm range and low LUMO level with promising PCE.<sup>195</sup>

<sup>192</sup> Y. Li, W. Huang, D. Zhao, L. Wang, Z. Jiao, Q. Huang, P. Wang, M. Sun, G. Yuan, *Molecules*, **2022**, 27, 1800

<sup>193</sup> G. Zhang, J. Zhao, P.C.Y. Chow, K. Jiang, J. Zhang, Z. Zhu, J. Zhang, F. Huang, H. Yan, *Chem. Rev.*, **2018**, 118, 3447–3507

<sup>194</sup> J. Zhao, Y. Li, G. Yang, K. Jiang, H. Lin, H. Ade, W. Ma, H. Yan, *Nat. Energy*, **2016**, 1, 15027.

<sup>195</sup> Y. Lin, J. Wang, Z.-G. Zhang, H. Bai, Y. Li, D. Zhu, X. Zhan, *Adv. Mater.* **2015**, 27, 1170–1174

<sup>196</sup> H. Fu, Z. Wang, Y. Sun, *Angew. Chem. Int. Ed.*, **2019**, 58, 4442–4453

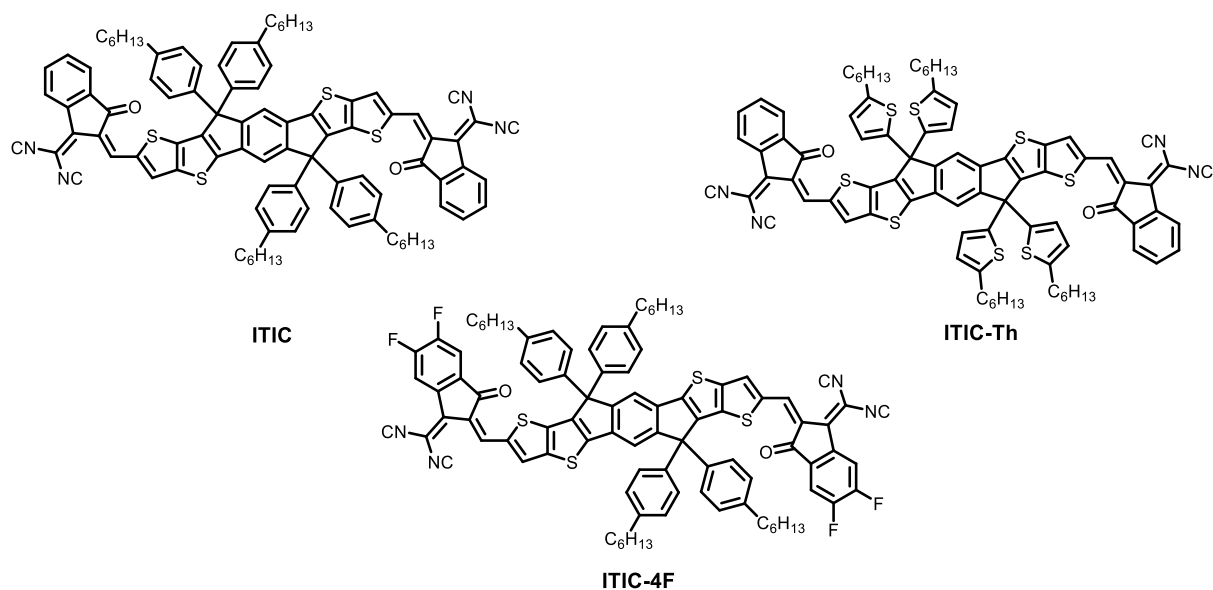


*Figure 82: Common Small molecules NFAs*

The efficiency of BHJ approaches 19 % using a small molecule NFAs **ITIC-4F** known as **IT4F** in **PM6/IT4F** blend (Figures 82 and 88).<sup>197</sup>

In 2019, new NFA with A-DA'D-A structure, **Y6**, which is another type of small molecules NFAs has showed one of the highest PCE (15.7 %) with high  $V_{oc}$  of 0.825 V, fill factor of 74 % and  $J_{sc}$  of 25.2 mA cm<sup>-2</sup> due to the preservation of the conjugation along the length of the molecule due to the fused dithienothiophen[3,2-b]-pyrrolobenzothiadiazole (**TPBT**) unit, which allows the tuning of the electron affinity with -5.65 eV HOMO level and -4.10 eV LUMO level and 1.33 eV band gap.<sup>198</sup> Therefore, series of **Y6** derivatives have been developed such as **Y6-Se** which has enhanced quinoidal character leading to lower band gap because of better orbital overlap in  $\pi$ -conjugated system with more polarizable delocalization of the electron cloud in Se compared to S atom in thiophene but their absorption range is not broad enough compared to **Y6** (Figure 83). With appropriate donor materials, the PCE reached 18.1 % in **PM7:PM7: Y6: PC71BM** quaternary OSCs.<sup>199</sup>

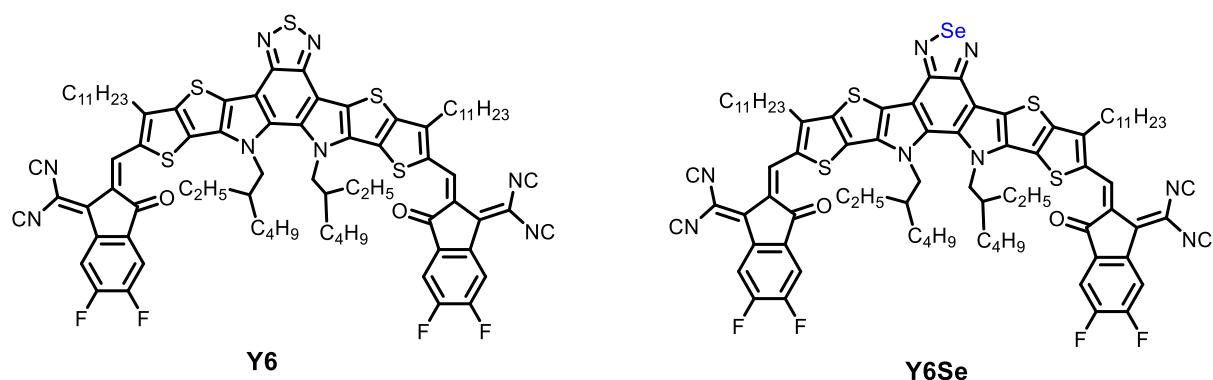


*Figure 83: Small molecules NFAs with A-DA'D-A structure*

<sup>197</sup> T. H. Lee, Y. Dong, R. A. Pacalaj, S. Y. Park, W. Xu, J.-S. Kim, J. R. Durrant, *Adv. Funct. Mater.*, **2022**, 2208001

<sup>198</sup> J. Yuan, Y. Zhang, L. Zhou, G. Zhang, H.-L. Yip, T.-K. Lau, X. Lu, C. Zhu, H. Peng, P. A. Johnson, M. Leclerc, Y. Cao, J. Ulanski, Y. Li and Y. Zou, *Joule*, **2019**, 3, 1140–1151.

<sup>199</sup> Q. Guo, Q. Guo, Y. Geng, A. Tang, M. Zhang, M. Du, X. Sun, E. Zhou, *Mater. Chem. Front.*, **2021**, 5, 3257–3280



Recently, polymeric NFAs acceptors are developed. The most known building blocks in this type are perylene diimide (**PDI**), naphthalene diimide (**NDI**), bithiophene imide (**BTI**) and B-N bridged bipyridine (**BN-Py**) and some D-A copolymers including the small NFAs as acceptor units such as PDI-vinylene (**PDI-V**), NDI-bithiophene **NDI-2T** and cyclopenta-dithiophene (**CPDT-TPD**)(Figure 84).<sup>200</sup> As all polymer solar cells, they have advantages as the structural flexibility, morphological stability and superlative mechanical properties.

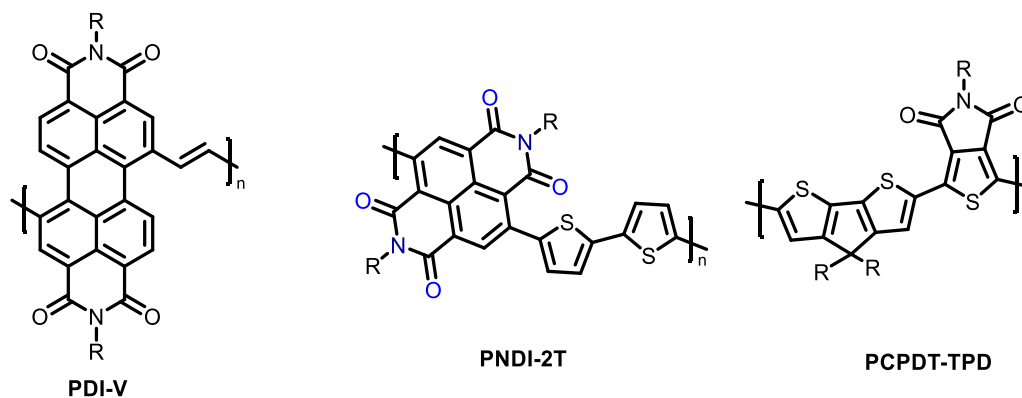


Figure 84: Examples of NFAs based on known building blocks (**PDI**, **BTI**, **BN-Py**).

In 2022, **PY-2S** has been synthesized with fluorine functionalized derivative **PY-2S-F** and two **PY-2Se** derivatives **Y-2Se-F**, and **PY-2Se-Cl** (Figure 85). The maximum PCE of 16.1 % achieved is with the use of **PY-2Se-Cl** as acceptor blended with **PM6** as donor material.<sup>201</sup>

<sup>200</sup> H. Sun, F. Chen, Z.-K. Chen, *Materials Today*, **2018**, 24, 94-118

<sup>201</sup> Q. Fan, H. Fu, Z. Luo, J. Oh, B. Fan, F. Lin, C. Yang, A. K.-Y. Jen, *Nano Energy*, **2022**, 92, 106718

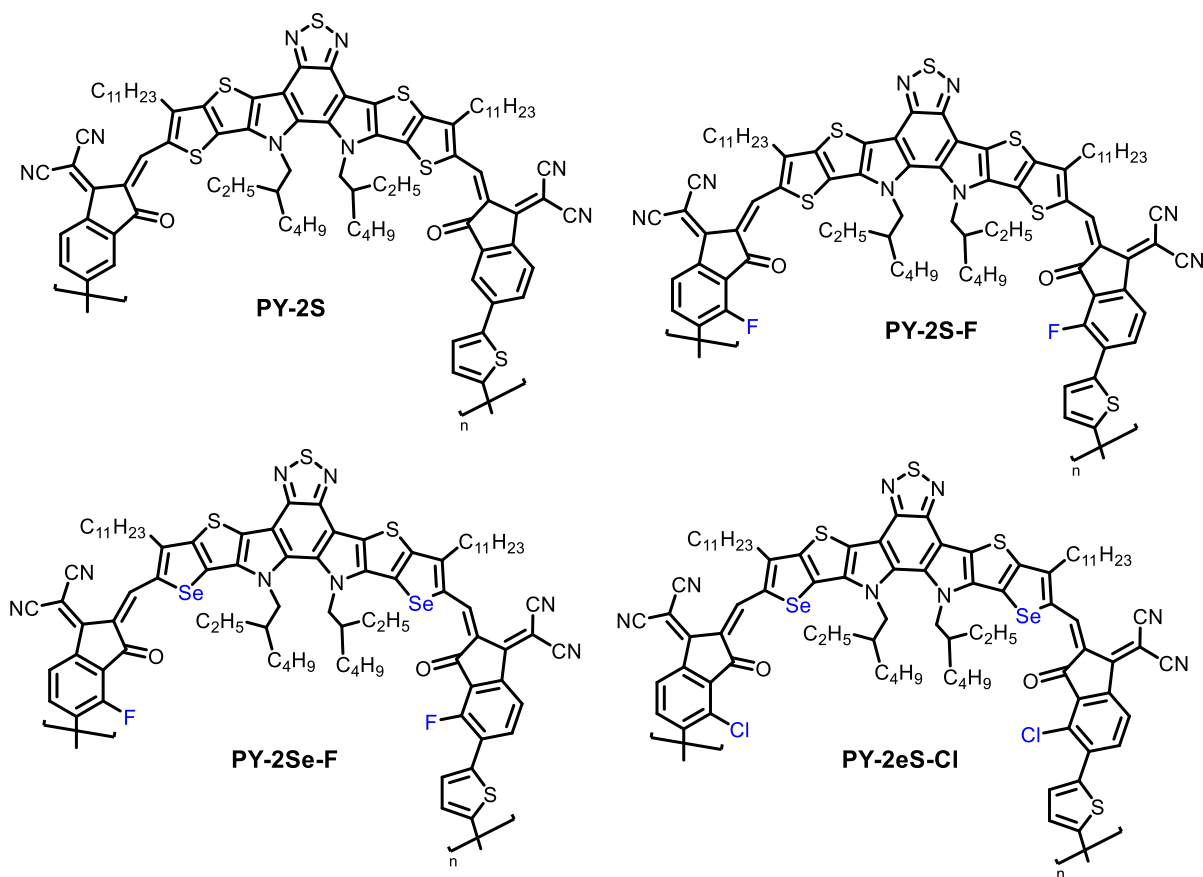


Figure 85: Polymeric NFAs used in high performance organic solar cells.

Fullerene derivatives have been widely used as electron acceptors in organic solar cells. Yet, NFAs materials have emerged as promising candidates to replace the fullerene molecules.

However, the active layer, including donor/ acceptor materials, has been a key factor for achieving high PCE values. Therefore, the progress in the efficiency of organic solar cells relies on developing both acceptor and donor materials. In the next paragraph, donor materials from the literature are discussed.

### 6.3.2. Donor materials:

The small band gap is not a guarantee for high PCE value. Proper HOMO and LUMO levels are crucial for the efficient charge transfer to the acceptor material and to obtain large  $V_{oc}$  of the device. More properties are essential such as high charge carrier mobility and favorable morphology when blended with the acceptor.<sup>202</sup> Donor materials are classified into three main types: small molecules, conjugated polymers and metallooligomers.

<sup>202</sup> G. Li, R. Zhu, Y. Yang, *Nat. Photon.*, **2012**, 6, 153

### 6.3.2.1. Small molecule donor materials:

The first generation of donor materials is composed of small molecules such as DPP-based small molecule materials, which offers advantages such as ease of fabrication and purification, determined and uniform structure, and high open circuit voltage  $V_{oc}$  compared to the polymers.<sup>203</sup>

A family of donor materials has been developed based on Diketopyrrolopyrrole (or pyrrolo[3,4-c]-pyrrole-1,4-dione) (Figure 86) that is a new pigment class, which is obtained in 1974, but it was not reported until 1993. In 2008, DPP-based small molecules and polymers were applied as organic semiconductors in organic photovoltaics and organic thin film transistors. Through the engineering of the energy levels of DPP derivatives, they could be used as p-type, n-type and ambipolar semiconductors.<sup>204</sup>

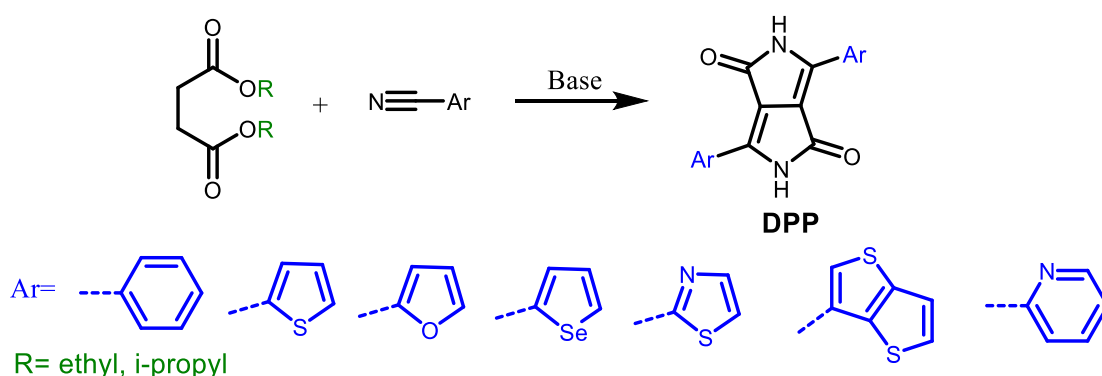


Figure 86: Chemical structures of DPP chromophores

This type of molecules has lower charge mobility compared to larger systems, and shorter effective carrier lifetime in a comparison between the efficiency between monoDPP molecule and bis-DPP molecule as p-type materials in organic solar cells. Developing a large conjugated system would be more promising in this application.

### 6.3.2.2. Polymer donor materials:

In 2016, the efficiency of polymer organic solar cells reached 11 % using a blend based on poly[(5,6-difluoro-2,1,3-benzothiadiazol-4,7-diyl)-alt-(3,3''-di(2-nonyltridecyl)-2,2';5',2'';5'',2'''-quaterthiophen-5,5'''-diyl)] (**PffBT4T-C<sub>9</sub>C<sub>13</sub>**) as donor and **PC<sub>71</sub>BM** as acceptor.<sup>205</sup>

Later, Benzodithiophene (**BDT**) is considered as one of the most important units as an electron donating block in the synthesis of D-A donor materials. **PBDB-T-2Cl** is a chlorinated copolymer, which consists of **BDT** as donor unit and 1,3-bis(4-(2-ethylhexyl)thiophen-2-yl)-

<sup>203</sup> R. S. Ashraf, I. Meager, M. Nikolka, M. Kirkus, M. Planells, B. C. Schroeder, S. Holliday, M. Hurhangee, C. B. Nielsen, H. Sirringhaus, I. McCulloch, *J. Am. Chem. Soc.*, **2015**, 137, 1314.

<sup>204</sup> A. Tang, C. Zhan, J. Yao, E. Zhou, *Adv. Mater.*, **2016**, 29,1600013

<sup>205</sup> J. Zhao, Y. Li, G. Yang, K. Jiang, H. Lin, H. Ade, W. Ma, H. Yan, *Nature Energy*, **2016**, 1, 1507

5,7-bis (2-alkyl)benzo[1,2-c:4,5-c']dithiophene-4,8-dione (**BDD**) as acceptor unit. Photovoltaic characterization of **PBDBT-T-2Cl: IT-4F** shows high PCE of 14.4 %<sup>206</sup> (Figure 87).

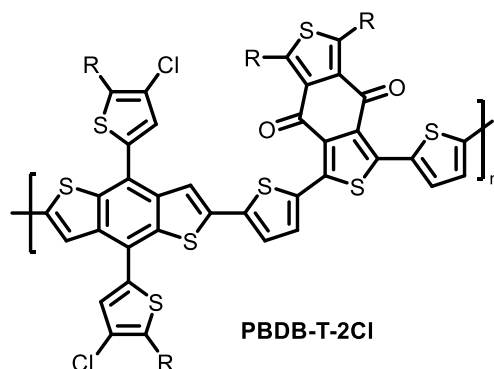


Figure 87: The structure of **PBDB-T-2Cl** polymeric NFAs

**PM6** is another copolymer based on fluorothieryl-substituted benzodithiophene with deep HOMO level (-5.50 eV), which leads to lower  $V_{oc}$  and reduced  $V_{loss}$ . It exhibits strong  $\pi$ - $\pi$  interaction and dominant face-on orientation. The performance of organic solar cells based on **PM6:IT-4F** is of high PCE around 13.5 % due to the fluorination effect.<sup>207</sup> The PCE using **PM6:IT-4F** blend approaches 19 %, <sup>208</sup> that makes fluorinated donor and acceptor blend **PM6:IT-4F** a promising candidate for large scale production (Figure 88).

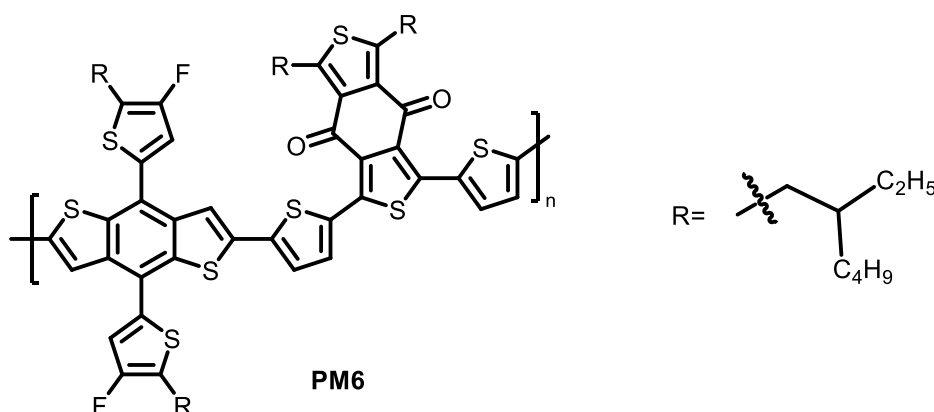


Figure 88: The structure of **PM6** NFAs used in the achieving the best PCE in organic solar cells

DPP is an interesting unit due to the planar conjugated bicyclic structure that leads to strong  $\pi$ - $\pi$  interactions, and the presence of a lactam part that provokes a strong electron withdrawing effect, which makes them good accepting units in optoelectronic materials (Figure 86). The solubility of these DPP based materials could be modified with solubilizing alkyl chains at the N moiety of the lactam using linear or branched alkyl chains.<sup>209</sup> DPP has been used as a building block in small molecules and in conjugated polymers.

<sup>206</sup>S. Zhang, Y. Qin, J. Zhu, J. Hou, *Adv. Mater.*, **2018**, 30, 1800868

<sup>207</sup> Q. Fan, W. Su, Y. Wang, B. Guo, Y. Jiang, X. Guo, F. Liu, T. P. Russell, M. Zhang and Y. F. Li, *Sci. China: Chem.*, **2018**, 61, 531–537

<sup>208</sup> T. H. Lee, Y. Dong, R. A. Pacalaj, S. Y. Park, W. Xu, J.-S. Kim, J. R. Durrant, *Adv. Funct. Mater.*, **2022**, 32, 2208001

<sup>209</sup> H. Zhan, Q. Liu, S.-K. So, W.-Y. Wong, *Journal of Organometallic Chemistry*, **2019**, 894, 1-9

DPP-based conjugated polymers with common feature used for photovoltaic is the small band gap in range 1.25-1.55 eV,<sup>210</sup> that creates a broad optical absorption up to 1000 nm, good film-forming characteristics and film morphology resulting in good FF and high short circuit current  $I_{sc}$ . Hence, a high and remarkable PCE exceeded 10 % in single junction and 11 % in multijunction organic solar cells were obtained.<sup>211</sup>

Several publications have been done in improving the PCE of photovoltaic by working on the developing various DPP-based conjugated polymers derivatives as donor materials through chemical modifications for higher charge mobility with keeping in mind the donor-acceptor approach.

**PBDTT-FDPP**, **PBDTT-DPP** and **PBDTT-SeDPP** (Figure 89) are three copolymers based on **BDT** as donor unit and DPP as the acceptor unit with promising efficiencies. The PCE is around 7 % in **PBDTT-SeDPP: PC<sub>71</sub>MB** and around 4.5 % in **PBDTT-FDPP: PC<sub>71</sub>MB** and 6.4 % in **PBDTT-DPP: PC<sub>71</sub>MB**.<sup>212</sup> The optical band gaps are 1.51, 1.46, and 1.38 eV, respectively. **DPP2TBP** (Figure 89) is another DPP based conjugated polymer flanked with two thiophene units and two phenyl rings with good PCE of 5.7 % in **DPP2TBP: PC<sub>71</sub>MB** with optical band gap of 1.63 eV.<sup>210</sup>

One of the electron donors with DPP unit is **PDPP3T**, which is a copolymer of DPP and terthiophene (Figure 89). **PDPP3T** affords high PCE of 7.4 % in organic solar cells with **PC<sub>71</sub>MB** as acceptor material. **PDPP3T $\alpha$ /tTPT** is a derivative of **PDPP3T** with enhanced PCE of 8 % in a blend with **PC<sub>71</sub>MB** material (Figure 89).<sup>213</sup>

---

<sup>210</sup> W. Li, A. Furlan, W. S. C. Roelofs, K. H. Hendriks, G. W. P. van Pruissen, M. M. Wienka, R. A. J. Janssen, *Chem. Commun.*, **2014**, 50, 679-681

<sup>211</sup> W. Li, K. H. Hendriks, M. M. Wienk, R. A. Janssen, *Acc. Chem. Res.*, **2016**, 49, 78

<sup>212</sup> L. Dou, W.-H. Chang, J. Gao, C.-C Chen, J. You, Y. Yang, *Adv. Mater.*, **2013**, 25, 825-831

<sup>213</sup> K. H. Hendriks, G. H. L. Heintges, V. S. Gevaerts, M. M. Wienk, R. A. J. Janssen, *Angew. Chem., Int. Ed.*, **2013**, 52, 8341

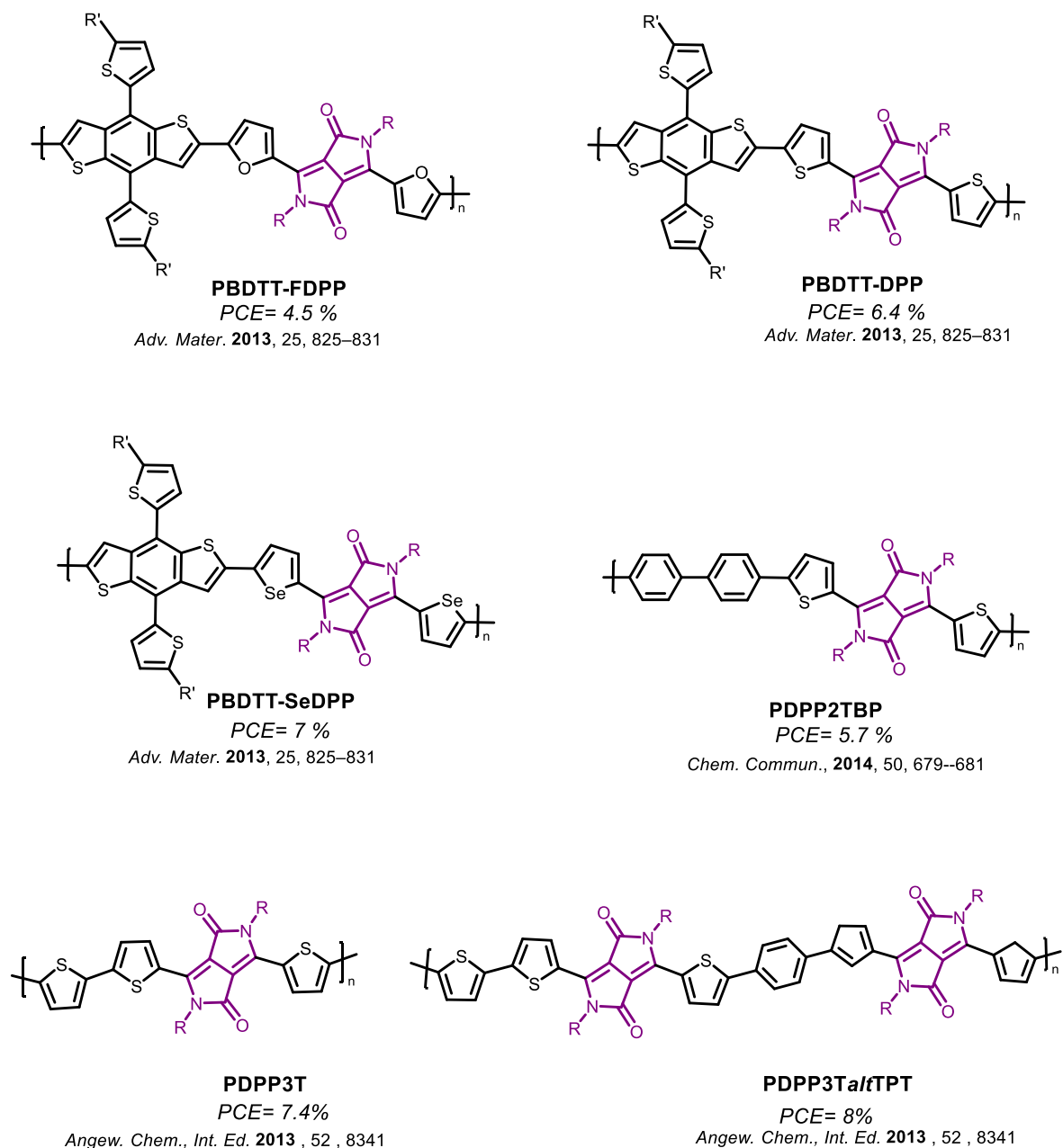


Figure 89: DPP based polymeric NFAs

Several analogues of DPP based conjugated polymers have been synthesized with phenyl **DPP-P**, thiophene unit **DPP-T** and with selenophene **DPP-Se**. The combination of these heterocyclic molecules with covalent bond to the lactam ring at position 3 and 6 opens the door in a multitude of D-A combinations for optimized electronic properties (Figure 90).

Thiophene unit has shown enhanced co-planarity and hence efficient  $\pi$ - $\pi$  stacking, where the donating strength and then the quinoidal form are affected due to the decrease in aromatic resonance energy compared to phenyl units.<sup>214</sup> Therefore, the DPP that is already widely used in the literature as a building block in donor materials attracts the attention for further chemical modifications while looking for enhanced PCE.

<sup>214</sup> J. Dhar, N. Venkatramaiah, Anitha A., S. Patil, *J. Mater. Chem. C*, **2014**, 2, 3457–3466

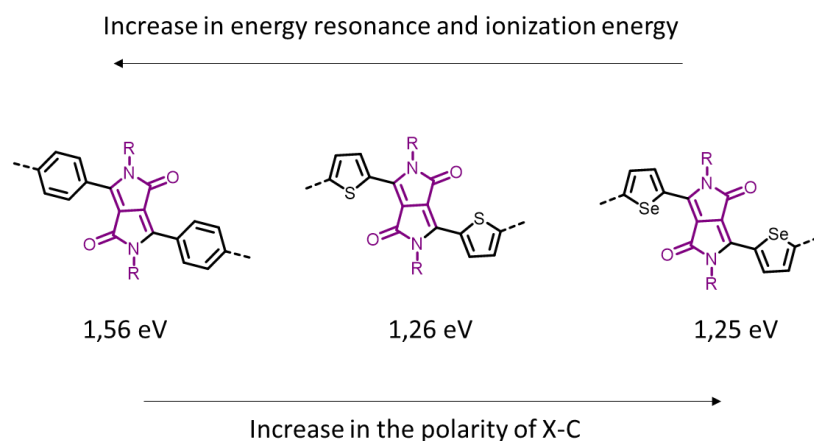


Figure 90: The differences in chemical properties of DPP unit engaged to different donor units

In extensive search for new semiconductors for optoelectronic applications, metallopolymers attracted attention due to their properties such as reversibility, solubility besides of their optoelectronic properties to be used as donor materials.

## 7. Metallopolymers:

Metallooligomers can be considered as the third type of donor materials. The main reason to use this type of polymers is the presence of a transition metal in the backbone of the conjugated polymer, which can change its coordination number or oxidation state. Hence, this process can modulate the conductive material between high and low conductivity.<sup>215</sup>

Metallopolymers offer the opportunity to tune the electronic structure of the polymer due to their small ionization potential. Upon direct contact with any illumination source, the excitons are generated followed with photon interaction leading to a reduced band gap. In main chain polymers this process is linked to the ligand used which represents the conjugated unit. These polymers are of tunable band gap nature, controlled morphology, long term stability, enhanced light absorption properties and high carrier mobility.<sup>216</sup>

### 7.1. Metal ligand coordination mode :

We can classify metallopolymers into two main types: Metallopolymer based on N-heterocyclic ligand and metallopolymer with metal-carbon alkyne conjugated system.

<sup>215</sup> J-C. Eloi, L. Chabanne, G.R. Whittell, I. Manners, *Mater. Today*, **2008**, 11, 28–36

<sup>216</sup> A. Verma, P. Chaudhary, R. K. Tripathi, A Singh, B. C. Yadav, *Inorg Organomet Polym*, **2022**, 32, 2807–2826

### 7.1.1. Metallopolymer based on N-heterocyclic ligand:

Several N-heterocyclic ligands have been used with transition metals due to their high binding affinity to metal ions to develop metallopolymers, as an example: Bis-terpyridine-Zn metallo-homo polymers derivatives (Figure 91).<sup>217</sup>

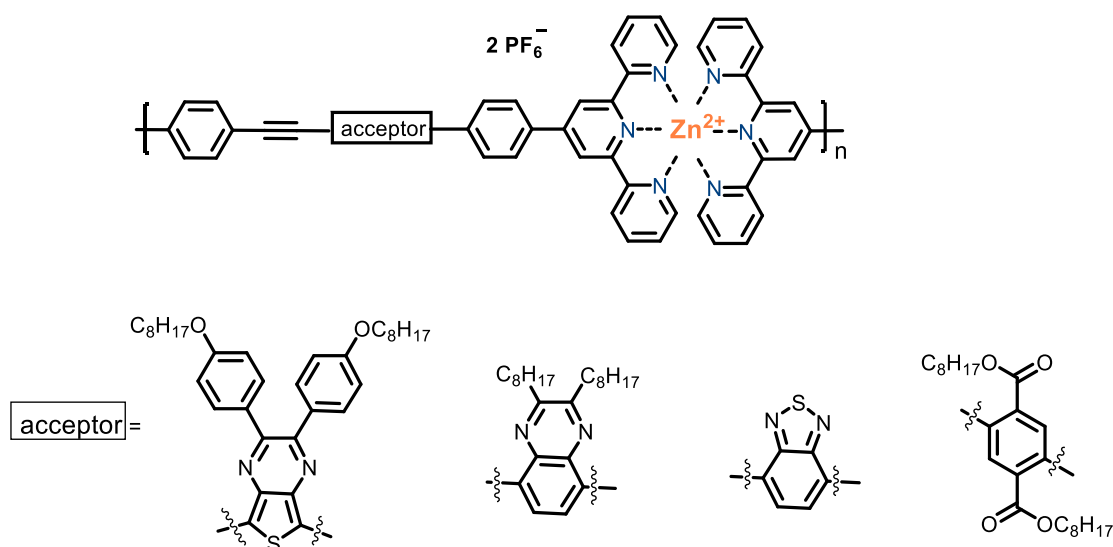


Figure 91: Zn metallopolymer derivatives

### 7.1.2. Metallopolymer based on metal-carbon alkyne conjugated system:

The second type of the conjugated system coupled with a transition metal for metallopolymers synthesis is the alkyne group system. There is a wide area of publications on this type of metal-carbon alkyne conjugated system. Therefore, poly(metal acetylide)s or so called Polymetallaynes, bis(acetylides) (Figure 92) are a well-studied class of main chain metallopolymers using ionic metal-carbon bond.<sup>218</sup>

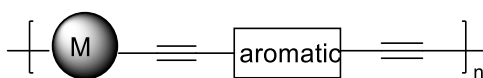


Figure 92: Poly(metal acetylide)s structure

The start of this metallopolymers was in 1970s with polymeric Pt and Pd by Sonogashira group.<sup>219</sup> These polymers involve group 8 to group 10 transition metals with increased stability with heavier metals that could be due to the increased ionic character of metal-carbon bond and the geometry type of the metal.

<sup>217</sup> F. Schlütter, A. Wild, A. Winter, M. D. Hager, A. Baumgaertel, C. Friebe, U. S. Schubert, *Macromolecules*, **2010**, 43, 6, 2759–2771

<sup>218</sup> A. La Groia, A. Ricci, M. Bassetti, D. Masi, C. Bianchini, C. Lo Sterzo, *J. Organomet. Chem.*, **2003**, 683, 406

<sup>219</sup> Y. Fujikura, K. Sonogashira, N. Hagihara, *Chem. Lett.*, **1975**, 1067



In this thesis we are interested in polymetallayne with Pt transition metal of group 10 and a spacer unit (Figure 93).

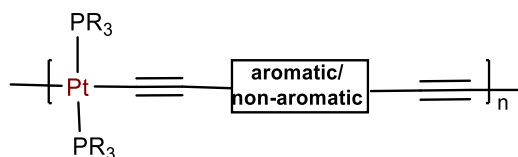


Figure 93: Structure for polymetallayne

Given all the consideration above and the intrinsic properties of the transition metal insertion in conjugated polymers backbone on the photophysical properties, DPP-based D-A metallooligomers attract a huge attention as donor materials for organic solar cells and more precisely in BHJ OSCs.

## 7.2. Metallooligomers in organic solar cells:

In 2019, Zhan, Wong and *al*<sup>220</sup> have reported a new series of conjugated organometallic D-A polymers with DPP core flanked with thiophenes ended with a triple bond connected to Pt-complex. These compounds are used as donors in BHJ solar cells, and the devices exhibit PCE from 0.33-1.40 %. However, the Pt containing metallooligomers attract widespread attention because of their additional advantages to enhance optical and optoelectronic properties. The solubility of the metallooligomer is increased with alkyl chain on lactam function and bulky phosphines, like **P1**, **P2** and **P3** represented in figure 94. Besides, the insertion of a supplementary thiophene for **P3** helps to increase the conjugation length, which can tune the levels of the bands from their electronic structure with a decrease of the optical band gap. But the rigidity of the organic part could increase, hence the decrease of the solubility could be overcome with the presence of a solubilizing chain  $n\text{-C}_6\text{H}_{13}$  on the additional thiophene moiety (Figure 94).

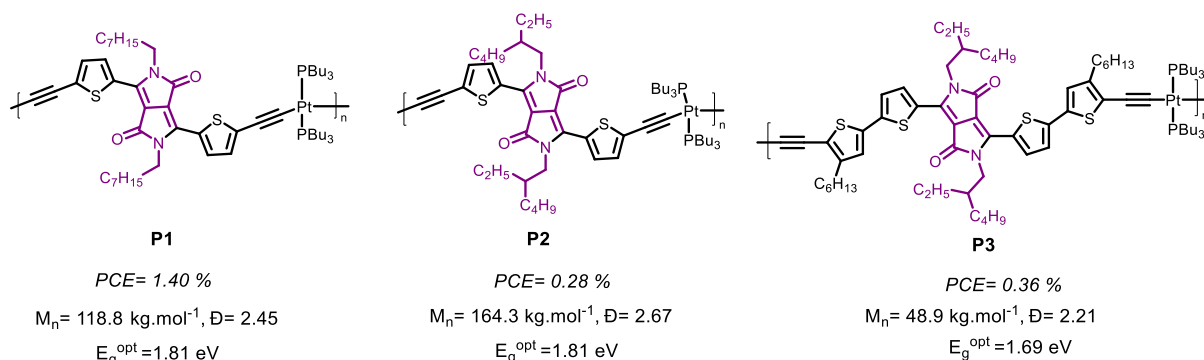


Figure 94: The DPP based metallooligomers synthesized by Zhan, Wong and *al*.<sup>220</sup>

In the literature, the increase of the average molar mass ( $M_n$ ) and the  $\pi$ -aggregation of the chain lead to the enhancement of optoelectronic properties.<sup>221</sup> A better solubility is favored using branched chains and bulky phosphines, it helps to prepare metallooligomers

<sup>220</sup> H. Zhan, Q. Liu, S.-K. So, W.-Y. Wong, *J. Organomet. Chem.*, **2019**, 894, 1.

<sup>221</sup> M.C. Scharber, D. Muhlbacher, M. Koppe, P. Denk, C. Waldauf, A.J. Heeger, C.J. Brabec, *Adv. Mater.*, **2006**, 18, 789-794

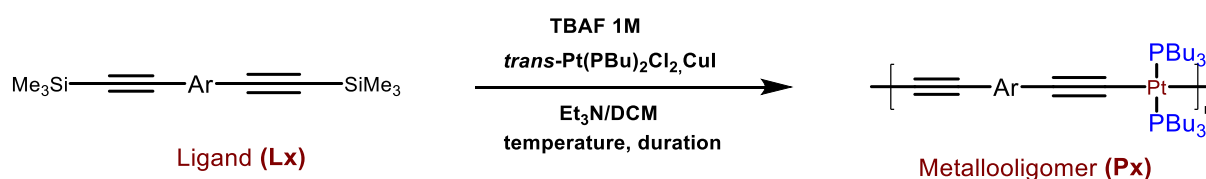
with higher  $M_n$ . However, the use of linear chain is still interesting to improve aggregation, but the risk is a decrease of the solubility. Hence, a balance must be made between good solubility with  $\text{PBU}_3$  and improved aggregation with linear chain  $n\text{-C}_8\text{H}_{17}$  as compound **P3** (Figure 94). It has a lower  $M_n$  but close to those of **P1** and it exhibits a better PCE of 1.40 % (**P1**, PCE= 0.28 %) with **PC<sub>71</sub>BM** as acceptor.

In addition, the advantages of the strategy applied for the preparation of **P3** is the increase in the conjugation length with the insertion of two thiophene units, the decrease of the optical band gap and the enhancements of the optical properties by increasing the wavelength range. Comparison of the absorption spectra of **P2** and **P3** shows a bathochromic shift of 28-30 nm of the absorption wave onset ( $\lambda_{\text{abs}}^{\text{(onset)}}$ ). A narrower optical band gap of 1.69 eV is obtained for **P3** with respect to 1.81 eV obtained for **P2**.<sup>222</sup>

Based on literature results, the team has decided to synthesis an analogue **P1'** of **P1** (Figure 95) as a reference compound. Our collaborator from LNMIIT in India, Pr. Ganesh D Sharma used **P1'** as donor with **PC<sub>71</sub>BM** in BHJ solar cells and the performances were evaluated with a PCE of 7.62 %. The significant difference with **P1** from the work of Wong and  $a^{\text{I}220}$  is the application solvent vapor annealing treatment (SVA) on the active layer to improve the molecular organization of the blend for an enhancement of the performances.<sup>223</sup> This work was made during the PhD of Mélodie NOS (2015-2018) in the group Polymers & Materials, POHET team. A part of it was dedicated to the preparation of narrow band gap metallooligomers to increase the wavelength range for enhanced optical properties to improve the solar cell performances. This work is summed up in the following part "preliminary results".

## 8. Preliminary results:

In the team POHET, the first metallooligomers have been prepared during the PhD of Mélodie Nos (2015-2018). As described in scheme 1, the metallooligomers are synthesized by a dehydrohalogenation reaction between a deprotected ligand and a  $\text{trans-PtCl}_2(\text{PBU}_3)_2$  complex in the presence of  $\text{CuI}$  and a base.



*Scheme 1: The general synthesis of metallooligomers using dehydrohalogenation reaction*

The metallooligomer **P1'** has been synthesized as a reference compound. In order to decrease the optical band gap, two strategies were applied based on the increase of the conjugation length as described in figure 95. The first strategy is to add two thiophene (T) units

<sup>222</sup> M. Nos, G. Marineau-Plante, D. Gao, M. Durandetti, J. Hardouin, P. Karsenti, G. Gupta, G. D. Sharma, P. D. Harvey, C. Lemouchi, L. Le Pluart, *J. Mater. Chem. C*, **2020**, 8, 2363-2380

<sup>223</sup> M. Jiang, H-r Bai, H-f Zhi, J-k Sun, J-l Wang, F. Zhang, Q. An, *ACS Energy Lett.*, **2021**, 6, 8, 2898–2906

with the preparation of **PA** and the second strategy is to use T-DPP-T dimers in the organic part of the ligand with the preparation of **P2'** (Figure 95).

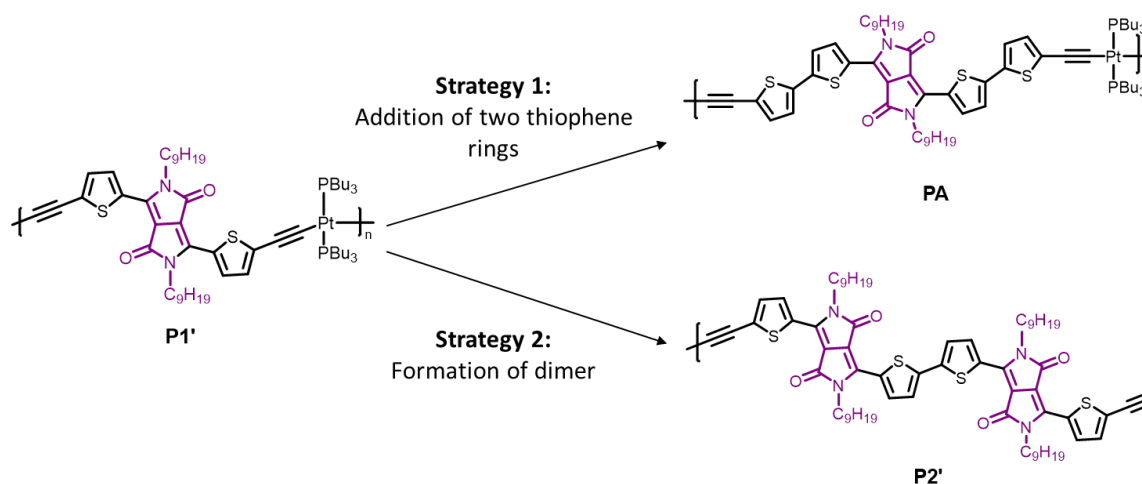


Figure 95: The two strategies followed to improve the properties of **P1'**

The metallooligomers were purified on biodead X1<sup>®</sup> then characterized by  $^1\text{H}$ ,  $^{31}\text{P}\{^1\text{H}\}$  NMR and by GPC for average molar mass determination. **P1'** has the higher average molar mass of  $18.2 \text{ Kg.mol}^{-1}$  with  $\mathcal{D}$  of 2.1 compared to **PA** ( $M_n = 12\text{-}13 \text{ Kg.mol}^{-1}$ ,  $\mathcal{D} = 2.3$ ) and **P2'** ( $M_n = 6\text{-}7 \text{ Kg.mol}^{-1}$ ,  $\mathcal{D} = 11.1$ ). **P2'** has the lowest  $M_n$  and the highest dispersity. This could be explained by an instability of the deprotected ligand during the preparation of the metallooligomer (Table 1).

Table 1: The analysis data of characterizations carried for **P1'**, **PA** and **P2'**

	$M_n$ $\text{Kg.mol}^{-1}$	$\mathcal{D}$	Number of units	$T_d$ ( $^\circ\text{C}$ )
<b>P1'</b>	18.2	2.1	15	221
<b>PA</b>	12-13	2.3	9-10	273
<b>P2'</b>	6.6	11.1	3-4	261

The optical properties were investigated by absorption spectroscopy. The spectrum of **PA** shows an increase in the  $\lambda_{\text{abs}}^{\text{(onset)}}$  of 66 nm in comparison to **P1'**, which evidenced the decrease of the optical band gap of 1.72 eV in **P1'** to 1.60 eV in **PA**. However, strategy 2 was more efficient in the decrease of  $E_g^{\text{opt}}$  because the absorption spectrum of **P2'** exhibits a bathochromic shift of  $\lambda_{\text{abs}}^{\text{(onset)}}$  of 156 nm, which corresponds to a narrower optical band gap of 1.42 eV for **P2'** in respect of 1.72 eV for **P1'** (Table2).

Table 2: The optical and electrochemical analysis data of **P1'**, **PA** and **P2'** and their corresponding ligands

	$\lambda_{\text{abs}}^{(\text{max})}$ ( $\epsilon\lambda$ )		$\lambda_{\text{abs}}^{(\text{max})}$ In Solution nm	$\lambda_{\text{abs}}^{(\text{onse})}$ nm	$E_{\text{g}}^{\text{opt}}$ eV	$E_{\text{ox}}^{\text{onset}}$ V/ESC	$E_{\text{red}}^{\text{onset}}$ V/ESC	HOMO eV	LUMO eV	$E_{\text{g}}^{\text{elec}}$ eV
<b>L1'</b>	<b>554 (3.71), 599 (4.44)</b>	<b>P1'</b>	599, 646	719	1.72	0.65	-0.97	-5.38	-3.76	1.62
<b>LA</b>	<b>347, 594 (4.89), 634 (5.02)</b>	<b>PA</b>	337, 663	785	1.60	0.71	-1.00	-5.44	-3.73	1.71
<b>L2'</b>	<b>648 (1.42), 669 (1.39)</b>	<b>P2'</b>	654, 718	875	1.42	0.63	-0.78	-5.36	-3.95	1.41

Onset potential (V vs SCE) for reduction ( $E_{\text{red}}^{\text{onset}}$ ) and oxidation ( $E_{\text{ox}}^{\text{onset}}$ ). HOMO and LUMO energies calculated with the equation  $E_{\text{HOMO}} = -(E_{\text{ox}}^{\text{onset}} + 4.73)$  eV,  $E_{\text{LUMO}} = -(E_{\text{red}}^{\text{onset}} + 4.73)$  eV.  $E_{\text{g}}^{\text{elec.}} = E_{\text{LUMO}} - E_{\text{HOMO}}$  (eV)

The values of HOMO and LUMO levels were determined from onset potentials obtained with cyclic voltammetry, as well as the corresponding band gap values of the three metallooligomers **P1'**, **PA** and **P2'**. **P2'** shows a band gap of 1.41 eV, which is smaller with respect to 1.71 eV and 1.62 eV band gaps of **PA** and **P1'**, respectively. The smaller band gap of **P2'** could be due to the extension in the conjugation length of the conjugated backbone. The bands electronic structure and the band gap values make **P1'**, **PA** and **P2'** promising candidates as donor materials associated to acceptors in solar cells.

Therefore, the photophysical properties of **P1'** and **P2'** were investigated to evaluate the time of electron transfer and recombination with fullerene acceptor **PCBM**. Both metallooligomers exhibit fluorescence lifetimes in ps timescale, which is long enough for efficient photo-induced electron transfer to the acceptor (**PCBM**).<sup>222</sup> These results are promising; hence, they were used in BHJ solar cells as donors. Nevertheless, because of limited quantities of **PA**, this metallooligomer was not used as a donor in BHJ solar cells.

The photovoltaic performances of BHJ solar cells were investigated with **P1'** and **P2'** as donors with **PC<sub>71</sub>BM** as acceptor with optimal weight ratio donor: acceptor of 1:1.5. The average values of PCE are 7.62 and 9.54 % for **P1'**: **PC<sub>71</sub>BM** and **P2'**: **PC<sub>71</sub>BM**, respectively (Table 3).

Table 3: Photovoltaic parameters of the optimized polymer solar cells based on **P1'** and **P2'** as donor and **PC<sub>71</sub>BM** as acceptor.

polymer	$I_{sc}$ (mA/cm <sup>2</sup> )	$\mu_e$ cm <sup>2</sup> /Vs	$\mu_h$ cm <sup>2</sup> /Vs	$V_{oc}$ (V)	FF	PCE (%)
<b>P1'</b>	12.96	$2.29 \times 10^{-4}$	$9.93 \times 10^{-5}$	0.92	0.597	7.12 (7.01) <sup>a</sup>
<b>P2'</b>	16.24	$1.15 \times 10^{-4}$	$2.38 \times 10^{-4}$	0.89	0.667	9.54 (9.42) <sup>a</sup>

<sup>a</sup> average of 8 devices

In the literature, Miyake and *al* have synthesized an analog of **PA**.<sup>224</sup> The difference is the functionalization of the lactam functions with branched alkyl chain instead of the linear chain of **PA**. This compound exhibits a lower average molar mass of 8.8 Kg.mol<sup>-1</sup>.<sup>224</sup> The electrochemical, optical and optoelectronic properties were not investigated because of its poor solubility contrary to **PA** which exhibits a good solubility (Figure 96).

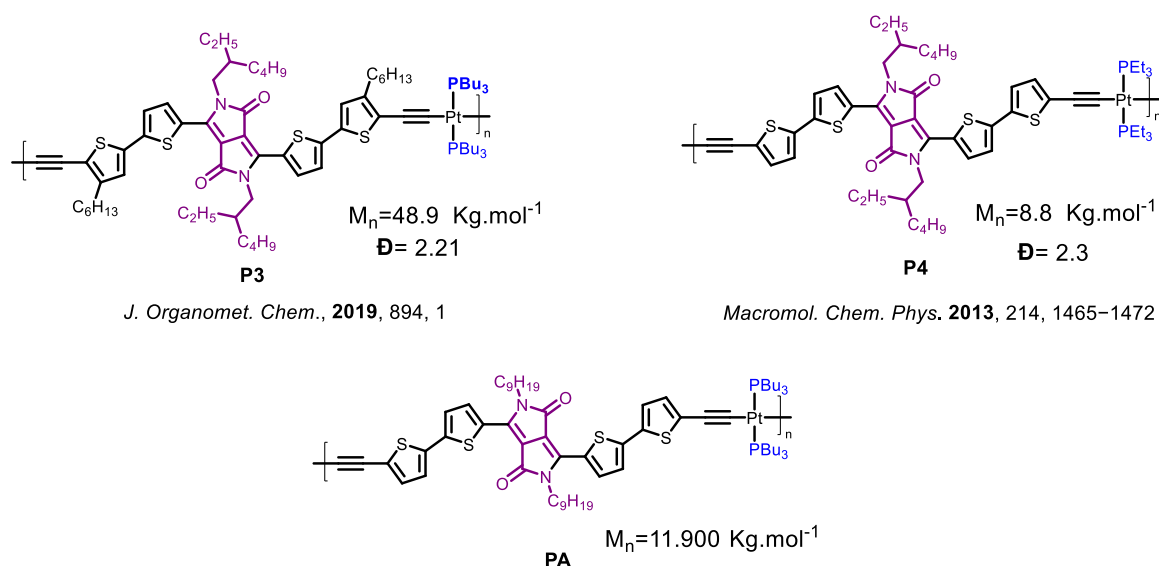


Figure 96: The metallooligomer synthesized in the team

Based on these preliminary results, it would be interesting to prepare larger quantities of **PA** and to use it as a potential donor in BHJ solar cells. Another aspect is to overcome the stability problems of the deprotected ligand **L2'** which prevents the formation of longer chains **P2'**. Therefore, the objectives are the preparation of longer chains metallooligomers of **PA** for studying its photovoltaic performance in BHJ solar cells and to synthesize new ligands with higher stability than **L2'** for a narrow optical band gap metallooligomers ( $E_g^{\text{opt.}} = 1.4\text{-}1.5 \text{ eV}$ ).

<sup>224</sup>Y. Yuan, T. Michinobu, J. Oguma, T. Kato, K. Miyake, *Macromol. Chem. Phys.*, **2013**, 214, 1465–1472

## II. New DPP based metallooligomers:

The objective of my project is to improve the strategies 1 and 2. For strategy 1, my work focused on the increase of the average molar mass by (1) the improvement of the reaction conditions of metallooligomers **PA** preparation and by (2) applying functionalization step of two thiophene moieties with solubilizing chains  $C_{12}H_{25}$ . For strategy 2, the aim is to overcome the stability problem of the deprotected ligand **L2'**. Hence, we have decided to synthesize a new ligand **LC** for the preparation of a new narrow band gap metallooligomer **PC** with the insertion of EDOT unit with a better stability and prepared from an easier synthesis. The targets are depicted in figure 97.

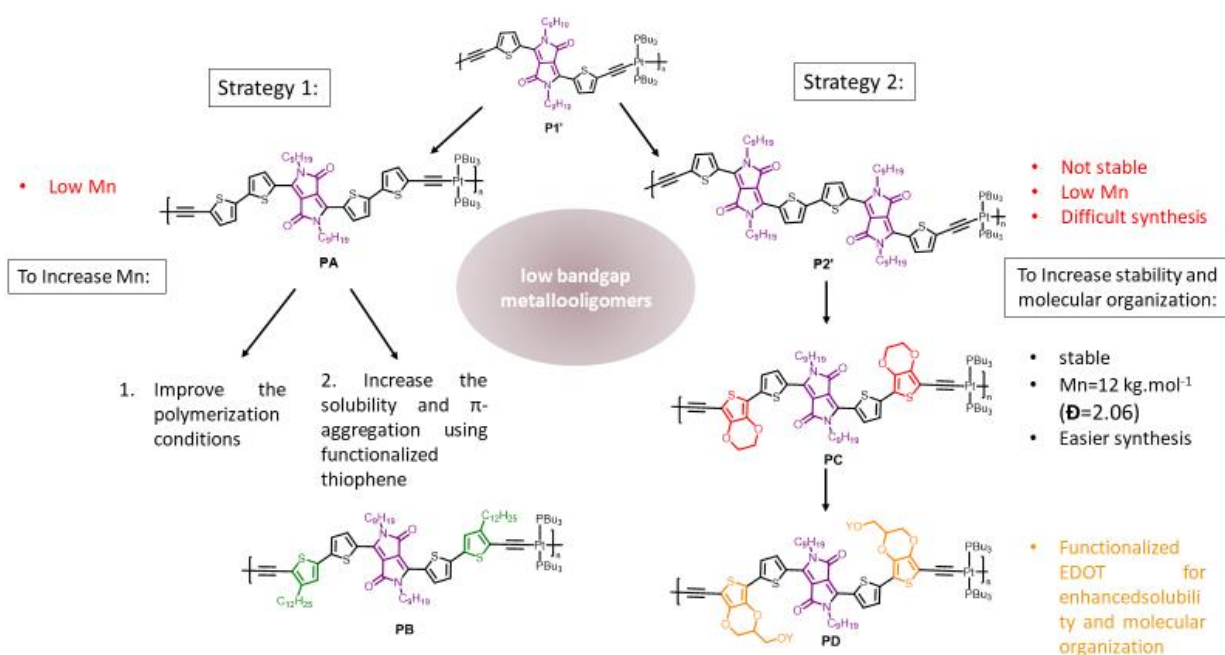


Figure 97: The general scheme for low band gap metallooligomers

The metallooligomers are prepared by a dehydrohalogenation reaction between deprotected ligands **Lx** and  $\text{trans PtCl}_2(\text{PBu}_3)_2$  in the presence of  $\text{CuI}$  and a base. The silyl groups TMS are removed in situ with a solution of tetrabutylammonium fluoride. In my project, we have decided to prepare the targets **A**, **B**, **C** and **D** depicted in figure 98, for the enhancement of the optical and optoelectronic properties of the donors.

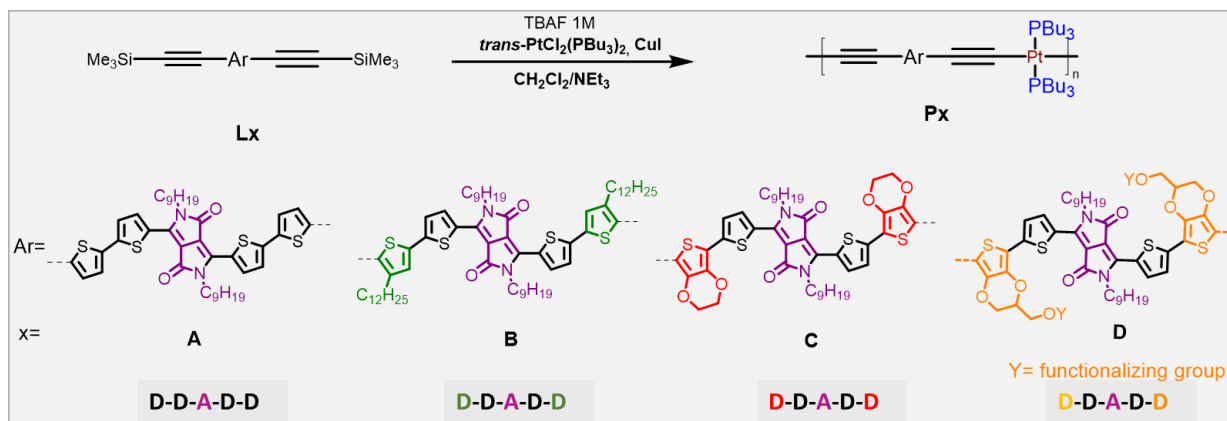


Figure 98: The synthesis overview of main targets of chapter 2

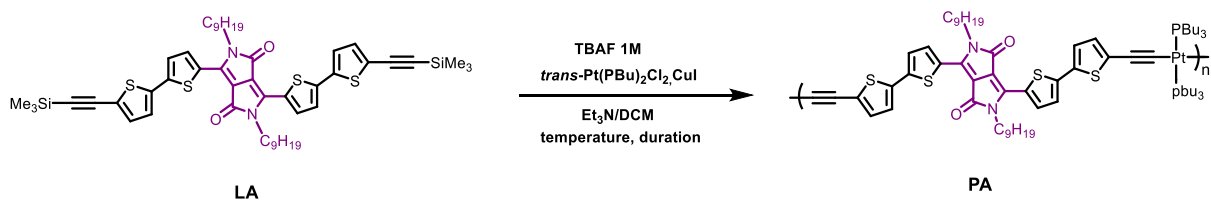
The metallooligomers are purified by biobead X1<sup>®</sup>. This exclusion steric static phase permits to remove the remaining ligand and impurities. The formation of the metallooligomers is checked by <sup>31</sup>P{<sup>1</sup>H} NMR with the observation of a single signal attributed to phosphorous atoms of the phosphines and a value of the coupling constant  $J_{\text{Pt-P}}$  close to 2200-2600 Hz, which corresponds to trans geometry of the ligands in the square planar [Pt]-complex. The complexation of the ligand to platinum is evidenced by <sup>1</sup>H NMR with a variation of the chemical shift of the protons from thiophene units. Then, the average molar masses of the obtained metallooligomers are determined by GPC. These data could be confirmed by MALDI-TOF analysis carried out by Julie Hardouin at PBS laboratory and PISSARO platform, Rouen. The optical properties are investigated by absorption spectroscopy on liquid and thin films with the determination of  $\lambda_{\text{abs}}(\text{onset})$  to calculate the optical band gap. In parallel, the electrochemical properties are studied by cyclic voltammetry, carried out by Muriel Durandetti in COBRA laboratory, Rouen to determine the HOMO and LUMO levels and the value of the electrical band gap ( $E_{\text{g}}^{\text{elec.}}$ ). In addition, the thermal properties were investigated. Thermogravimetric analysis (TGA) was carried to indicate the decomposition temperature of each metallooligomer as well as XRD was used to study the microstructure.

## 1. Strategy 1: to increase the molecular mass $M_n$ of DPP based metallooligomers:

The objective of this strategy is to increase the average molar mass by following two ways: (1) Improving the reaction conditions of metallooligomer **PA** preparations and (2) functionalizing of thiophene units with a solubilizing chain for the synthesis of a new metallooligomer **PB**.

### 1.1. Improving the reaction conditions of metallooligomer PA:

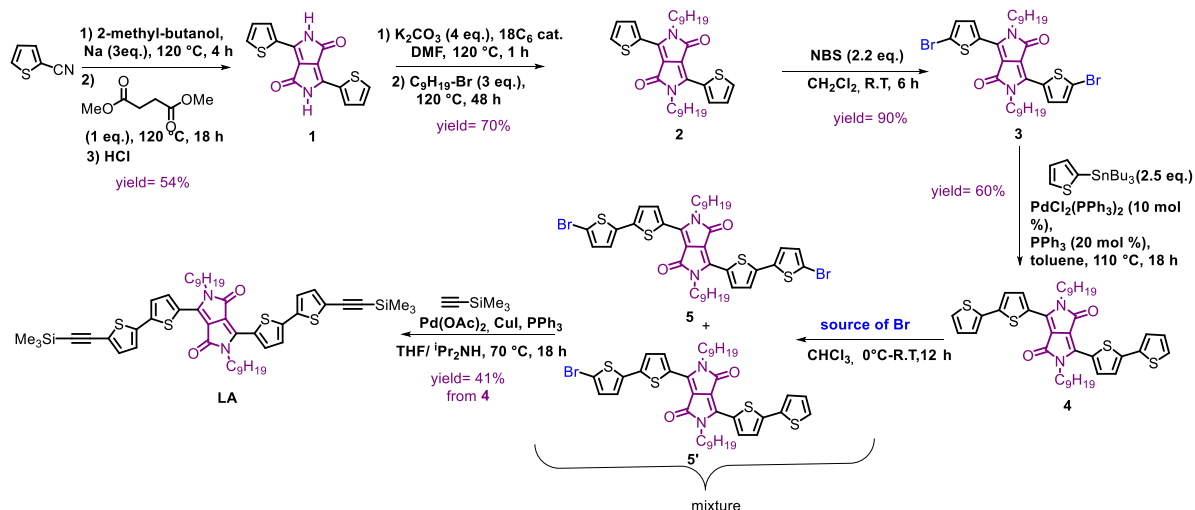
To begin with, the reaction conditions of the dehydrohalogenation, depicted in scheme 2, have been modified to increase the average molar mass of **PA**. In prior, larger quantities of ligand **LA** are required to test several conditions.



Scheme 2: The synthesis of metalloligomers **PA**

### 1.1.1. Synthesis of **LA** :

The synthesis of **LA** is prepared in six steps from 2-thiophenecarbonitrile according to modified procedures as illustrated in scheme 3.



Scheme 3: The synthetic scheme of **LA**

In the literature, several procedures exist to synthesize the DPP core from a double condensation reaction between two 2-thiophene carbonitrile and bis ester derivative. The yields vary from 20 % to 90 %.<sup>225,226,227</sup>

The procedure followed in the team is inspired by the work of *J. M. J. Fréchet*<sup>228</sup> with a yield of 54 %. The first step is the addition of excess of sodium to 2-methylbutanol for the formation of alcoholate. The next step is deprotonation of the ester to form enolate ion and its nucleophilic addition to the cyanide function. The same mechanism is repeated twice. The product **1** is isolated with a yield of 54 %.

The second reaction is the alkylation of lactam function. The linear alkyl chains are installed by nucleophilic substitution between deprotonated N of the lactam and halogenated chain in the presence of potassium carbonate and 18-crown-6 in DMF. Compound **2** is

<sup>225</sup> B. Fu, J. Baltazar, A. R. Sankar, P-H. Chu, S. Zhang, D. M. Collard, E. Reichmanis, *Adv. Funct. Mater.*, **2014**, 24, 3734.

<sup>226</sup> C. Wang, Y. Qin, Y. Sun, Y-S. Guan, W. Xu, D. Zhu, *ACS Appl. Mater. Interfaces*, **2015**, 7, 15978.

<sup>227</sup> R. Y. Mahale, S. S. Dharmapurikar, M. K. Chini, *Chemical Physics Letters*, **2018**, 696, 48.

<sup>228</sup> C. H. Woo, P. M. Beaujuge, T. W. Holcombe, O. P. Lee, J. M. J. Fréchet, *J. Am. Chem. Soc.* **2010**, 132, 15547



obtained with a yield of 70 %. Then, **2** was brominated at the position 2 of the thiophene moieties with N-bromosuccinimide (NBS) to form compound **3**. It is carried out away from light to avoid side reactions. The brominated compound **3** was isolated with a yield of 90 %. Afterwards, thiophenes are inserted after a Stille coupling reaction between compound **3** and 3-tributylstannyl-thiophene catalyzed with Pd(PPh<sub>3</sub>)<sub>2</sub>Cl<sub>2</sub>. The compound **4** was obtained with a yield of 60 %.

The bromination of compound **4** is the limiting step because of the formation of two products monobrominated **5** and bisbrominated **5'**, and with the consumption of the starting materials in a side reaction of oxidative polymerization. The purification step for separating the two compounds **5** and **5'** is tedious. Their presence was confirmed by <sup>1</sup>H NMR and mass spectrometry analysis. Therefore, the mixture was directly engaged in Sonogashira coupling reaction for the preparation of ligand **LA**.

To improve the yield of the formation of ligand **LA**, the reaction conditions of the bromination step have been optimized. The tested conditions are listed in table 4. The comparisons are made from the yields of the formation the ligand **LA** calculated for the two last steps from intermediate **4**, since the mixture **5** and **5'** was directly engaged in Sonogashira coupling reaction. For the calculated yields listed in table 4, the same reaction conditions for the Sonogashira coupling have been applied (the best condition is described in scheme 4 and in the next paragraph). The initial condition (Entry 1, Table 4) is inspired from the manuscript of Mélodie NOS and reported procedure.<sup>220</sup> The yield of the formation of ligand **LA** is low of 14 % yield. This could be explained by the formation of insoluble side product of oxidative polymerization.<sup>229</sup> To prevent the side reaction, the number of equivalents of NBS was decreased from 2.25 to 2.00 eq. and it was added in several portions (Entry 2, Table 4), but the yield was not improved. Then, bromine was used instead of NBS inspired from reported procedure.<sup>230</sup> Bromine was added at 0 °C, then the reaction was carried out at room temperature (Entry 3, table 4). The yield was significantly improved to 40 %, but the reaction suffers from a lack of reproducibility. Hence, the reported conditions have been modified by keeping the temperature in the temperature range -5 to 0 °C during the reaction (Entry 4, Table 4, conditions optimized during the project of resynthesis of **PC**). These new conditions permit to improve the yield from 14 to 41 % with a good reproducibility.

Table 4: The conditions of bromination reaction for the synthesis of intermediate **5**

Entry	Source of Br	Solvent	Temperature	Duration	Yield
<b>1</b> <sup>231</sup>	NBS (2.25 eq.)	CH <sub>2</sub> Cl <sub>2</sub>	0 °C to R.T	12 h	14 %
<b>2</b>	NBS (2.1 eq.)	CHCl <sub>3</sub>	0 °C to R.T	12 h	14 %
<b>3</b>	Br <sub>2</sub> (2 eq.)	CHCl <sub>3</sub>	0 °C to R.T	3 h	40 %
<b>4</b>	Br <sub>2</sub> (2 eq.)	CHCl <sub>3</sub>	< 0 °C	3 h	41 %

<sup>229</sup>A. Patra, V. Agrawal, R. Bhargav, Shahjad, D. Bhardwaj, S. Chand, Y. Sheynin, M. Bendikov, *Macromolecules*, **2015**, 48, 24, 8760–8764

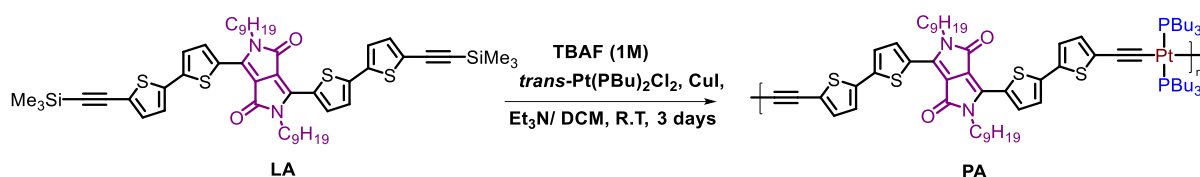
<sup>230</sup>C. Kanimozhi, N. Yaacobi-Gross, E. K. Burnett, A. L. Briseno, T. D. Anthopoulos, U. Salzner, S. Patil, *Phys. Chem. Chem. Phys.*, **2014**, 16, 17253-17265

<sup>231</sup> Manuscript sygal\_fusion\_28082-nos-melodie

The final step is a Sonogashira coupling reaction between brominated compounds **5** and **5'** and trimethylsilylacetylene (TMSA) in the presence of Pd catalyst, CuI and a base. From the initial conditions,<sup>232</sup> the yield was increased by changing Pd(OAc)<sub>2</sub> by Pd(PPh<sub>3</sub>)<sub>2</sub>Cl<sub>2</sub>, the solvents, the base (<sup>i</sup>Pr<sub>2</sub>NH instead of Et<sub>3</sub>N) and by heating, inspired from reported procedure<sup>233</sup>. Thanks to these optimizations, larger quantities of **LA** have been prepared for the synthesis of metallooligomer **PA**. It helps us to test different reaction conditions to increase the average molar mass of **PA**.

### 1.1.2. Synthesis of PA :

In this part, the reaction conditions have been modified to increase the average molar mass ( $M_n$ ) of **PA** (Scheme 4).



Scheme 4: The synthesis of **PA**

After several attempts, the optimal condition is the use of an excess of ligand (1.8 eq. instead of 1.0 eq.) and CuI (0.5 eq. instead of 0.1 eq.) and longer reaction time (3 days instead of 1 day), Table 5. Metallooligomers with two-fold higher  $M_n$ ,  $M_n = 23.8 \text{ Kg.mol}^{-1}$  with  $\mathcal{D} = 2.8$  have been prepared (Entry 2, Table5).

Table 5: The best condition for the preparation of **PA** (Entry 2) compared to the initial condition (Entry 1)

Entry.	<b>LA</b>	trans-Pt(PBu) <sub>2</sub> Cl <sub>2</sub>	CuI	temperature	Duration	$M_n$ Kg.mol <sup>-1</sup>	$\mathcal{D}$
1	1.0 eq.	1 eq.	0.1 eq.	R.T	3 days	12.4	2.3
2	1.8 eq.	1 eq.	0.5 eq.	R.T	3 days	23.8	2.8

### 1.1.3. Characterizations of PA

The metallooligomer **PA** has been purified on X1<sup>®</sup> bio beads. The metallooligomer formation was confirmed by <sup>31</sup>P{<sup>1</sup>H} NMR. The spectrum represented in figure 32 displays a single signal at 3.55 ppm with a coupling constant  $J(^{31}\text{P}-^{195}\text{Pt})$  of 2306 Hz, which confirms the trans-geometry of the ligands in the square planar [Pt] complex. The NMR spectra of the two metallooligomers **PA**: short chains ( $M_n = 12\text{-}13 \text{ Kg.mol}^{-1}$ ) and long chains ( $M_n = 23\text{-}24 \text{ Kg.mol}^{-1}$ ) are compared in figure 99. <sup>31</sup>P{<sup>1</sup>H} NMR spectrum of **PA** consists of a second low intense signal at 7.5 ppm attributed to end-chain L-Pt(PBu<sub>3</sub>)<sub>2</sub>-Cl, which proves the presence of short chain metallooligomer. This signal is not present in the spectrum of long chains **PA**. After

<sup>232</sup> Q. Liu, C-L. Ho, Y. H. Lo, H. Li, W-Y. Wong, *J Inorg Organomet Polym.*, **2015**, 25, 159.

<sup>233</sup> Y. Yuan, T. Michinobu, J. Oguma, T. Kato, K. Miyake, *Macromolecule.chem.phys.*, **2013**, 214,1465-1472

complexation of the ligand to Pt(II)-complex, a chemical shift of -0.38 ppm of thiophene terminated proton nearby the triple bond is observed.

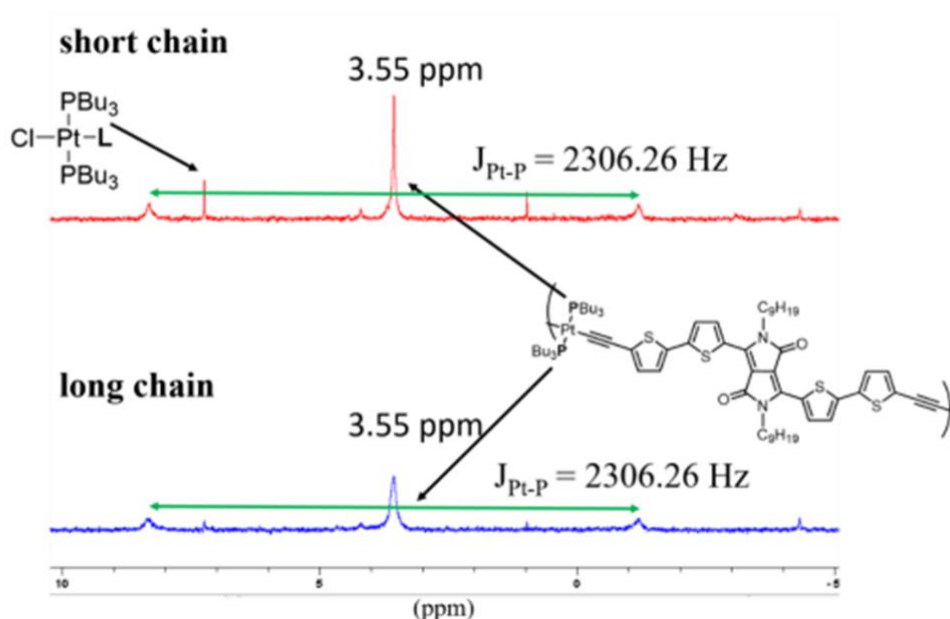


Figure 99: The  $^{31}\text{P}\{^1\text{H}\}$  NMR spectrum of **PA** of short ( $M_n = 12\text{-}13 \text{ Kg.mol}^{-1}$ ) and long chains ( $M_n = 23\text{-}24 \text{ Kg.mol}^{-1}$ )

Therefore, the formation of **PA** is confirmed by the variation of  $^1\text{H}$  chemical shift of protons from thiophene and by the comparison of IR-ATR spectra of ligand **LA** and polymer **PA**. A decrease in the vibration frequency of the band  $\nu(\text{C}\equiv\text{C})$  from 2140 to 2083  $\text{cm}^{-1}$  is observed. This is similar to the characterizations of **P1'** (Table 2). Then, the mass distribution is determined by GPC. The comparison of the chromatograms of **PA** short chains (Condition 1) and long chains (Condition 2), represented in figure 100, shows an increase in the  $M_n$  with the application of optimized reaction conditions 2. Using condition 2, the average molar mass is increased twice to 23-24  $\text{Kg.mol}^{-1}$  with  $\mathbf{D}$  of 2.8 in comparison with **PA** (short chains, condition 1) ( $M_n = 12\text{-}13 \text{ Kg.mol}^{-1}$ ,  $\mathbf{D} = 2.3$ ) (Figure 100). This corresponds to chains with an average length of 17-18 repeating units in comparison to 9-10 units for **PA** short chains (Condition 1).  $M_n$  of **PA** long chains is close to those of **P1'** with  $M_n = 18\text{-}19 \text{ Kg.mol}^{-1}$ ,  $\mathbf{D} = 2.1$ , and 14-15 repeating units (Table 2). Moreover, the decomposition temperature of **PA** is tested at 5 wt % loss and compared to that of **P1'**. The analysis is summarized in table 6.

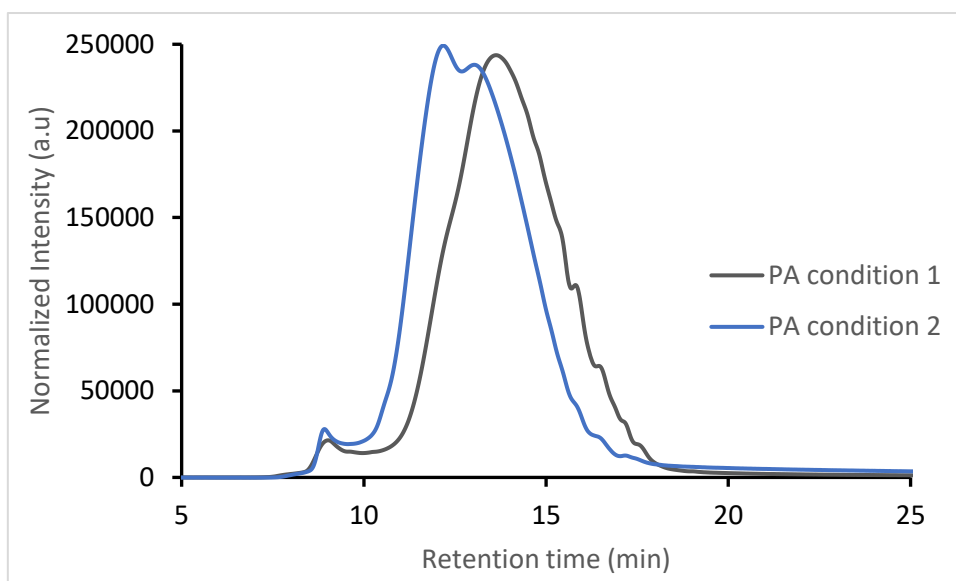


Figure 100: Comparison of GPC chromatograms of **PA** between condition 1, short chains,  $M_n=12-13 \text{ Kg.mol}^{-1}$  and condition 2, long chains,  $M_n=23-24 \text{ Kg.mol}^{-1}$

Table 6: The analysis data of **PA**

	$M_n$ ( $\text{Kg.mol}^{-1}$ )	$\mathcal{D}$	Number of units	$T_d$ ( $^{\circ}\text{C}$ ) <sup>a</sup>	$\Delta\delta\text{Ha}^b$ (ppm)	$\Delta\delta\text{Hb}^b$ (ppm)	$^{31}\text{P}$ (ppm)	$J_{P-Pt}$ (Hz)
<b>P1'</b>	18.2	2.1	14-15	221	0.13	-0.38	3.96	2289
<b>PA</b>	23.8	2.8	17-18	273	0.00	-0.38	3.55	2306

<sup>a</sup>Temperature at 5 wt % loss. <sup>b</sup>Ha and Hb refer to the first proton nearby the DPP acceptor unit and the first proton nearby the triple bond.

**PA** was analyzed with MALDI-TOF/MS with the 2-[(2E)-3-(4-tert-butylphenyl)-2-methylprop-2-enylidene]malononitrile (DCTB) matrix by Julie Hardouin, PBS, PISSARO, Rouen. The spectrum is represented in figure 101. It displays ion series from  $m/z$  1000 to 9000 with mass gap of 1360-1362 Da, which is equal to molecular mass of the repeating unit.

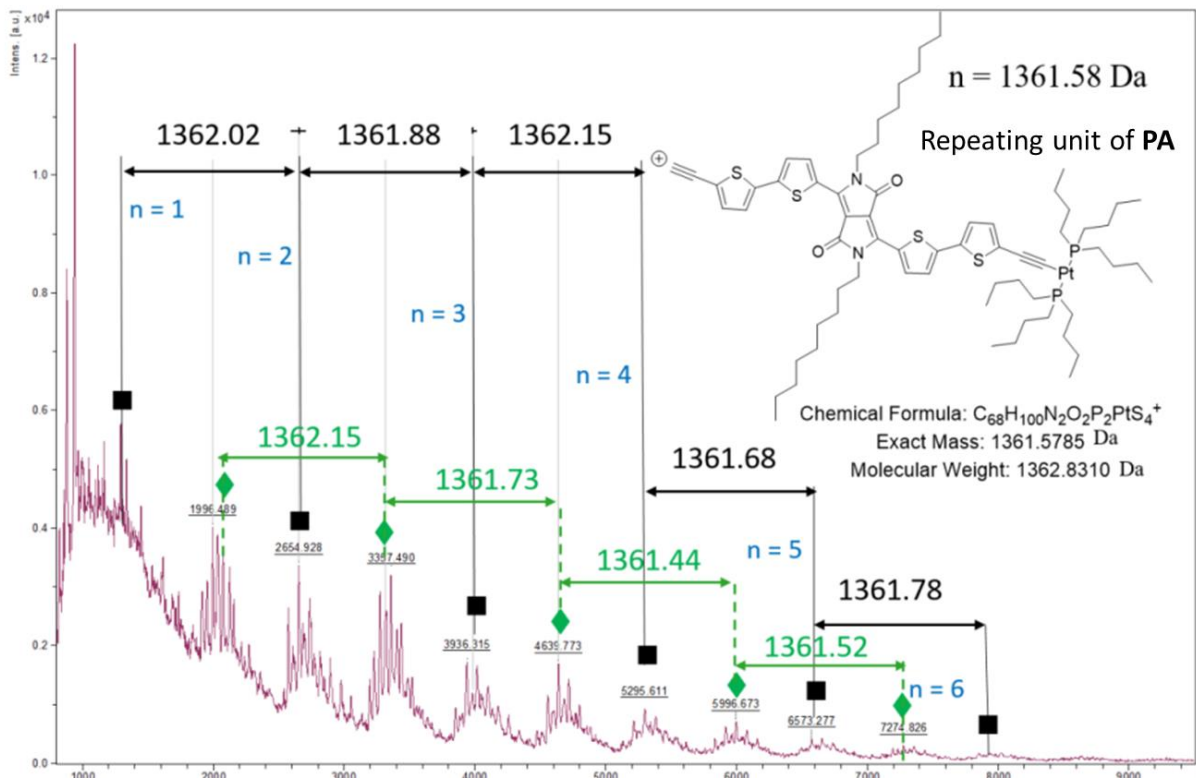


Figure 101: MALD-TOF spectrum of PA with the DCTB matrix

The optical properties of ligand **LA** and metallooligomer **PA** have been investigated by absorption spectroscopy on the liquids and on thin films with the determination of wavelength onset ( $\lambda_{\text{abs}}^{\text{(onset)}}$ ) to calculate the optical band gap and compared to those of **L1'** and **P1'**. The spectra are represented in figure 102 and figure 103 and the data are listed in table 7.

The absorption capacity of **LA** was investigated with the determination of the molar extinction coefficient ( $\epsilon_{\lambda}$ ). It is higher ( $4.89 \times 10^4 \text{ mol}^{-1} \text{ L cm}^{-1}$ ,  $5.02 \times 10^4 \text{ mol}^{-1} \text{ L cm}^{-1}$ ) than those of **L1'** ( $3.71 \times 10^4 \text{ mol}^{-1} \text{ L cm}^{-1}$ ,  $4.44 \times 10^4 \text{ mol}^{-1} \text{ L cm}^{-1}$ ). The comparison of the absorption spectra of the solutions in figure 102 shows a bathochromic shift of absorption band at the lowest energy from **LA** to **PA**, similar to **L1'**, **P1'**. It is explained by the increase of the conjugation length after the complexation reaction.

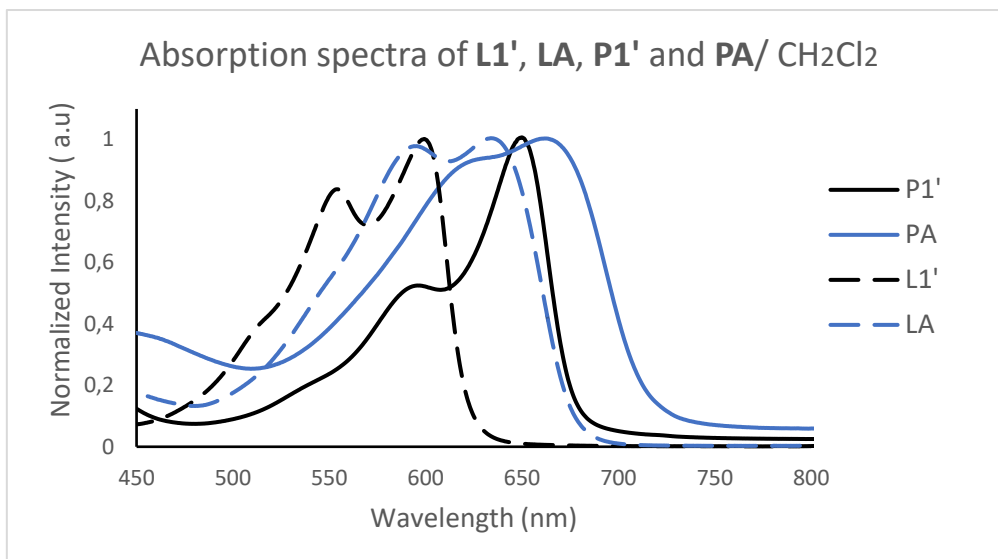


Figure 102: The absorption spectra of **L1'**, **LA**, **P1'** and **PA** in  $\text{CH}_2\text{Cl}_2$

Absorptions of **PA** were measured on thin films to evaluate the  $\lambda_{\text{abs}}^{\text{(onset)}}$  and to calculate the optical band gap ( $E_g^{\text{opt}}$ ). The spectra of **PA** and **P1'** are compared in figure 103 and the data are listed in table 7. As expected, a bathochromic shift of  $\lambda_{\text{abs}}^{\text{(onset)}}$  of 66 nm is observed from **P1'** to **PA**, which corresponds to a decrease of the optical band gap from 1.72 eV for **P1'** to 1.58 eV for **PA**.

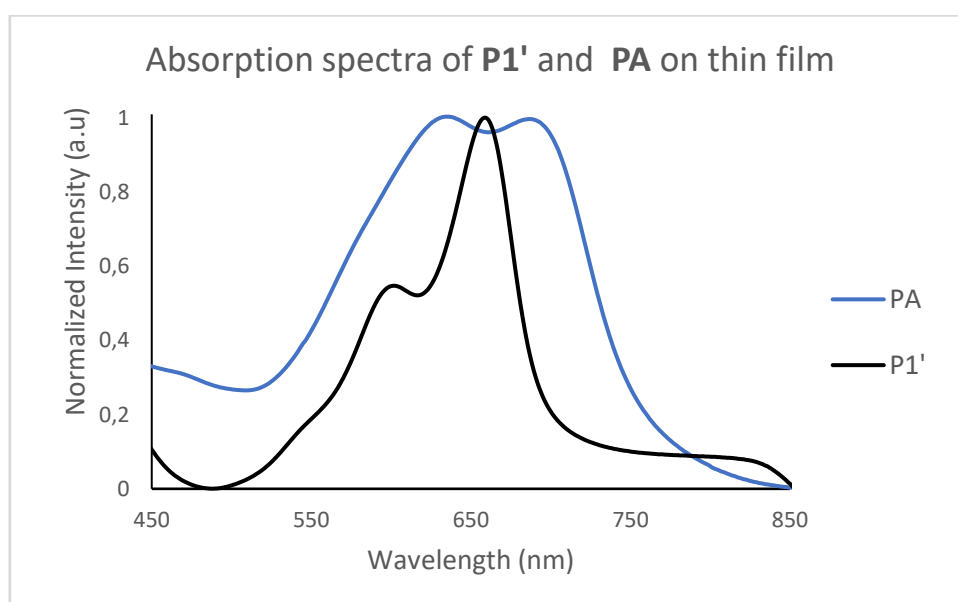


Figure 103: The absorption spectra of **P1'** and **PA** on thin film

The electrochemical properties of **PA** have been studied by cyclic voltammetry and compared to those of **P1'**. The bands electronic structures of **P1'** and **PA** are represented in figure 104 and they are compared to band levels of the acceptor **PC<sub>71</sub>BM** and **PC<sub>61</sub>BM**. The data are summarized in table 7. There is a decrease in the HOMO level for **PA** which is favorable to increase the  $V_{\text{oc}}$ . Otherwise, the values of LUMO levels are similar. The obtained

$E_g^{\text{elec}}$  are similar with 1.62 and 1.71 eV for **P1'** and **PA**, respectively. An increase of  $E_g^{\text{elec}}$  is observed. This trend is different to the decrease of the optical band gap from **P1'** (1.72 eV) to **PA** (1.58 eV), this decrease in the optical band gap is expected due to the extra two thiophene unit and the increase in the conjugation length. However, the deeper HOMO level obtained in cyclic voltammetry allows an increase in the  $V_{\text{oc}}$  value and consequently a higher solar cell performance.

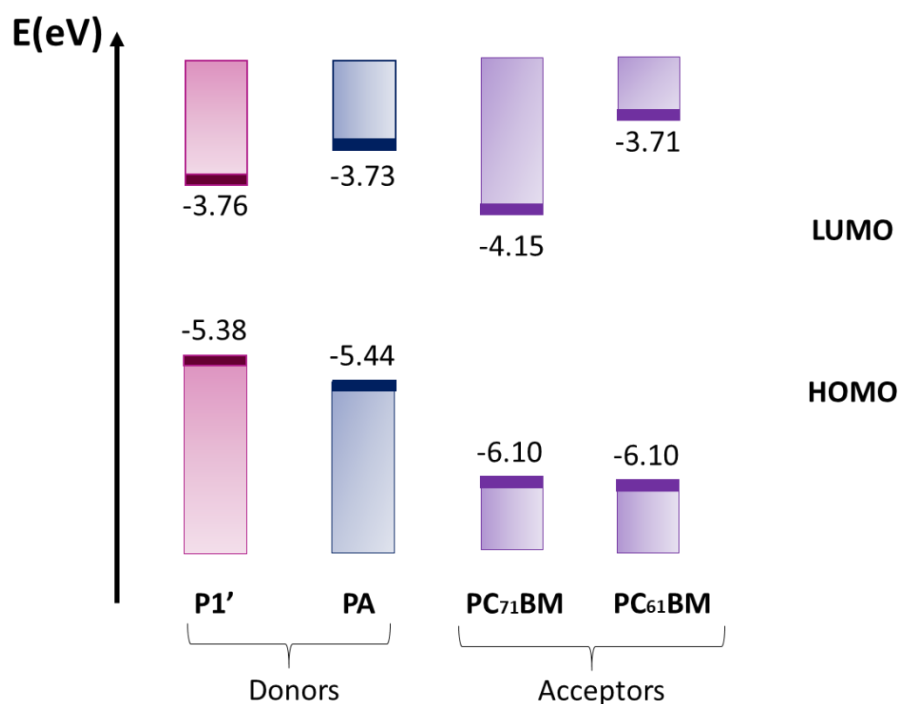


Figure 104: The bands electronic structure of **P1'**, **PA** (donors) and fullerene acceptors

Table 7: Optical and electrochemical properties data of the ligands **L1'**, **LA** and the metallooligomers **P1'**, **PA**

	$\lambda_{\text{abs}}^{\text{(max)}}(\epsilon_{\lambda})$ nm ( $10^4 \text{ mol}^{-1} \text{ Lcm}^{-1}$ )		$\lambda_{\text{abs}}^{\text{(max)}}$ Solution nm	$\lambda_{\text{abs}}^{\text{(onset)}}$ nm	$E_g^{\text{opt}}$ eV	$E_{\text{ox}}^{\text{onset}}$ V/ESC	$E_{\text{red}}^{\text{onset}}$ V/ESC	HOMO eV	LUMO eV	$E_g^{\text{elec}}$ eV
<b>L1'</b>	<b>554</b> <b>(3.71),599</b> <b>(4.44)</b>	<b>P1'</b>	599, 646	719	1.72	0.65	-0.97	-5.38	-3.76	1.62
<b>LA</b>	<b>595 (4.89),</b> <b>634 (5.02)</b>	<b>PA</b>	337, 663	785	1.58	0.71	-1.00	-5.44	-3.73	1.71

Onset potential (V vs SCE) for reduction ( $E_{\text{red}}^{\text{onset}}$ ) and oxidation ( $E_{\text{ox}}^{\text{onset}}$ ). HOMO and LUMO energies calculated with the equation  $E_{\text{HOMO}} = -(E_{\text{ox}}^{\text{onset}} + 4.73)$  eV,  $E_{\text{LUMO}} = -(E_{\text{red}}^{\text{onset}} + 4.73)$  eV.  $E_g^{\text{elec}} = E_{\text{LUMO}} - E_{\text{HOMO}}$  (eV)

After following the first way to increase the average molar mass by carrying optimization on the reaction conditions of the dehydrohalogenation reaction, we successively obtained long chains metallooligomer **PA** with twice the average molar mass of **PA** synthesized with the initial condition. Therefore, **PA** was investigated in photophysics to evaluate the phototransfer and electronic transfer with fullerene acceptor (**PC<sub>71</sub>BM**) and to study the recombination's time.

## 1.2. Photophysical study of PA:

After obtaining the suitable electronic structure for electron transfer between the donor metallooligomer **PA** and the used acceptor **PC<sub>71</sub>BM**, the photophysical properties are studied for the metallooligomer by our collaborator Pr. D. Harvey from Sherbrooke University, Canada. **MCzM** (Figure 105) was also studied as an acceptor with **PA**.

### 1.2.1. Photoreductive electron transfer between PA and electron acceptor:

The objective of these studies is to evaluate the times of phototransfer between the donor such as **PA** and an acceptor and the time of charge recombinations.

After formation of the exciton in the donor (<sup>1</sup>polymer\*), an electron transfer occurs from the donor like a polymer and in our case the metallooligomer to the acceptor like **PC<sub>71</sub>BM** (<sup>1</sup>polymer\* + acceptor → polymer<sup>+</sup>• + acceptor<sup>-</sup>•). Based on the investigation of **P2'**, this process occurs in femtosecond time scale, and the recombination with the back-electron transfer occurs in picoseconds with the formation of triplet state (polymer<sup>+</sup>• + acceptor<sup>-</sup>• → <sup>3</sup>polymer\* + polymer + acceptor).<sup>234</sup> However, fullerene acceptors suffer from low absorptivity values in the visible region, which cause small relative number of excitations generated by the direct excitation of the **PC<sub>71</sub>BM** acceptor. Consequently, **MCzM** was used as non-fullerene acceptor to overcome this potential problem in this study with **PA** as donor material.

The absorption, excitation and fluorescence spectra of the donor metallooligomer and the **MCzM** acceptor are reported in figure 106. Both the metallooligomer and the acceptor are weakly fluorescent.

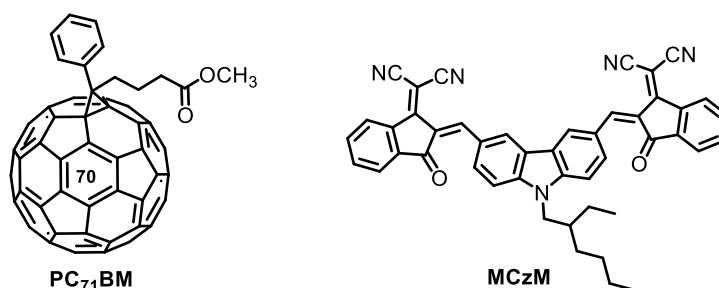


Figure 105: the structures of **PC<sub>71</sub>BM** and **MCzM** acceptors

<sup>234</sup>G. Marineau-Plante, M. Qassab, A. Schlachter, M. Nos, M. Durandetti, J. Hardouin, C. Lemouchi, L. Le Pluart, P. D. Harvey, *Journal of Inorganic and Organometallic Polymers and Materials*, **2022**, 32, 1266-1276



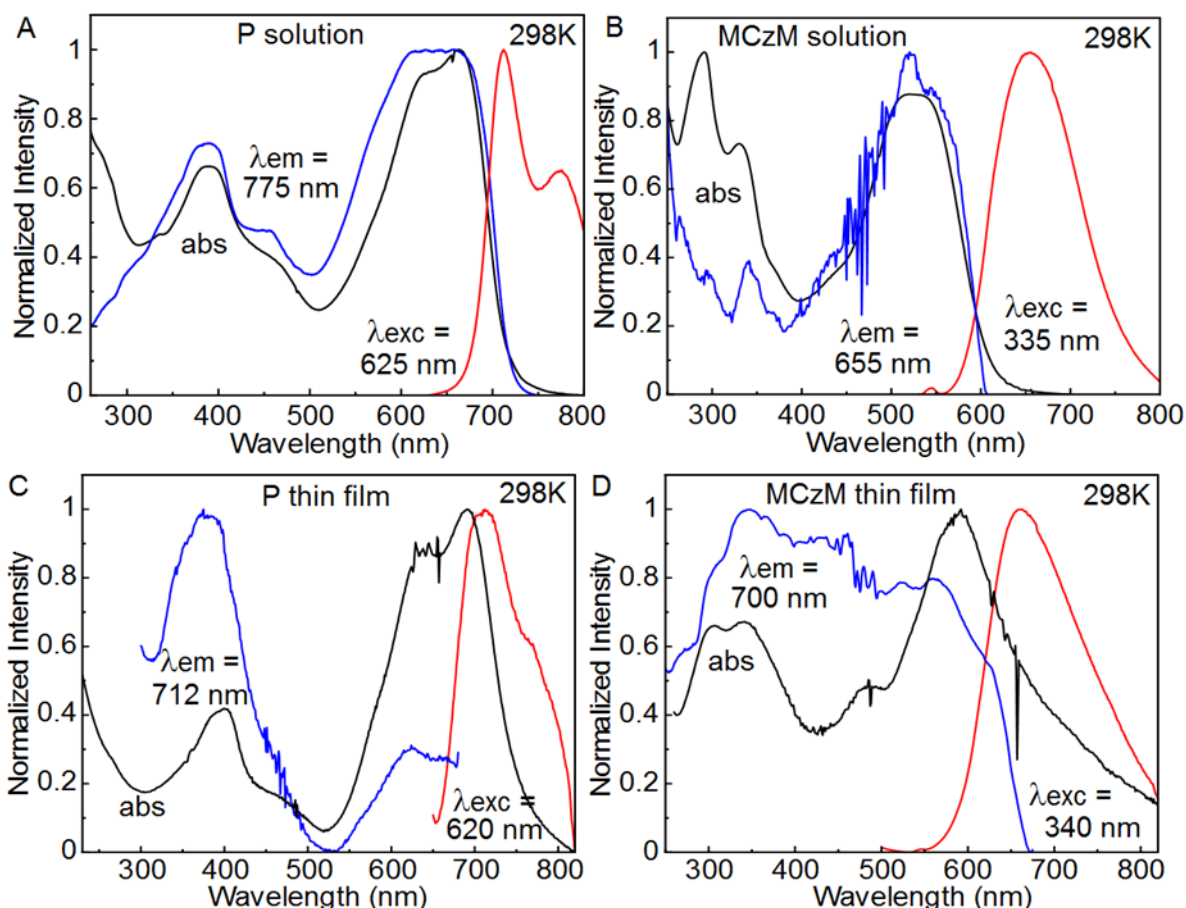


Figure 106: Normalized absorption (black), excitation (blue) and fluorescence (red) spectra of **PA** in  $CH_2Cl_2$  (A) and drop-casted thin film (C), and of **MCzM** in  $CH_2Cl_2$  (B) and drop-casted thin film (D).

### 1.2.2. Stability test:

**PA** discloses instability when the solutions of **PA** are exposed to room light or to a high intensity irradiation source. It is noteworthy that the physical parameter study was carried with fresh samples under soft power light. To study this instability, **PA** was dissolved in degassed  $CH_2Cl_2$  solvent and subjected to an irradiation  $\lambda_{exc} = 623$  nm and flux power intensity 20 times to that used in solar cell design. The Quasi-total photo conversion or polymer decomposition occurred in 10 minutes of irradiation. Hence, **PA** is not stable enough to be used as a donor in BHJ solar cell (Figure 107).

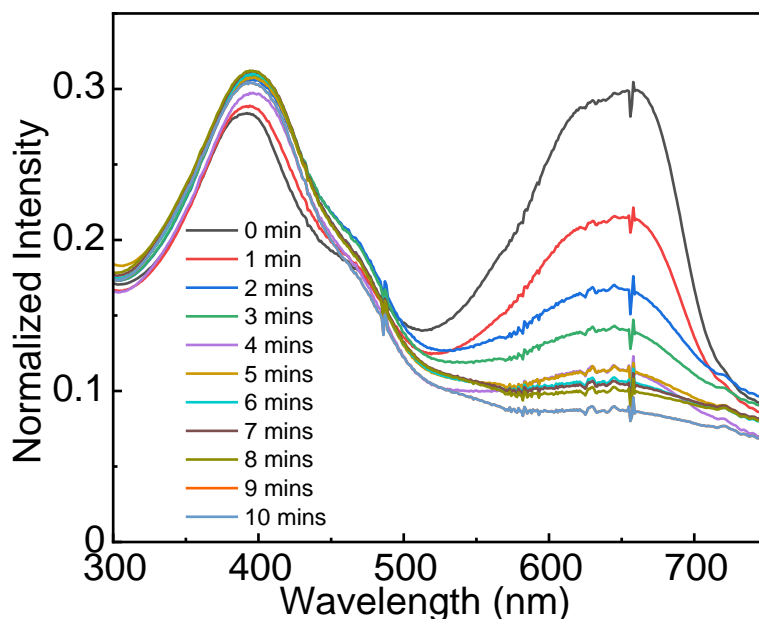
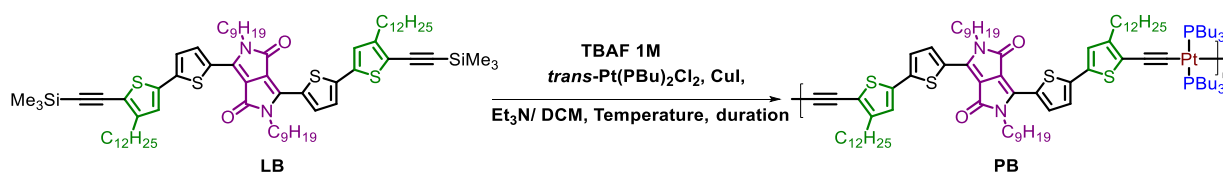


Figure 107: Time-dependence of the absorption spectra of **PA** in  $\text{CH}_2\text{Cl}_2$  upon irradiation at 623 nm (flux power density =  $19.7 \times 10^3 \text{ W/m}^2$ ). Note that the flux density at AM 1.5 is  $1 \times 10^3 \text{ W/m}^2$ .

So, these results were published in 2022 in Journal of Inorganic and Organometallic Polymers and Materials. However, due to the instability issue of **PA**, we followed another way to increase the average molar mass  $M_n$ , which is functionalizing of the conjugated system with a solubilizing group to enhance the solubility of the ligand and the metallooligomer. This approach was inspired from the reported work of Wong and *al*,<sup>220</sup> hence, a new ligand **LB** was prepared with two thiophenes functionalized with a solubilizing linear alkyl chain  $\text{C}_{12}\text{H}_{25}$ .

### 1.3. Functionalizing with solubilizing chain to increase the average molar mass:

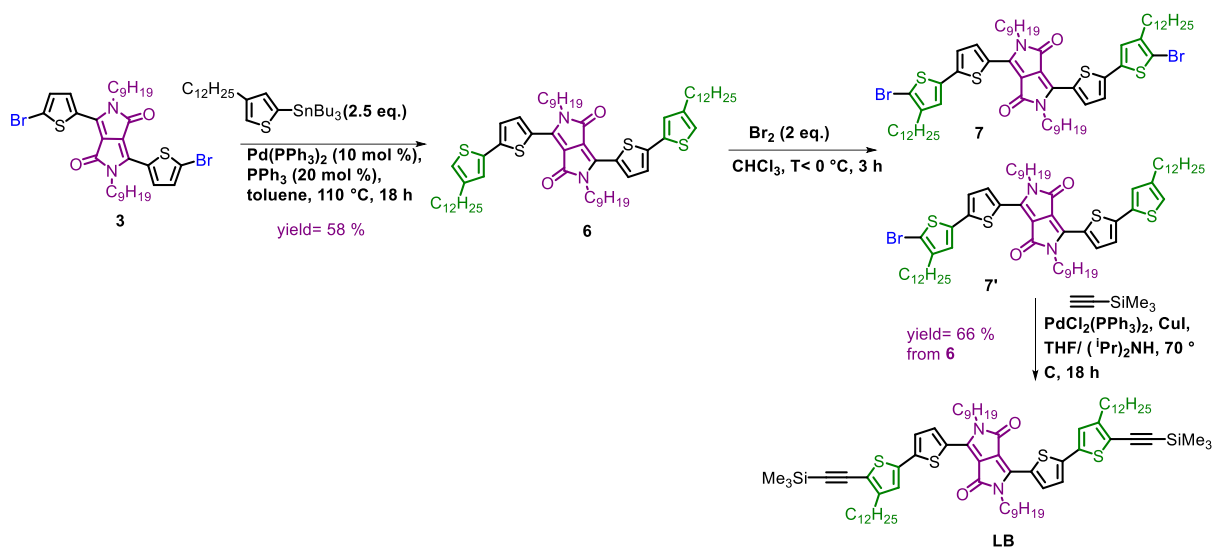
In this part, we describe the second way of strategy 1, which aims to increase the average molar mass of the metallooligomer. Linear alkyl side chain is used as a solubilizing chain on thiophene units, which could improve the solubility of ligand **LB**, and the metallooligomer **PB** and this helps to reach higher average molar mass. Indeed, Linear alkyl chains have been chosen to maintain important aggregation with reduced  $\pi$ - $\pi$  stacking distances for enhanced electronic mobilities. Moreover, linear alkyl side chains could be utilized to promote the nanostructural order of the active layer and further to enhance the photovoltaic performance. **LB** was used in dehydrohalogenation reaction for **PB** preparation (Scheme 5).



### Scheme 5: The synthesis of metallooligomers **PB**

#### 1.3.1. Synthesis of **LB**

The goal of this part is to synthesize ligand **LB**, that is an analog of **LA**, the difference is the presence of linear alkyl chain  $n\text{-C}_{12}\text{H}_{25}$  on the second thiophene. The synthesis of ligand **LB** is inspired by the work of Zhan, Wong and *al.*,<sup>220</sup> it is represented in scheme 6. It is like the route followed for the synthesis of ligand **LA**.



Scheme 6: The synthetic route of ligand **LB**

The insertion of  $\text{C}_{12}\text{H}_{25}$  functionalized thiophene is made by a Stille coupling reaction between the brominated DPP containing compound **3** and the freshly prepared stannic of  $\text{C}_{12}\text{H}_{25}$ -thiophene. The compound **6** is isolated with a yield of 67%. The next step is the bromination of compound **6** using the same optimized conditions applied in **LA** synthesis, with bromine at range temperature of  $-5$  to  $0\text{ }^\circ\text{C}$ . This yields to a mixture of mono- and bis-brominated compounds **7** and **7'** with tedious purification. Hence, they were not separated. The last step is a Sonogashira coupling reaction between the mixture **7**, **7'** and trimethylsilylacetylene catalyzed with  $\text{Pd}(\text{PPh}_3)_2\text{Cl}_2$  in the presence of  $\text{CuI}$  and the base  $i\text{Pr}_2\text{NH}$ . The ligand was isolated with a yield of 66% in the two last steps from intermediate **6** (Scheme 6). As expected, the solubility of **LB** is better than for **LA**.

All intermediates and ligands were characterized with  $^1\text{H}$  and  $^{13}\text{C}$  NMR, ESI, HRMS and MALDI TOF were carried out to complete the characterizations of the ligands. The ligand **LB** was used for the preparation of metallooligomer **PB**.

#### 1.3.2. Optical properties of **LB**

The absorption spectra in CH<sub>2</sub>Cl<sub>2</sub> of the different ligands **L1'**, **LA** and **LB** have been represented in figure 108. The comparison between **LA** and **LB** spectra shows a very small bathochromic shift in the absorption band for **LB**. So, there is no significant impact of functionalizing the thiophene units with a solubilizing chain on the absorption wavelength range. Hence, the optical band gap is not affected.

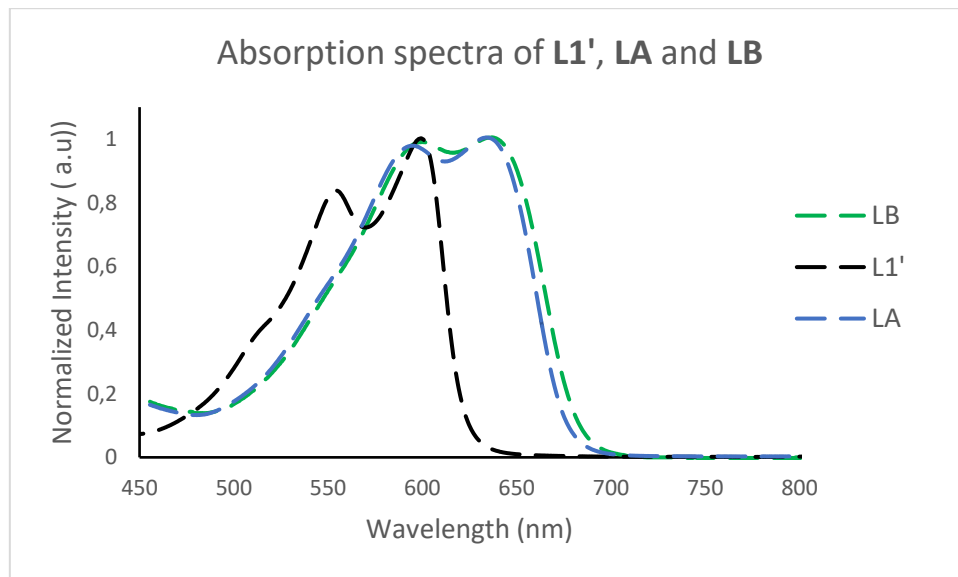
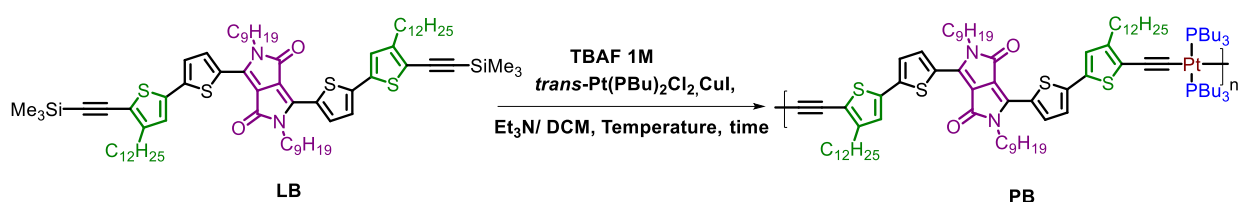


Figure 108: The absorption spectra of **L1'**, **LA** and **LB** in CH<sub>2</sub>Cl<sub>2</sub>

### 1.3.3. Synthesis of PB

The metallooligomer **PB** was synthesized according to the optimized protocol applied for long chains **PA** (Scheme 7, Table 8).



Scheme 7: The synthesis of metallooligomer **PB**

The progress of the reaction was monitored by <sup>31</sup>P{<sup>1</sup>H} NMR. It was noticed that the metallooligomer **PB** was not formed at room temperature (Entry 1, Table 8). Hence, the reaction temperature was increased to 45 °C. After two hours, <sup>31</sup>P{<sup>1</sup>H} NMR spectrum exhibits two signals at 4.8 and 3.5 ppm attributed to distinct complexes with coupling constant  $J_{\text{Pt-P}} = 2330$  Hz for both. The purification on biobeads® X1 didn't succeed in separating the two complexes and some ligand remained evidenced by TLC monitoring.

Table 8: The different conditions for polymerization reaction of **PB**

Entry.	LB	<i>trans</i> -Pt(PBu) <sub>2</sub> Cl <sub>2</sub>	CuI	temperature	Duration	<sup>31</sup> P{ <sup>1</sup> H} ppm	J <sub>Pt-P</sub> Hz
<b>1</b>	<b>1.8 eq.</b>	1 eq.	0.5 eq.	RT	3 days	/	/
<b>2</b>	<b>1.8 eq.</b>	1 eq.	0.5 eq.	45°C	2h	4.8, 3.5	2330

The mixture was analysed by GPC. The GPC chromatogram of **PB** (Figure 109) shows two main broad peaks, which evidences, the presence of several populations of metallooligomers and the majority is of ligand **LB**. The poor progress of the reaction for the preparation of **PB** even after heating could be explained by a poor reactivity during the polymerization due to the steric hindrance generated by the alkyl chain on the thiophene and butyl groups of the phosphine despite the better solubility of **LB**.

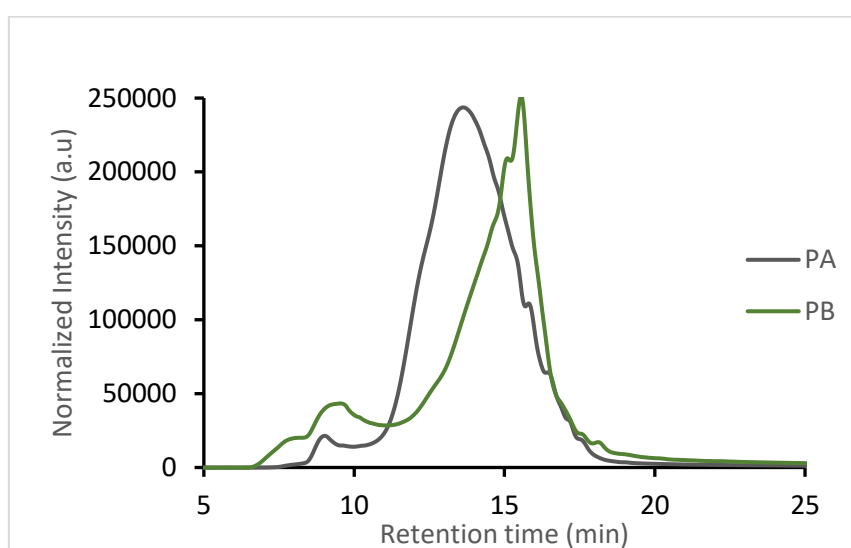


Figure 109: GPC chromatogram of **PB**

Following strategy 1, it results in improving the average molar mass of metallooligomer **PA**. This result was published in 2022 in Journal of Inorganic and Organometallic Polymers and Materials. But the synthesis of the desired metallooligomer **PB** with solubilizing chain was not succeeded. The photophysical properties of **PA** were studied. Nevertheless, **PA** shows instability to irradiation, which prevents using it as a donor material in BHJ solar cells. Hence, we focused on strategy 2 for the synthesis of a new narrow band gap DPP based metallooligomer **PC**. The objective of strategy 2 is to obtain a narrow band gap metallooligomer with higher stability than **P2'** and with easier synthesis for preparing large quantities. Synthesizing enough quantity allows our collaborator Pr. Ganesh D. Sharma to try different conditions for binary systems and to apply distinct architectures as ternary systems with two acceptors (donor/ acceptor1/ acceptor2) or as tandem solar cells.

## 2. Strategy 2: Narrow band gap metallooligomers:

In the team, a narrow band gap metallooligomer **P2'** was prepared by Mélodie NOS during her PhD project (2015-2018). It exhibits an electrical band gap of 1.41 eV and a wide absorption wavelength range from 550 to 850 nm. These good optical properties and suitable band's electronic structure for obtaining efficient electronic transfer explain the good performances of the BHJ solar cells. They exhibit an average PCE of 9.42 % with **P2'** as a donor and **PC<sub>71</sub>BM** as an acceptor. The modification of the organic part (**Ar**) of the ligand with dimers (T-DPP-T)<sub>2</sub> permits the enhancement of the optoelectronic properties with a better PCE than **P1'** (PCE= 7.05 %, **P1'**: **PC<sub>71</sub>BM**).

The drawbacks of **P2'** are instability issue of deprotected ligand **L2'**, low M<sub>n</sub>, difficult synthesis and difficulties to apply chemical functionalizations.<sup>222</sup> For that, the aim of my PhD project is to prepare a new narrow band gap metallooligomer **PC** by replacing the second thiophene ring of **PA** by 3,4- Ethylenedioxythiophene unit (EDOT).

Based on a reported work on EDOT and DPP containing conjugated polymers,<sup>235</sup> the insertion of EDOT moiety in the organic part (**Ar**) of the ligand brings benefits such as an increase in the conjugation length, providing strong electron donor character to increase the intramolecular charge transfer and leading to a narrow the band gap.<sup>227</sup> The presence of S...O interactions increases the planarity of the conjugated backbone. This permits to increase charge mobilities.<sup>235</sup> Besides, alkoxy groups of the cycle of EDOT unit increases the stabilization of the quinoid structure, which helps to decrease the band gap.

Moreover, the cycle of EDOT can easily be functionalized with a side chain carrying a function with the preparation of metallooligomer **PD** depicted in figure 110. This side chain permits to increase the solubility and the molecular organization of the donor, to improve the morphology of the active layer and the dissociation of excitons (Figure 110). The side chain used could be carrying an organizing group as triphenylene,<sup>236</sup> solubilizing group as a branched extended alkyl chain.<sup>237</sup> Also, the siloxane chain is interesting to improve the separation of donor/ acceptor in the active layer.<sup>238</sup> Moreover, polar chains like ethylene glycol could decrease the binding energy in exciton and consequently increase the exciton dissociation leading to an increase in the charge's generation.<sup>239</sup>

---

<sup>235</sup> C. J. Mueller, C. R. Singh, M. Thelakkat, *Journal of polymer Science, Part B: Polymer Physics*, **2016**, 54, 639–648

<sup>236</sup> K. J. Lee, J. H. Woo, E. Kim, Y. Xiao, X. Su, L. M. Mazur, A.-J. Attias, F. Fages, O. Cregut, A. Barsella, F. Mathevet, L. Mager, J. W. Wu, A. D'Aléo, J.-C. Ribierre, *Phys. Chem. Chem. Phys.*, **2016**, 18, 7875-7887

<sup>237</sup> C. Grand, W. Zajaczkowski, N. Deb, C. K. Lo, J. L. Hernandez, D. G. Bucknall, K. Mü llen, W. Pisula, J. R. Reynolds, *ACS Appl. Mater. Interfaces*, **2017**, 9, 15, 13357–13368

<sup>238</sup> J. Mei, D. H. Kim, A. L. Ayzner, M. F. Toney, Z Bao, *J. Am. Chem. Soc.*, **2011**, 133, 20130–20133

<sup>239</sup> J. Kosco J, S. Gonzalez-Carrero S, C. T. Howells CT, W. Zhang W, M. Moser M, R. Sheelamanthula R, L. Zhao L, B. Willner, T. C. Hidalgo, H. Faber, B. Purushothaman, M. Sachs, H. Cha, R. Sougrat, T. D. Anthopoulos, S. Inal, J. R. Durrant, I. McCulloch, *Adv Mater.*, **2022**, 34, 22

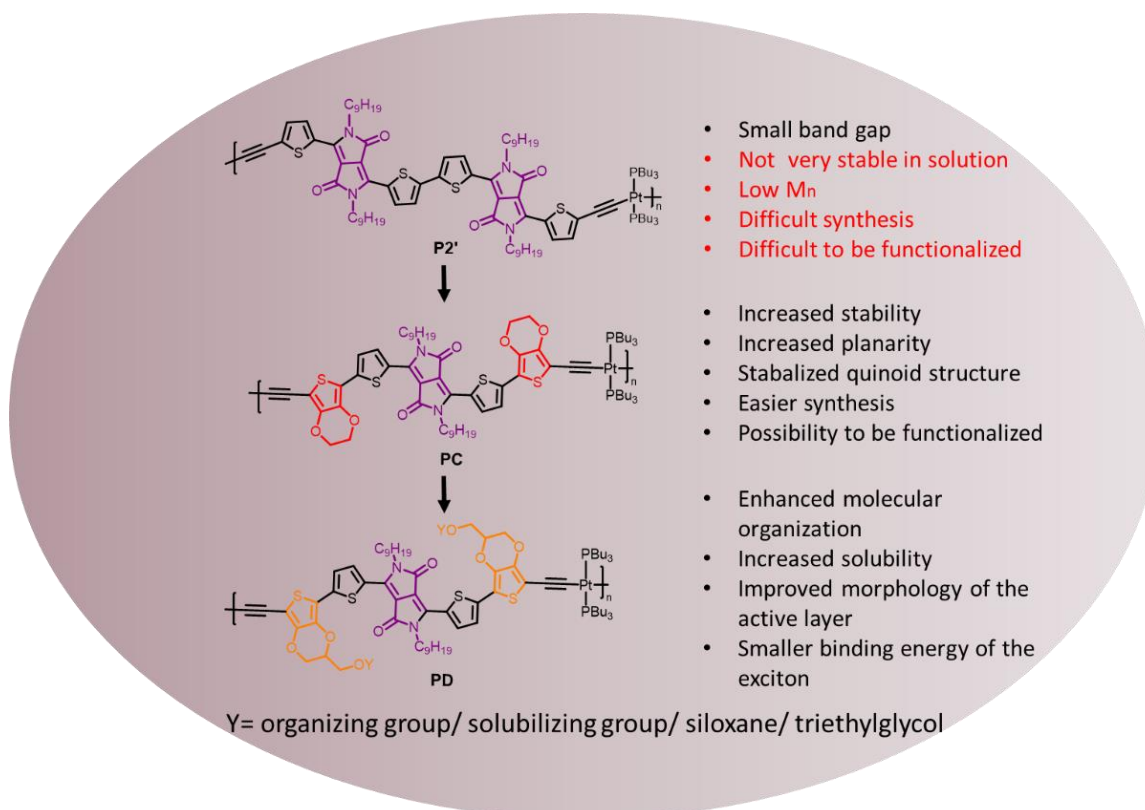
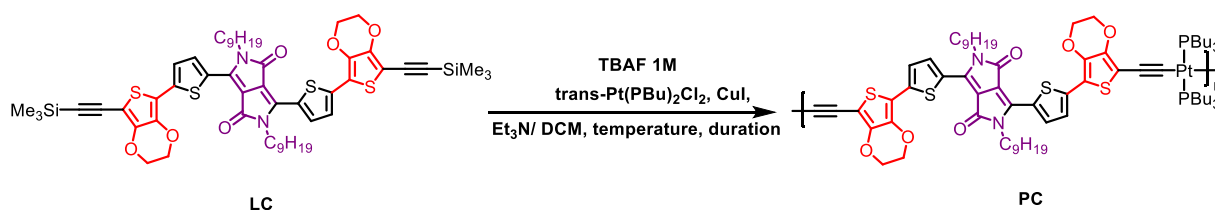


Figure 110: The general scheme of low band gap metallooligomers developed in strategy 2.

## 2.1. Synthesis of PC:

The synthesis of **PC** includes the synthesis of ligand **LC** followed by Cu-catalyzed dehydrohalogenation reaction to obtain the desired metallooligomer (Scheme 8).

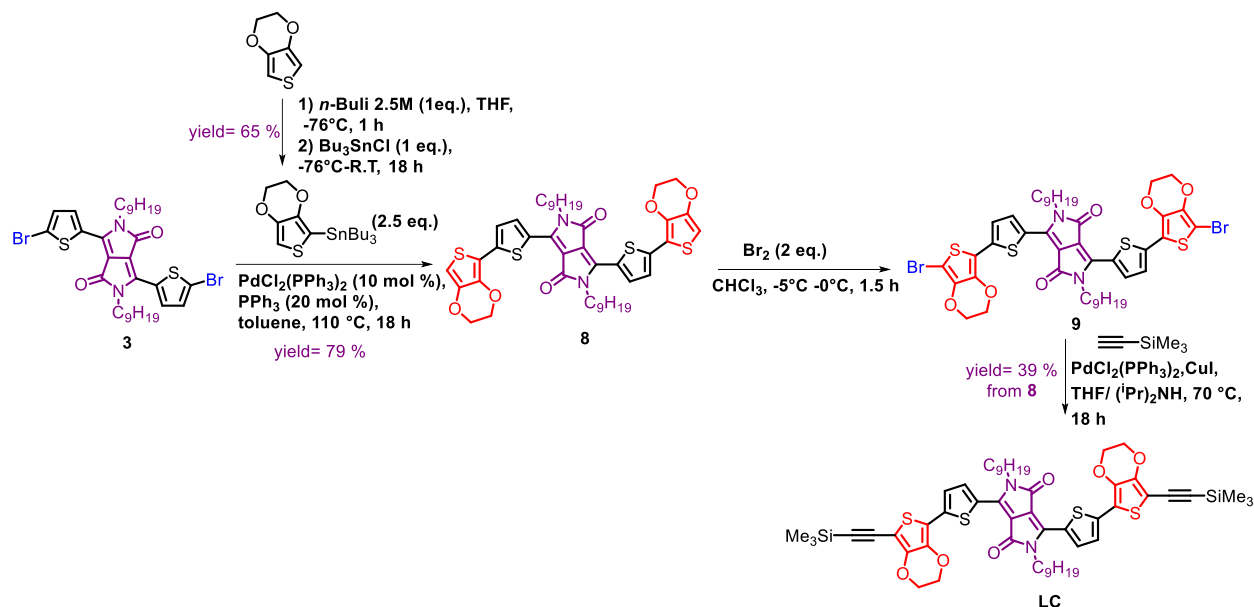


Scheme 8: The synthesis of **PC**

### 2.1.1. Preparation of Ligand LC:

The ligand **LC** is prepared in a similar strategy to that of **LA** and **LB**. EDOT unit was inserted after a  $\text{Pd}(\text{PPh}_3)_2\text{Cl}_2$  catalyzed Stille coupling reaction between the bisbrominated intermediate **3** and freshly prepared EDOT stannic derivative. The EDOT containing compound **8** was isolated with a yield of 67%. The next reaction is the bromination of compound **8**. It is the limiting step. The formation of the compound **9** is confirmed by  $^1\text{H}$  NMR and mass spectrometry with the formation of insoluble side products formed from oxidative

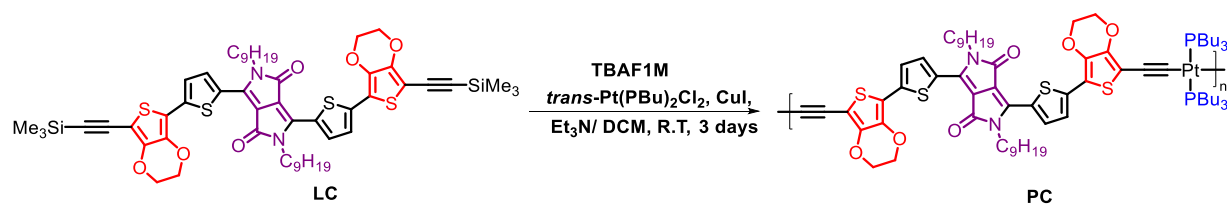
polymerization.<sup>240</sup> A strict control of the temperature and maintaining it in the range of -5 °C to 0 °C, in dark with shorter reaction time of 1.5 hours limit the side reaction. Compound **9** was directly engaged in the next step, which is a Sonogashira coupling reaction to install the triple bonds protected with silyl groups (TMS). Hence, **LC** was isolated with a good purity and a global yield of 39 % from **8** (Scheme 9).



Scheme 9: The synthetic route of ligand **LC**

### 2.1.2. Synthesis of PC:

**PC** was prepared with same reaction conditions applied for **PA**; conditions 1 and 2, by CuI-dehydrohalogenation reaction at R.T for three days (Scheme 10) to give a turquoise compound, which was purified by steric exclusion on bio-beads® X1.



Scheme 10: The synthesis of metallooligomer **PC**

<sup>240</sup> A. Patra, V. Agrawal, R. Bhargav, Shahjad, D. Bhardwaj, S. Chand, Y. Sheynin, M. Bendikov, *Macromolecules*, **2015**, 48, 24, 8760–8764



### 2.1.3. Characterizations of PC

**PC** formation was confirmed by  $^{31}\text{P}\{^1\text{H}\}$  NMR with a signal at 2.56 ppm with  $J_{\text{Pt-P}} = 2317.81$  Hz. An infrared spectroscopy brings out vibration frequency for the triple bond at  $2078\text{ cm}^{-1}$ . The average molar mass has been evaluated in gel permeation chromatography; it is found to be  $M_n = 12\text{ Kg.mol}^{-1}$  with  $\mathcal{D} = 2.06$  close to that of **PA** ( $M_n = 12.4\text{ Kg.mol}^{-1}$ ) using the first condition. In comparison to the previous metallooligomer **P2'** ( $M_n = 6.6\text{ Kg.mol}^{-1}$ ,  $\mathcal{D} = 11.1$ ), it is of higher average molar mass and smaller dispersity. In our work we compared the average molar mass of **PC** to metallooligomer **PA**, it has been found that they have close values (Figure 111).

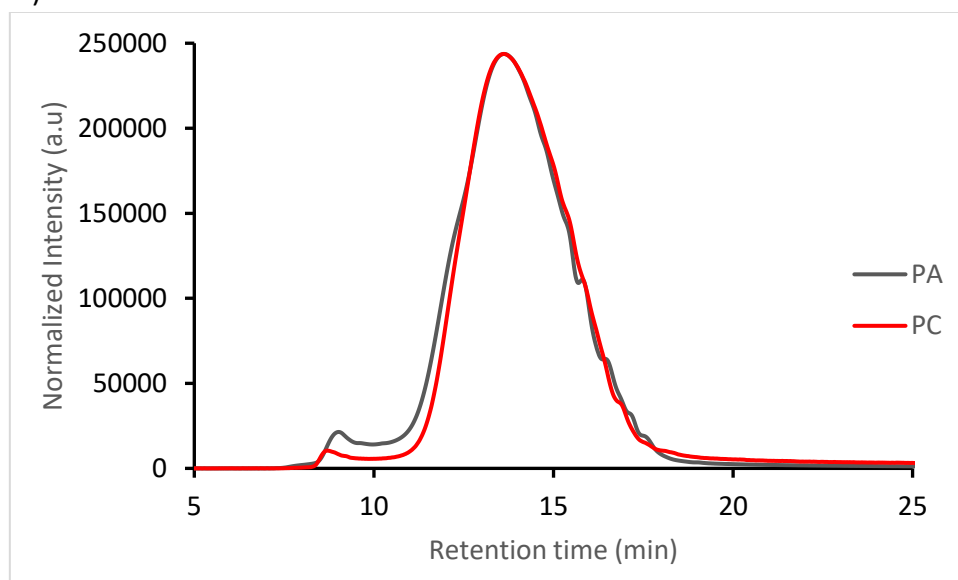


Figure 111: Comparison of GPC chromatograms of **PA** and **PC**

The decomposition temperature of **PC** has been tested and compared to **P2'** to evaluate the improvement from **P2'** to **PC**. The data from the analysis of **P1'**, **P2'** and **PC** are listed in table 9.

Table 9: The analysis data of characterizations carried for **P1'**, **P2'** and **PC**

	$M_n$ ( $\text{Kg.mol}^{-1}$ )	$\mathcal{D}$	Number of units	$^{31}\text{P}$ (ppm)	$J_{\text{P-Pt}}$ (Hz)
<b>P1'</b>	18.2	2.1	14-15	3.96	2289
<b>P2'</b>	6.6	11.1	3-4	3.88	2290
<b>PC</b>	12	2.06	8-9	2.56	2318

The optical properties of ligand **LC** and metallooligomer **PC** have been investigated by absorption spectroscopy on the liquid and on thin films with the determination of wavelength onset to calculate the optical band gap and to be compared to those of **L2'** and **P2'**. The spectra are represented in figure 112 and figure 113 and the data are listed in table 10.

The absorption capacity of **LC** was investigated with the determination of the molar extinction coefficient ( $\epsilon_\lambda$ ). **LC** shows  $\epsilon_\lambda$  ((609 nm)  $4.81 \times 10^4\text{ mol}^{-1}\text{ L cm}^{-1}$ , (658 nm)  $5.17 \times 10^4$

mol<sup>-1</sup> L cm<sup>-1</sup>) much higher than those of **L2'** (1.39 x10<sup>4</sup> mol<sup>-1</sup> L cm<sup>-1</sup>, 1.42 x10<sup>4</sup> mol<sup>-1</sup> L cm<sup>-1</sup>). The comparison of the absorption spectra of the solutions in figure 111 shows a bathochromic shift of absorption band at the lowest energy from **LC** to **PC**. Moreover, **PC** is with higher  $\lambda_{\text{abs}}^{(\text{max})}$  of 710 nm compared to **LC** with  $\lambda_{\text{abs}}^{(\text{max})}$  of 658 nm. The same bathochromic shift is observed between **L2'** and **P2'** with higher  $\lambda_{\text{abs}}^{(\text{max})}$  for **P2'** (718 nm) compared to **L2'** (669 nm). This means a smaller band gap by increasing the conjugation length.

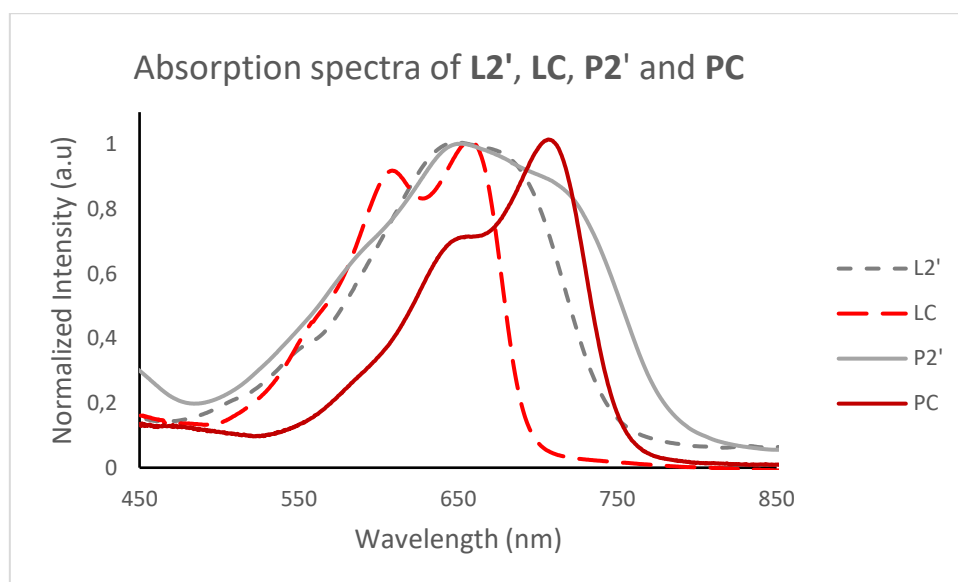


Figure 112: The absorption spectra of **L2'**, **LC**, **P2'** and **PC** in CH<sub>2</sub>Cl<sub>2</sub>

Absorptions of **PC** and **P2'** were measured on thin films to evaluate the  $\lambda_{\text{abs}}^{(\text{onset})}$  and to calculate the optical band gap ( $E_g^{\text{opt}}$ ). The spectra of **PC** and **P2'** are compared in figure 113 and the data are listed in table 10. The values of  $\lambda_{\text{abs}}^{(\text{onset})}$  are about 840 nm and 875 nm for **PC** and **P2'**, respectively. So, the  $E_g^{\text{opt}}$  was calculated with 1.48 eV for **PC**, which is close to that of **P2'** (1.42 eV).

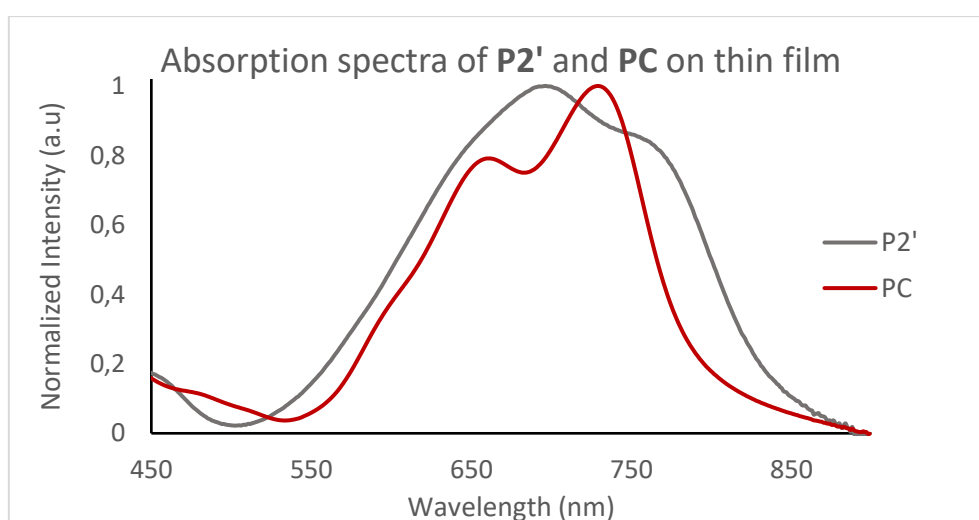


Figure 113: The absorption spectra of **P2'** and **PC** on thin film

Cyclic voltammetry was carried by Muriel Durandetti from COBRA laboratory, Rouen. The results confirm the narrow band gap of  $E_g^{\text{elec}} = 1.42$  eV, which is close to the calculated

$E_g^{opt}$  (1.48 eV) with LUMO= -3.85 eV and higher level for HOMO at -5.27 eV for **PC** with respect to the HOMO level of **P2'**. The data are listed in table 10. The bands electronic structures of **PC** and **P2'** are represented in figure 114.

Strategy 2 is based on the insertion of EDOT, which permits a decrease in the band gap to 1.42 eV in comparison to **P1'** ( $E_g^{elec} = 1.62$  eV) and with close value to that of **P2'** ( $E_g^{elec} = 1.41$  eV). The risk of the insertion of a strong donor like EDOT is level rising of EHOMO which leads to decrease in  $V_{OC}$ . But regarding the cyclic voltammetry analysis, the HOMO energy level of **PC** is slightly higher of 0.09 eV than those of **P2'**. However, the LUMO level of **PC** is slightly higher than that of **P2'** allowing a higher  $\Delta E1$  value (Figure 114).  $\Delta E1$  and  $\Delta E2$  are calculated according to the following equations:

$$\Delta E1 = LUMO^A - HOMO^D$$

$$\Delta E2 = LUMO^D - LUMO^A$$

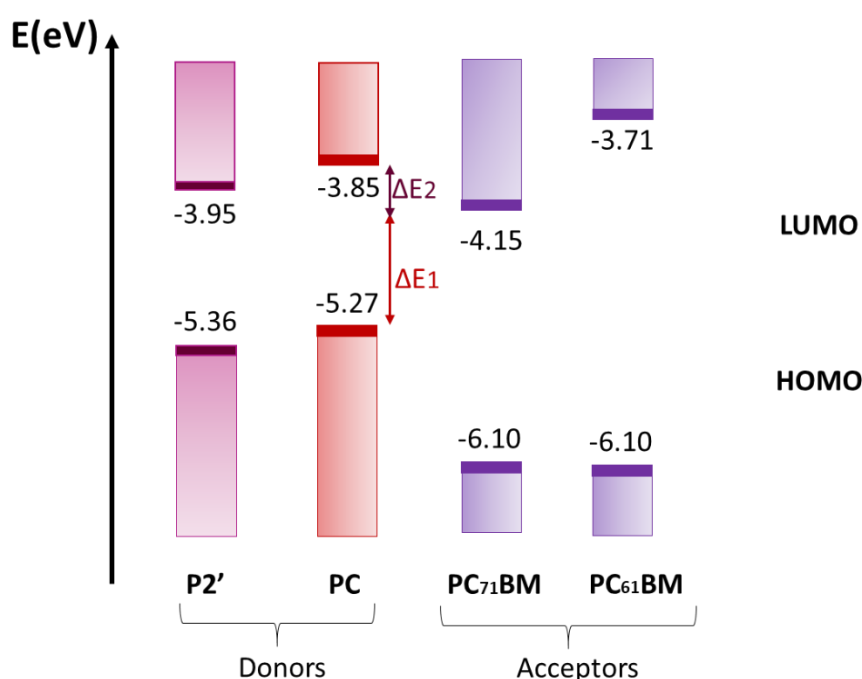


Figure 114: The electronic structure of **P2'**, **PC** and **PCBM**

Table 10: The optical and electrochemical analysis data of **P2'**, **PC** and their corresponding ligands.

	$\lambda_{abs}^{(max)}$ ( $\epsilon_{\lambda}$ )		$\lambda_{abs}^{(max)}$	$\lambda_{abs}^{(onset)}$	$E_g^{opt}$	$E_{ox}^{onset}$	$E_{red}^{onset}$	HOMO	LUMO	$E_g^{elec}$
	nm ( $10^4 mol^{-1} Lcm^{-1}$ )		In solution nm	On thin film nm	eV	V/ESC	V/ESC	eV	eV	eV
<b>L2'</b>	<b>648 (1.42), 669 (1.39)</b>	<b>P2'</b>	654, 718	875	1.42	0.63	-0.78	-5.36	-3.95	1.41
<b>LC</b>	<b>609 (4.81), 658 (1.39)</b>	<b>PC</b>	650, 710	840	1.48	0.54	-0.88	-5.27	-3.85	1.42

Onset potential (V vs SCE) for reduction ( $E_{red}^{onset}$ ) and oxidation ( $E_{ox}^{onset}$ ). HOMO and LUMO energies calculated with the equation  $E_{HOMO} = -(E_{ox}^{onset} + 4.73)$  eV,  $E_{LUMO} = -(E_{red}^{onset} + 4.73)$  eV.  $E_g^{elec} = E_{LUMO} - E_{HOMO}$  (eV)

Based on these promising preliminary results, a collaborative project was started in 2021 between the members of the team to resynthesize the metallopolymer **PC** in larger

quantities (300-500 mg) to fully characterize it and to study this compound in photophysics and finally to use it as a donor in BHJ solar cells. The challenge was to prepare larger quantities (to multiply the synthetic scale by 10). The re-synthesis was conducted by Jean-François Lohier, an engineer in organic chemistry and Romuald Herbinet an engineer specialized in GPC and thermal properties characterization in the team POHET at the LCMT. The collaborative work allows optimizations on the bromination and Sonogashira steps described previously (Scheme 9). This permits the increase of the yields and the purity of the intermediates. The collaboration between Jean-François Lohier and Romuald Herbinet leads to an improvement of the dehydrohalogenation step. Thanks to GPC monitoring, which leads to the increase of the purity and the average molar mass of **PC** (15.1 Kg.mol<sup>-1</sup>,  $\bar{M}_n = 2.5$ ). This project leads to the preparation of 300 mg of **PC**. It was fully characterized in <sup>1</sup>H, <sup>31</sup>P{<sup>1</sup>H} NMR, IR-ATR, GPC and MALDI-TOF. The data from cyclic voltammetry confirms the preliminary results ( $E_{\text{HOMO}} = -5.27$  eV,  $E_{\text{LUMO}} = -3.85$  eV). The photophysical properties of **PC** were investigated by Pr. Pierre D. Harvey.

During the photophysical properties investigations, the stability test shows **PC** is much more stable than **P2'** in the solid state. In addition, **PC** and the mixture **PC/PCBM** in solution are stable even after one month. Hence, by now **PC** is the most stable metallooligomer prepared in the team.

Based on these promising results, 150 mg from the 300 mg batch was used as a donor in BHJ solar cell with **PC<sub>71</sub>BM** and non-fullerenes acceptors like **IT-4F** and **Y6**, to test different ratio donor/acceptor. The SVA treatment was applied to improve the morphology of the active layer. The solar cells achieve good performances with an average value of PCE at 8.96 % with **PC<sub>71</sub>BM** which is close to the PCE of 9.42 % for **P2': PC<sub>71</sub>BM**. These performances increased significantly to 11.94 % with **IT-4F** and 14.12 % with **Y6**. It was planned to prepare ternary systems to increase the PCE. We plan to publish these results in 2023 in ACS macromolecules.

Thanks to the collaborative work, we were able to end by promising results, where **PC** was synthesized in large quantities with improved purity allowing the preparation of BHJ solar cells using **PC** as a donor material with different types of acceptors. The manufactured BHJ solar cells show good performances.

After the promising results of **PC**, we have decided to develop another type of metallooligomers **PD** with the functionalization of the cycle from EDOT moiety with side chains carrying distinct functions **Y** to enhance the performance of solar cells.

## 2.2. Synthesis of functionalized EDOT containing metallooligomers PD:

Functionalization of **PD** could be applied for different purposes versus the type of function **Y** carried by the side chain. For conjugated polymers, side chains have an effective impact on solubility, processability, intermolecular packing and an impact on the morphology of BHJ organic solar cells.<sup>241</sup> **PD** could be functionalized with a solubilizing group ( **Y**= alkyl

---

<sup>241</sup> D. Liu, Q. Zhu, C. Gu, J. Wang, M. Qiu, W. Chen, X. Bao, M. Sun, R. Yang, *Adv. Mater.*, **2016**, 28, 8490

chain) to increase the average molar mass, polar group (  $Y$ = ethylene glycol) to increase the exciton dissociation, siloxane chains (  $Y$ = SiOR) <sup>242</sup> which increases the D/A segregation in the active layer, and by organizing group such as  $Y$ = triphenylene to enhance the molecular organization and to increase the compatibility with the acceptor. Among solubilizing groups, we chose the extended branched alkyl chain, which favors good solubility, and promotes better aggregation with shorter  $\pi$ -stacking distances (Figure 115).

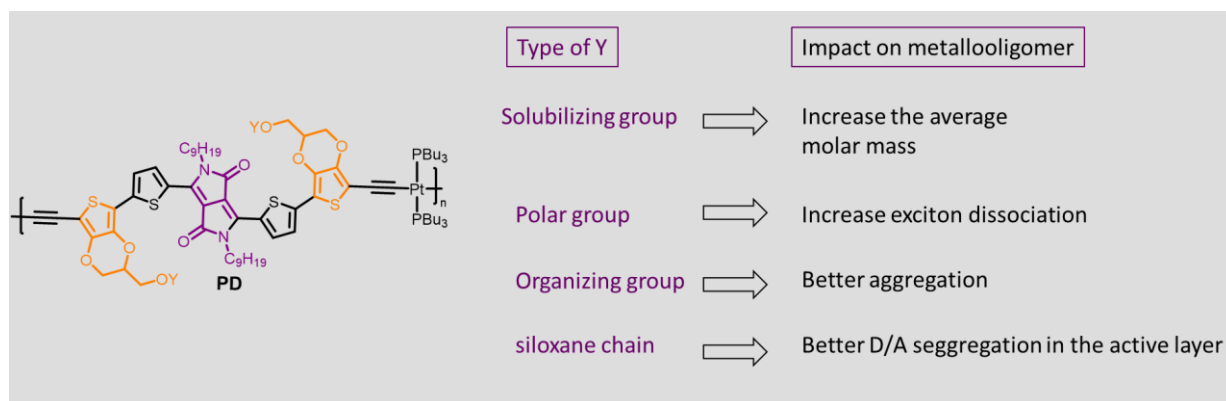
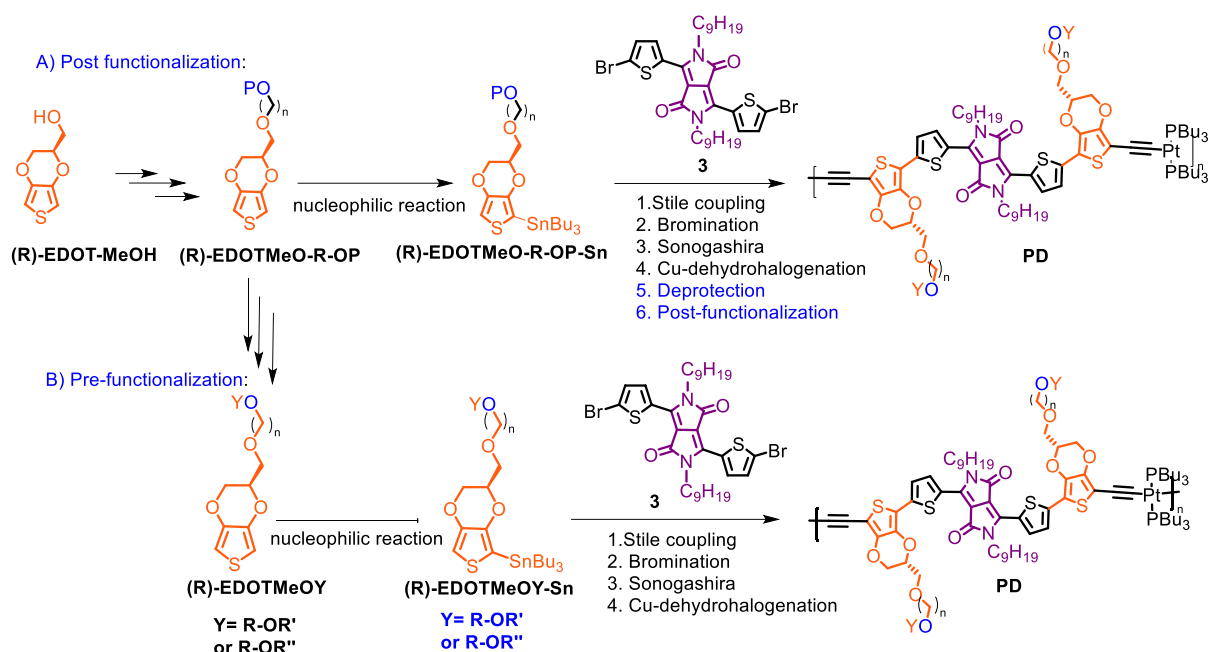


Figure 115: The impact of the side chains with the function  $Y$

The global synthesis of functionalized metallooligomer **PD** is illustrated in scheme 8. The strategy is to insert functionalized EDOT (**EDOT-Me-R-OY**) on DPP intermediate **3** after a Stille coupling reaction. It starts with the synthesis of the key synthon **EDOT-MeO-R-OP** from racemic (**R/S**)-**EDOT-MeOH** and enantiomeric pure (**R**)-**EDOT-MeOH**. The key synthon is represented in figure 116. It is composed of a spacer **R** terminated by a protected alcohol **OP**. The function  $Y$  could be attached to the alcohol function after a Williamson or esterification reaction. Then, depending on the nature of the function  $Y$  and its compatibility with the reaction conditions, a pre- or post-functionalization could be made as described in scheme 11. If function  $Y$  is compatible with bromination and basic medium with Sonogashira reaction as alkyl or ethylene glycol chain, the pre-functionalization could be carried out. However, if  $Y$  is composed of sensitive, fragile function, molecules like aromatic ring or siloxane chain sensitive to bromination or base respectively, a post-functionalization could be applied which use the generic synthon **EDOT-MeO-R-OP**. After the deprotection, the  $Y$  function could be attached on the alcohol functions after an O-alkylation or esterification.

<sup>242</sup> B. Fan, L. Ying, P. Zhu, F. Pan, F. Liu, J. Chen, F. Huang, Y. Cao, *Adv. Mater.*, **2017**, 29, 1703906



Scheme 11: The general synthetic route of metallooligomers **PD** with functionalized **EDOT** from the key synthon **3**

**(R)-EDOT-MeOR-OP** (Figure 116) is considered as the generic and the common synthon of the two strategies and it is used for the synthesis of functionalized metallooligomer **PD** (Scheme 11). This unit is composed of the EDOT rings to keep the same advantages than for **PC**. The second component is the presence of an alkyl spacer to increase the flexibility for an enhancement of the molecular organization. The third part is the protected alcohol function OP with silyl group (**P**). Generation of the alcohol function after deprotection permits to graft **Y** functions. The last part is the chiral center, which allows preparing stereoregular metallooligomers to improve the molecular organization and to enhance the charge transport.<sup>243</sup> **(R)-EDOT-MeOR-OP** is described in figure 116.

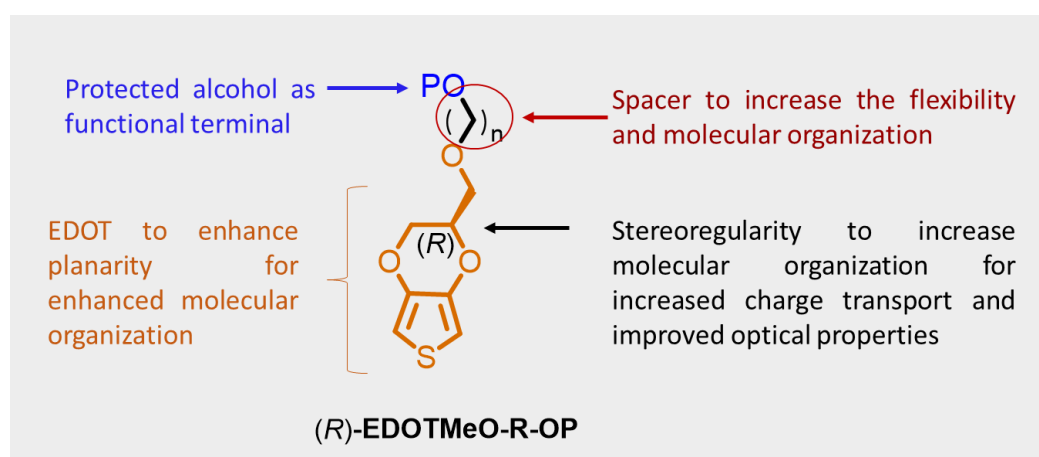


Figure 116: The descriptive skeleton of the generic synthon

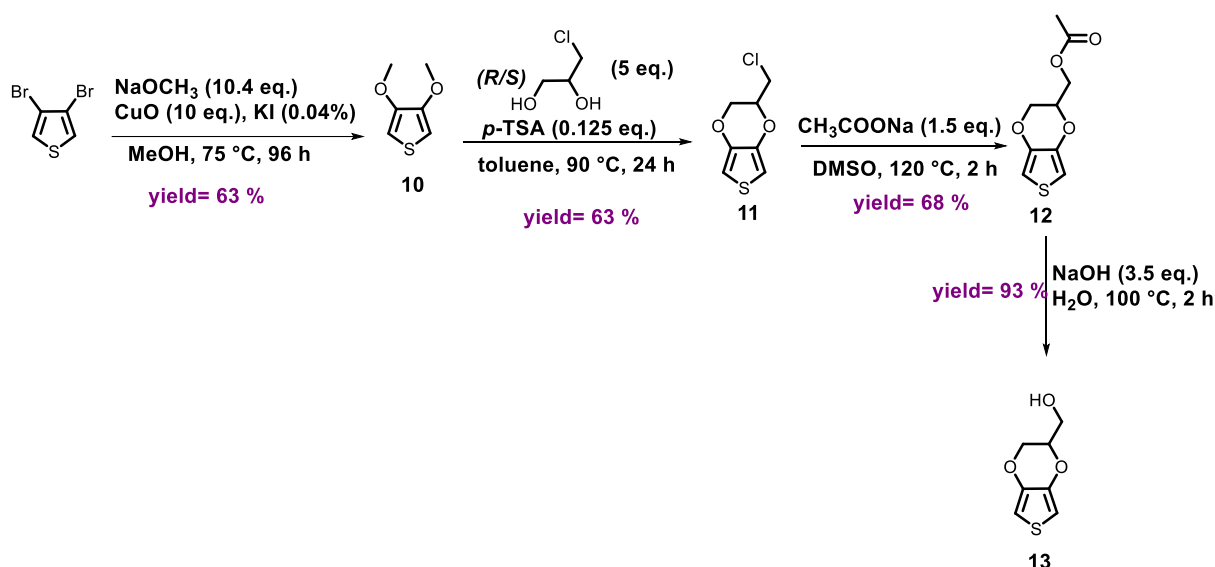
<sup>243</sup> D. Amsallem, A. Bedi, F. Tassinari, O. Gidron, *Macromol.*, **2020**, *53*, 9521–9528

The syntheses of this part were conducted by Victor Boshveski during his research project for his M2 internship (January -June 2022) period. It was an opportunity for me to train an M2 student with Cyprien Lemouchi and Loïc Le Pluart.

## 2.2.1. Preparation of the generic Synthon (*R*)-EDOT-MeOR-OP

### 2.2.1.1. Synthesis of (*R/S*)-EDOT-MeOH:

Due to the high cost of commercially available (*R/S*)-EDOT-MeOH (362 euros/g). The synthesis has been carried in four steps according to the literature starting from commercially available and cheaper 3,4-dibromothiophene (12 euros/g, Sigma-Aldrich, Meck) with optimized procedures inspired from the literature<sup>244</sup> (Scheme 12).



Scheme 12: The synthesis of the racemic mixture (*R/S*)-EDOT-MeOH 13

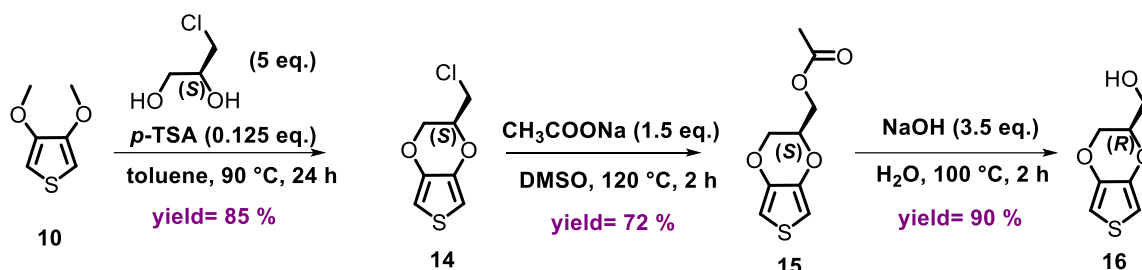
The first step was carried according to Cu catalyzed reported procedures,<sup>244</sup> but the product was isolated with a yield of 10 %. So, reaction conditions have been modified by adding an excess of sodium methanoate. The reaction was monitored by TLC, sequential additions of CuO and base are required to increase the progress of the reaction. With these optimizations, the yield of compound **10** was increased from 10 % to 63 %. The second step is an intermolecular cyclization reaction between the compound **10** and (*R/S*)-3-chloro-1,2-propanediol, activated in the presence of para-toluene sulfonic acid (*p*-TSA). Compound **11** was obtained with a yield of 63 %. The third step is the formation of the ester derivative **12** from sodium carboxylate to give compound **12** with a yield of 68 %. The last step is a hydrolysis reaction of the ester **12** to obtain (*R/S*)-(EDOT-MeOH) **13** in a good yield of 93 %.

<sup>244</sup> S. Zhang, J Xu, B. Lu, L. Qin, L. Zhang, S. Zhen, D. Mo, *J. Polym. J. Polym. Sci., Part A: Polym. Chem.*, **2014**, 52, 1989–1999

**(R/S)-EDOT-MeOH** was isolated with a global yield of 25 % from the commercially available 3,4-dibromothiophene.

### 2.2.1.2. Synthesis of (R)-EDOT-MeOH

Stereoregular conjugated polymers have attracted attention in numerous applications. They show better optical and optoelectronic properties, and better molecular organization.<sup>245</sup> Therefore, it is interesting to prepare stereoregular metallooligomers from enantiopure **(R)-EDOT-MeOH**. We could study the benefits of the presence of a chiral center on the molecular organization and charge transport properties. The chiroptical properties of this synthon have been investigated in the literature.<sup>245</sup> To study the benefits of the presence of a chiral center, we synthesized the *(R)*- isomer of **EDOT-MeOH** to be used as a building block in DPP based metallooligomer. The synthesis is inspired from the literature (Scheme 13).<sup>246</sup>



Scheme 13: The synthesis of *(R)*-EDOT-MeOH **16**

The synthesis of the chiral EDOT *(R)*-EDOT-MeOH **16** is of the same protocol used for the preparation of the racemic mixture *(R/S)*-EDOT-MeOH **13**. The first step is a reaction between intermediate **10** and *(S)*-3-chloro-1,2-propanediol to form intermediate **14** with a yield of 85 %. The second step is a nucleophilic substitution to form compound **15** followed by hydrolysis of the ester **15** using basic conditions to form compound **16**. *(R)*-EDOT-MeOH **16** is prepared with a global yield of 45 % from 3,4-dibromothiophene. The difference in the global yield between the racemic mixture and compound **16** is the use of dry *p*-TSA in the second step. The formation of the enantiomeric pure compounds **14** and **16** are confirmed by high performance liquid chromatography HPLC analysis carried out by Fabien Le Cavalier in LCMT laboratory. An HPLC column with chiral stationary phase has been used for the separation of the two enantiomers in the racemic mixture. The comparison of the chromatograms of the compounds **14** and **16** with the one of the racemic products confirms the enantiomeric purity of the samples with the presence of only one peak, which justifies the presence of a single enantiomer.

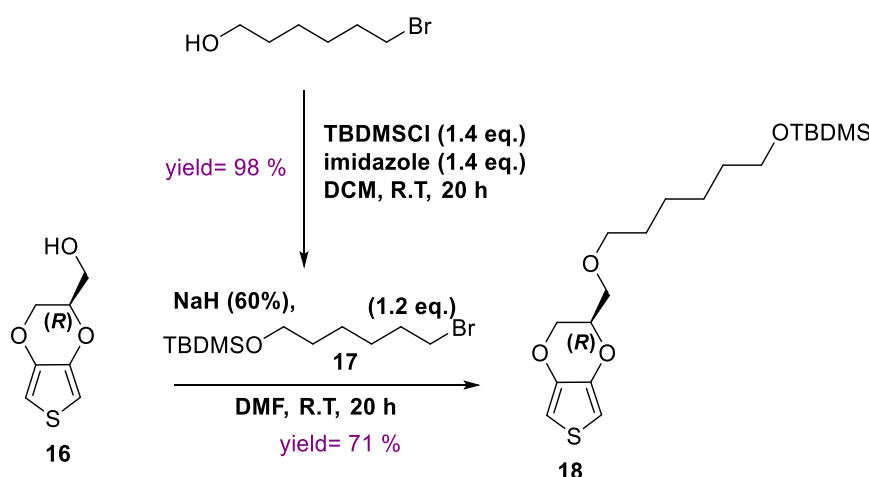
<sup>245</sup> D. Amsallem, A. Bedi, F. Tassinari, O. Gidron, *Macromol.*, **2020**, 53, 9521–9528

<sup>246</sup> L. Dong, Y. Zhang, X. Duan, X. Zhu, H. Sun, J. Xu, *Anal. Chem.*, **2017**, 89, 9695–9702



### 2.2.1.3. Synthesis of (*R*)-EDOT-MeO-ROP:

The aim of this part is to synthesize the generic synthon (*R*)-EDOT-MeO-R-OP **18**. As represented in scheme 14, it is prepared from the attachment of an alkyl chain as spacer of 6 carbon atoms terminated by a protected alcohol (OTBDMS). The spacer increases the flexibility and the alcohol function generated after removing silyl group permits to functionalize EDOT with side chains and **Y** functions. The synthesis of a similar compound **EDOT-MeO-R-OP** is reported. It's a racemic sample, and the alcohol function is protected with tetrahydropyran (THP).<sup>247</sup> The synthetic route is illustrated in scheme 14, where tert-Butyldimethylsilyl (TBDMS) protecting group was used because it is more robust and compatible with several reaction conditions. The synthetic route of (*R*)-EDOT-MeO-R-OP **18** is illustrated in scheme 14.



Scheme 14: The synthesis of (*R*)-EDOT-MeO-R-OP **18**

The synthesis of (*R*)-EDOT-MeO-R-OP **18** requires the preparation of a halogenated chain terminated with protected alcohol **17**, which is successively synthesized with a very good yield of 98 % from reported procedure.<sup>248</sup> This chain was engaged in Williamson O-alkylation reaction with deprotonated compound **16**. The generic synthon (*R*)-EDOT-MeO-R-OP **18** was isolated with a yield of 71 %. However, a series of optimizations was carried out to increase the yield from 0 % to 71 %. The data of the reaction condition are listed in table 11.

For the first attempts inspired by reported examples of O-alkylation of **EDOT-MeOH**,<sup>249</sup> a large excess of sodium hydride (20 eq.) has been used in THF at room temperature (Entry 1, Table 11). However, no product was obtained, and the starting material has been isolated. For next attempts, the number of equivalents has been decreased to 4 eq. (Entry 2) and to 2 eq.

<sup>247</sup> S.C.Ng, H.S.O. Chan, W.-L. Yu, *Journal of Materials Science Letters*, **1997**, *16*, 809-811.

<sup>248</sup> Patent : Kozlowski, R. Z., et al. Lipo- or amphiphilic scintillators and their use in assays, WIPO, W02002014290, **2002**

<sup>249</sup> G. Trippé, F. Le Derf, J. Lyskawa, M. Mazari, J. Roncali, A. Gorgues, E. Levillain, M. Sallé, *Chem. Eur. J.*, **2004**, *10*, 6497-6509.

(Entry 3) but the reaction didn't proceed. Other experiments have been carried out with a moderate heating to 45-65 °C,<sup>250</sup> but it failed (Entry 4). The base has been replaced by KOH, inspired from an example of alkylation of EDOT,<sup>251</sup> only the starting material was isolated. According to alkylation of an oxazole-R-OH heterocycle,<sup>248</sup> the reaction has been carried with excess of NaH (10 eq.) at room temperature in DMF instead of THF and the product **18** has been obtained with a good yield of 71 % (Entry 5).

Table 11: The different conditions of the O-alkylation of **EDOT-MeOH** for the synthesis of compound **18** from **16**

Entry	Base	Equivalents	Solvent	Temperature	Yield of <b>18</b>
1	NaH (60 %)	20	THF	R.T	0 %
2	NaH (60 %)	4	THF	R.T	0 %
3	NaH (60 %)	2	THF	R.T	0 %
4	NaH (60 %)	4	THF	45-65 °C	0 %
5	KOH (85 %)	4	THF	R.T	0 %
6	NaH (60 %)	10	DMF	R.T	71 %

After the synthesis of **(R)-EDOT-MeO-R-OP**, the objective is to synthesize the stannic compound to be attached to DPP intermediate by Pd-catalyzed Stille coupling reaction for applying the post functionalization strategy. Hence, it is important to work on the preparation of stannic derivatives from the protected synthon **(R)-EDOT-MeO-R-OP**.

### 2.2.2. Example of pre- functionalization with the direct functionalization of **(R)-EDOT-R-OP** with alkyl chains:

To test the first strategy of pre-functionalization represented in scheme 11, we have decided to use an alkyl chain as **Y** function, because it is compatible to all reaction conditions.

Initially, the preparation of extended alkyl branched chains was decided to increase the solubility of n-type conjugated polymers (Chapter 3). They were prepared during M2 internship (Viktor BOSHEVSKI, January-June 2022) from reported procedures.<sup>252</sup> As these chains were synthesized in limited quantities (100-200 mg), they were engaged in the direct functionalization of the generic synthon. The presence of branching point induces better solubility, while the presence of a linear spacer allows good  $\pi$ -stacking.

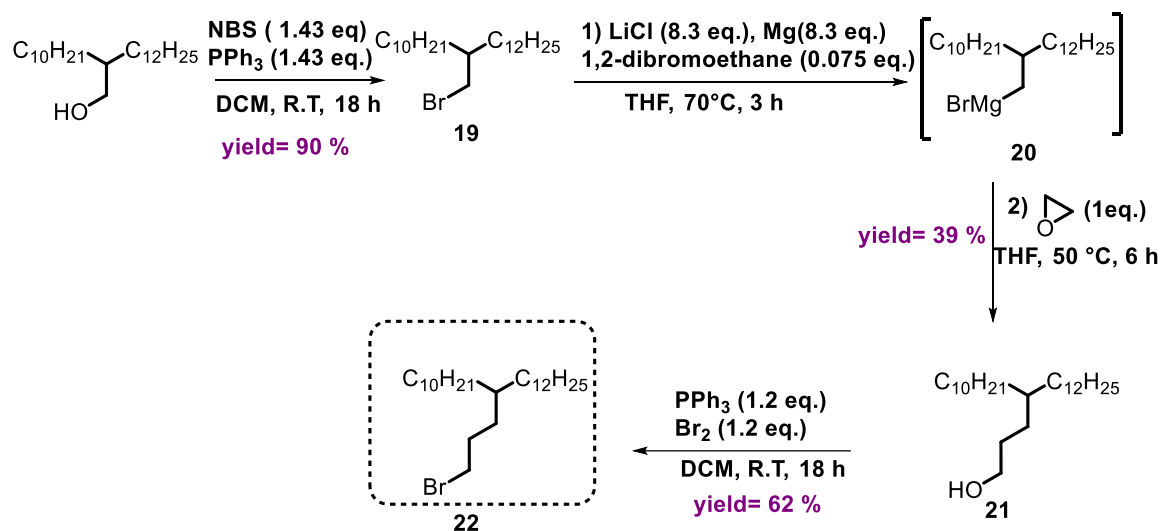
<sup>250</sup> K. Krishnamoorthy, M. Kanungo, A.Q. Contractor, A. Kumar, *Synth. Met.* **2001**, *124*, 471-475.

<sup>251</sup> S. Macher, M. Schott, M. Sassi, I. Facchinetti, R. Ruffo, G. Patriarca, L. Beverina, U. Posset, G. A. Giffin, P. Löbmann, *Adv. Funct. Mater.*, **2019**, *30*, 1906254

<sup>252</sup> Kohsuke Kawabata, Masahiko Saito, Itaru Osaka, and Kazuo Takimiya, *J. Am. Chem. Soc.* **2016**, *138*, 7725

### 2.2.2.1. Synthesis of branched alkyl chain:

The synthesis of the extended alkyl branched chain is already described in the literature. It is inspired by the work of Takimiya and *al'* in two steps from the brominated compound **19** using ethylene oxide<sup>59</sup> (Scheme 15).



Scheme 15: The synthesis alkyl branched chain with 3 carbon spacer **18**

The first step through the preparation of the extended branched chain is the formation of brominated compound **19** from the alcohol starting material, which is commercially available. Two conditions were tested for bromination to obtain compound **19**, the data of the reaction conditions are listed in table 12. The yield of the reaction was increased from 52 % to 90%.

Table 12: The different conditions of bromination reaction for the synthesis of intermediate **19**

Entry	NBS	PPh <sub>3</sub>	Temperature	Duration	Yield
1	1.5 eq.	2 eq.	R. T	16 h	52 %
2	1.43 eq.	1.43 eq.	R. T	16 h	90 %

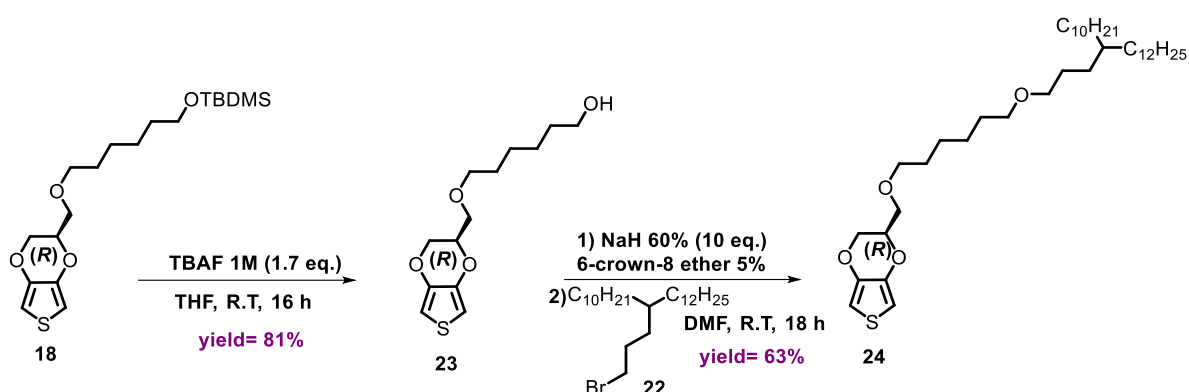
The next step in the preparation of extended branched chain is a nucleophilic addition of freshly prepared Grignard intermediate **20** from compound **19** to ethylene oxide to obtain alcohol with three carbon spacer **21**. From reported procedure,<sup>59, 253</sup> the compound **21** was obtained with a yield of 39 %. The next step is bromination reaction with bromine<sup>59</sup> to obtain the desired molecule **22** in a yield of 62 %.

The extended branched chain **22** was synthesized in small quantity. Therefore, it was tested in the functionalization of EDOT by applying a pre-functionalization strategy to attach Y= extended branched alkyl chain on (*R*)-EDOT-MeO-R-OP to prepare (*R*)-EDOT-MeO-R-OR'.

<sup>253</sup> K. Kawabata, M. Saito, N. Takemura, I. Osaka, K. Takimiya, *Polymer Journal*, **2017**, 49, 169-176

### 2.2.2.2. Synthesis of *(R)*-EDOT-R-OR'

*(R)*-EDOT-R-OR' has been synthesized in two steps starting from *(R)*-EDOT-R-OP **18**, the first step is deprotection of the alcohol terminal using TBAF at R.T to obtain compound **23** with a yield of 81 %. This step is followed by nucleophilic substitution of the deprotonated alcohol of **23** on the halogenated extended alkyl branched chain **22**. The functionalized EDOT **24** was isolated with a yield of 63 % (Scheme 16).



Scheme 16: The synthesis of *(R)*-EDOT-MeO-R-OR' **24**

The pre-functionalization strategy was successively applied with obtaining functionalized EDOT with branched extended alkyl chain **24**. This compound is suitable to be used for obtaining a stannic derivative and then the stannic derivative could be used in Stille coupling reaction in the presence of DPP intermediate.

### 2.2.3. Example of post-functionalization with the insertion of *(R)*-EDOT-R-OP in the DPP containing ligand:

In case the Y function is sensitive to reactions conditions, the post-functionalization of the generic ligand **L'** could be carried out as represented in figure 117 to overcome these difficulties.

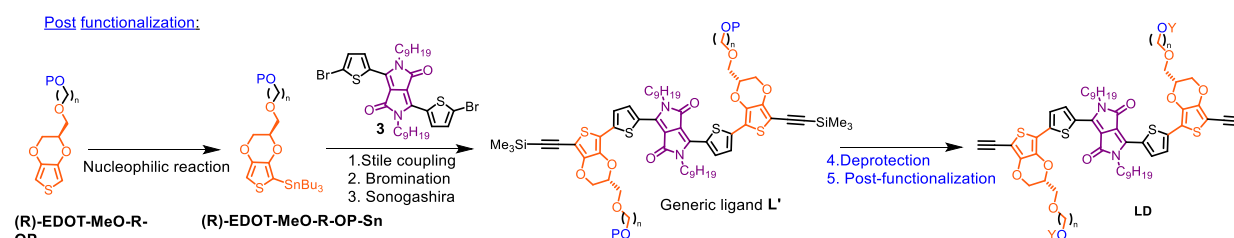
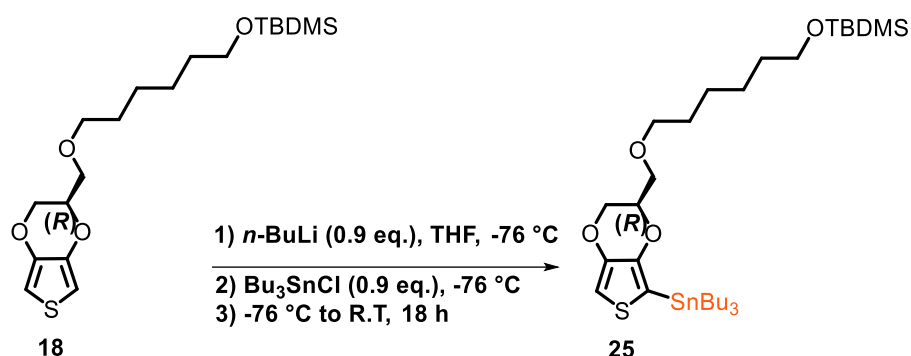


Figure 117: An example of post-functionalization strategy

Post-functionalization strategy consists of attaching the generic synthon *(R)*-EDOT-R-OP to T-DPP-T moiety, followed by a bromination reaction of EDOT moieties and then a Sonogashira coupling reaction to prepare the generic ligand **L'**. Then, the silyl group is

removed to generate the alcohol function, which was used to attach the **Y** function to prepare **LD**. This ligand will be engaged in dehydrohalogenation reaction for the preparation of metallooligomer **PD**. The key step in this synthesis is the formation of the stannic derivative of **(R)-EDOT-R-OP 25** (Figure 117).

The stannic derivative **25** was prepared from compound **18** (Scheme 17). It is inspired from a reported procedure.<sup>254</sup>



*Scheme 17: The synthesis of monostannic functionalized EDOT 25*

The monostannic compound **25** is obtained in one step according to scheme 17. It starts with deprotonation reaction of the hydrogen in alpha position of thiophene with *n*-BuLi, followed by a nucleophilic substitution on tributyltin chloride to obtain the desired compound **25** with 75 % conversion according to <sup>1</sup>H NMR analysis. This step required an optimization, listed in table 13.

*Table 13: The different conditions for the synthesis of compound 25*

Entry	<i>n</i> -BuLi(2.5M)	Bu <sub>3</sub> SnCl	Solvent	Duration	[ <b>18</b> ] mmol/mL	Conversion
1	1.0 eq.	1.0 eq.	THF	18 h	1.5	0 %
2	0.9 eq.	0.9 eq.	THF	18 h	13	75 %

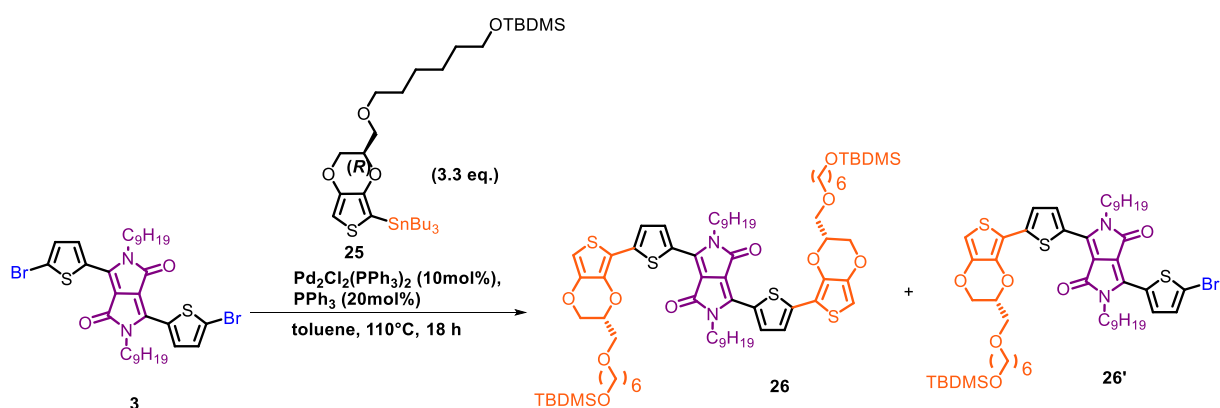
At the beginning the stannylation reaction has been tested on 1 equivalent of the base and 1 equivalent of the stannic reagent. However, the <sup>1</sup>H NMR spectrum showed the absence of the monostannic product. To increase the reactivity of the base, the concentration has been increased from 1.5 mmol/mL to 13 mmol/mL and the number of equivalents is reduced to 0.9 for each of the base and the stannic reactant to minimize the formation of bis stannic EDOT.

To verify the formation of the desired compound, a comparison between the <sup>1</sup>H NMR spectra of the starting material and the isolated compounds was made. For compound **25**, the hydrogen signal at the alpha position has a chemical shift of 6.57 ppm instead of 6.3 ppm in the starting product. And the presence of the signal of the protons of butyl groups was observed around 1.5 ppm, which confirms the formation of monostannic compound **25**. It was directly engaged in the next step without further purifications.

<sup>254</sup> L. Huang, G. Zhang, K. Zhang, Q. Peng, M. S. Wong, *macromolecule*, **2019**, 52, 12, 4447–4457

#### 2.2.4. Synthesis of the generic ligand **L'** with the preparation of the EDOT and DPP containing intermediate **26**:

post-functionalization was carried out from the generic ligand **L'**. It brings the advantage to be functionalized with different functions **Y** to prepare distinct ligands **LD** and metallooligomer **PD**. In order to prepare **L'**, the intermediate **26** must be synthesized (Scheme 18). The generic synthon is attached to T-DPP-T moiety with a Pd-catalyzed Stille coupling reaction in the presence of dibrominated DPP **3** and the monostannic function of compound **25** according to scheme 18.



Scheme 18: The synthesis of intermediate **26**

Intermediate **26** was obtained with a yield of 45 % with a Stille coupling reaction in the presence of Pd<sub>2</sub>Cl<sub>2</sub>(PPh<sub>3</sub>)<sub>2</sub>. Upon completing the reaction, a secondary product **26'** was obtained with a yield of 12 %. These two compounds were characterized by <sup>1</sup>H and <sup>13</sup>C NMR. Even with the difficulty to analyze such molecules with ASAP or ESI due to the low solubility, the molecular peak of each compound has been detected with ASAP and ESI by Karine Jarsale, LCMT, Caen. Intermediate **26** could be subjected to bromination reaction and then Sonogashira coupling reaction for the preparation of the generic ligand **L'** as an intermediate in **LD** preparation.

Indeed, the expected metallooligomer from **26'** could be of our interest in other type of metallooligomers with one EDOT unit per monomer to study the impact of the quantity of the organizing group.

To conclude with, (*R*)-EDOT-MeO-R-OP was synthesized as a generic synthon for both pre- and post-functionalization. It was successively functionalized with extended branched alkyl chain to obtain (*R*)-EDOT-MeO-R-OR' **24** as a key step in pre-functionalization strategy. In addition, (*R*)-EDOT-MeO-R-OP intermediate was directly used in the formation of stannic derivative **25**. Intermediate **25** was integrated in the preparation of a generic ligand **L'** using a Stille coupling reaction, which could be followed by bromination reaction and Sonogashira coupling. This is as an example of a post-functionalization strategy.

### 3. Conclusion and Perspectives:

The main objective of the work demonstrated in chapter 2 is decreasing the optical band gap of metallooligomers synthesized in the team to increase the absorption wavelength range and to decrease energy losses. Increasing the conjugation length, changing the nature of organic part of the ligand and improving the planarity of the conjugated system backbone are of the methodologies applied. Therefore, two strategies were applied to enhance optical and optoelectronic properties of the metallooligomers and increasing the absorption wavelength range. The first strategy aimed to insert two thiophenes with the preparation of **PA**. We succeeded to obtain **PA** with an increased absorption wavelength range compared to **P1'** and with an increased average molar mass with optimization of the reaction condition of dehydrohalogenation. The insertion of solubilizing chain on thiophenes could increase the solubility of the ligand **LB**, but **PB** was not isolated because we faced reactivity problems. Concerning the second strategy, we successively obtained a new metallooligomer **PC**. This strategy aimed to overcome the drawbacks of a previous metallooligomer **P2'** and mostly the instability issue of the deprotected ligand **L2'** and the difficulties of the synthesis. It is applied by the insertion of strong donor (EDOT), which can play a remarkable role in improving the planarity of the backbone of the conjugated system and consequently can increase the absorption wavelength range of the obtained metallooligomer. This strategy results in a low optical band gap comparable to **P2'**, but **PC** exhibit a remarkable good stability and it is prepared with easier synthetic route (Figure 118).

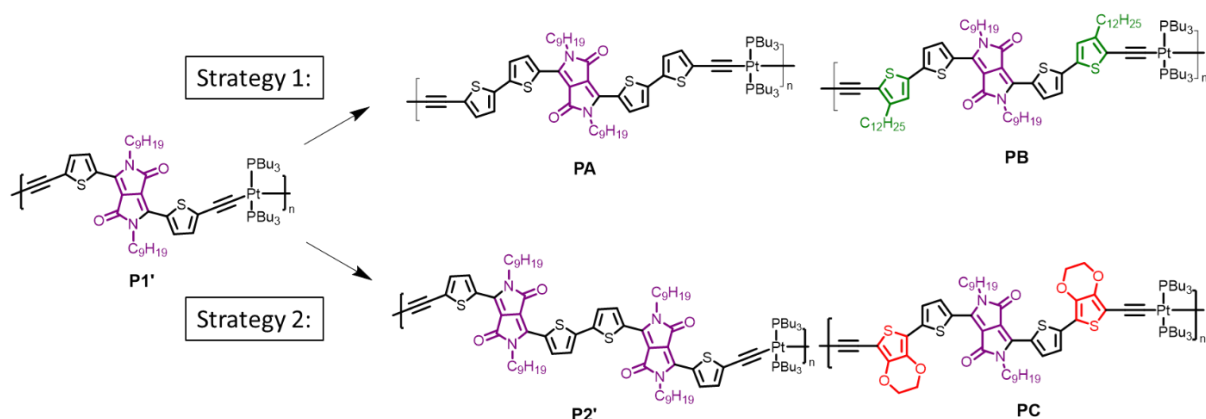


Figure 118: The structure of different metallooligomers synthesized in this thesis.

Thanks to the collaborative project with Jean-François Lohier and Romuald Herbinet, 300 mg of **PC** was resynthesized with improved purity. This permits its investigation in Photophysics and its use as a donor in BHJ solar cell. The highest performances reach 15.12 % with the acceptor **Y6** with an average value of 14.12 %. This good result will be published soon in ACS macromolecules.

Hence, **PC** is considered now as a reference for the next generation of **DPP** based metallooligomers accompanied with EDOT. Its performances could be enhanced with the functionalization of EDOT with side chains and functions **Y**. We have tested two strategies of pre and post functionalization to prepare these functionalized metallooligomers **PD**. Some intermediates of functionalized EDOT have been already synthesized.

In perspectives of this part, the major goal is to resynthesize the intermediate **26** to be used as a donor unit in the preparation of functionalized EDOT contained metallooligomer **PD**. So, the distinct side chain could be grafted by applying post-functionalization strategy to have an impact on the molecular organization of the obtained metallooligomer (Figure 119) and on its optoelectronic properties, to enhance solar cell performance.

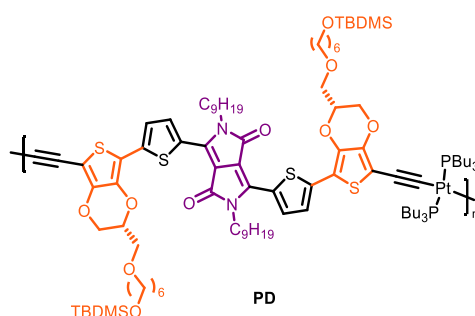
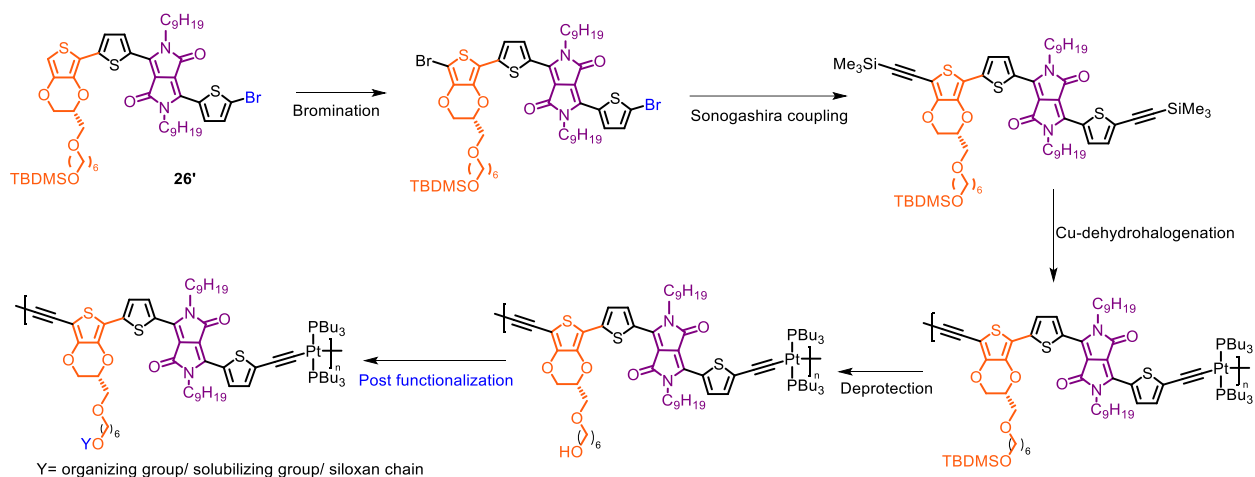


Figure 119: Structure of functionalized EDOT contained metallooligomer **PD**

Moreover, new type of metallooligomers using one unit of EDOT per monomer as **26'** intermediate could be synthesized (Scheme 19) to study the impact of the quantity of organizing groups on the charge mobility and solar cell performance.



Scheme 19: The synthesis of new type of metallooligomers using one unit of EDOT per monomer as **26'** intermediate



# Chapter 3

## I. Introduction:

Electron-deficient or n-type polymers have high electron affinity value due to a low lying LUMO (Lowest Unoccupied Molecular Orbital), which allows negative charge transport. It is crucial of importance to develop efficient ones to be used as semiconductors for n-type OFET (Organic Field Effect transistors) application and as conducting polymers, after a doping process, for n-type materials preparation into organic thermoelectric (OTEs) devices, when they are associated to counterpart p-type materials (Figure 120). However, n-type polymers are still rare because of their difficult synthesis, poor solubility and lower performances compared to p-type (donor, giving electron, hole transport). The greatest limitation is the lack of the stability of n-type polymers to O<sub>2</sub> and H<sub>2</sub>O, which decreases charges transport time limit. One strategy to overcome these limitations is lowering the LUMO level. Therefore, it is important to increase the electro-deficient nature of the conjugated polymer and to improve its  $\pi$ -stacking of the chains. The narrow band gap of these polymers is an additional advantage for doping step effectiveness and to develop ambipolar OFET,<sup>255</sup> the greatest advantage is the use of a single material for both holes and electrons transport.

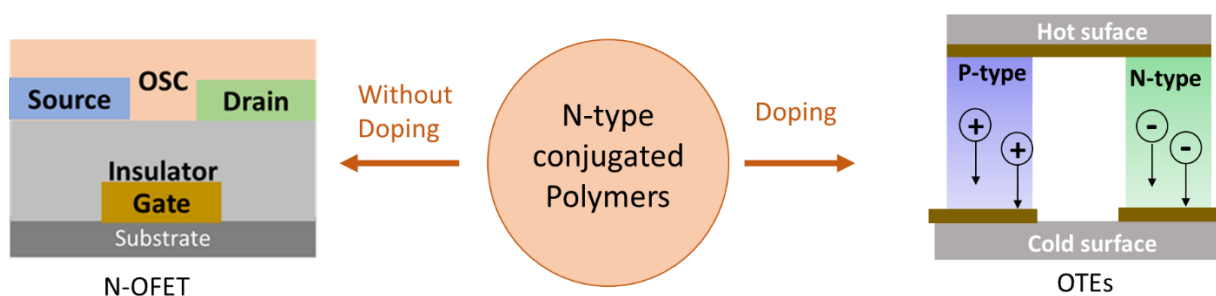


Figure 120: Applications of conjugated polymers

### 1. Thermoelectric materials:

Nowadays, thermoelectric materials attract widespread attention because they can generate electricity from gradient temperature. They can increase renewable energy production part by recycling heat loss from human activity (e.g., industrial activity).

Over the history, in 1794, the first hints of thermoelectric effect were observed with Alessandro Volta's work. However, the story of thermoelectric devices started with the discovery of Thomas J. Seebeck effect in 1821, where he noticed circuit made between two unlike metals with different temperature. Many materials have considered useful for thermoelectricity generation. Starting with the inorganic materials, they are of three main categories: metal, intermetallic system, and metallic oxide. The first semiconductors and conductors used were based on metals such as copper and iron. The next generation in the 20<sup>th</sup> century was using materials as ceramics and composites.<sup>256</sup> However, among the intermetallic system the best thermoelectric material is bismuth telluride Bi<sub>2</sub>Te<sub>3</sub><sup>257</sup> and some

<sup>255</sup> J. Yang, Z. Zhao, S. Wang, Y. Guo, Y. Liu., *chem*, **2018**, 4, 2748-2785

<sup>256</sup> A. Polozine, S. Sirovinskaya, L. Schaeffer, *Materials Research.*, **2014**, 17(5): 1260-1267

<sup>257</sup> H. J. Goldsmid, *Materials* **2014**, 7(4), 2577-2592

of its alloy.<sup>258,259</sup> These materials are the most efficient at near room temperature and up to 100 °C. Indeed, it is the only material utilized and well-trying in commercially available converters with high performance calculated by figure of merit (ZT), which is with values between 1 and 2 for both n-type and p-type materials.<sup>260</sup> Recently, organic semiconductors have been used in thermoelectric devices.

### 1.1. Principle of thermoelectric devices:

There are two modes of function for thermoelectric device.<sup>261</sup> It is used as a power generator with Seebeck effect and as a refrigerator device with Peltier effect according to the configuration of the system (Figure 121).

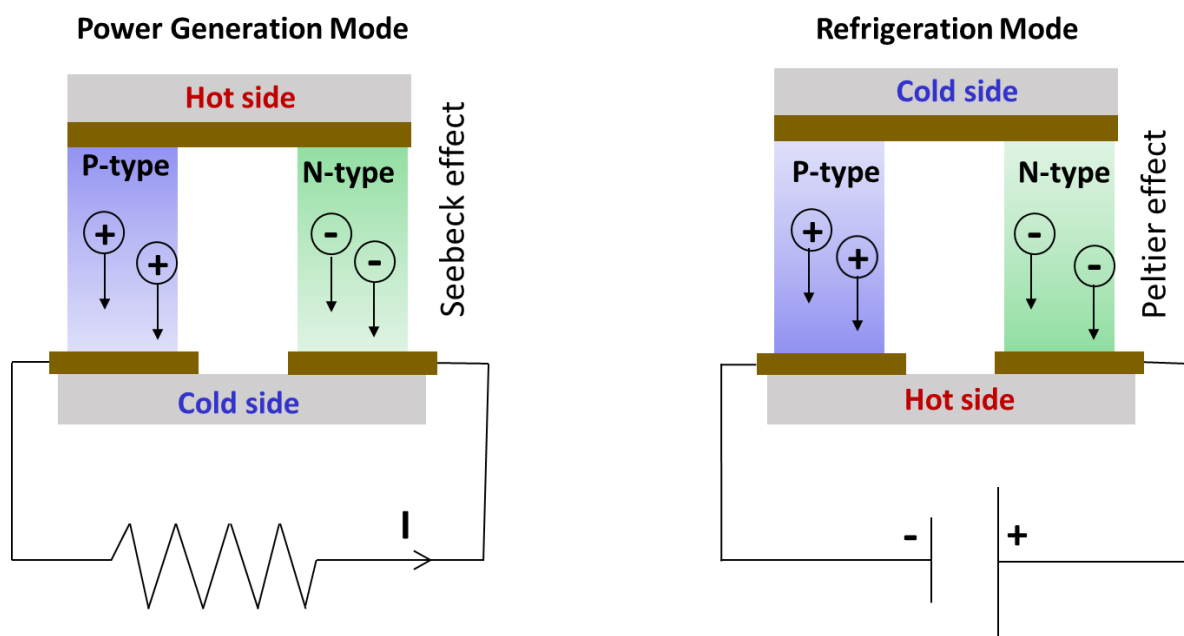


Figure 121: The different function principles of thermoelectric device according to their fabrication form

Seebeck effect is used in thermoelectric generators that work as heat engines to produce electricity from heat, which could be recycled from heat generated from human activities (transportation, industrial activity, ...). Peltier effect is used to form a refrigerator. In my PhD project, we focus on Seebeck effect.

Thermoelectric device consists of a pile made up of a number of two types of materials pairs: n-type and p-type (Figure 122). These materials are connected in series with conductors. The difference in temperature between the two conductors allows the generation of electric

<sup>258</sup> L. D. Hicks, M. S. Dresselhaus, *Phys. Rev. B.*, **1993**, 47, 12727-12731.

<sup>259</sup> B. Poudel, Q. Hao, Y. Ma, Y. Lan, A. Minnich, B. Yu, X. Yan, D. Wang, A. Muto, D. Vashee, X. Chen, J. Liu, M. S. Dresselhaus, G. Chen, Z. Ren, *Science*, **2008**, 320, 634-638

<sup>260</sup> B. Rijal, A. Baimyrza, T. Parein, Q. Lonné, D. Blond, R. Retoux, F. Gascoin, L. Le Pluart, C. Lemouchi, *Nano-Structures & Nano-Objects*, **2021**, 25, 100629

<sup>261</sup> Y. Du, J. Xu, B. Paul, P. Eklund, *Applied Materials Today*, **2018**, 12, 366–388

potential. The sum of these potentials is known as electromotive force. Increasing the number of pairs leads to increase in the electromotive force.

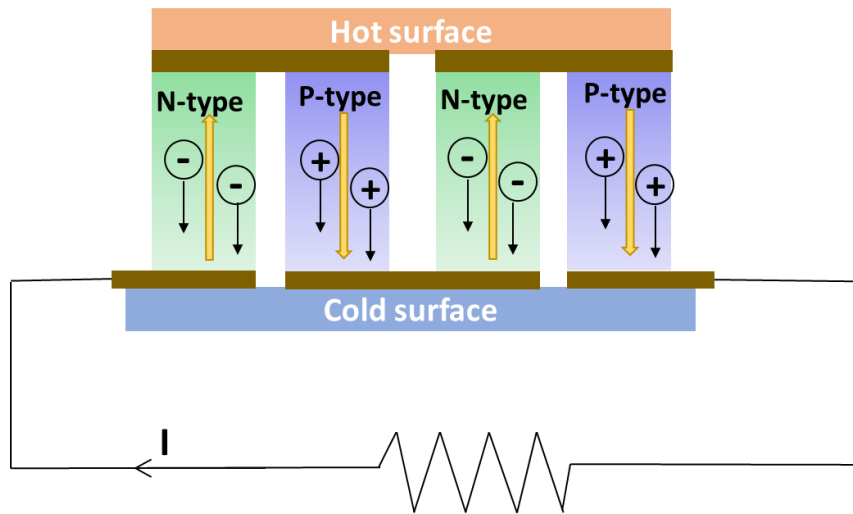


Figure 122: Structure of thermoelectric device

## 1.2. Performance of thermoelectric devices:

The energy conversion energy efficiency of thermoelectric device can be estimated by dimensionless figure, the figure of merit  $ZT$  with the equation below:<sup>262</sup>

$$PCE = ZT = \frac{S^2 T}{\rho \kappa} = \frac{S^2 \sigma T}{\kappa}$$

Where,  $S$  is the Seebeck coefficient,

$\sigma$  is the electrical conductivity.

$\rho$  is the electrical resistance.

$T$  is the absolute temperature between the cold side and hot side

$\kappa$  is the thermal conductivity between the cold side and hot side

$Z$  takes into consideration the electrical resistance of the thermoelements in series ( $R$ ) and thermal conductivity of thermoelements Connected in parallel ( $K$ ).<sup>263</sup>

$$Z = \frac{S^2}{RK}$$

The electrical conductivity is determined with  $\sigma = n e \mu$ , where  $e$  the charge carrier,  $n$  the density of charge carrier and  $\mu$  carrier mobility.

After calculating the Seebeck coefficient and electrical conductivity, power factor (PF) can be calculated.

$$PF = S^2 \sigma$$

<sup>262</sup> D. Enescu, E.O. Virjoghe, *Renewable and Sustainable Energy Reviews*, **2014**, 38, 903–916

<sup>263</sup> G. Min, D.M. Rowe, *Energy Convers Manag.*, **2000**, 2(41), 163–71

Over the past years, scientists are working to manage increasing the ZT values of thermoelectric devices. Therefore, based on the figure of merit, the aim is to meet three qualitative criteria: high Seebeck coefficient, high electrical conductivity and low thermal conductivity to obtain high temperature difference between the two conductors and low electrical resistance for large circuit current.<sup>264</sup>

On the other hand, the increase in electrical conductivity usually is followed by an increase in the thermal conductivity. Moreover, if the electrical conductivity sharply increased, the Seebeck coefficient drops as summarized in the graph below:

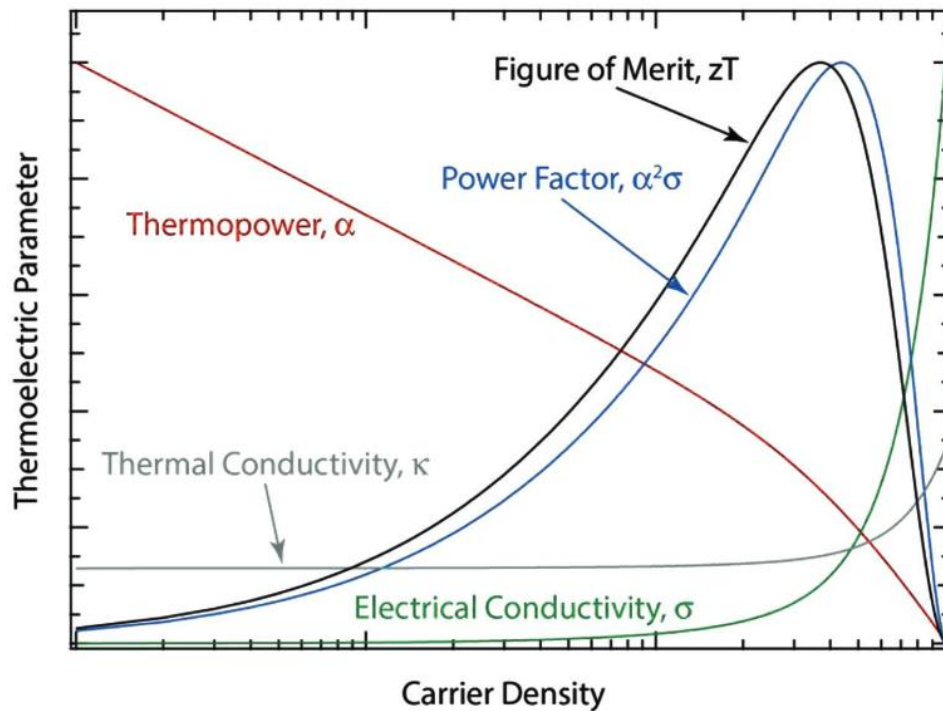


Figure 123: Graph showing the coupled dependence of the various TE properties on carrier concentration<sup>265</sup>

The current applied strategy for high performance thermoelectric materials is to develop materials with high electrical conductivity and low thermal conductivity. Typically, enhancement of electrical conductivity is by increasing  $n$  using doping technique. The first type of materials is based on inorganic compounds (metals, intermetallic system, and metallic oxide). Bismuth telluride  $\text{Bi}_2\text{Te}_3$ , and more recently, silicon are among the high performance materials, for thermoelectric (TE) applications near room temperature. The best performing  $\text{Bi}_2\text{Te}_3$ , typically, p-type alloys exhibit high ZT of 2.42 at 700 K, while n-type  $\text{Bi}_2\text{Te}_3$  alloys are of lower values due to higher thermal conductivities. Concerning silicon (Si), it is a tetravalent metalloid, which is recently studied in TE industry, when it is used in the form of nano-wires, the ZT value is around 1 at 200 K.<sup>266</sup> SnSe crystals are among type inorganic materials that

<sup>264</sup> Q. Zhang, Y. Sun, W. Xu, D. Zhu, *Adv. Mater.*, **2014**, 26, 6829.

<sup>265</sup> J.L. Blackburn, A.J. Ferguson, C. Cho, J.C. Grunlan, *Adv. Mater.*, **2018**, 30, 35.

<sup>266</sup> Md. N. Hasan, H. Wahid, N. Nayan, M. S. Mohamed Ali, *Int J Energy Res.* **2020**, 1–53

shows good thermoelectric performance, where it allows obtaining the highest ZT value so far of 2.62 at 923K.<sup>267</sup>

Despite the high ZT values of inorganic materials, they suffer inherent disadvantages such as rarity, toxicity, poor processability and expensive manufacturing. Also, this type of materials requires high operation temperature that is generally above 200 °C.<sup>268</sup> Therefore, nowadays, the current strategy is to decrease the thermal conductivity with porous materials preparation like the preparation of Bi<sub>2</sub>Te<sub>3</sub> nanotubes developed in the team with Aigerim 's PhD and publication of an article.

Another strategy is the use of doped organic conjugated polymers. They are good candidates to overcome the disadvantages of inorganic materials. Currently, doped conjugated polymers show low thermal conductivity, but also low electrical conductivity. Hence, the aim of researchers is to increase the electrical conductivity.

Conjugated polymers attract attention for the preparation of p- and n-type materials for OTE applications because they have low thermal conductivity low-cost fabrication and good mechanical flexibility. They are semiconductors and reach a conductive state after a doping process. Doping process is an electronic transfer between a doping agent and the conjugated polymer and it is of two types: p-type and n-type doping. The "p-doping" is an oxidation of donor conjugated polymer, and the "n-doping" is the reduction of an electron-deficient polymer. The efficiency of doping depends on the ionization potential (IP) value for p-type doping and on the electron affinity (EA) for n-doping. Hence, the doping efficiency is affected by the energy bands levels of the conjugated polymer. So, doping process could be enhanced by tuning the energy levels by modifying the structure of the conjugated polymer for enhanced electronic transfer. In this thesis, we are interested in n-doping of conjugated polymers. The first reported high conductivity was after doping of trans-polyacetylene using naphthalenide of about 80 S cm<sup>-1</sup> in 1978.<sup>269</sup>

However, they have lower electrical conductivity. So, the challenge is to increase the electrical conductivity. One strategy is to increase charge mobility by improving the molecular organization of the polymer with edge-on  $\pi$ -stacking orientation and better  $\pi$ -stacking of the chains.

In the literature, we can identify the best p-type and n-type doped conjugated materials for thermoelectric applications.

### 1.3. P-type conjugated polymers for OTEs:

Polythiophene, poly(3,4-ethylenedioxythiophene) (**PEDOT**), polyacetylene (**PA**), polyaniline (**PANI**), polypyrrole (**PPY**) and polyphenylvinylene (**PPV**) are common families, which are used as p-type materials in thermoelectric materials. They show several interesting

---

<sup>267</sup> L-D. Zhao, S-H Lo, Y. Zhang, H. Sun, G. Tan, C. Uher, C. Wolverton,, V. P. Dravid, M. G. Kanatzidis, *Nature*, **2014**, 508(7496), 373–377.

<sup>268</sup> C-J Yao, H-L Zhang, Q. Zhang, *Polymers*, **2019**, 11, 107

<sup>269</sup> C. K. Chiang, M. A. Druy, S. C. Gau, A. J. Heeger, E.J. Louis, A. G. MacDiarmid, Y. W. Park, H. Shirakawa, *J. Am. Chem. Soc.*, **1978**, 100, 1013–1015.

properties such as low density, low cost, easy synthesis and processing.<sup>270</sup> P-type conjugated polymers, exhibit low thermal conductivity between 0.11 and 0.4 W/mK, and after the doping process an electrical conductivity from  $10^{-16}$  to  $10^{-5}$  S.cm<sup>-1</sup> with power factor in range of  $10^{-6}$  to  $10^{-10}$  Wm<sup>-1</sup> K<sup>-2</sup>.<sup>271</sup>

One of the highest ZT values obtained using organic material is 2.17, which is obtained at 45 K using polyaniline conducting polymer (**PANI**) doped with sulfonic acid due to the giant Seebeck coefficient up to 0.6 V/K.<sup>272</sup>

The first thermoelectric device based on **PEDOT** was fabricated in 1988, where **PEDOT** is a member of polythiophene derivatives used as p-type conducting material.<sup>273</sup> In 2011, **PEDOT** doped with iron(III) p-toluenesulfonate (**PEDOT: Tos**) achieved the highest power factor over 300  $\mu\text{W}\cdot\text{m}^{-1}$  and low thermal conductivity of 0.37 W m<sup>-1</sup> K<sup>-1</sup> leading to ZT of 0.25 at room temperature.<sup>274</sup> The system **PEDOT** doped with polystyrene sulfonic acid (**PSS**) (**PEDOT: PSS**) is famous with their high electrical conductivity and good stability to water and oxygen. In 2013, a higher power factor of 469  $\mu\text{W}\cdot\text{m}^{-1}$  has been reported and ZT of 0.42 at room temperature with (**PEDOT: PSS**) system by mixing DMSO organic solvent to commercial **PEDOT: PSS**.<sup>275</sup>

Among the p-type conjugated polymer with good power factor, there are **PTbTTVT** and **PTbTTVT-F**. They are thieno(3,4-b)thiophene derivatives **TbT**. **PTbTTVT** has electrical conductivity of 180.7 Scm<sup>-1</sup>, Seebeck coefficient of 17.7  $\mu\text{V}\cdot\text{K}^{-1}$  and power factor of 5.6  $\mu\text{W}\cdot\text{m}^{-1}\text{K}^{-2}$ . **PTbTTVT-F** is with slightly higher power factor of 7.2  $\mu\text{W}\cdot\text{m}^{-1}\text{K}^{-2}$  with electrical conductivity of 111.1 Scm<sup>-1</sup>, and Seebeck coefficient of 25.5  $\mu\text{V}\cdot\text{K}^{-1}$  with CuTFSI dopant (Figure 124).<sup>276</sup>

In 2019, a selenium substituted DPP polymer **PDPPSe-12** (Figure 124) has been developed with high performance. After doping with FeCl<sub>3</sub> to reach ZT about 0.25 at RT with high electrical conductivity of 997 S cm<sup>-1</sup>, Seebeck coefficient of 62.3  $\mu\text{V}\cdot\text{K}^{-1}$ , and high-power factor of 364  $\mu\text{V}\cdot\text{K}^{-1}$ .<sup>277</sup>

---

<sup>270</sup> Y. Du, S.Z. Shen, K. Cai, P.S. Casey, *Progress in Polymer Science*, **2012**, 37, 820–841

<sup>271</sup> C-J Yao, H-L Zhang, Q. Zhang, *Polymers*, **2019**, 11, 107

<sup>272</sup> C. Nath, A. Kumar, Y-K Kuo, G. S. Okram, *Appl. Phys. Lett.*, **2014**, 105, 133108

<sup>273</sup> F. Jonas, G. Heywang, W. Schmidtberg, J. Heinze, M. Dietrich, Polythiophenes, Process for Their Preparation and their Use. Bayer AG German Patent DE 3813589A1, 22 April 1988.

<sup>274</sup> O. Bubnova, Z. U. Khan, A. Malti, S. Braun, M. Fahlman, M. Berggren, X. Crispin, *Nature Materials*, **2011**, 10, 429-433

<sup>275</sup> Q. Wei, M. Mukaida, K. Kirihara, Y. Naitoh, T. Ishida, *Materials*, **2015**, 8(2), 732-750

<sup>276</sup> S. Wu, W. Xing, M. Zhu, Y. Zou, Y. Sun, W. Xu, D. Zhu, *J. Mater. Chem. C*, **2021**, 9, 4158–4163

<sup>277</sup> J. Ding, Z. Liu, W. Zhao, W. Jin, L. Xiang, Z. Wang, Y. Zeng, Y. Zou, F. Zhang, Y. Yi, Y. Diao, C. R. McNeill, C-a. Di, D. Zhang, D. Zhu, *Angew. Chem. Int. Ed.*, **2019**, 19, 18893

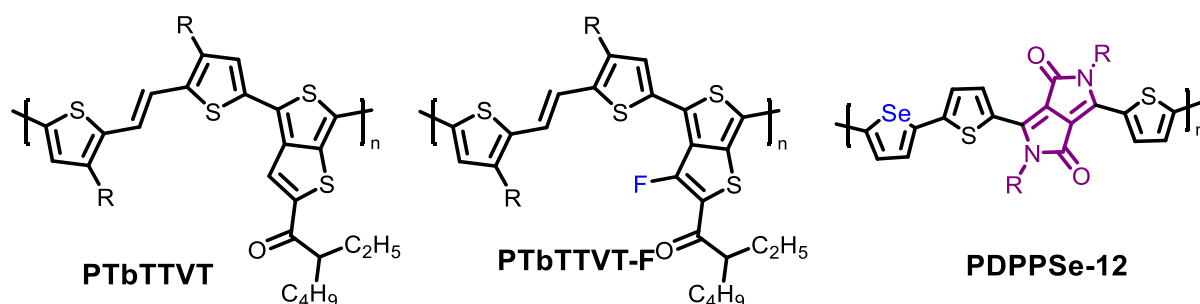


*Figure 124: Examples of p-type conjugated polymers*

N-type conjugated polymers are the second leg for building organic thermoelectric devices. Developing high performance n-type conjugated polymers is a necessity.

#### 1.4. N-type conjugated polymers for OTHes:

N-type counterparts are still rare and suffer from poor thermoelectric behavior due to inefficient doping process or too low conductivity. Most n-type conjugated polymers are of insufficient air and water stability, which restrict them from being efficient under ambient conditions. However, it is well-known that the stability of n-type conjugated polymers strictly related to low LUMO level.<sup>278</sup> Usually conjugated polymers with good charge mobility are used in organic field effect transistors and as n-type materials after doping in organic thermoelectrics.

Therefore, in this thesis we are more interested in the synthesis of stable n-type conjugated polymers with good conductivity. N-type conjugated polymers with low LUMO level are essential for n-type organic field effect transistors and for obtaining n-type thermoelectric materials with high stability and an efficient doping process. The main parameters that must be considered in choosing the building block of n-type conjugated polymers is the deep LUMO level below  $-4.9$  eV,<sup>279</sup> which is required to avoid the electrochemical oxidation by H<sub>2</sub>O and O<sub>2</sub>. The second parameter is the planarity of the backbone. Furthermore, the most promising strategy to achieve low band gap polymer is to alternate donor (D) and acceptor (A) monomers because of the frontier orbitals hybridization effect. Electro-deficient feature increases with a low lying LUMO level that depends on acceptor's nature.

Perylene bisimide (**PBI**) is among the most promising candidate for molecular design and achieving high performance requirement.<sup>280</sup> Naphthalenediimide (**NDI**) is well-known electronic material, which can be subjected to molecular modifications to yield cores as Naphtho dithiophenediimide (**NDTIs**), which is one of lowest LUMO level compounds ( $-4.0$  eV) and small band gap around 2.1 eV with attractive electronic and optical properties, which make it promising candidate as building block for n-type conjugated polymers.<sup>281</sup> Bithiophene

<sup>278</sup> H. Yao, Z. Fan, H. Cheng, X. Guan, C. Wang, K. Sun, J. Ouyang, *Macromol. Rapid Commun.*, **2018**, 39, 22

<sup>279</sup> Y-Q. Zheng, T. Lei, J-H. Dou, X. Xia, J-Y. Wang, C-J. Liu, J. Pei, *Adv. Mater.*, **2016**, 28, 7213-7219

<sup>280</sup> R. Schmidt, J. H. Oh, Y-S. Sun, M. Deppisch, A-M. Krause, K. Radacki, H. Braunschweig, M. Konemann, P. Erk, Z. Bao, F. Wurthner, *J. Am. Chem. Soc.*, **2009**, 131, 17, 6215–6228

<sup>281</sup> Y. Fukutomi, M. Nakano, J-Y. Hu, I. Osaka, K. Takimiya, *J. Am. Chem. Soc.*, **2013**, 135(31), 11445-11448



imide (**BTI**) and its derivatives are another building block have been developed as promising acceptor units (Figure 125).<sup>282</sup>

Other families are used as a core for n-type conjugated polymers benzodifurandione (**BDFD**)<sup>283</sup> and benzodithiophenedione (**BDTD**) (Figure 125).<sup>284</sup>

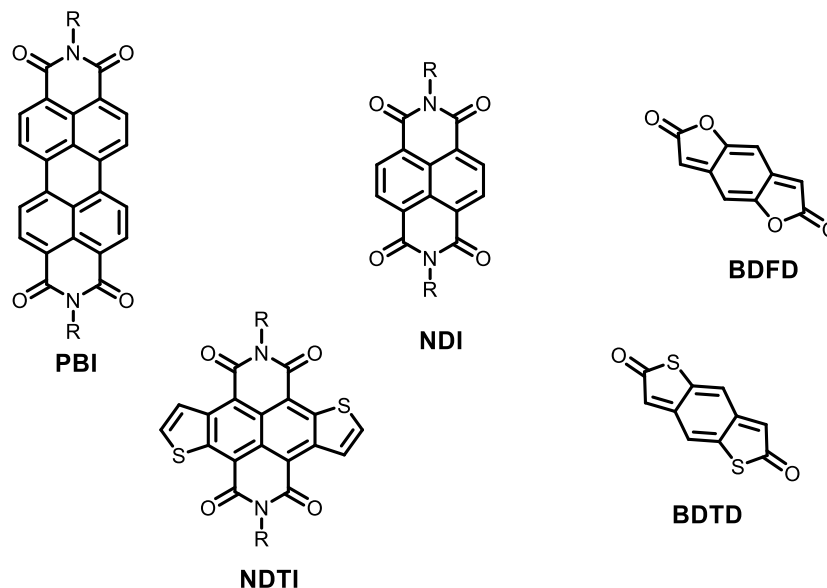


Figure 125: Structure of building blocks of n-type conjugated polymers.

**NDI** based D-A copolymers are widely investigated due to the coplanarity of the building block unit and the high electron affinity. Several **NDI** derivatives have been synthesized with different donor units resulting in low LUMO levels with the lowest value of -4.46 eV and small band gap of 1.55 eV with thiophene units. However, the smallest band gap of 1.28 eV was achieved using benzodithiophene as a donor unit with LUMO of -4.42 eV. In 2020, a family of **NDTI** based conjugated polymer has been developed with low LUMO level below -4.0 eV (Figure 126).<sup>285,286</sup>

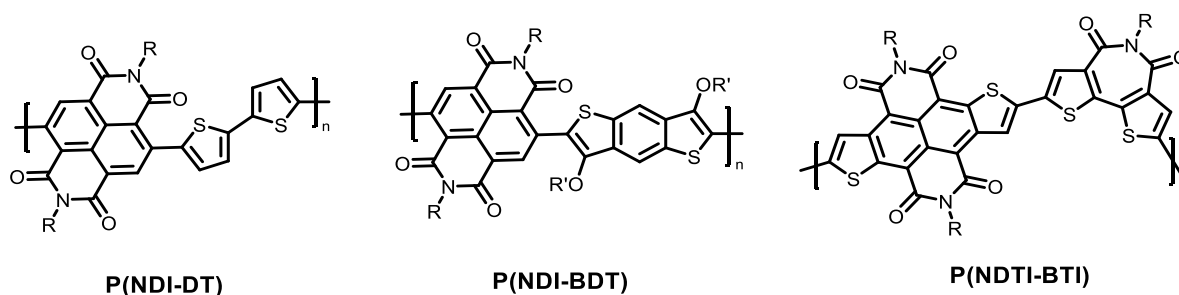


Figure 126: N-type conjugated polymers based on **NDI** and **NDTI** units

<sup>282</sup> K. Feng, H. Guo, J. Wang, Y. Shi, Z. Wu, M. Su, X. Zhang, J. H. Son, H. Y. Woo, X. Guo, *Journal of the American Chemical Society*, **2021**, 143, 3, 1539-1552

<sup>283</sup> W. Ma, K. Shi, Y. Wu, Z. Lu, H. Liu, J-Y. Wang, J. Pei, *ACS Appl. Mater. Interfaces*, **2016**, 8, 37, 24737-24743

<sup>284</sup> M. Nakatsuka, K. Nakasuji, I. Murata, I. Watanabe, G. Saito, T. Enoki, H. Inokuchi, *Chem. Lett.*, **1983**, 12, 905.

<sup>285</sup> Y. Wang, K. Takimiya, *Adv.Mater.*, **2020**, 32, 2002060

<sup>286</sup> H. Ran, F. Li, R. Zheng, W. Ni, Z. Lei, F. Xie, X. Duan, R. Han, N. Pan, J-Y Hu, *ACS Appl. Electron. Mater.*, **2021**, 3, 12, 5573-5583

Poly(p-phenylene vinylene) (**PPV**) derivatives are based on benzo[1,2-b:4,5-b']-difurran-2,6-dione (**BDFD**) as acceptor unit, they are nearly of torsion free backbone, where the fused electron deficient rigid structure lead to less conformational disorder, low LUMO level up to -4.49 eV and a very narrow band gap of 0.89 eV with electron mobility of  $0.16 \text{ cm}^2\text{V}^{-1}\text{s}^{-1}$  and high electrical conductivity of  $1.1 \text{ S cm}^{-1}$  and power factor up to  $1.96 \mu\text{Wm}^{-1}\text{K}^{-2}$  and then **LPPV** conjugated polymers show excellent air stability.<sup>287</sup> **FBDPPV**<sup>288</sup> is one of the n-type conjugated polymers with highest power factor up to  $28 \mu\text{Wm}^{-1}\text{K}^{-2}$  and high electrical conductivity of  $14\text{-}22 \text{ S.cm}^{-1}$  with LUMO level of -4.17, which synthesized by the group of Pei. These n-type conjugated polymers are used in THEs (Figure 127). In the literature, benzo[1,2-b:4,5-b']-dithiophene-2,6-dione (**BDTD**) is a promising acceptor since it leads to polymers with LUMO levels lower than -4.00 eV. Hence, these polymers show the best electron mobility ( $\mu_e$ ) with high air stability and high TE performances (Figure 127).<sup>283</sup>

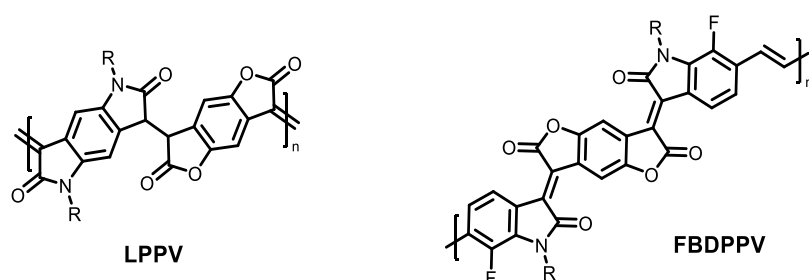


Figure 127: The structure of LPPV and FBDPPV conjugated polymers

**BDTD** based conjugated polymers were used in OFETs applications, as example **BDTD-4T** with LUMO level of -4.04 eV, small band gap of 1.16 eV and ambipolar behavior with an electron mobility of  $0.30 \text{ cm}^2\text{V}^{-1}\text{s}^{-1}$ .<sup>59</sup>

Another **BDFD** based conjugated polymer which owns low lying LUMO level are **BDOPV**.<sup>289</sup> This type of conjugated polymers shows high electron mobility in their initial state before the doping process; Therefore, they are applicable in n-type field effect transistors with LUMO level of -4.15 eV and 1.57 eV band gap with an electron mobility of  $1.74 \text{ cm}^2\text{V}^{-1}\text{s}^{-1}$ . The addition of fluorine atoms **FBDOPV**<sup>279</sup> leads to high apparent electron mobility up to  $14.9 \text{ cm}^2\text{V}^{-1}\text{s}^{-1}$ . Moreover, the fluorine atom leads to a lower LUMO of -4.32 eV keeping the band gap of the same value.<sup>279</sup> These n-type conjugated polymers are used in OFET (Figure 128).

<sup>287</sup> Y. Lu, Z-D. Yu, R-Z. Zhang, Z-F. Yao, H-Y. You, L. Jiang, H-I. Un, B-W. Dong, M. Xiong, J-Y. Wang, J. Pei, *Angew. Chem. Int. Ed.*, **2019**, 58, 11390–11394

<sup>288</sup> K. Shi, F. Zhang, C. Di, T-W. Yan, Y. Zou, X. Zhou, D. Zhu, J-Y. Wang, J. Pei, *J. Am. Chem. Soc.*, **2015**, 137, 22, 6979–6982

<sup>289</sup> T. Lei, J-H. Dou, X-Y. Cao, J-Y. Wang, J. Pei, *Adv. Mater.*, **2013**, 25, 6589–6593

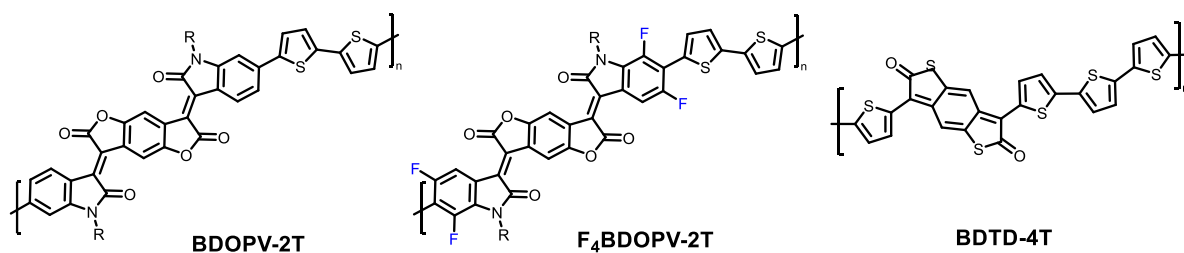


*Figure 128: Structure of n-type conjugated polymers with low LUMO level*

## 1.5. Doping:

N-doping of conjugated polymers is when the dopant plays the role of a donor, so it donates electron to the LUMO level of the n-type conjugated polymer; therefore, creating electrons. As examples of dopants, there are the small atoms like alkali metals such as Lithium, cesium and Lewis acids. However, small molecule dopants can diffuse and then provoke device instability. Therefore, using large and aromatic molecules as good as donor are more efficient in the preparation of stable devices, but large enough not to diffuse in the thin film neither to act as a trap, where they must be allowed to inject an electron to the LUMO level of the conjugated polymer. Hence, the HOMO level must lie above the LUMO of the matrix.<sup>290</sup> This type of doping is still complicated due to the limited molecules combining the stability with appropriate high LUMO state compared to the organic conjugated polymers because the stability of the dopant against oxidation decreases as the HOMO level increases.

Among the n-dopant in organic thermoelectrics **PyB**,<sup>291</sup> (4-(1,3-dimethyl-2,3-dihydro-1H-benzimidazol-2-yl)phenyl)dimethyl amine (**N-DMBI-H**) and trisaminomethane (**TAM**) (Figure 129).<sup>292</sup>

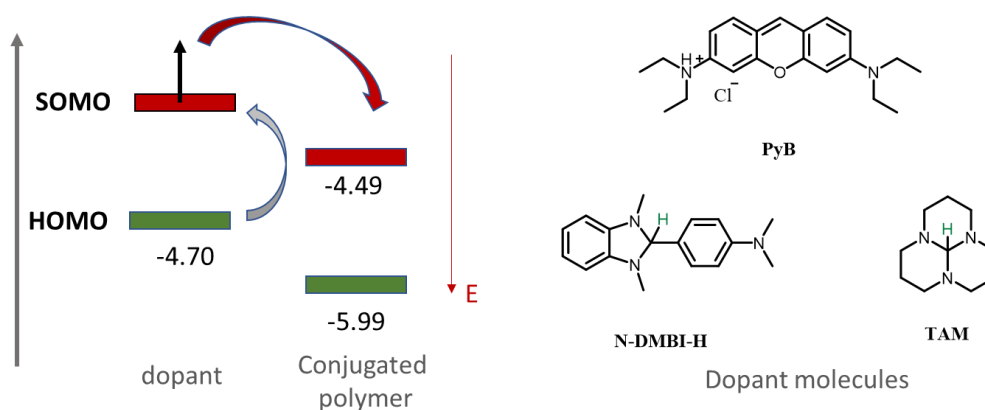


*Figure 129: common n-dopant in organic thermoelectrics*

<sup>290</sup> B. Lüssem, M. Riede, K. Leo, *Phys. Status Solidi A*, **2013**, 210(1), 1-232

<sup>291</sup> S. Kobayashi, T. Takenobu, S. Mori, A. Fujiwara, Y. Iwasa, *Appl. Phys. Lett.*, **2003**, 82(25), 4581

<sup>292</sup> Y. Lu, Z-D. Yu, Y. Liu, Y-F. Ding, C-Y. Yang, Z-F. Yao, Z-Y. Wang, H-Y. You, X-F. Cheng, B. Tang, J-Y. Wang, J. Pei, *J. Am. Chem. Soc.*, **2020**, 142, 15340–15348

**N-DMPI-H** represents the state of art as n-doping reagent, which is widely used in n-type conjugated polymers because of its high doping efficacy.<sup>293</sup> In contrast, **TAM** even has smaller size and consequently it is highly miscible with cycloalkyl edge increasing the side chain affinity, after ionization it has “Y-aromaticity” that reduces the  $\pi$ -affinity, while **N-DMBI<sup>+</sup>** have large  $\pi$ -system and molecular volume resulting in a potential overlap of frontier orbitals. Even though the **TAM<sup>+</sup>** display dramatic effects on the conformation of the doped conjugated polymer due to its motif structure. In table 14, there are examples of the effect of dopant on the thermoelectric properties of two of the best conjugated polymers.

Table 14: Promising n-type material prepared from n-doping of electron deficient conjugated polymer.<sup>294</sup>

Conjugated polymer/Dopant	$\sigma$ ( $S\text{ cm}^{-1}$ )	S ( $\mu\text{ V K}^{-1}$ )	PF ( $\mu\text{Wm}^{-1}\text{K}^{-2}$ )
<b>LPPV/ TAM</b>	$3.7 \pm 0.3$	$-204 \pm 5$	$33.9 \pm 0.9$
<b>LPPV/ N-DMBI-H</b>	$0.9 \pm 0.2$	$-170 \pm 3$	$1.7 \pm 0.2$
<b>FBDPPV/ TAM</b>	21	-170	51
<b>FBDPPV/ N-DMBI-H</b>	14	-200	28

Till now there is no clear explanation concerning the doping stage. It is still affected with different parameters rather than the structure and size, where the doping percentage is quite difficult to be expected depending on the conjugated polymer backbone.

Lowering the LUMO level of the conjugated polymers is an important factor to have efficient doping.<sup>295</sup> In addition, launching electron withdrawing groups is widely used strategy to lower the LUMO level for high electron mobility n-type conjugated polymers.<sup>296</sup>

Doping is a way to increase the conductivity in conjugated polymers for thermoelectric materials, but it is not enough to achieve high conductivity. Increasing the charge carrier transport is a must for further enhancement in the electrical conductivity and consequently the power factor.

## 1.6. Increase the charge carrier transport:

After the generation of charge carrier via doping process, the charge carrier transport has a significant effect on the electrical conductivity, where the transfer of polaron is in two ways. Intrachain transport that is the major and strongly related to the planarity of the conjugated system. And interchain transport off carriers that is forcefully correlated by the morphology and microstructure in the film state with the aggregation of the conjugated

<sup>293</sup> P. Wei, J.H. Oh, G. Dong, Z. Bao, *J. Am. Chem. Soc.*, **2010**, 132, 8852–8853.

<sup>294</sup> C-Y. Yang, Y-F. Ding, D. Huang, J. Wang, Z-F. Yao, C-X. Huang, Y. Lu, H-I. Un, F-D. Zhuang, J-H. Dou, C. Di, D. Zhu, J-Y. Wang, T. Lei, J. Pei, *Nature Communications*, **2020**, 11, 3292

<sup>295</sup> D. Huang, H. Yao, Y. Cui, Y. Zou, F. Zhang, C. Wang, H. Shen, W. Jin, J. Zhu, Y. Diao, W. Xu, C.A. Di, D. Zhu, *J. Am. Chem. Soc.*, **2017**, 139, 13013–13023.

<sup>296</sup> X.K. Gao, Y.B. Hu, *J. Mater. Chem. C*, **2014**, 2, 3099–3117

polymer. One of parameters leading to strong  $\pi$ - $\pi$  stacking and aggregation is long  $\pi$ -conjugated backbone. Here there are three main criteria to follow:

- Planarity of the conjugated backbone to increase the delocalization of intra chain transport.
- The morphology and microstructure tuning to enhance aggregation.
- High molecular weight of the conjugated polymer.

### 1.6.1. Planarity

Donor-acceptor conjugated polymers suffer of large torsion angles between the two building blocks, which restrict the planarity and thus the localization of polaron in the backbone and consequently the interchain transport is blocked.<sup>297</sup> Therefore, maintaining planarity is an urgent need for high charge carrier transport. polybenzimidazobenzophenanthroline **BBL** is an example of a torsion free backbone resulting in high conductivities up to  $2.4 \text{ S}\cdot\text{cm}^{-1}$ .<sup>298</sup> Another example is **LPPV** that is nearly torsion free with electrical conductivity of  $0.6 \text{ S}\cdot\text{cm}^{-1}$  after 76 days under ambient conditions (Figure 130).

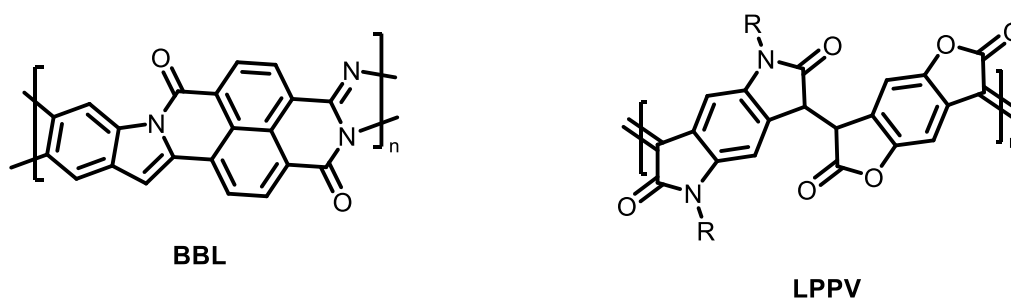


Figure 130: Examples of *n*-type conjugated polymers with high planarity

The second parameter quietly linked to the increased conductivity is the suitable molecular morphology of the conjugated polymer for thermoelectric device.

### 1.6.2. Molecular morphology:

Another issue is the morphology of the conducting polymer, for instance, it is common understanding that conjugated polymers with a pseudo straight line backbone can be arranged with edge-on orientation and show high electron mobilities in organic thermoelectric (Figure 131).<sup>299</sup>

<sup>297</sup> D. Fazzi, M. Caironi, C. Castiglioni, *J. Am. Chem. Soc.*, **2011**, 133, 19056–19059.

<sup>298</sup> S. Wang, H. Sun, U. Ail, M. Vagin, P.O. Persson, J.W. Andreasen, W. Thiel, M. Berggren, X. Crispin, D. Fazzi, S. Fabiano, *Adv. Mater.*, **2016**, 28, 10764–10771.

<sup>299</sup> Y. Wang, T. Hasegawa, H. Matsumoto, T. Mori, T. Michinobu, *Adv. Funct. Mater.*, **2017**, 27, 1604608

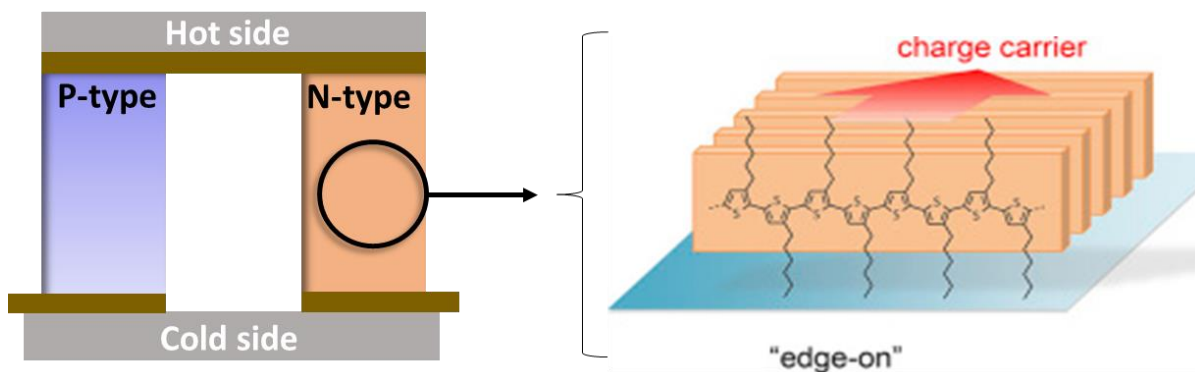


Figure 131: Edge-on orientation in organic thermoelectrics<sup>300</sup>

In the work of Pie, they studied the relation between the thin film morphology and the thermoelectric performance.<sup>283</sup> They used **FBDDPV** as n-type conjugated polymer and **N-DMBI** as a dopant. Grazing incident wide-angle X-ray scattering (GIWAXS) is one of the methods used to study the morphology. In this study, it has been noticed the role of dopant is further than enhancing the charge carrier but also it affects the molecular packing of **FBDDPV**. The use of suitable proportion of the dopant improves the molecular packing and consequently the charge carrier is increased (Figure 132).

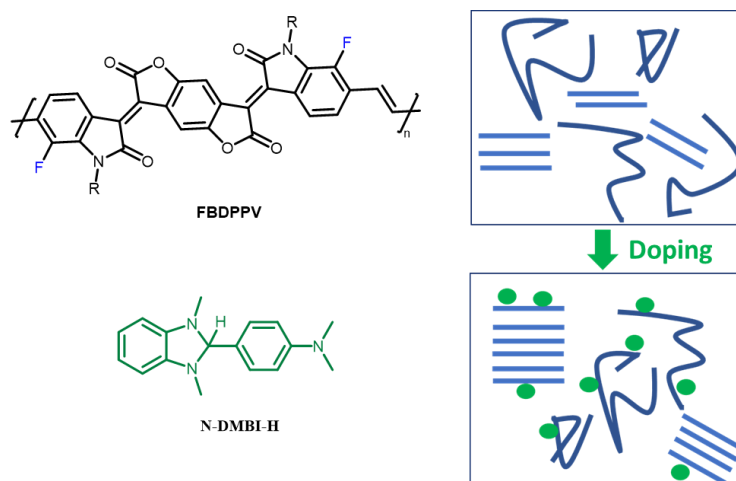


Figure 132: The effect of doping on molecular organization of conjugated polymers<sup>283</sup>

However, changing the percentage of dopant used has an impact on the orientation of the  $\pi$ - $\pi$  stacking between face-on and edge-on orientation.

<sup>300</sup> I. Osaka, K. Takimiya, *Polymer*, **2015**, 59, A1-A15

### 1.6.3. Average molar mass:

The last critical factor will be explained, which the mobility critically linked to is the molecular weight.<sup>301</sup> Neher and *al*<sup>302</sup> have demonstrated that average molar mass has a dominant effect on the mobility. They have concluded that the mobility increases as the average molar mass increases even with reduced crystallinity. This could be explained by better interconnectivity within the polymer with higher average molar mass. However, for lower average molar mass, the molecules are more like isolated microstructure. Moreover, it has been obtained that charged polarons are delocalized over several chains unless for low average molar mass the degree of polaron delocalization is lower, which explain the effect of average molar mass on the charge mobility. As an example, **DPP-DTT** based polymer have been synthesized with high average molar mass of 110 Kg.mol<sup>-1</sup>, which exhibits a very high mobility up to 10.5 cm<sup>2</sup>V<sup>-1</sup> s<sup>-1</sup> contrary to low average molar mass polymer with mobility of 1 cm<sup>2</sup>V<sup>-1</sup> s<sup>-1</sup>.<sup>303</sup>

### 1.7. Enhance the device stability:

The stability of conducting polymers is challenging parameter. Until now doped n-type conjugated polymers are still of poor stability. This parameter is divided into two principles: the stability of the polymer to chemical reactions and the electrochemical stability.<sup>304</sup> Water and oxygen are the main active components in the air. It should be noted that p-type polymers can accept electrons; therefore, they play the role of oxidation agent while n-type can donate an electron and then they play the role of reducing agent. Hence, one way to enhance the stability is lowering the LUMO level of n-type doped conjugated polymers. A comparison between **PNDIT2** and **2S-trans-PNDIT2** with -3.75 eV and -3.96 eV as LUMO level respectively, it showed enhanced stability to the lower LUMO level in **2S-trans-PNDIT2** that permits electron to relax on energy level less subjected to a redox process under ambient conditions (Figure 133).<sup>305</sup> Another way to improve the stability is to prevent the trapping species from reaching the charge transporting area of the polymer, where the mobile electrons are thermodynamically unaffected by trapping. This could be achieved by the water and oxygen exclusion by using molecular semiconductors packed in in sufficiently dense motif to resist the penetration by these species or via appropriate encapsulation keeping the device under inert atmosphere.<sup>306</sup>

---

<sup>301</sup> J-F. Chang, J. Clark, N. Zhao, H. Sirringhaus, D. W. Breiby, J. W. Andreasen, M. M. Nielsen, M. Giles, M. Heeney, I. McCulloch, *Phys. Rev. B*, **2006**, 74(11), 115318

<sup>302</sup> A. Zen, J. Pflaum, S. Hirschmann, W. Zhuang, F. Jaiser, U. Asawapirom, J. P. Rabe, U. Scherf, and D. Neher, *Adv. Funct. Mater.*, **2004**, 14, 757

<sup>303</sup> J. Li, Y. Zhao, H. S. Tan, Y. Guo, C. A. Di, G. Yu, Y. Liu, M. Lin, S. H. Lim, Y. Zhou, H. Su and B. S. Ong, *Sci. Rep.*, **2012**, 2, 754

<sup>304</sup> D.M. de Leeuw, M.M.J. Simenon, A.R. Brown, R.E.F. Einerhand, *Synthetic Metals*, **1997**, 87, 53-59

<sup>305</sup> D. Nava, Y. Shin, M. Massetti, X. Jiao, T. Biskup, M. S. Jagadeesh, A. Calloni, L. Duò, G. Lanzani, C. R. McNeill, M. Sommer, M. Caironi, *ACS Appl. Energy Mater.*, **2018**, 1, 9, 4626–4634

<sup>306</sup> B. A. Jones, A. Facchetti, M. R. Wasielewski, T. J. Marks, *J. Am. Chem. Soc.*, **2007**, 129, 49, 15259–15278

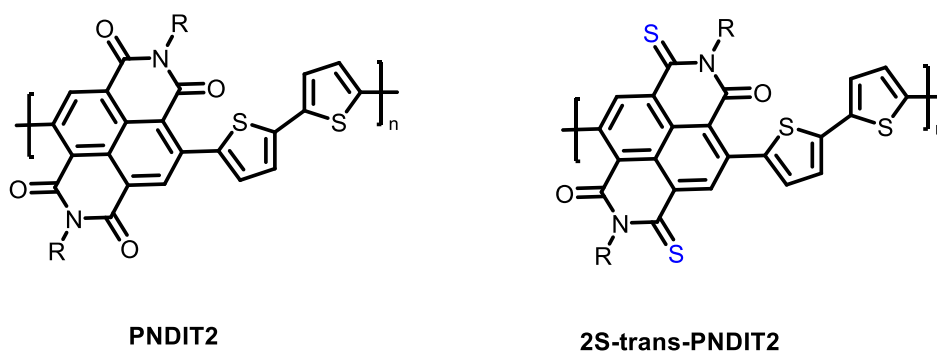


*Figure 133: N-type conjugated polymers with remarkable stability*

## 1.8. Side chain engineering:

Conjugated polymers usually are made up of a core and side chains, these chains have an impact on the solubility of the conjugated polymer, intermolecular packing and optoelectronic properties.<sup>307</sup> Side chain engineering is a simple and effective method to tailor the conjugated polymer without changing the core unit. They are believed to have interchain aggregation in solution, which could play a critical role in crystallization. Knowing that, side chains might provide a way to tune the interchain interactions of conjugated polymers, so, it affects the solution-state aggregation. Strong intermolecular interactions allow the conjugated polymers to have pre-aggregates in solution.<sup>308</sup> The packing of conjugated polymers depends on several parameters according to the pre-aggregation mechanism. However, pre-aggregation mechanism is affected by several parameters such as solvent, dissolution temperature, and solution aging time, bulkiness of the side chain, and interactions between the polymeric chain, polymer and solvent and polymer and the substrate.<sup>309</sup> So, it is still difficult to forecast the type of molecular organization by only choosing the type of the side chain. The choice of our chain is based on reported examples, which exhibit an increase of charge transport, but the comparison is limited because the polymer backbone is different. We are more interested in studying the impact of linear, branched extended alkyl chains and perfluorinated alkyl chains.

### 1.8.1. Alkyl side chains:

Alkyl side chains are the key factor affecting the solubility and the self-assembly of a conjugated polymer. It has been established to take part in intermolecular interactions and supramolecular self-assembly.<sup>310</sup>

<sup>307</sup> D. Wang, L. Liu, X. Gao, C. Di, D. Zhu, *CCS Chem.*, **2021**, 3, 2212–2225

<sup>308</sup> J-H Dou, Y-Q Zheng, T. Lei, S-D Zhang, Z. Wang, W-B Zhang, J-Y Wang, J. Pei, *Adv. Funct. Mater.* **2014**, 24, 6404-6404

<sup>309</sup> Z. Xu, K. S. Park, Y. Diao, *Sec. Polymer Chemistry*, **2020**, 8

<sup>310</sup> L. Ding, H.-B. Li, T. Lei, H.-Z. Ying, R.-B. Wang, Y. Zhou, Z.-M. Su, J. Pei, *Chem. Mater.*, **2012**, 24, 1944



The position of the alkyl side chain can affect the optoelectronic properties because it could generate steric hindrance and decrease the planarity of the polymer. Thomas Heiser and al prepared two polymers with alkyl chains at different positions a and b, illustrated in (Figure 134). For position b the distance between the R chains is larger than in the position a, which decreases the steric hindrance. This agrees with absorption spectroscopy data. For the position b, the absorption band at the lowest energy is red shifted in comparison to those of position a. In position b, the backbone of the polymer is less sterically twisting and therefore enhanced coupling between the donor and acceptor units and increased charge transfer, which favors the reduction of the band gap. Another parameter has been tested is the length of the linear alkyl side chain, however, no significant impact on the absorption peaks. Hence, the length of the alkyl side chain does not affect the band gap. Replacing the linear position at b position by a branched chain had blue shift due to the more steric hindrance. On the other hand, the conjugated polymer with linear chain results an aggregation in solution designating the lower polymer solubility.<sup>311</sup>

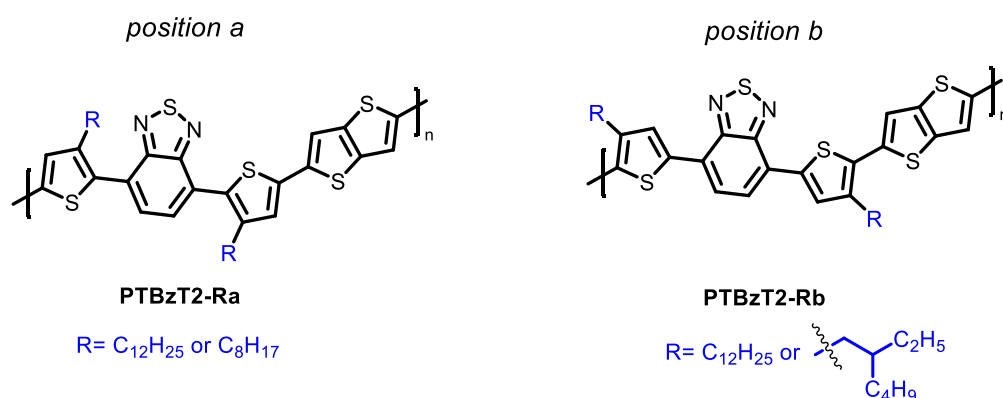


Figure 134: Examples of conjugated polymers with different alkyl side chain

Therefore, the position of the side chain has an influence on the HOMO and LUMO levels of the conjugated polymer, the impact was more on the HOMO level that was increased by 0.34 eV in b position. And the change of the type affected the solubility and the degree of aggregation, while the change in the length almost with no impact on the absorption spectra.

In 2013, a work has been carried to see the impact of utilizing different solubilizing groups on the charge transport and thin film morphology. Branched alkyl side chains increase more the solubility of the polymer than linear ones, but the steric hindrance generated by the branching point nearby the conjugated backbone of the polymer could cause torsion/binding of the chain with higher energy disorder and larger  $\pi$ - $\pi$  spacing into the packing. This is detrimental to high charge transport. However, linear alkyl chain, less bulky leads to more ordered structure with shorter  $\pi$ - $\pi$  spacing and hence better anisotropic transport as reported on the work of Thomas Heiser and *al.* (Figure 135a).<sup>312</sup> Besides, linear chains have a lower solubilizing effect than branched ones, but this increases the pre-aggregation mechanism speed, which favors the packing of the chains with an edge-on orientation.<sup>313</sup> It is beneficial

<sup>311</sup> L. Biniek, C. L. Chochos, G. Hadziioannou, N. Leclerc, P. L  v  que, T. Heiser, *Macromolecular Rapid Communication*, **2010**, 31, 651-656

<sup>312</sup> S. Fall, L. Biniek, Y. Odarchenko, D. V. Anokhin, G. de Tournadre, P. L  v  que, N. Leclerc, D. A. Ivanov, O. Simonetti, L. Giraudet, T. Heiser, *J. Mater. Chem. C*, **2016**, 4, 286-294

<sup>313</sup> T. Marszalek, M. Li, W. Pisula, *Chem. Commun.*, **2016**, 52, 10938-10947

for the enhancement of charges transport. This is illustrated by the reported work of Fréchet and *al* with the preparation of n-C<sub>16</sub>H<sub>33</sub> linear chain functionalized DPP-containing polymers. Polymers with linear chains exhibit lower solubility and an edge-on orientation with higher a degree of crystallinity and shorter  $\pi$ - $\pi$  spacing. Hence, their hole mobility is twice higher than for branched chains functionalized (Figure 135b).<sup>128</sup>

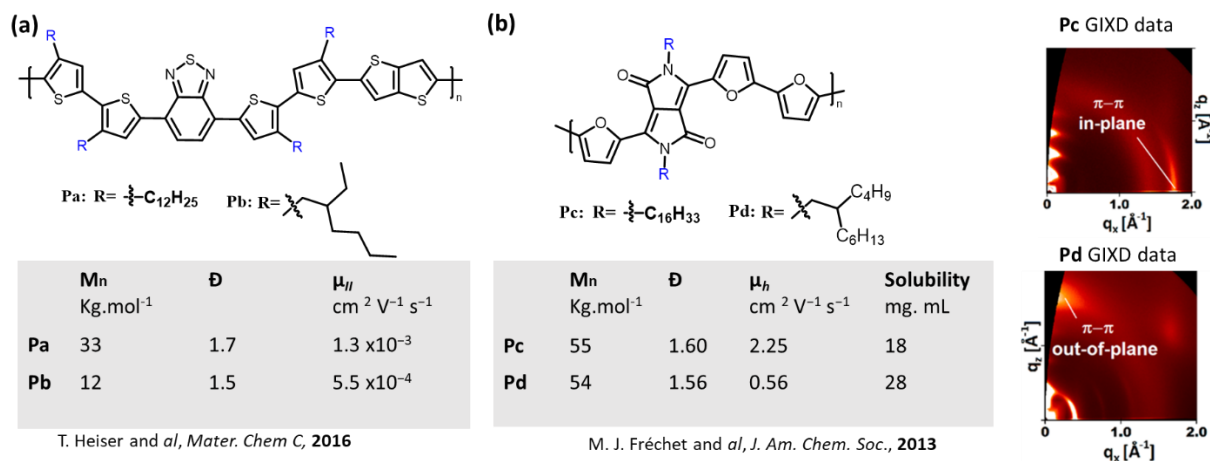


Figure 135: (a) Polymers synthesized by T. Heiser and *al*, (b) polymers synthesized by Fréchet and *al*.

So, linear alkyl chains are interesting side chains to trigger good molecular organization and suitable packings to reach efficient charge transport. But they can lower the solubility of the conjugated polymer.

Therefore, keeping a suitable molecular organization and having a good solubility of the polymer is a challenge for the researchers. One solution is the use of branched extended alkyl chains. They are composed of a linear spacer terminated by a branched chain. The increase of spacer length (number of carbon atoms n) enables move away bulky branching point, which helps for the improvement of the aggregation and to guarantee a good solubility with the branched alkyl part. They could trigger a preferential edge on orientation with an electron mobility of 14.9 cm<sup>2</sup>.V<sup>-1</sup>s<sup>-1</sup> as reported by the group of Pei and *al*.<sup>279</sup> However, it's difficult to predict the molecular organization like the  $\pi$ -stacking orientation because of the influence of several parameters like the length of the spacer, the length of alkyl branched chains, the position of this chain on the conjugated backbone and their number per repeating units. This could lead to detrimental orientation face-on or usually to a mixture of edge-on and face-on orientations. Optimizations are required to select this chain according to the type of conjugated polymer.

The length of the linear spacer and so the position of the branching point have an impact on the molecular organization. As illustrated by the work of Pei and *al* with the preparation of **F4-BDOPV** polymers. They correlate the enhancement of the mobility with the increase of the spacer length, number of CH<sub>2</sub> before the branching point from 1 to 5 (Figure 136a). The three polymers with different branching point show similar 2 theta, which reveals

similar lamellar distance due to the same total length of the three branched alkyl chains (Figure 136b).<sup>314</sup>

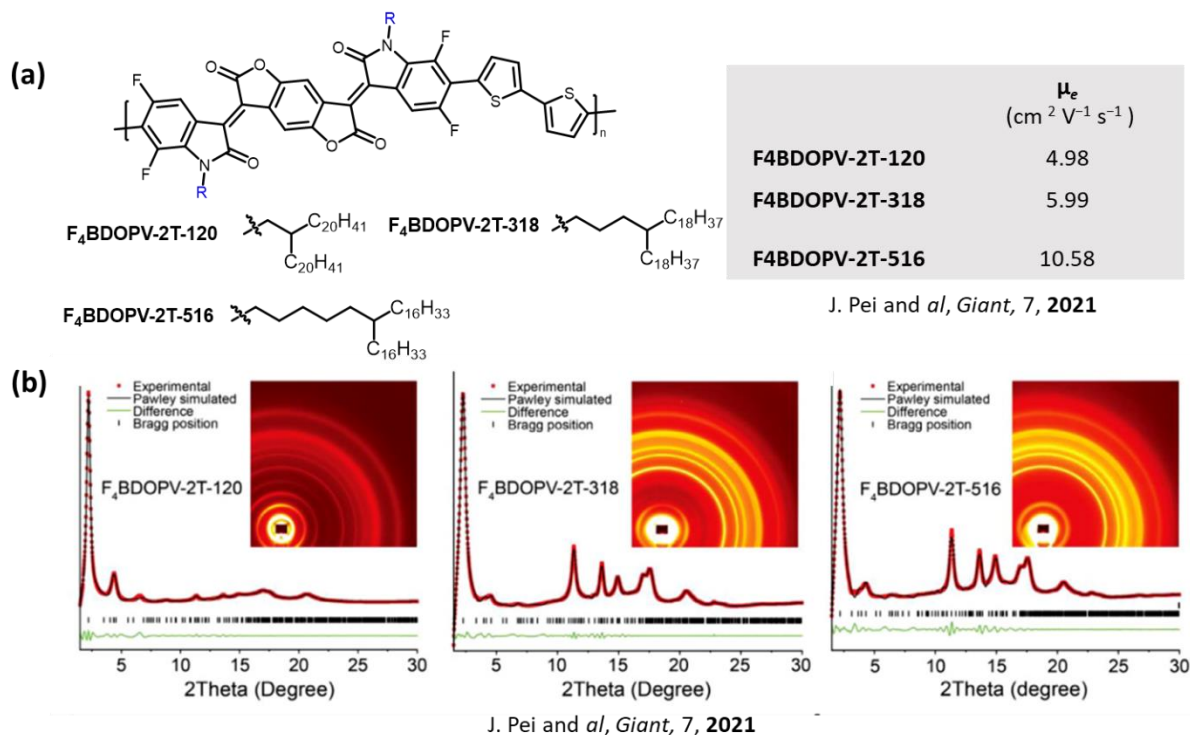


Figure 136: (a) **F4-BDOPV** polymers and their electron mobility, (b) the PXRD data of the different polymers

Another example from the work of Jian Pie group about the preparation of isoindigo-based conjugated polymers (**IIDDT**) for better understanding of maintaining planarity, aggregation, and solubility. Four conjugated polymers with different branched alkyl chains have been synthesized **IIDDT-C1**, **IIDDT-C2**, **IIDDT-C3** and **IIDDT-C4**. The different alkyl chains were attached in the same position, their difference in the number of  $\text{CH}_2$  in the-spacer (Figure 137). **IIDDT-C3** and **IIDDT-C4** showed a red-shifted absorption band at lowest energies. This could be attributed to a better planarity of the conjugated backbone or/and an improvement of chains aggregation with shorter  $\pi$ - $\pi$  spacing. These observations are in correlation with GPC analysis that showed some aggregation for these two conjugated polymers with longer spacer. It has been noticed, when the branching point is away of the backbone (**IIDDT-C4**) the  $\pi$ - $\pi$  stacking distance decreases from 3.57 to 3.75 Å. Moreover, the length of the spacer affects the molecular organization. The XRD measurements show an edge-on orientation of the chains stacking for **IIDDT-C3** but a face-on orientation for **IIDDT-C2** and **IIDDT-C4**. As expected, the highest hole mobility of  $3.62 \text{ cm}^2 \text{V}^{-1} \text{s}^{-1}$  is obtained for **IIDDT-C3** with edge-on orientation (Figure 137).<sup>315</sup>

<sup>314</sup> Y-Q Zheng, Z-F Yao, J-H Dou, Y. Wang, W. Ma, L. Zou, S. Nikzad, Q-Y Li, Z-H Sun, Z-A Yu, W-B Zhang, J-Y Wang, J. Pei, *Giant*, 2021, 7, 100064

<sup>315</sup> T. Lei, J-H. Dou, J. Pei, *Adv. Mater.*, 2012, 24(48), 6457-6461

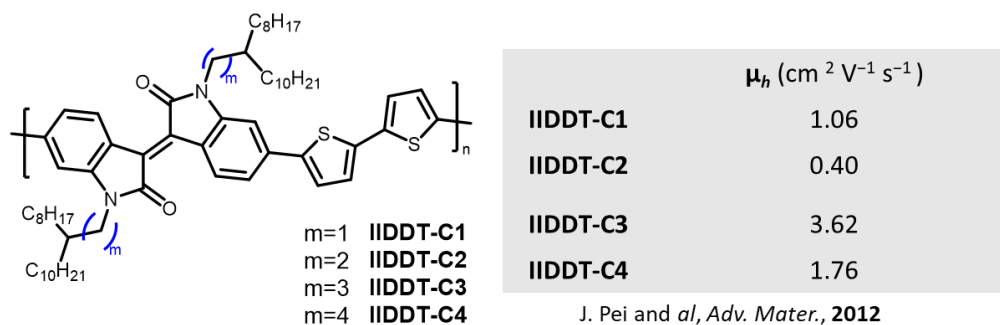


Figure 137: Examples of conjugated polymers with alkyl side chain with different length of spacer

This example shows that with one chain it is difficult to forecast an edge-on orientation. For one type of conjugated polymer, an optimum length of the spacer must be found to favor this orientation. However, these examples are a guideline, but it is important to test several branched extended chains with different length of the spacer and of the terminated branched chain. Usually a mixture of face-on and edge-on is obtained.

Moreover, the density of the alkyl side chain has an impact on the overall conformation, where the decrease in the side chain grafting along the polymer backbone form helicoidal form instead of lamellar structure and then give rise to face-on orientation that is unfavorable for thermoelectric devices.<sup>316</sup>

Therefore, the position of the side chain has an influence on the HOMO and LUMO levels of the conjugated polymer, the impact was more on the HOMO level that was increased by 0.34 eV in b position. And the change of the type affected the solubility and the degree of aggregation, while the change in the length almost with no impact on the absorption spectra.

Side chain is not limited with alkyl chains, perfluoroalkyl side chains attract the attention for conjugated polymers used as n-type materials in organic thermoelectric materials and organic field effect transistors.

### 1.8.2. Perfluoroalkyl side chains:

Perfluoroalkyl chains are of our interest to integrate it to the backbone we have as a side chain attached to the organizing group in the conjugated polymer since the presence of fluorine atoms gives unique properties, such as hydrophobicity, rigidity, thermal stability, chemical/oxidative resistance and an ability to self-organize,<sup>317</sup> which make them promising solubilizing groups. Fluorinated alkyl side chains have a closely packed structure which prevents the diffusion of water and oxygen into films. Consequently, they permit the stability under ambient condition. Moreover, fluorine atoms allow the presence of fluorophobic

<sup>316</sup> S. Fall, L. Biniek, Y. Odarchenko, D. V. Anokhin, G de Tournadre, P. L v  que, N. Leclerc, D. A. Ivanov, O. Simonetti, L. Giraudet, T. Heisera, *J. Mater. Chem. C*, 2016, **4**, 286-294

<sup>317</sup> V. Percec, M. Glodde, T.K. Bera, Y. Miura, I. Shiyonovskaya, K.D. Singer, V.S.K. Balagurusamy, P.A. Heiney, I. Schnell, A. Rapp, H.W. Spiess, S.D. Hudson, H. Duan, *Nature*, 2002, 419, 384-387.

interactions leading to self-organized architectures, which could enhance the charge transport.<sup>318</sup>

In a literature study, semi-fluoroalkyl side chains have been introduced to an electron-accepting naphthalene diimide (NDI) unit alternated with an electron donating unit such as bithiophene **T2** and thienylene-vinylene-thienylene (TVT) giving two semiconducting polymers **PNDIF-T2** and **PNDIF-TVT** (Figure 138). The two polymers show air stability and high crystallinity due to self-organization leading to rigid polymer backbone. The electron mobilities are up to 6.50 and 5.64  $\text{cm}^2 \text{V}^{-1} \text{s}^{-1}$  for **PNDIF-T2** and **PNDIF-TVT**, respectively, which are higher than those of **PNDI2OD-T2** ( $0.1 \text{ cm}^2 \text{V}^{-1} \text{s}^{-1}$ ) and **PNDIDT-TVT** ( $1.84 \text{ cm}^2 \text{V}^{-1} \text{s}^{-1}$ ) (Figure 138).<sup>319</sup>

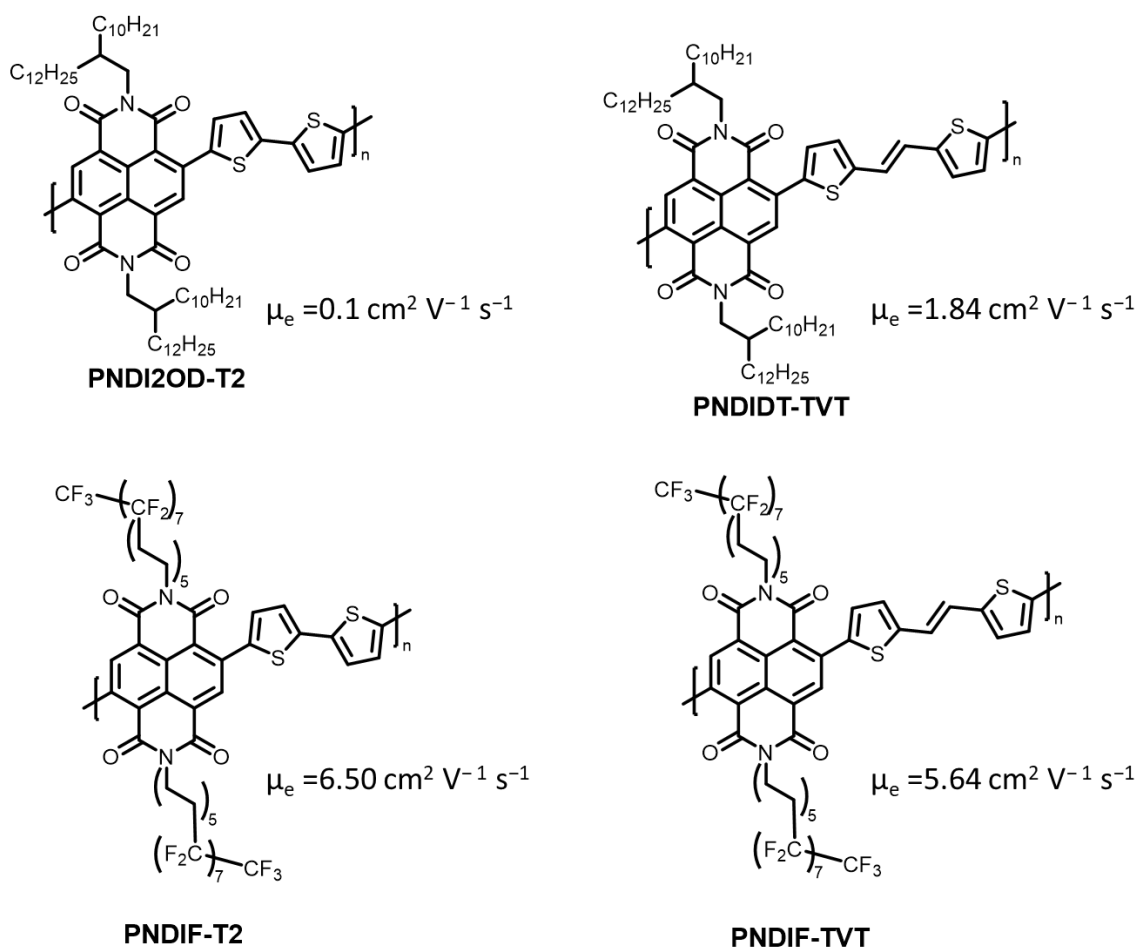


Figure 138: Examples of n-type conjugated polymers with high  $\mu_e$

Therefore, perfluoroalkyl side chains allow us to have stable n-type low band gap conjugated polymer under ambient conditions with high charge enhanced charge mobility. According to the literature, Perfluoroalkyl and ether perfluoroalkyl PEDOT and ester analogue are other examples of conjugated polymers functionalized with perfluoroalkyl side chains in

<sup>318</sup> B. Kang, R. Kim, S. B. Lee, S-K. Kwon, Y-H. Kim, K. Cho, *J. Am. Chem. Soc.*, **2016**, 138, 3679–3686

<sup>319</sup> R. Kim, P. S. K. Amegadze, I. Kang, H-J. Yun, Y-Y. Noh, S.-K. Kwon, Y-H. Kim, *Advanced Functional Materials*, **2013**, 23(46), 5719–5727

the group of Marc Sallé (Figure 139).<sup>320</sup> The presence of fluorinated terminal fragment might allow a higher degree of organization.

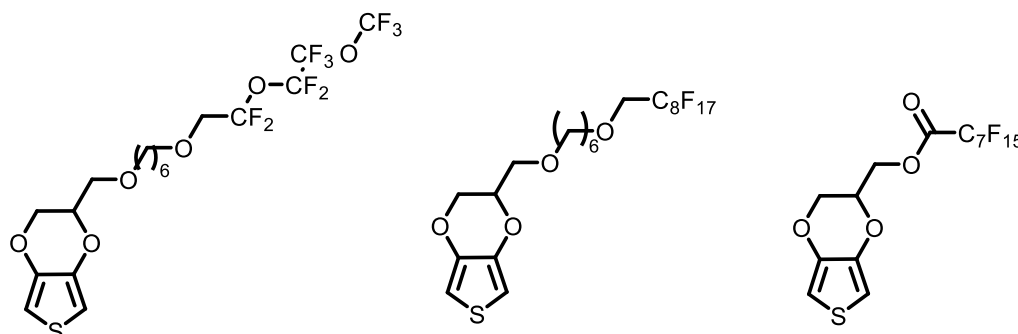


Figure 139: The structure of Perfluoroalkyl and ether perfluoroalkyl PEDOT and ester analogue

**PCTV-BTzF** is a D-A conjugated polymer with semi-fluorinated alkyl side chain with good solubility in common organic solvents (figure 140).<sup>321</sup> The semi-fluorinated chain allows the self-organization behavior by self-aggregate between the alkyl part and fluorocarbon part. Also, it affects the molecular orientation with planar back structure. Moreover, due to the fluorophobic effect and self-segregation of the chains, strong self-aggregation is induced leading to small  $\pi$ - $\pi$  stacking distance (3.62 Å).

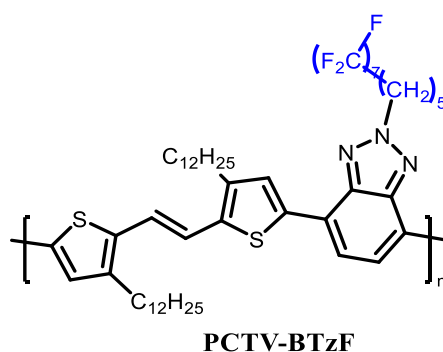


Figure 140: Conjugated polymer with superior self-assembly

The presence of fluorinated side chain shows superior self-assembly morphology with small  $\pi$ - $\pi$  distance after thermal annealing, which could be due to the repulsive interaction of hydrocarbon and fluorocarbon in the solvent with no dramatic impact on the LUMO and HOMO levels compared to the non-fluorinated polymer. Therefore, fluorinated side chains weakly change the electrochemical properties but widely affect the morphology and the stability of a conjugate polymer.

<sup>320</sup> A. Benedetto, M. Balog, H. Rayah, F. Le Derf, P. Viel, S. Palacin, M. Sallé, *Electrochimica Acta*, **2008**, 53, 3779–3788

<sup>321</sup> M-H. Lee, M. Kang, H-G. Jeong, J-J. Park, K. Hwang, D-Y. Kim, *Macromol. Rapid Commun.*, **2018**, 39, 1800431

### 1.8.3. Ethylene Glycol polar group:

Polar side chains such as oligoethylene glycol side chain increase the compatibility between the conjugated polymers and dopant used in thermoelectrics through enhancing miscibility between them.<sup>292</sup> Then, polar side chains can allow complete p-doping efficiency of conjugated polymers such as polythiophenes by **F4TCNQ** leading to high conductivity of  $100 \text{ S cm}^{-1}$  for a low dopant fraction (10 %) with thermal stability.<sup>322</sup>

Naphthalenediimide-bithiophene copolymer **p(gNDI-gT2)** is a structural analogue of **P(NDI2OD)** functionalized with oligoethylene glycol side chain (Figure 141). A comparison with **P(NDI2OD-T2)** with non-polar side chains shows that the polar oligoethylene side chains prevent the aggregation of dopant (**N-DMBI**) up to a concentration of 20 mole %, which proves the enhanced polymer/ dopant miscibility. The obtained electrical conductivity is above  $10^{-1} \text{ S cm}^{-1}$ , which is at least 2 orders of magnitude higher than **P(NDI2OD-T2)**.<sup>323</sup>

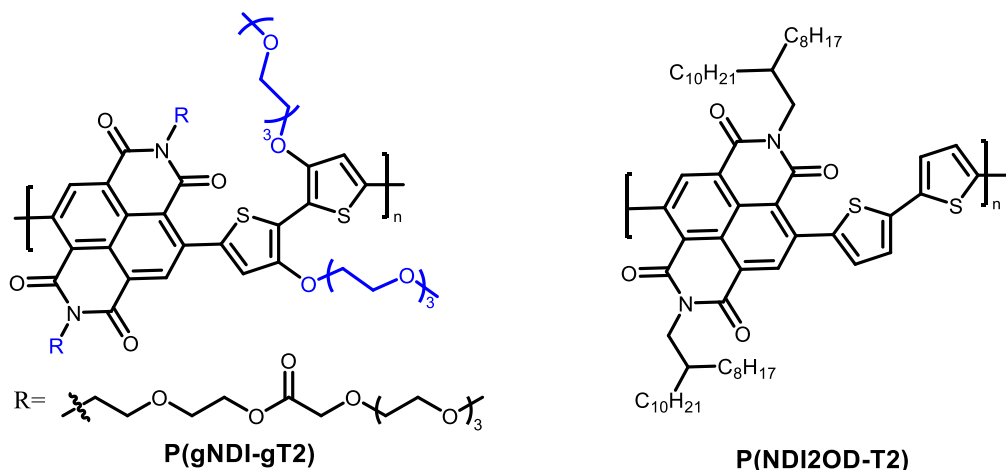


Figure 141: The structure of **P(NDI2OD-T2)** and its structural analogue **p(gNDI-gT2)**

N-type conjugated polymers have apportioned considerable improvement for many applications other than thermoelectrics such as n-type organic field effect transistors (OFETs).

## 2. Organic field effect transistors:

The concept of field effect transistors was proposed by 1930.<sup>324</sup> Then, in 1986, Tsumura and al have discovered the organic field effect transistors OFETs.<sup>325</sup> Figure 142 shows the structure of an OFET device.

<sup>322</sup> R. Kroon, D. Kiefer, D. Stegerer, L. Yu, M. Sommer, C. Müller, *Adv. Mater.*, **2017**, 29, 1700930

<sup>323</sup> D. Kiefer, A. Giovannitti, H. Sun, T. Biskup, A. Hofmann, M. Koopmans, C. Cendra, S. Weber, L. J. Anton Koster, E. Olsson, J. Rivnay, S. Fabiano, I. McCulloch, C. Müller, *ACS Energy Lett.*, **2018**, 3, 278–285

<sup>324</sup> US 1745175, Lilienfeld, Julius Edgar, "Method and apparatus for controlling electric currents", published 1930-01-28

<sup>325</sup> A. Tsumura, H. Koezuka, T. Ando, *Appl. Phys. Lett.*, **1986**, 49, 1210–1212.

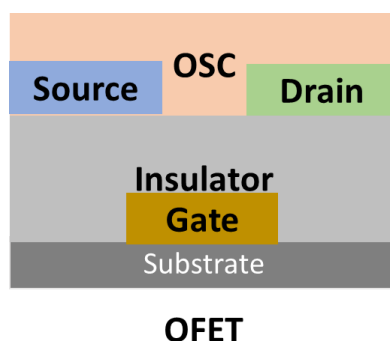


Figure 142: The structure of an organic field effect transistors based on OSC (organic semiconductor)

In a context of semiconductors worldwide shortage, it is crucial to develop efficient organic semiconductors as transistors or sensors instead of traditional ones (silicon, metals or metal oxides) because of low cost, less toxicity, light weight and mechanical flexibility, low operating voltages, ease of low temperature yet large-scale manufacturing and, they have good compatibility with large-area and flexible substrates/materials.<sup>220, 326</sup>

An Organic field-effect transistor (OFET) is a switching device, basically from a gate electrode, a dielectric layer, source and a drain electrode; Both are in contact with an organic semiconductor (OSC) layer, whose charge density is modified by an electric field applied between the semiconductor and a gate electrode (Figure 142), with no requirement for doping process. According to the position of the gate and the electron semiconductors, four configurations can be obtained.

To obtain the ideal n-type OFET, high electron affinities correlated to the lowest LUMO level are required for better charges injection under ambient conditions with high electron mobility.<sup>227</sup>

## 2.1. Principle of OFET:

In a field effect transistor, when the gate voltage  $V_G$  is applied, the free charges are produced between the semiconductor and the dielectric layer. In addition, a small source/drain voltage  $V_{DS}$  is formed leading to a current in the channel controlled by  $V_G$ . Another term is  $V_T$ , the threshold voltage that is the minimum gate voltage needed to induce a current. When  $V_G$  and  $V_{DS}$  applied are different, the behavior is different (Figure 143).<sup>327</sup>

<sup>326</sup> Y. Zhao, Y. Guo, Y. Liu, *Adv. Mater.* **2013**, 25, 5372–5391

<sup>327</sup> J. Yang, Z. Zhao, S. Wang, Y. Guo, Y. Liu, *Chem*, **2018**, 4(12), 2748–2785



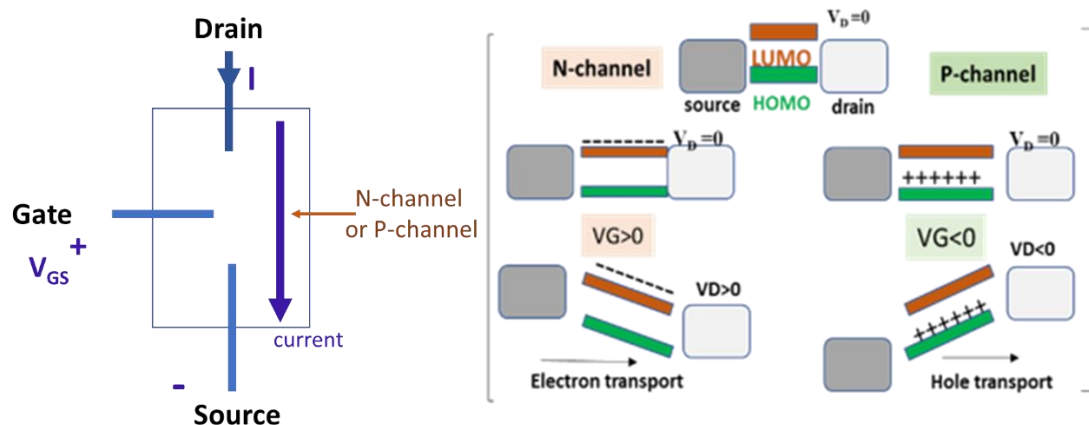


Figure 143: The principle of an OFET

Therefore, developing organic semiconductors with good charge mobility and stability is attracting researchers interest for obtaining organic field effect transistors with high performances.

## 2.2. Organic semiconductors OSC:

OSC can be oligomers or polymers knowing that there are two types of OSC, p-type and n-type.<sup>328</sup> P-type OFETs are of good performance on the other hand, n-OFETs are still behind.

In order to have n-type performance with suppressed p-type behavior, it is crucial to have a deep LUMO level to facilitate the electron injection and Low-lying HOMO level to prevent holes accumulation. This type of conjugated polymer can act as unipolar n-type performance; therefore, formation of n-channel.<sup>329</sup> One of the highest electron mobility in the literature is D-A conjugated polymer **F4BDOPV-2T** with an electron mobility of  $14.9 \text{ cm}^2\text{V}^{-1}\text{s}^{-1}$  (Figure 144).

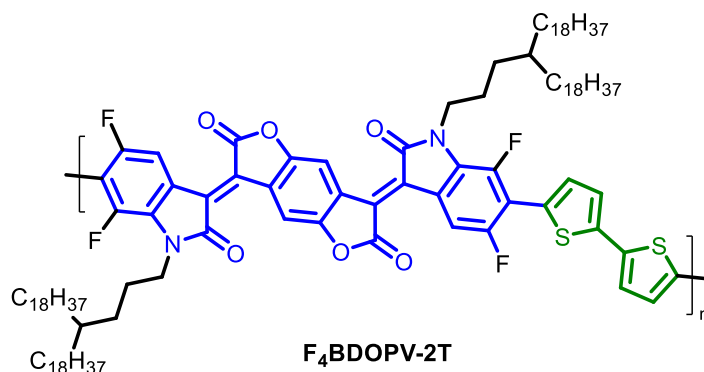


Figure 144: N-type conjugated polymer with high electron mobility

<sup>328</sup> L. Torsi, M. Magliulo, K. Manoli, G. Palazzo, *Chem. Soc. Rev.*, **2013**, 42, 8612-8628

<sup>329</sup> Y. Wang, H. Guo, A. Harbuzaru, M. A. Uddin, I. Arrechea-Marcos, S. Ling, J. Yu, Y. Tang, H. Sun, J. T. L. Navarrete, R. P. Ortiz, H. Young Woo, X. Guo, *J. Am. Chem. Soc.*, **2018**, 140, 19, 6095-6108

Hence, synthesizing new n-type D-A conjugated polymers is crucial for n-type OFETs and organic thermoelectric materials.

To the best of our knowledge, 2,2'-Bithiophene-5,5'-dione (**BTD**) and benzo[1,2-b:4,5-b']dithiophene-2,6-dione (**BDTD**) are two acceptor units of promising performance in D-A conjugated polymers. In the work of Kohsuke Kawabata and *al* three acceptor units have been used including **BTD** and **BDTD** (Figure 145).

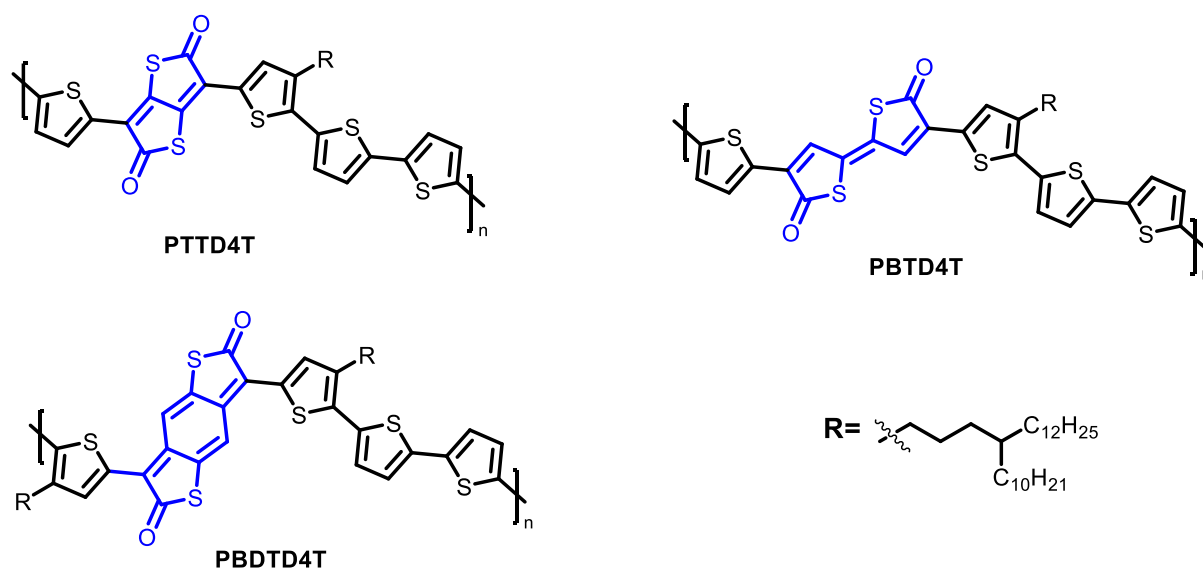


Figure 145: N-type donor-acceptor conjugated polymers

### 3. Preliminary results:

A n-type conjugated polymer was previously synthesized with LUMO level at -4.52 eV, which is one of the lowest levels reported in the literature. This is a significant advantage to guarantee stable electronic properties at ambient conditions. However, lower average molar mass and a face-on  $\pi$ -stacking orientation of the chains are detrimental to reach high charge mobilities and certainly larger electrical conductivity after doping step. Hence, the aim of my PhD project is to enhance the solubility of the conjugated polymer for an increase in the average molar mass value to favor edge-on molecular orientation using functionalization with different alkyl side chains, and to improve the blend between the conjugated polymer and doping agent by introducing polar side chains such as triethylene glycol to the backbone of the conjugated polymer.

The objective was to prepare a narrow band gap electro-deficient conjugated polymer with a LUMO lower than -4.0 eV to guarantee stable charge transport properties at the ambient condition for ambipolar OFET and n-type OTE applications. The narrow band gap is interesting for ambient stable ambipolar OFETs development.<sup>330</sup> The increase of the planarity

<sup>330</sup> R. Ozdemir, D. Choi, M. Ozdemir, G. Kwon, H. Kim, U. Sen, C. Kim, H. Usta, *J. Mater. Chem. C*, **2017**, 5, 2368-2379

and the quinoid form stabilization favor higher electrical conductivity values of n-type materials after a doping process for n-type efficient OTE preparation. Inspired from the work of Pei and *al*,<sup>283</sup> who used benzo[1,2-b:4,5-b']-difurran-2,6-dione as an acceptor. The idea was to use an acceptor with a stronger quinoid character as the sulfur-analog benzo[1,2-b:4,5-b']-dithiophene-2,6-dione (**BDTD**) developed by the Takimiya and *al*<sup>59</sup> and to replace the two thiophenes by EDOT unit to increase quinoid stabilization for increased polaron charge delocalization and enhanced electronic properties. In addition, the presence of EDOT increases the planarity with formation of non-covalent interactions S...O, which improve the  $\pi$ -stacking aggregation. In the synthesized conjugated polymer, the backbone is functionalized with branched alkyl chain to guarantee a good solubility to the polymer. The structure of the target polymer **DG90** is depicted in figure 146.

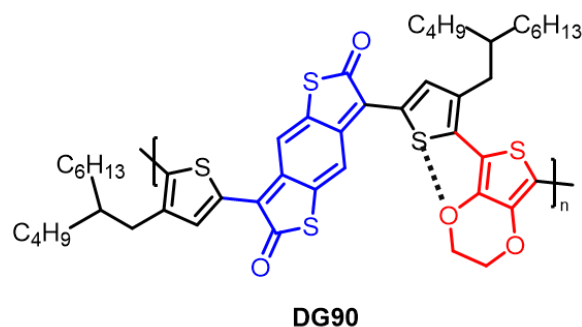


Figure 146: The chemical structure of the conjugated polymer **DG90**

The planarity is increased by the insertion of EDOT moiety. The non-covalent intramolecular interaction S...O lock the conformation and improve the rigidity of the conjugated polymer.<sup>331</sup> Furthermore, they improve the molecular organization with a better  $\pi$ -stacking of the chains, which enhances charge transport.<sup>332</sup> Quinoid form stabilization is improved with the use of quinoid acceptor benzo[1,2-b:4,5-b']-dithiophene-2,6-dione (**BDTD**), and it is reinforced with the presence of EDOT unit.

The project concerning the synthesis of n-type conjugated polymers for organic thermoelectric materials has been started in 2017 with the work of a post-doctoral Di Gao, who found the synthesis of an electro-deficient conjugated polymer, **BDTD-2T-EDOT**. It has one of the lowest LUMO in the literature (-4.52 eV) with a narrow band gap ( $E_g^{\text{elec}} = 0.88$  eV), hence, it is a promising candidate for n-OFET and OTEs.

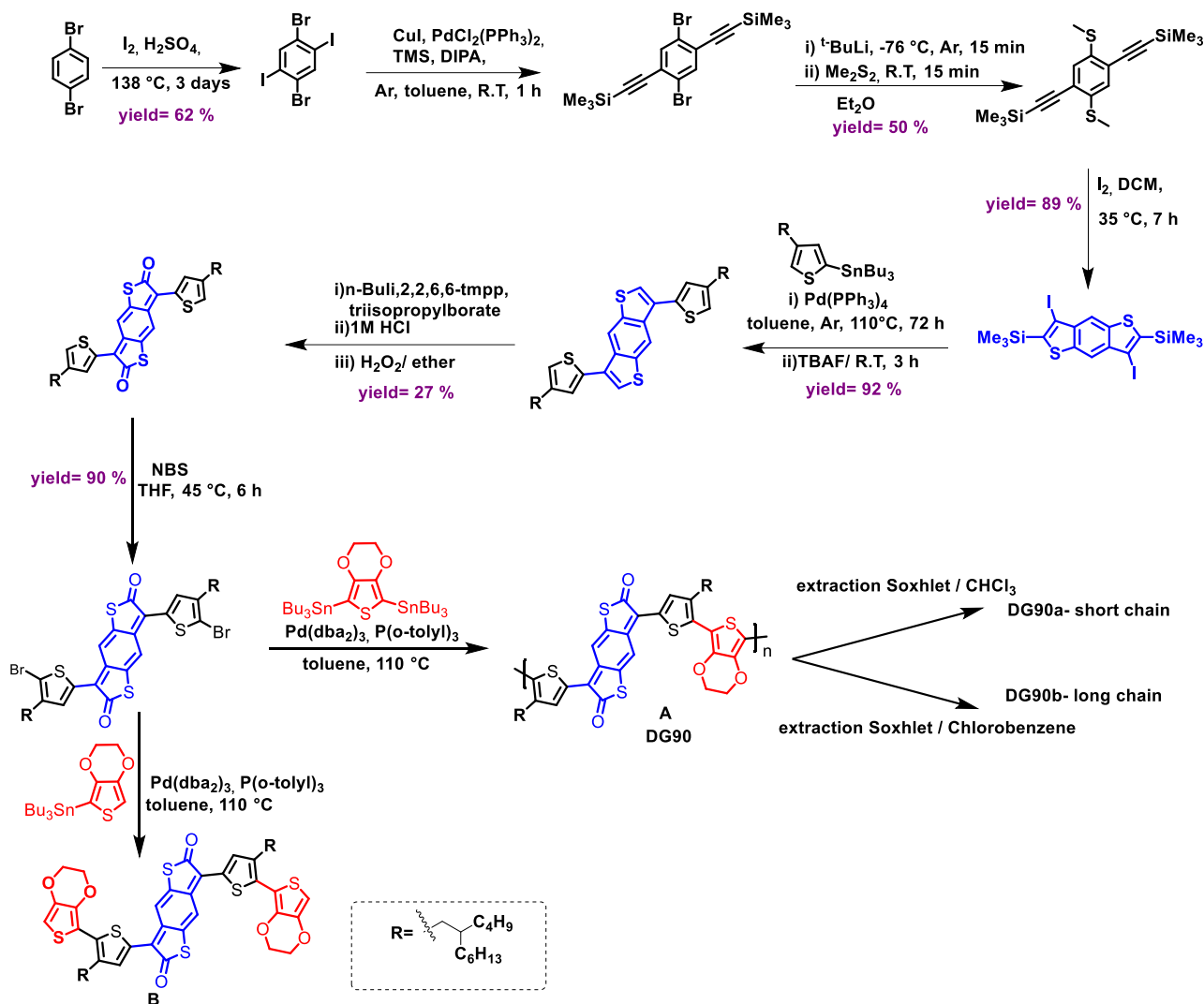
The synthesis of the polymer **DG90** (A) has been inspired of a reported procedure.<sup>333,334,59</sup> It is a multi-step synthesis depicted at scheme 20. The difference is the nature of the alkyl chain R carried by the thiophene ring and the final Stille coupling reaction, which allows the insertion of EDOT moiety. Compound **B** is an analogue of **DG90**. It was prepared to study the optical properties of an analogue of the monomer.

<sup>331</sup> A. S. Zen, C. Atilgan, G. Sonmez, *J. Phys. Chem. C*, **2007**, 111, 16362 – 16371.

<sup>332</sup> N. Kamatham, O. A. Ibraikulov, P. Durand, J. Wang, O. Boyron, B. Heinrich, T. Heiser, P. L  v  que, N. Leclerc, S. M  ry, *Adv. Funct. Mater.*, **2020**, 2007734

<sup>333</sup> S. Duhovi  , M. Dinc  , *Chem. Mater.*, **2015**, 27, 16, 5487–5490

<sup>334</sup> H. Ebata, E. Miyazaki, T. Yamamoto, K. Takimiya, *Org. Lett.*, **2007**, 9, 22, 4499–4502



Scheme 20: The general synthetic route of the polymer **DG90** including the two compounds **A** and **B**

After purification, the intermediates were characterized by  $^1\text{H}$ ,  $^{13}\text{C}$  NMR and mass spectrometry (ESI). **DG90** has been purified with a Soxhlet with hot chloroform, which yields to a first fraction **DG90a**, isolated after evaporation. The solid residue was re-extracted with a Soxhlet with hot chlorobenzene, a second fraction **DG90b** was obtained after solvent evaporation. The fractions were characterized by  $^1\text{H}$  NMR. The average molar masses were determined by size exclusion chromatography (GPC) with polystyrene (PS) standards, the data shows that the first fraction **DG90a** is composed of polymer chains with shorter length, ( $M_n=14.6 \text{ Kg.mol}^{-1}$ ,  $\bar{D}=1.94$ , 11-12 units) in comparison to those from the second fraction **DG90b** ( $M_n=23.8 \text{ Kg.mol}^{-1}$ ,  $\bar{D}=2.58$ , 23-24 units). MALDI-TOF analysis was carried out with DCTB (2-[(2E)-3-(4-tert-butylphenyl)-2-methylprop-2-enylidene]malononitrile) matrix by Julie Hardouin from PBS laboratory, Rouen. The mass spectrum of **DG90b** exhibited several ion series from  $m/z$  3000 to 11000 with a mass gap of 859-860 Da between a series of molecular

masses equal to the repeating units. It demonstrates the formation of an oligomer composed of 11-12 repeating units at least (Figure 147).

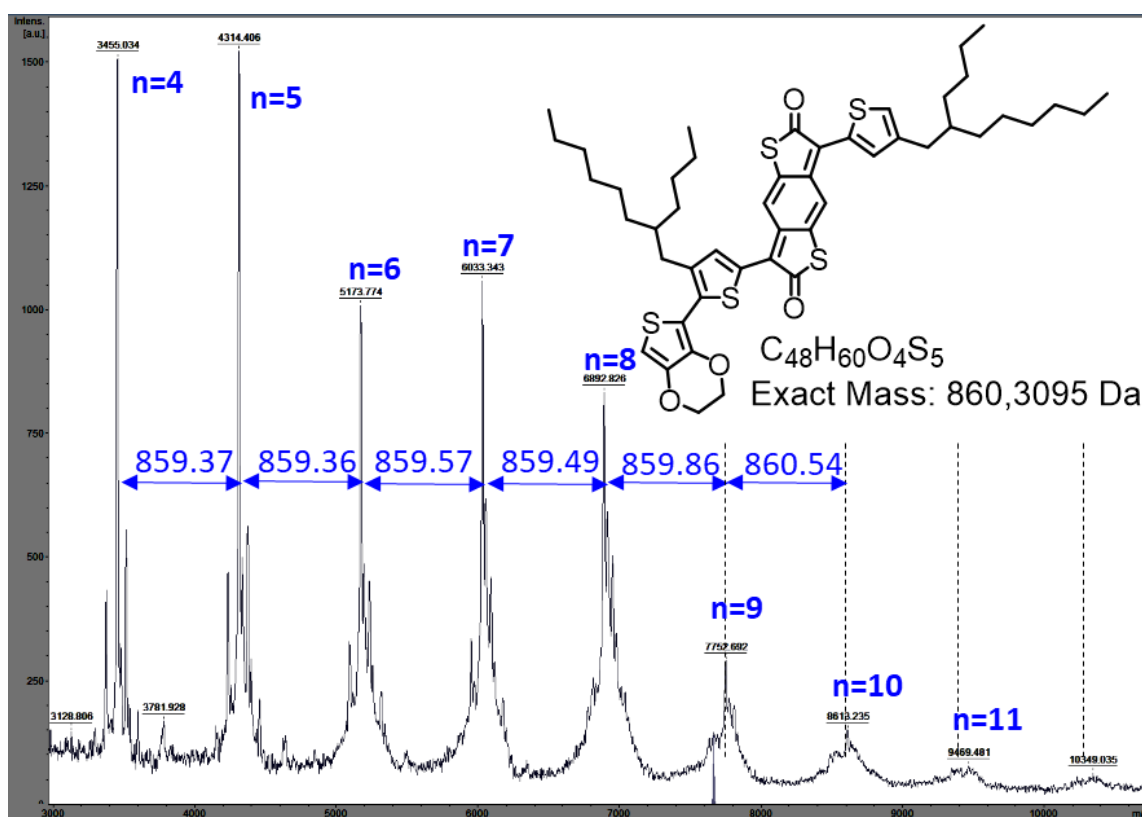


Figure 147: The MALDI-TOF spectrum of **DG90b** with DCTB matrix

The two obtained fractions showed different decomposition temperature with interesting behaviour with **DG90a** of  $T_d$  of 341 °C that is higher than that of **DG90b** that is 329 °C (Table 15). The optical properties of the two fractions were investigated by absorption spectroscopy from 300 to 2400 nm with Julien Cardin in CIMAP laboratory, Caen. The data are summarized in table 15.

In order to evaluate the capacity of absorption, the value of molar extension coefficients ( $\epsilon_\lambda$ ) for intermediate **A** and analogue **B** of the monomer (Scheme 20) were determined at  $6.50$  and  $5.45 \times 10^4 \text{ mol}^{-1} \text{ L cm}^{-1}$ , respectively. These values demonstrate a good absorption capacity. According to the absorption spectrum, both **DG90** values absorb from 300 nm to 2400 nm. **DG90a** has an onset absorption at 1644 nm and maximum absorption at 1285 nm that corresponds to an optical band gap of 0.76 eV (Table 15). But **DG90b** shows onset absorption at 1999 nm with an absorbance maximum at  $\lambda_{\text{max}}$  of 1285 nm, which corresponds to a narrower band gap of 0.62 eV (Figure 148). The decrease in the band gap is in agree with the literature due to the increase in the conjugation length (Table 15). In the absorption spectra of the two fractions in thin film, **DG90a** shows maximum absorption at 1191 nm, while **DG90b** shows maximum absorption at 2126 nm. These values correspond to optical band gaps of 0.65 eV and 0.58 eV, respectively. The insertion of the EDOT allows smaller band gap in comparison to the value of band gap obtained for **PBDTD4T** that is of 0.88 eV.<sup>59</sup>

Besides these exceptional optical properties, **DG90** could be valorised for their use in near infrared NIR photodetector.<sup>335</sup>

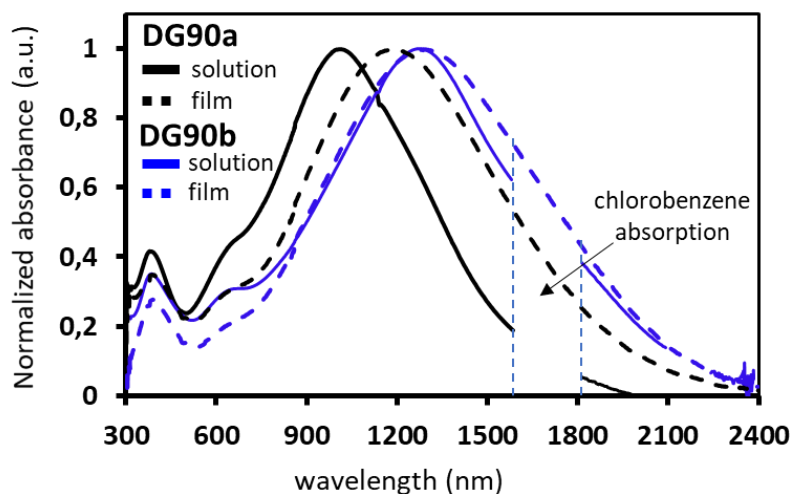


Figure 148: The absorption spectra of the fraction **DG90a** and **DG90b**.

Table 15: The different analysis data of **DG90a** and **DG90b** compared to the literature example.

	chlorobenzene							Thin film		
	$M_n$ (Kg.mol <sup>-1</sup> )	$\mathcal{D}^a$	$T_d$ (°C) <sup>b</sup>	$\lambda_{max}$ nm	$\lambda_{max}^{calc}$ nm <sup>c</sup>	$\lambda_{onset}$ nm	$E_g^{opt}$ eV <sup>d</sup>	$\lambda_{max}$ nm	$\lambda_{onset}$ nm	$E_g^{opt}$ eV <sup>d</sup>
<b>DG90a</b>	14.6	1.94	341	1001	1003	1644	0.76	1191	1916	0.65
<b>DG90b</b>	23.9	2.58	329	1285	1361	1999	0.62	1295	2126	0.58
<b>PBDTD4T</b> <sup>59</sup>	58	3.10	/	/	/	/	/	1207	1415	0.88

<sup>a</sup> Dispersity calculated by  $M_w/M_n$ . <sup>b</sup> The temperature measured at 5 wt% loss. <sup>c</sup> Electronic transitions calculated by DFT. <sup>d</sup> The band gap calculated using the  $\lambda_{onset}$

The electrochemical properties of **DG90b** have been studied by cyclic voltammetry by Muriel Durandetti from COBRA laboratory, Rouen. The data are listed in table 16. The levels of HOMO and LUMO are calculated from onset oxidation and reduction potentials, respectively. **DG90** has one of the lowest LUMO in the literature (-4.52 eV) with a narrow band gap ( $E_g^{ele} = 0.82$  eV), hence, it is a promising candidate for n-OFET and n-OTE applications.

<sup>335</sup> L. Zhang, T. Yang, L. Shen, Y. Fang, L. Dang, N. Zhou, X. Guo, Z. Hong, Y. Yang, H. Wu, J. Huang, Y. Liang, *Adv. Mater.*, **2015**, 27, 6496–6503

Table 16: The analysis data of the cyclic voltammetry of **DG90**

	$E_{\text{ox}}^{\text{onset}}$ V/ESC	$E_{\text{red}}^{\text{onset}}$ V/ESC	HOMO eV <sup>a</sup>	LUMO eV <sup>a</sup>	$E_{\text{g}}^{\text{elec}}$ eV <sup>b</sup>	$E_{\text{g}}^{\text{opt}}$ eV <sup>c</sup>
<b>DG90</b>	0.61	-0.21	-5.34	-4.52	0.82	0.58
<b>PBDTD4T</b>	0.22	-0.76	-5.02	-4.04	0.98	0.88

<sup>a</sup> Onset potential (V vs SCE) for reduction ( $E_{\text{red}}^{\text{onset}}$ ) and oxidation ( $E_{\text{ox}}^{\text{onset}}$ ). HOMO and LUMO energies calculated with the equation  $E_{\text{HOMO}} = -(E_{\text{ox}}^{\text{onset}} + 4.73)$  eV,  $E_{\text{LUMO}} = -(E_{\text{red}}^{\text{onset}} + 4.73)$  eV. <sup>b</sup>  $E_{\text{g}}^{\text{elec}} = E_{\text{LUMO}} - E_{\text{HOMO}}$  (eV). <sup>c</sup> The optical band gap in thin film.

The hole and electron mobilities of **DG90a** and **DG90b** have been measured on OFET device by Pr. Thomas Heiser from ICUBE laboratory at Strasbourg (Figure 149).

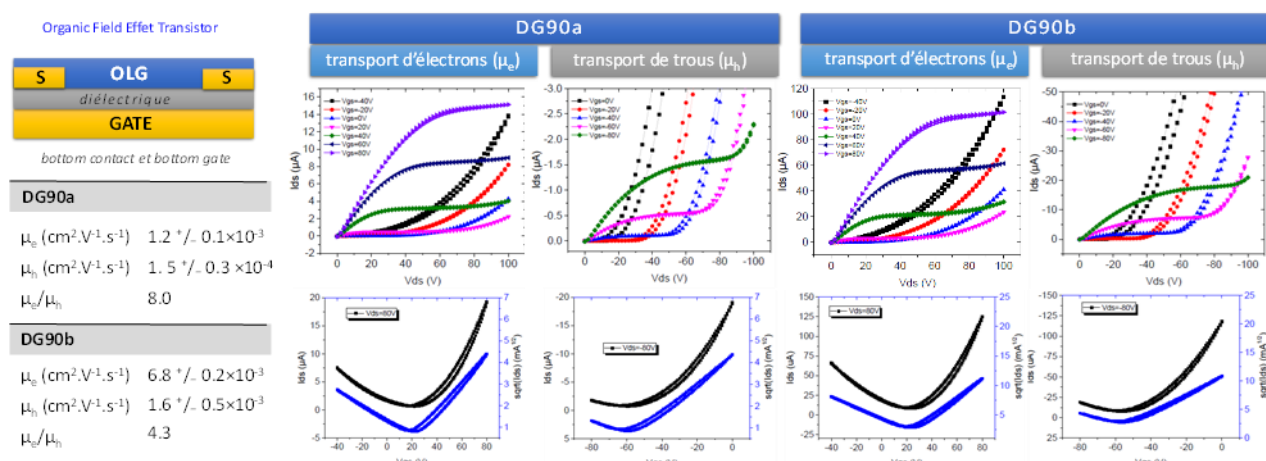


Figure 149: The hole and electron mobilities of **DG90a** and **DG90b**

Ambipolar behavior has been noticed, with hole and electron mobilities after calculating the hole to electron mobilities ratio, which is about 8 and 4.3 for **DG90a** and **DG90b**, respectively. For **DG90b** the obtained values ( $\mu_e = 6.8 \times 10^{-3} \text{ cm}^2 \text{ V}^{-1} \text{ s}^{-1}$  and  $\mu_h = 1.6 \times 10^{-3} \text{ cm}^2 \text{ V}^{-1} \text{ s}^{-1}$ ) are higher than those of **DG90a** ( $\mu_e = 1.2 \times 10^{-3} \text{ cm}^2 \text{ V}^{-1} \text{ s}^{-1}$  and  $\mu_h = 1.5 \times 10^{-4} \text{ cm}^2 \text{ V}^{-1} \text{ s}^{-1}$ ), which could be due to the higher average molar mass in agreement with impact of molar mass on charges transport explained in chapter 1. After annealing treatment (molecular organization improvement under heating) the values of charge mobilities have been increased. However, these values are lower than those from the literature (**PBDTD4T**,  $\mu_e = 0.35 \text{ cm}^2 \text{ V}^{-1} \text{ s}^{-1}$  and  $\mu_h = 0.30 \text{ cm}^2 \text{ V}^{-1} \text{ s}^{-1}$ ). These values could be explained by the lower average molar mass and by the molecular organization of the chains, like face-on  $\pi$ -stacking orientation, which is detrimental to charge transport. So, we decided to carry out GIWAXD measurement to determine the orientation of the  $\pi$ -stacking in **DG90b** for further understanding.

GIWAX measurements were carried out in CRISMAT laboratory in Caen to study the  $\pi$ -stacking orientation. The XRD pattern illustrated in figure 150 shows a “face-on” orientation of the  $\pi$ -stacking for **DG90b**. It is not favorable for good charge mobilities for OFET or OTE applications.

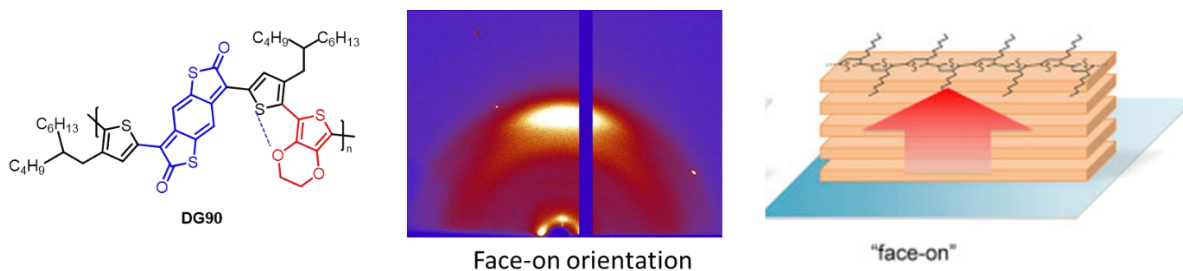


Figure 150: GIWAX XRD pattern of **DG90b**

Hence, both the face-on orientation and low average molar mass could explain the low electron mobility ( $\mu_e = 6.8 \cdot 10^{-3} \text{ cm}^2\text{V}^{-1}\text{s}^{-1}$ ).

From these preliminary results, the objective of my PhD project is to enhance the electronic properties of the electro-deficient polymer. The strategy followed is to change the nature of the side chain R carried by thiophene rings from **(BDTD-2T-EDOT)<sub>n</sub>** inspired from reported examples by suitable types of chains, which will be chosen to increase the average molar mass,  $\pi$ - $\pi$  aggregation, air/water stability and to trigger “edge-on”  $\pi$ -stacking orientation for the enhancement of the charge transport.

## II. New n-type Conjugated Polymers:

The objective is to synthesize a new narrow band gap and low lying LUMO n-type conjugated polymers with high electron mobility for n-type or ambipolar OFET applications and with high electrical conductivity for n-type OTE material preparation. From the preliminary results and a bibliographic study, a suitable chemical functionalization is applied on **(BDTD-2T-EDOT)<sub>n</sub>** with different side chains R carried on **BDTD** acceptor and R' on **EDOT** moiety **(1)** to increase the solubility and the average molar mass ( $M_n$ ), **(2)** to enhance the  $\pi$ - $\pi$  aggregation, **(3)** to trigger edge-on stacking orientation and **(4)** to have better air/moisture stability. The main target polymer is represented in figure 151.

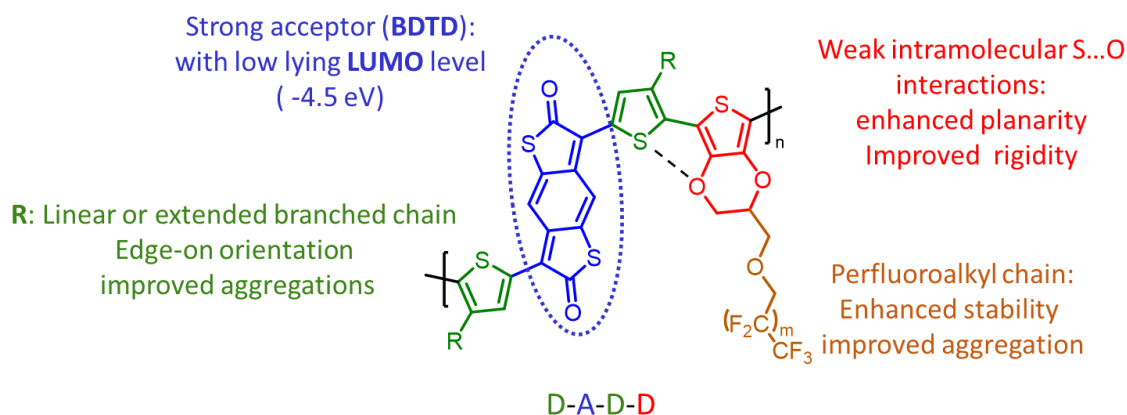
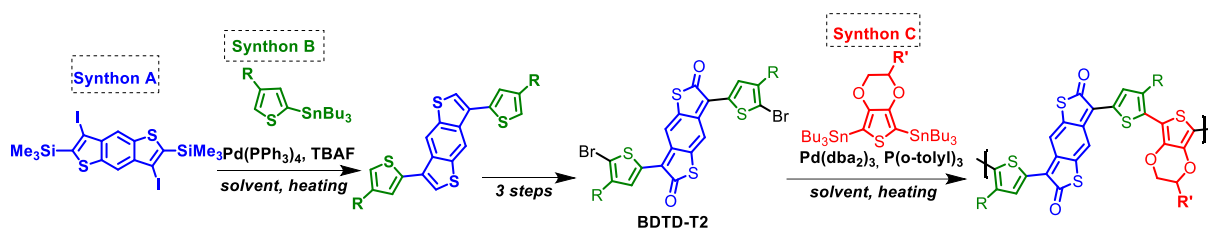


Figure 151: The description of the main target polymer



Different targets have been imagined to study progressively the impact of each side chain on the solubility and the molecular organization. The generic synthesis is the same applied for the first polymer described in the preliminary results. The advantage of this synthetic route is testing one by one different side chains **R** and **R'** because they are carried on the distinct synthons **B** and **C**, respectively (Scheme 21). This helps to evaluate their impact on the solubility and molecular organization. The synthons **A**, **B** and **C** are attached sequentially after coupling reactions (Scheme 21).



*Scheme 21: Generic synthesis of n-type conjugated polymer from the synthons **A**, **B** and **C** with side chains **R** and **R'***

Based on the bibliographic study reported (paragraph 1.8 “side chain engineering” of this chapter), insertion of linear chains on conjugated polymers could improve aggregation with closest  $\pi$ - $\pi$  spacing and more crystallinity. In contrast to branched chain, the solubility of the polymer could be lower, but this is favorable for increasing pre-aggregation chains mechanism and to trigger to preferential edge-on orientation.<sup>336</sup> This is demonstrated by the reported work of Fréchet and *al* with the preparation of  $n$ -C<sub>16</sub>H<sub>35</sub> alkyl chain functionalized DPP-furane polymers. Compounds functionalized with linear chains exhibit better molecular organization and twice higher holes mobility values in comparison to the polymers with branched chains.<sup>128</sup> Hence, for the first target **T1**, linear chain  $n$ -C<sub>12</sub>H<sub>15</sub> has been chosen to improve aggregation and to trigger edge-on  $\pi$ -stacking orientation. Besides, it would be easier to prepare rapidly the first **BDTD** derivatives (**BDTD-1**) and **T1** (Figure 152), because 1-bromododecane required in the synthesis is commercially available contrary to the extended branched alkyl chain, which is prepared in three steps (Scheme 15).<sup>59</sup> The solubilizing chain on the EDOT with target **T2** could improve the solubility of the polymer and its average molar mass. If the solubility of **BDTD-1** is not good enough for the syntheses, the extended branched alkyl chain could be used instead of linear ones in the preparation of **BDTD-2** and the target **T4** (Figure 152). These chains permit to maintain a good solubility of the polymer and improve molecular organization, which leads to the increase of the average molar mass and the enhancement of the charge transport.<sup>337</sup> Besides, the variation of the length ( $n$ : number of carbon atoms) of the spacer has an impact on the molecular organization, the size of the crystalline nanodomains and on the electronic properties.<sup>338</sup> The insertion of perfluoroalkyl chain (**T3** and **T6**) on EDOT moiety permits higher degree of organization, inspired from reported work of Marc Sallé and *al*, with a gain of stability of  $n$ -type OFET as in the work of Kilwon Cho.<sup>318</sup> A final aspect is to improve molecular organization with the assistance of amphiphilic mesogenic groups, like triphenylene cores synthesized in the group with the

<sup>336</sup> M. Li, C. An, T. Marszalek, M. Baumgarten, H. Yan, K. Müllen, W. Pisula, *Adv. Mater.*, **2016**, 28, 9430-9438

<sup>337</sup> S. Chen, B. Sun, W. Hong, H. Aziz, Y. Meng and Y. Li, *J. Mater. Chem. C*, **2014**, 2, 2183

<sup>338</sup> K. Kawabata, M. Saito, N. Takemura, I. Osaka, K. Takimiya., *Polymer Journal*, **2017**, 49, 169–176

target **T7**.<sup>339</sup> Triphenylene groups self-assemble into columnar architectures.<sup>340</sup> The five alkyl chains per triphenylene group favor a good solubility of the polymer (Figure 152).

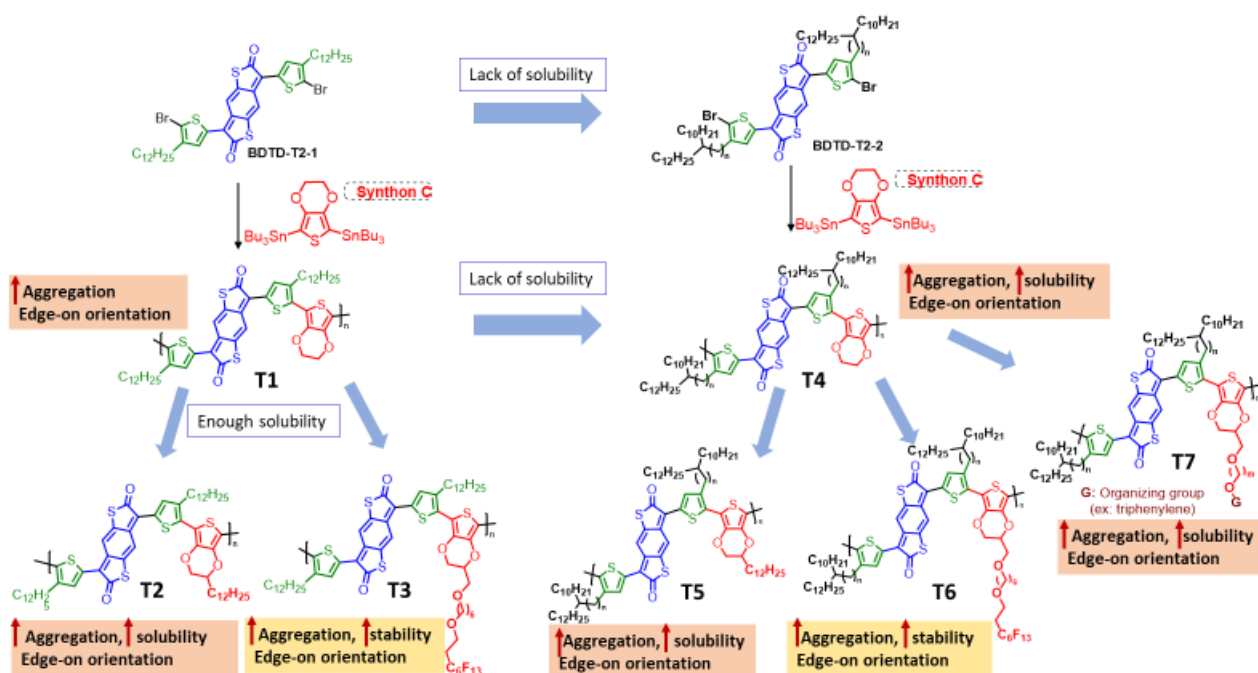


Figure 152: Explanations of the choice of targets **T1-T7**

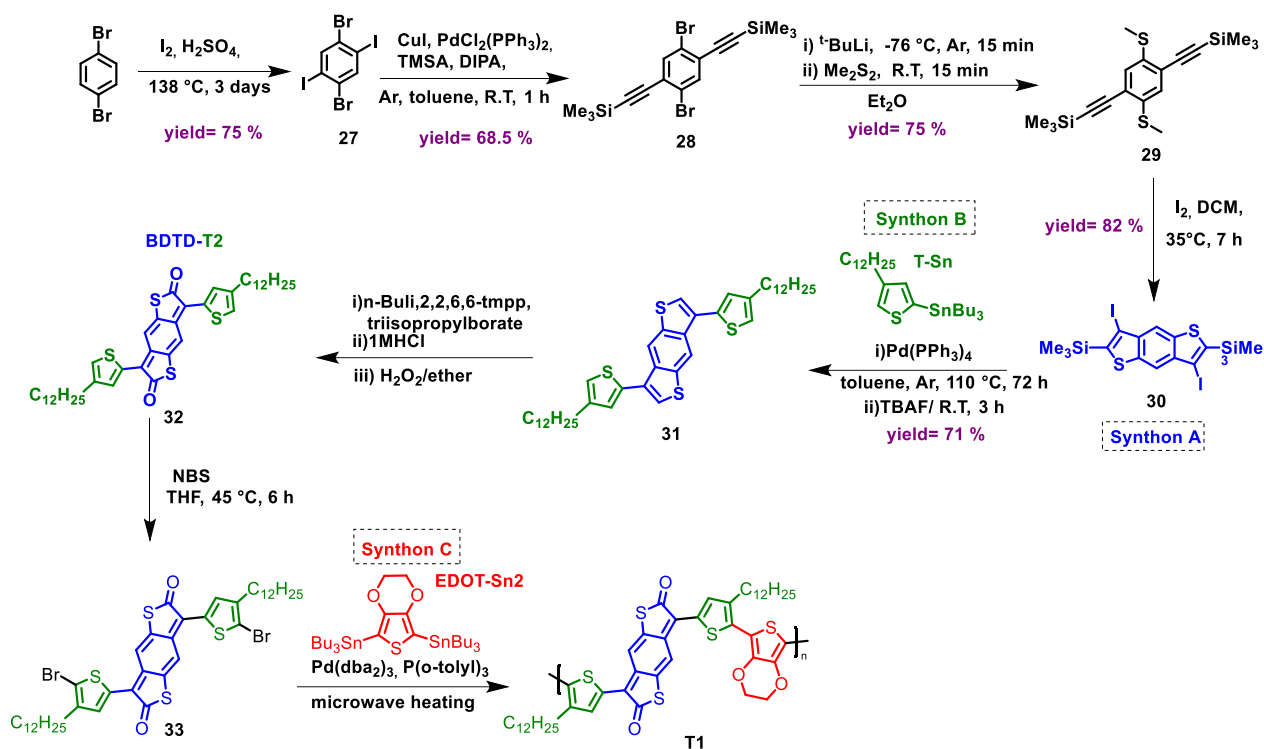
The average molar mass will be determined by GPC. The microstructure of polymer thin films will be investigated by XRD to evaluate the crystallinity and the orientation of the  $\pi$ -stacking. The charge mobilities will be measured on OFET device by Pr. Thomas Heiser from ICUBE laboratory in Strasbourg to evaluate the impact of the functionalization. In the final stage, the materials with the highest charge mobilities will be doped with different molar quantities of **N-DMBI** or **TAM** to achieve high electrical conductivity for OTE applications.

## 1. Synthesis of new n-type conjugated polymer T1:

The synthesis of the first target **T1** is performed using multi-step reactions inspired from the literature<sup>59, 333, 334</sup> with optimization in the procedures. The synthesis is represented in scheme 22.

<sup>339</sup> G. Marineau-Plante, M. Nos, D. Gao, M. Durandetti, J. Hardouin, P-L Karsenti, C. Lemouchi, L. Le Pluart, G. D. Sharma, P. D. Harvey, *ACS Appl. Polym. Mater.*, **2021**, 3, 2, 1087–1096

<sup>340</sup> Y. Xiao, D. Zeng, L. M. Mazur, A. Castiglione, E. Lacaze, B. Heinrich, B. Donnio, D. Kreher, A-J Attias, J-C Ribierre, F. Mathevet, *Polymer Journal*, **2017**, 49, 31–39



Scheme 22: The synthetic scheme for the synthesis of the conjugated polymer **T1**

The synthesis includes the formation of three synthons: the acceptor **BDT 30** (synthon A), the stannic functionalized thiophene unit **T-Sn** (synthon B) and the distannic **EDOT-Sn2** (synthon C).

### 1.1. Synthesis of the acceptor unit

The synthesis of **synthon A (30)** consists of four steps starting from 1,4-dibromobenzene from a reported procedure.<sup>59, 333, 334</sup> The first step is iodination reaction using iodine as the source of iodine in sulfuric acid, which also played the role of solvent under controlled heating 125-135 °C to avoid further iodination that makes the separation of the desired product and by-product difficult. The large excess of acid causes many difficulties in the work up and the purification process. Hence, this step must be carried out with safety precaution. In addition, the precipitation of the product into hard-solid stones complicates the and restricts the purification step. Work-up optimizations have been carried to increase the yield. After the resynthesis of this compound, I supposed to carry out extraction of the liquid part, and to crash well the obtained stones with a maul into fine powder. The excess of iodine in the powder was removed after several triturations in pentane and a crystallization in chloroform. Since the presence of iodine traces with the compound prevents the formation of compound **28** after the Sonogashira coupling reaction. The yield was improved from 62 % in the reported procedures to 75 %. The second step is Sonogashira coupling reaction under inert atmosphere, which leads to diacetylenic compound **28** with triple bonds protected with trimethylsilyl (TMS) isolated with a yield of 68.5 %. It is prepared from bihalogenated derivative **27** and trimethylsilylacetylene (TMSA) in presence of protecting groups using (triphenylphosphine)palladium chloride as catalyst, CuI and diisopropylamine as base, which is dried and degazed with Argon. The yield of this step was significantly increased after improving the purification of the compound **27** for removing all traces of iodine.

The third step is a thiophilic reaction where bromine is replaced by methylsulfur group. The reaction of bishalogenated compound **28** and  $t\text{-BuLi}$  yields to the formation of the organolithium derivative, which reacts with dimethyldisulfide (DMDs) to form compound **29**. The yield was increased from 50 % in the reported procedure<sup>334</sup> to 84 % by purifying the product with a precipitation instead of a column chromatography.

The acceptor **30** was obtained after an electrophilic cyclization reaction in the presence of iodine. The mechanism is represented in figure 153. The desired compound is isolated with a yield of 82 %.

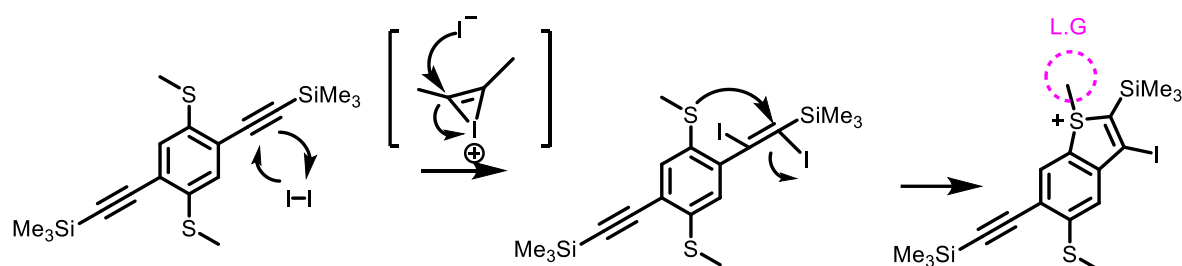
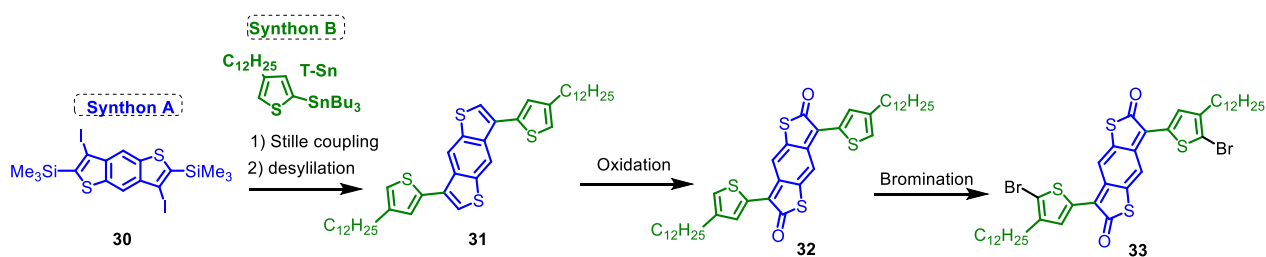


Figure 153: The mechanism of the cyclization reaction in the synthesis of intermediate **30**

## 1.2. Synthesis of the acceptor of D-A-D unit BDTD-2TR1 (Synthon A-Synthon B) (32)

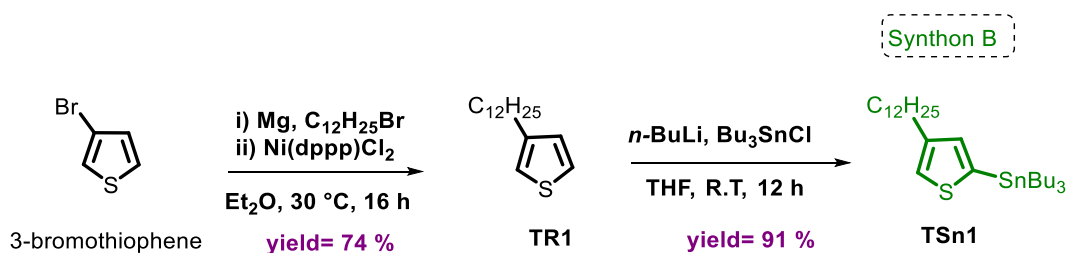
The synthesis of the acceptor is composed of three stages: (1) the attachment of the **synthon B**,  $n\text{-C}_{12}\text{H}_{25}$  functionalized thiophene ring to the **Synthon A** with a Stille coupling reaction, (2) the oxidation reaction to generate the thioesters functions after, which provides the electro-deficient nature to the acceptor **BDTD 32** and (3) the bromination of the acceptor **32**. The oxidation step is the limiting step in this synthesis, since the synthetic route was inspired by the work of Takimiya and *al* (Scheme 23) with the preparation of the same acceptor nature with branched alkyl chain with a yield of 47 %, <sup>59</sup> but in our synthesis, we use linear alkyl chain. This procedure was applied for the synthesis of the same acceptor functionalized by branched alkyl chains with a lower yield of 27 % for the preparation of **DG90** (See part of preliminary results in this chapter).



Scheme 23: The synthetic route followed for the synthesis of intermediate **33** (BDTD-T2)

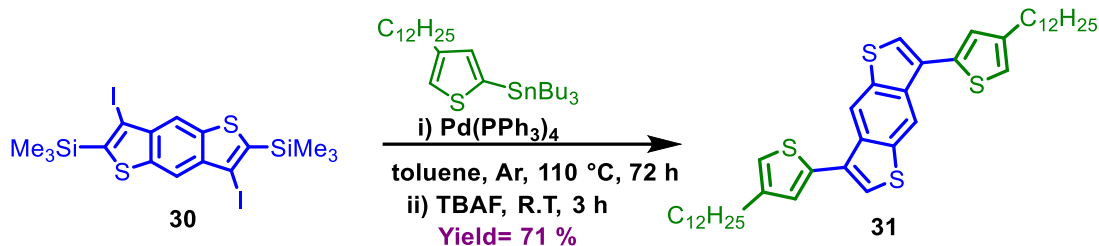
The synthesis of intermediate **31** requires the synthesis of the donor unit that is a stannic thiophene molecule substituted with linear alkyl side chain.

The functionalized thiophene **TSn1** is synthesized by two steps, which are inspired by the literature (Scheme 24).<sup>254</sup> The first step is a Kumada cross-coupling reaction, which involves preparing a Grignard reagent from bromododecane. The linear chain functionalized thiophene **TR1** is isolated after purifications using silica column chromatography and vacuum distillation with a yield of 74 %. The second step is the organotin formation from the reaction between anion formed by lithiation at -78 °C of **TR1** and tributyltin chloride. **TSn1** is isolated after an extraction with no further purification with a yield of 91 % (Scheme 24).



Scheme 24: The synthesis of **TSn1** (Synthon B)

After preparing synthon A and synthon B, the next step is a Stille coupling reaction between the bisiodine acceptor **30** (Synthon A) and the organotin thiophene derivative **TSn1** (Synthon B) in the presence of tetra triphenylphosphine palladium catalyst under a reflux of three days. Then, 1M TBAF solution is added to remove TMS groups (Scheme 25).



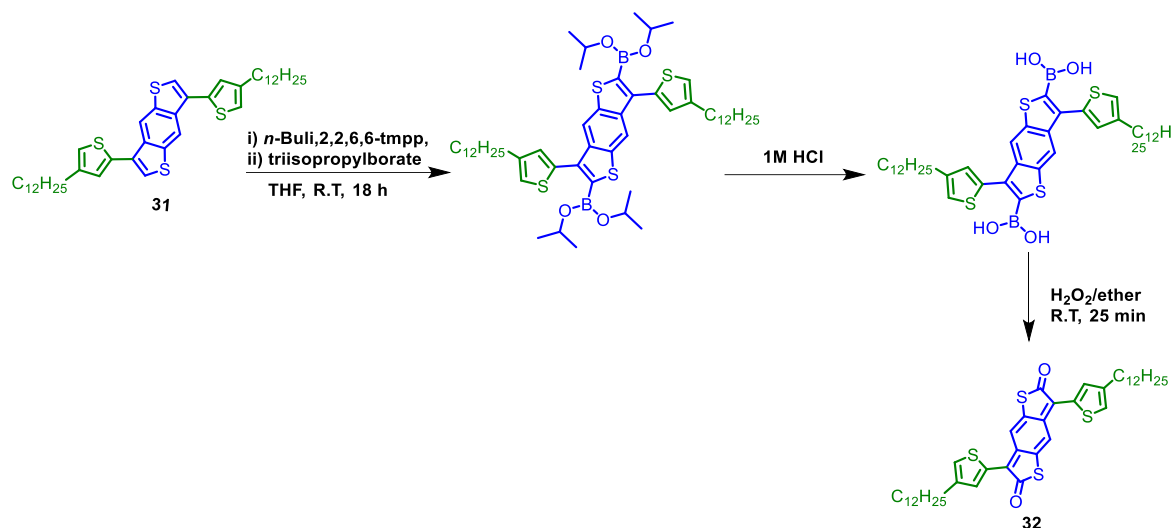
Scheme 25: The synthesis of intermediate **31**

The overall yield of these two successive steps is 71 % yield after optimization on the reaction conditions and purification step summarized in table 17. At the beginning, the procedure was applied according to the literature. The obtained product was isolated with low yield (25 %). After a progressive increase in the number of equivalents of Pd(PPh<sub>3</sub>)<sub>4</sub> from 0.01 to 0.1 allows an increase in the yield from 25 % to 48 %. However, the addition of **TSn1** in portions during 24 hours results in higher yield of 71 %.

Table 17: The different reaction conditions are used for the synthesis of intermediate **31**

	Number of equivalent of Pd(PPh <sub>3</sub> ) <sub>4</sub>	Number of equivalents of TSn1	Number of portions	Yield
1	0.01	2.2	1	25 %
2	0.05	2.2	1	34 %
3	0.1	2.2	1	48 %
4	0.1	4.2	4	71 %

The next reaction is the oxidation reaction of the intermediate **31** to generate the acceptor **BTD** with the formation of withdrawing thioester functions, illustrated in scheme 26. This is the limiting step of the synthetic route. The reaction procedure was inspired by the work in the literature<sup>59</sup> of the same acceptor with different side chain.



Scheme 26: The synthesis of intermediate **32**

The synthesis of intermediate **32** consists of deprotonation of the compound **31** with the strong base lithium tetramethylpiperidine freshly prepared from *n*-Buli (2.5 M) and 2,2,6,6-tetramethylpiperidine. The anionic intermediate reacts with triisopropylborate to give the boronic ester derivative. It is followed by hydrolysis of the boronic ester to boronic acid with 1M HCl solution. Then oxidation takes place at the boronic acid position with hydrogen peroxide at room temperature (Scheme 26). This limiting step requires strict anhydrous and inert conditions. Several attempts were carried out to improve the reactivity of the reaction and the yield.

First, the reaction conditions used for **DG90** synthesis have been tested, inspired from the literature (Entry 1, Table 18), but the desired product was not isolated even if the reaction time was increased (Entry 2). However, the reaction took place when the base 2,2,6,6-tmpp is being freshly dried over calcium hydride and freshly distilled under vacuum (Entry 3). For better understanding, the reaction was monitored by <sup>1</sup>H NMR to evidence the formation of the boronic and the desired compound **31**.

The formation of the desired compound **32** is confirmed by  $^1\text{H}$  NMR and by mass spectrometry with the determination of the exact mass. The low solubility of the intermediates could explain the lack of reactivity and reproducibility but also the low stability of the compounds. Hence, Different solvents have been tried in order to increase the solubility of the intermediate during the deprotonation step. However, all the tested solvents result in poor solubility, keeping in mind we must control the molar concentration of the base (2.5 M) The conditions are listed in table 18.

Table 18: The different conditions tested in the synthesis of oxidized compound

	n-BuLi (2.5 M)	2,2,6,6- tetramethylpip- yridine	triisopropylborate	Solvent	Temperature for deprotonation	Duration
Ref.	2.4 eq.	2.4 eq. (No distillation)	4.7 eq.	THF	-76 °C	5 h
1	2.4 eq.	2.4 eq. (No distillation)	6.55 eq.	THF	-76 °C	15 h
2	2.4 eq.	2.4 eq. (Distillation)	6.55 eq.	THF	-76 °C	15 h
3	2.4 eq.	2.4 eq. (Distillation)	6.55 eq.	THF	-76 °C	3 h
4	2.4 eq.	2.4 eq. (Distillation)	6.55 eq.	THF	-76 °C	4 h
5	2.4 eq.	2.4 eq. (Distillation)	6.55 eq.	DMF	-76 °C	15 h
6	2.4 eq.	2.4 eq. (Distillation)	6.55 eq.	diethylether	-76 °C	15 h
7	2.4 eq.	2.4 eq. (Distillation)	6.55 eq.	Toluene	-76 °C	15 h

After confirming the presence of intermediate **BDTD-1 32**, it was engaged in bromination reaction with NBS to obtain the final intermediate **33**. It was not stable enough in solutions nor in deuterated solvents to be well characterized in  $^1\text{H}$  and  $^{13}\text{C}$  NMR. But the  $^1\text{H}$  NMR spectrum analysis revealed the absence of the proton signal at 7.25 ppm, which corresponds to the proton at the alpha position of the thiophene ring, which agrees with the presence of bromine. Besides, the compound was characterized by mass spectrometry with the detection of the molecular peak with the presence of 2 bromines and a peak from ionic fragment in the presence of one bromine. The exact mass confirmed the formation of the product **33**. Hence, this product was directly engaged in the final step to form the conjugated polymer **T1**. In perspective, to increase the solubility and the stability. It was planned to synthesize the analogous intermediate **BDTD-2** (Figure 152) with extended branched chains, introduced in the chapter 2. This intermediate will be used for the preparation of the target **T4**.

### 1.3. Synthesis of EDOT-containing units (Synthon C):

This part is dedicated to the description of the synthesis of the three EDOT containing **synthons C** represented in figure 154. **Synthon C1** was synthesized since it is the same intermediate engaged for the preparation of **DG90** polymer. This will help us to compare **T1** and **DG90**. Hence, we can study the impact of the linear chain on the molecular organization

and the electronic properties. For **synthon C2**, it is like **synthon C1** but with additional linear chain  $C_{12}H_{25}$  that is inserted on the cycle of EDOT to increase the solubility of the polymer and maintain a good aggregation. For **Synthon C3**, a perfluoroalkyl chain was added to increase the aggregation and the electron mobility with the improvement of the stability of the material inspired from reported example (Figure 154).<sup>341</sup>

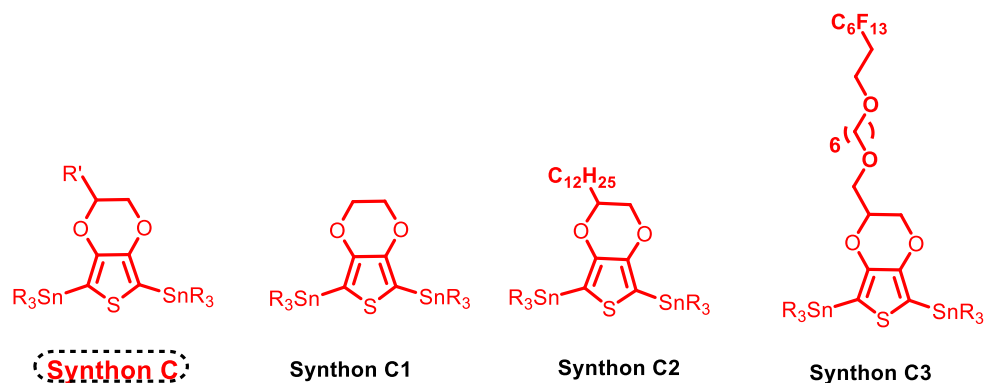
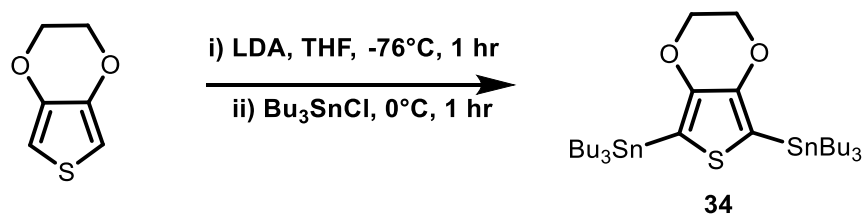


Figure 154: The structure of different synthons C

### 1.3.1. Synthesis of Distannic EDOT

**Synthon C1 (34)** is required for the synthesis of **T1**. The synthesis of **34** starts with a lithiation of EDOT with  $n\text{-BuLi}$  at  $-76\text{ }^\circ\text{C}$  followed by a reaction with tributyltin chloride as reported procedure.<sup>342</sup> The bis-stannic derivative was isolated after an extraction and engaged in the preparation of **T1** without further purification (Scheme 27) with complete conversion according to  $^1\text{H}$  NMR spectrum.



Scheme 27: The synthesis of di stannic EDOT (**Synthon C1**) **34**

### 1.3.2. Synthesis of Functionalized EDOT Synthon C2 (41)

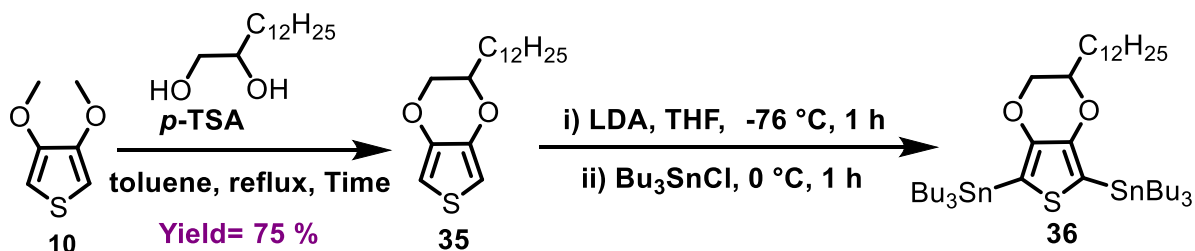
The **Synthon C1 (36)** is required for the preparation of the target **T3**. This compound was prepared with Cyprien Lemouchi in three steps from dibromothiophene. The first step is the formation of dimethoxythiophene from reported procedures. The second step is the preparation of  $C_{12}H_{25}$ -EDOT (**35**). First the compound was not isolated by following the

<sup>341</sup> V. Percec, M. Glodde, T.K. Bera, Y. Miura, I. Shiyonovskaya, K.D. Singer, V.S.K. Balagurusamy, P.A. Heiney, I. Schnell, A. Rapp, H.W. Spiess, S.D. Hudson, H. Duan, *Nature*, **2002**, 419, 384-387.

<sup>342</sup> N. I. Abdo, J. Ku, A. A. El-Shehawy, H-S. Shim, J-K. Min, A. A. El-Barbary, Y. H. Jang, J-S. Lee, *J. Mater. Chem. A*, **2013**, 1, 10306-10317



reported procedures.<sup>343</sup> Sequential additions of *p*-TSA with excess permit to obtain the target compound with a yield of 75 %. Bis-stannic derivative (**Synthon C2**, **36**) can be prepared from the same procedures described for EDOT moiety (Scheme 28).



Scheme 28: The synthesis of di stannic EDOT-R1 (**Synthon C2**) **36**

### 1.3.3. Synthesis of Synthon C3: Functionalization of (R)-EDOT-MeOH and (R)-EDOT-MeCl with perfluoroalkyl chain

Concerning the synthesis of **Synthon C3**, the strategy is the functionalization of the EDOT with perfluoroalkyl side chain. These chains have attracted our attention due to their hydrophobic character which plays a role in increasing the thermal and chemical stability of the polymer. Another interesting character is their ability to self-organize. The synthesis of **Synthons C3** was carried during Master 2 internship period of Victor Boshevski. That was an opportunity for me to train a Master 2 trainer on this research project with the participation of Cyprien Lemouchi and Loïc Le Pluart.

The synthesis of perfluoroalkyl chain functionalized EDOT has been reported, by the group of Mark Sallé.<sup>320</sup> The compound was prepared in two steps from EDOT-CH<sub>2</sub>OH (Figure 155a).

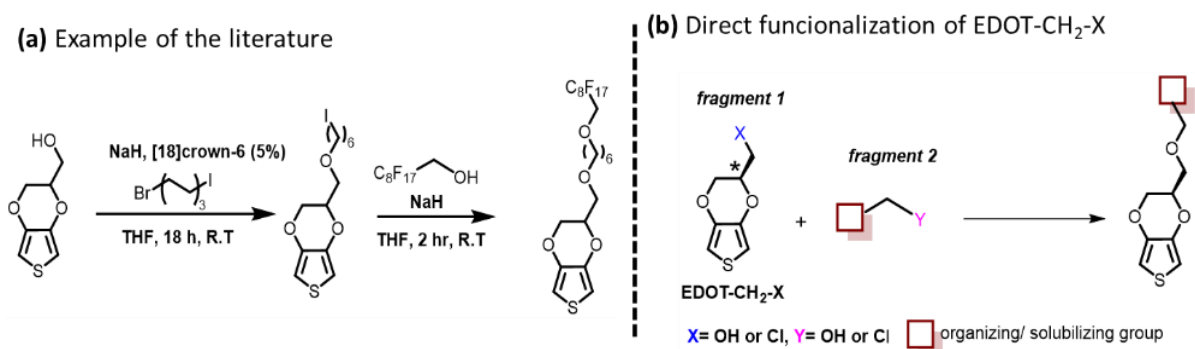


Figure 155: The strategy followed in literature to functionalize EDOT

The first step is the introduction of halogenated alkyl chain. The second step is the nucleophilic substitution with the perfluoroalcoholate on the halogenated derivative to form

<sup>343</sup> S. Zhang, J. Xu, B. Lu, L. Qin, L. Zhang, S. Zhen, D. Mo, *J. Polym. Sci., Part A : Polym. Chem.* **2014**, 52, 1989–1999

the target compound (Figure 155a). In our group, we were interested to test more convergent synthesis with the direct functionalization of the enantiopore **EDOT-CH<sub>2</sub>-X** with different types of chains for the insertion of solubilizing chain or amphiphilic organizing groups as described in figure 155b.

### 1.3.3.1. Direct Functionalization of (*R*)-EDOT-MeOH and (*R*)-EDOT-MeCl with perfluoroalkyl chain

For the synthesis of **Synthon C3**, we worked on the direct functionalization of the starting material EDOT-CH<sub>2</sub>-OH **13** prepared in four steps or EDOT-CH<sub>2</sub>-Cl **11**, which is prepared in two steps from dibromothiophene, (Chapter 2, Scheme 12). Besides, the reactions have been carried out from the enantiopure (*R*) compounds **13** or **11**, which are described in chapter 2 to prepare stereoregular conjugated polymer with enhanced molecular organization and increased charge transport.<sup>344</sup> For the synthesis of the functionalized **EDOT** there are two routes exist in the literature for Williamson reaction described in figure 156.

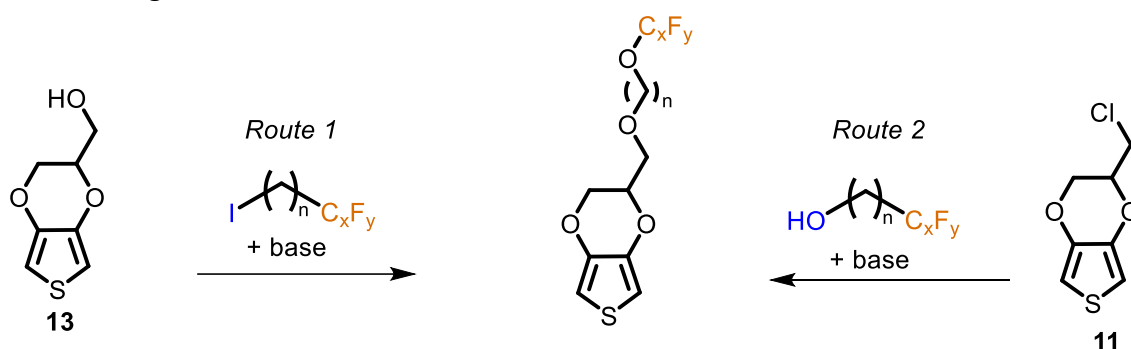


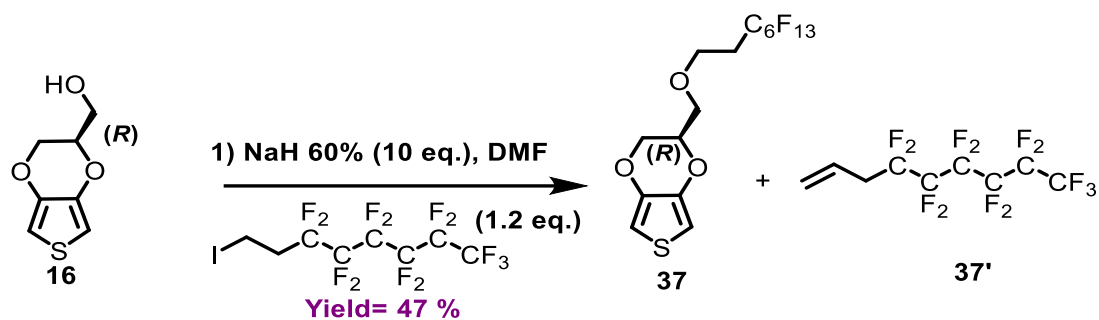
Figure 156: Routs followed to functionalize EDOT with perfluorinated chains (**Synthon C3**)

Following route 1, the EDOT functionalized with perfluorinated chain is prepared from the reaction between a halogenated perfluoroalkyl chain and an alcoolate obtained from EDOT-CH<sub>2</sub>-OH **13** after deprotonation in the presence of a base. However, in route 2, the reaction is between the halogenated EDOT (EDOT-CH<sub>2</sub>-Cl) **11** and perfluoroalcoolate, which is obtained after the deprotonation of perfluoroalkyl chain.

To begin with, route 1 was explored with the preparation of the perfluorinated EDOT **37** as described in scheme 29 and inspired by the work of S. Geribaldi and *al.*<sup>345</sup>

<sup>344</sup> D. Amsallem, A. Bedi, F. Tassinari, O. Gidron, *Macromol.*, **2020**, 53, 9521–9528

<sup>345</sup> H. Trabelsi, F. Szönyi, S. Geribaldi, *J. Fluor. Chem.*, **2001**, 107, 177–181



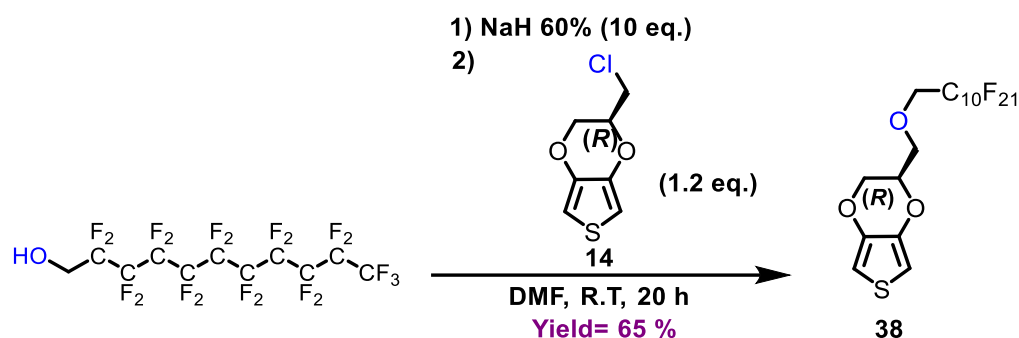
*Scheme 29: Route 1 for the synthesis of intermediate 37*

According to S. Geribaldi and al in such type of reactions,  $\beta$ -elimination side reaction is a risk on the iodinated perfluorinated chain. Therefore, we have decided to start from their condition to prevent the elimination.<sup>345</sup> So, the reaction was carried at room temperature in THF but with 2.5 eq. of NaH (Entry 1, Table 19). However, the target product was not isolated even with the increase of the number of equivalents of NaH to 4, 10 and 20 (entries 2-4, Table 19). Then, the reaction was heated to 67 °C, but as expected the heating promoted the elimination reaction with formation of the compound **37'** (Entry 5, Table 19). Finally, the use of DMF as solvent instead of THF with a large excess of NaH (10 eq.) permits us to isolate the compound **37** with a yield of 40 % with traces of the elimination product **37'** (5 %) (Entry 6, Table 19) according to <sup>1</sup>H NMR analysis. The Williamson reaction was favored by the better solubility of perfluorinated chain in DMF. Nevertheless, the separation of the desired compound from the byproduct **37'** is tedious.

*Table 19: The different conditions of Williamson reaction for the synthesis of compound 37*

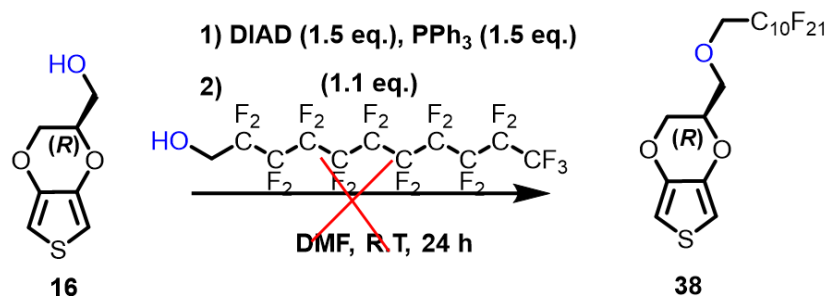
Entry	Base	Equivalent	Solvent	Temperature	Result
1	NaH (60 %)	2.5	THF	R.T	Starting product
2	NaH (60 %)	4	THF	R.T	Starting product
3	NaH (60 %)	10	THF	R.T	Starting product
4	NaH (60 %)	20	THF	R.T	<b>37</b> + elimination product
5	KOH 85 % aq.	20	THF	67°C	<b>37</b> + elimination product
6	NaH (60 %)	10	DMF	R.T	<b>37</b> , 40% yield + elimination product <b>37'</b> 5% yield

For route 2, the best reaction condition of route 1 (Entry 6, Table 19) was first applied. This route starts by deprotonation of the alcohol terminal of perfluorinated chain followed by the reaction with **EDOT-CH<sub>2</sub>-Cl 14** (Scheme 30). The formation of the alcoholate leads to more polar product and then better solubility in DMF. The yield of the reaction increases significantly with a vigorous stirring. Compound **38** was obtained as yellowish oil with a yield of 65 %.



Scheme 30: Route 2 for the synthesis of intermediate **38**

At the same time, another method was applied for the synthesis of compound **38** via Mitsunobu reaction to avoid the inconvenient deprotonation step (Scheme 31).



Scheme 31: The synthesis of intermediate **38**

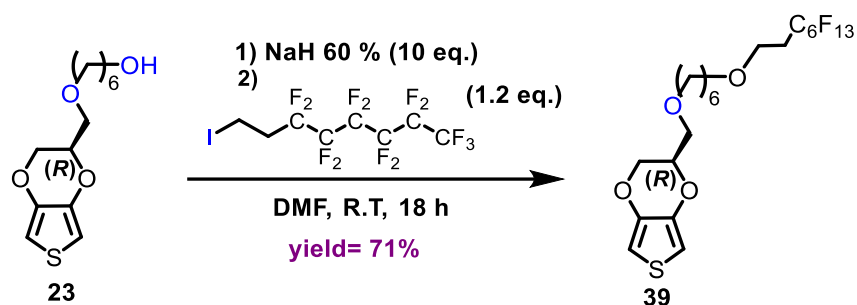
Several attempts have been tested with activation of **(R)-EDOT-MeOH** or perfluorinated alcohol. However, the desired product was not obtained. So, the precursor **38** of **Synthon C3** was obtained with a better yield of 65 % following the route 2.

Otherwise, we have also tested the synthesis of an analog of **synthon C3** (**39**) with the presence of an alkyl spacer, because we have decided to use the intermediate **23** developed in chapter 2 for DPP containing metallooligomers preparation (Scheme 16). Besides the addition of spacer separates the fluorinated terminal from the heterocyclic backbone, which leads to a higher degree of organization.<sup>320</sup> Hence, the presence of aliphatic spacer could help to enhance the charge mobility. Indeed, preserving the stereoregularity will allow better aggregation.<sup>346</sup>

<sup>346</sup> J.-M. Park, D. W. Kim, H. Y. Chung, J. E. Kwon, S. H. Hong, T.-L. Choi, S. Y. Park, *J. Mater. Chem. A*, **2017**, 5, 16681-16688

### 1.3.3.2. Synthesis of (R)-EDOT-R-OC<sub>10</sub>F<sub>21</sub> with spacer:

#### a) Insertion of the spacer on the EDOT moiety:

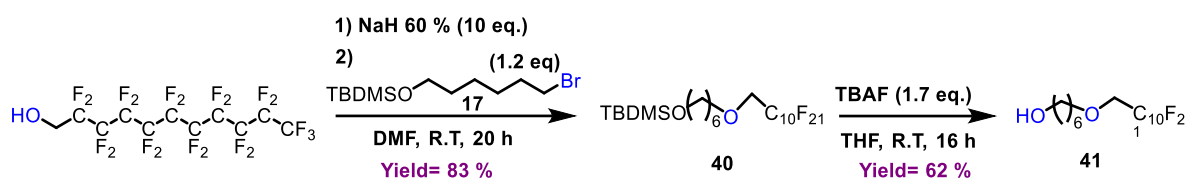


Scheme 32: The synthesis of intermediate **39**

Following the same strategy of Williamson reaction (Entry 6, Table 19) of route 1, compound **23** was deprotonated using NaH in DMF, followed by nucleophilic substitution reaction of the alcoholate on the iodinated perfluorinated chain to obtain compound **39** in a yield of 71 %. Formation of the target compound was confirmed by <sup>1</sup>H NMR and mass spectrometry. We have decided also to test the opposite strategy to insert the spacer on the perfluoroalkyl chain and to make it react on **EDOT-CH<sub>2</sub>-Cl**.

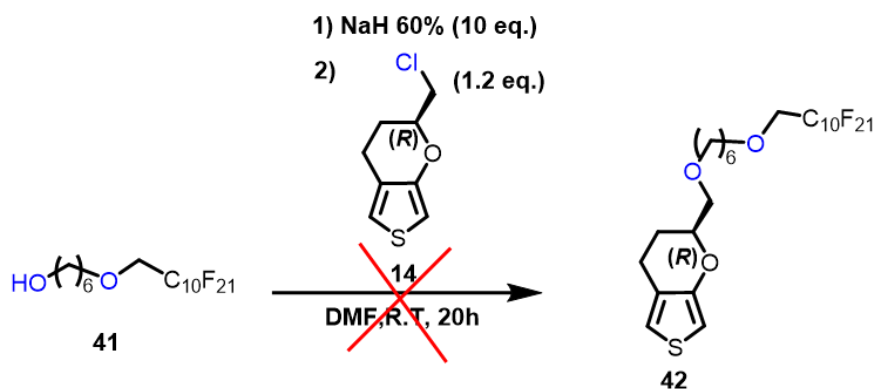
#### b) Insertion of the spacer on the perfluoroalkyl chain:

The spacer has been linked to the perfluorinated chain, and the deprotonated alcohol reacts on **EDOT-CH<sub>2</sub>-Cl** (Scheme 33). The chain with spacer **41** was prepared in two steps. The first step is the reaction between perfluorinated alcoholate and the bromoalkyl chain **17** with alcohol function protected with TBDMS to form compound **40** with a yield of 83 %. Then, the deprotection of the TBDMS groups is carried out with TBAF. The yield of the obtained compound **41** is 62 % (Scheme 33).



Scheme 33: The synthesis of compound **41**

Besides, we have tested the reaction conditions of route 2 to compare the yields. But the reaction of perfluoroalcoholate on on **(R)-EDOT-CH<sub>2</sub>Cl** didn't work (Scheme 34).



Scheme 34: The synthesis of *(R)*-EDOT-MeO-R-OC<sub>12</sub>H<sub>4</sub>F<sub>21</sub> **42**

After the obtention of the first **Synthons A**, **B** and **C**, we have decided to synthesize the first polymer **T1**. It is prepared from the **Synthon C1** and the brominated acceptor **BDTD-1 (33)**.

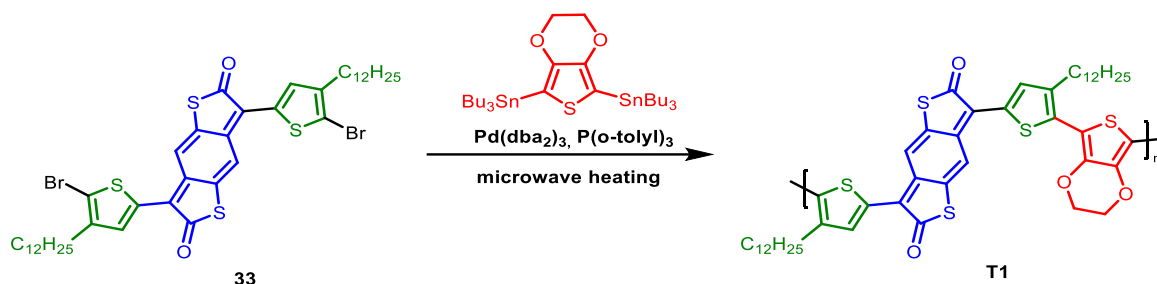
#### 1.4. Synthesis of the polymer T1:

Despite efforts made to improve the reaction conditions, **BDTD-1 33** was obtained in too limited quantity to allow the synthesis of all the targets, therefore we decided to focus on the synthesis of the reference target **T1**.

From preliminary results, (**BDTD-2T-EDOT**)<sub>n</sub> polymer (**DG90**) was synthesized with a Stille coupling reaction under a heating at 90 °C for 16 hours in toluene.

For the synthesis of **T1**, due to the limited quantities of the compound **33**, we decided to directly carry out the Stille coupling reaction with microwave heating in order to increase the reactivity and decrease the reaction time based on reported examples for other conjugated polymers (Scheme 35).<sup>347</sup> We carried out the same coupling reaction but with microwave heating as higher activation process by microwave heating could help to increase average molar mass of the polymers ( $M_n$ ). Because of a few quantities of **33**, we have tested two conditions, the data are listed in table 20. For condition 1 (**MQ187**), the reaction was carried out in toluene like for **DG90** and heated at 95 °C for twice 30 min with 200 W as power. The reaction was monitored by TLC after 30 min until no more starting material. The second condition (**MQ192**) was carried out in chlorobenzene to increase the temperature to 120 °C for 1 hour 30 min with 150 W as power (For these conditions the temperature was set (it's the power required to reach the temperature set)).

<sup>347</sup> W. Li, L. Yang, J. R. Tumbleston, L. Yan, H. Ade, W. You, *Adv.Mater.*, **2014**, 26, 4456–4462



Scheme 35: The synthesis of polymer **T1**

Table 20: The different polymerization conditions used in the synthesis of **T1**

	Solvent	Temperature	Power	Duration
Condition 1 ( <b>MQ187</b> )	Toluene	95 °C	200 watt	60 min
Condition 2 ( <b>MQ192</b> )	Chlorobenzene	120 °C	150 watt	90 min

### 1.5. Characterization of T1

The average molar masses ( $M_n$ ) were determined by GPC with UV-visible calibration based on polystyrene (PS) standards to confirm polymer formation. Figure 156 illustrates the superposition of chromatograms from **DG90-CHCl<sub>3</sub>** referred to **DG90a** ( $M_n=14.6 \text{ Kg.mol}^{-1}$ ), **DG90-CB** referred to **DG90b** ( $M_n= 23.8 \text{ Kg.mol}^{-1}$ ) and **T1** for the two microwave heating conditions (**MQ187**, **MQ192**). Concerning **T1**, the analyses show two types of polymers populations: long and short chain polymers with the presence of two peaks. In the first condition, we got two peaks of small difference in intensity, the first one corresponds to polymer with longer chains ( $M_n= 48.3 \text{ Kg.mol}^{-1}$ ,  $\mathcal{D}= 2.79$ ) that those of **DG90b**. However, for the second condition (**MQ192**), we got two peaks in big difference of their intensity, where the less intense one corresponds to a much higher average molar mass ( $M_n= 330 \text{ Kg.mol}^{-1}$ ,  $\mathcal{D}= 4.4$ ) than those of **DG90b**. For the two conditions retention time of the first peak is shorter than that of **DG90bs** one. So, **T1** has a higher  $M_n$  than **DG90b** (colored arrow in figure 157). Conditions 1 (**MQ187**) has the advantage of having the higher proportion of long chain polymers, while condition 2 (**MQ192**) has the advantage to form the highest average molar mass polymer even if the long chain polymers proportion is smaller. This is a promising result. Hence, further modifications of the microwave conditions are required as using longer heating time or other solvents like m-xylene that is of higher boiling point, allowing us to use higher heating temperature with longer reaction time.

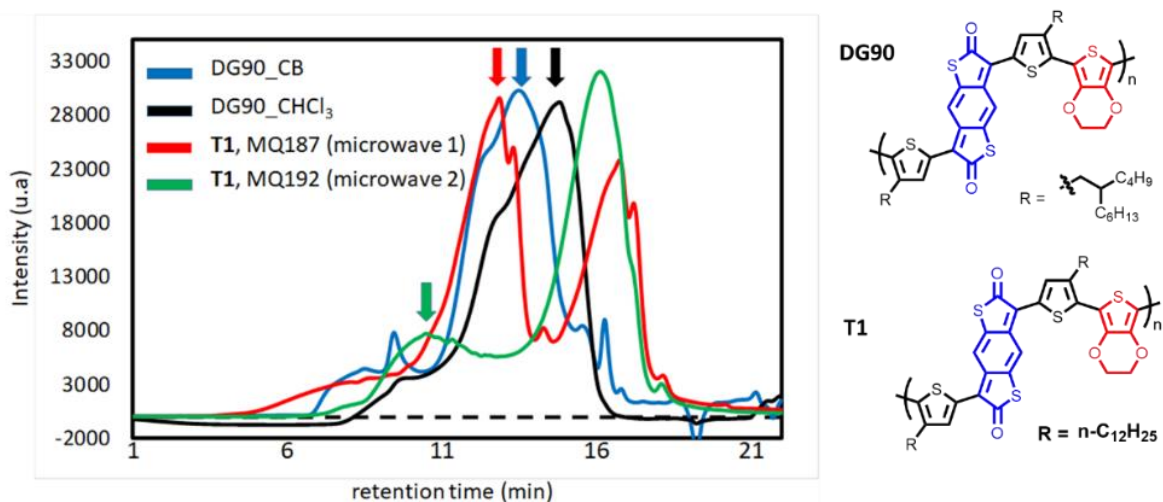


Figure 157: The GPC chromatograms of **DG90a** (**DG90-CHCl<sub>3</sub>**), **DG90b** (**DG90-CB**) and **T1** for the two conditions

Preparation of the polymer **T1** is difficult due to the low yield obtained from the oxidation reaction. Only limited quantities of the intermediate **33** were prepared. The lack of reactivity, stability of the final intermediates and the reproducibility of the oxidation step could be explained by a lower solubility of the samples. In perspective, this could be overcome by changing the linear chain by extended branched chains in order to improve the solubility and to check the improvement of the reactivity with the preparation of **T4** (Cf. Objectives part, Figure 152).



### III. Conclusion and Perspectives

During the work of this chapter, most of **Synthons C** have been synthesized, except **synthon C3**, which is the **EDOT** functionalized with perfluorinated chain. It requires the addition of the stannic function. Concerning **Synthon B**, it is successively synthesized to be integrated in the synthesis of **BDTD** intermediate after Stille coupling reaction.

However, the synthesis of **BDTD** acceptor is quite difficult due to the limitation in the oxidation step. This limitation mainly was because of the poor solubility of the intermediate used as an impact of the presence of the linear alkyl chain as well as not enough stability of intermediates and products obtained during the three successive steps for obtaining the ketone function. After several attempts we were able to obtain the desired molecule with low yield.

Therefore, only one of the designed targets **T1** has been synthesized, which is the reference conjugated polymer to compare with the previously synthesized polymer in the team **DG90**. After applying two polymerization conditions using microwave and different solvents, we were able to obtain two samples of **T1**, **MQ187** and **MQ192**. **MQ187** has the advantages of obtaining a higher proportion of long chain polymers than short chain polymers. However, **MQ192** has the advantage to have the highest molecular weight polymer of 330 Kg.mol<sup>-1</sup>, which is a promising result.

The next approach is to functionalize our polymer with extended branched chain instead of linear chain to alternate acceptor group **BDTD** with higher solubility and probably better reactivity. This will allow us to study the impact of the organizing groups (**Synthons C**) that is the functionalized EDOT. Therefore, this allows the synthesis of target **T4** as exemplified in figure 158. The solubility and stability will be tuned using various functionalized EDOT groups, which are already prepared leading to a new family of targets **T4-T6**.

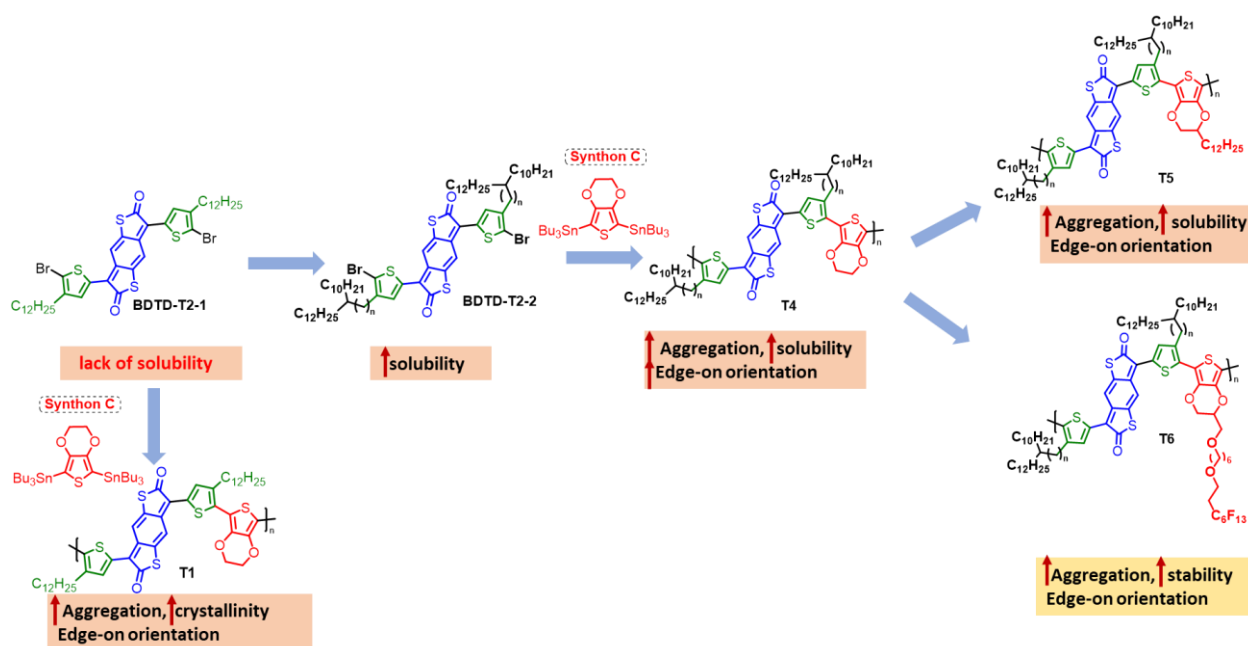


Figure 158: The next approach toward the synthesis of new family of conjugated polymers **T4-T6**.

In the same manner of **T1** preparation, the key intermediate **AA** of polymer **T4** synthesis would be prepared from **synthon B'** (Figure 159). The synthesis of **synthon B'** requires the preparation of extended branched chain **22a** or **22b** with change in the length of spacer according to synthetic strategies reported in the literature and described in chapter 2 of this manuscript.

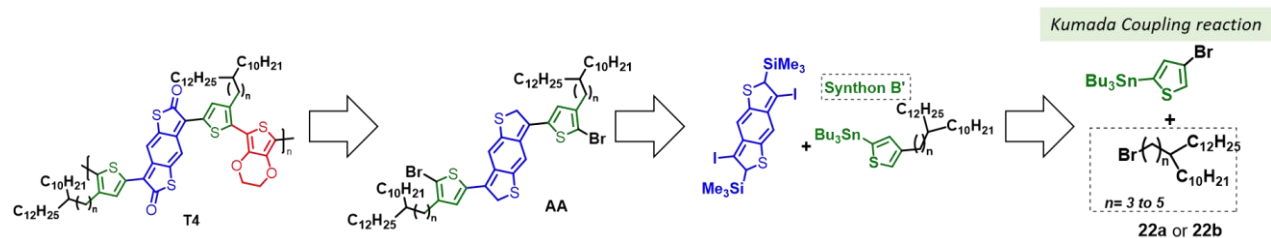


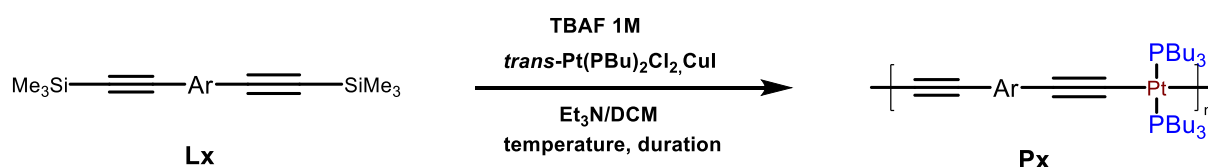
Figure 159: The retrosynthesis of the electro-deficient conjugated polymer **T4**

# General Conclusion

## General Conclusion:

Fabricating organic electronics such as organic solar cells, and organic field effect transistors requires the synthesis of organic semiconductors. These materials are mainly conjugated polymers and they are of two types: p-type and n-type. Both types are required to be designed and studied by researchers for obtaining organic electronic and photovoltaic devices with high performances. In this manuscript, two types of materials have been synthesized: Diketopyrrolopyrrole DPP based metallooligomers as donor materials for bulk heterojunction solar cells (BHJSCs) as well as electro-deficient conjugated polymers (n-type) for n-type organic field effect transistors or for thermoelectric materials after doping.

New metallooligomers with enhanced performances for solar cell applications were synthesized from a dehydrohalogenation reaction from a ligand **Lx** with  $\text{trans-PtCl}_2(\text{PBu}_3)_2$  in the presence of  $\text{CuI}$  and a base (Scheme 36). The metallooligomers are composed of DPP containing organic part (**Ar**) with a lactam function functionalized with a linear alkyl chain for better  $\pi$ -aggregation. The triple bonds from **Ar** are connected to Pt-transition metal (Scheme 36). The presence of transition metal offers additional benefits in respect with analog conjugated polymers. It helps tuning the electronic structure of the polymer and induce specific properties such as: long term stability, upper triplet state formation, enhanced light absorption and high carrier mobility.<sup>216</sup> In this work, two strategies have been developed for the enhancement of the optical and optoelectronic properties of the metallooligomers. The objectives were decreasing the optical band gap in order to reduce energy losses with broadened absorption wavelength range and improving the molecular organization in order to increase charge mobilities.



*Scheme 36: The general synthesis of metallooligomers using dehydrohalogenation reaction*

The methodology of the first strategy was increasing the conjugation length by inserting two thiophene rings to the **Ar** part with respect to an already synthesized **P1'** with the preparation of **PA** (Figure 160). The goal was increasing the average molar mass of **PA** by improving the reaction conditions of the dehydrohalogenation step and by increasing the solubility of the metallooligomer through functionalization the ligand with a solubilizing alkyl chain.

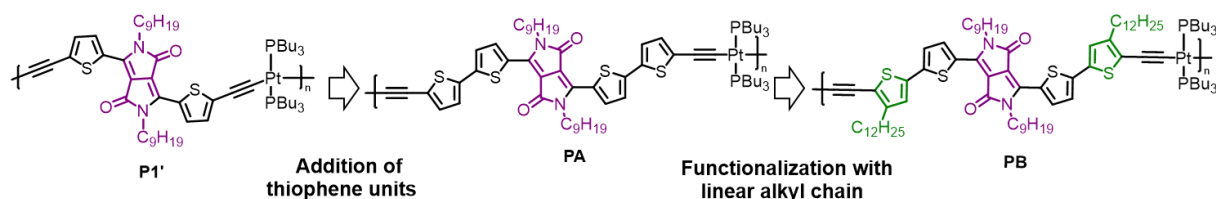


Figure 160: The methodology of strategy 1

The optimization of the dehydrohalogenation step permits to double the Mn value. Yet, the obtained metallooligomer **PA** shows instability issues under illumination and irradiation, which prevents its use as a donor in BHJSCs. These results have been published in 2022 in JIOP. Hence, the metallooligomer **PB** was prepared with a solubilizing linear alkyl chain added on the second thiophene to increase the solubility and to maintain a good  $\pi$ - $\pi$  aggregation. Nevertheless, the metallooligomer **PB** was not isolated because of lower reactivity of the ligand **LB** in the dehydrohalogenation step (Figure 161). Therefore, a second strategy has been applied to synthesize new metallooligomers with better properties.

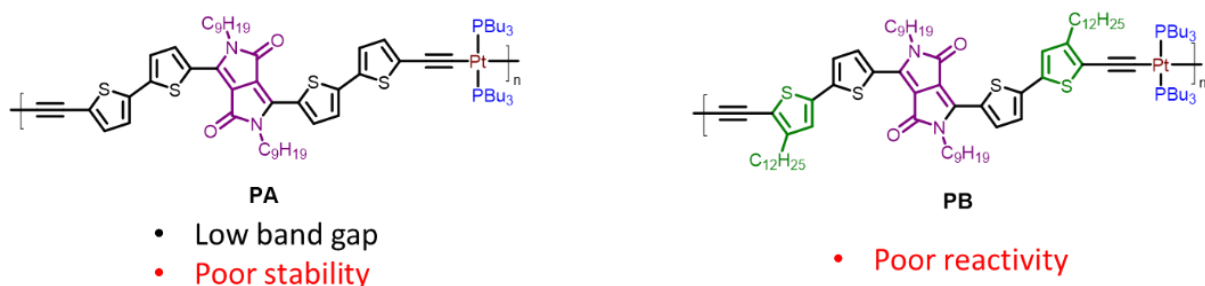


Figure 161: The structure of metallooligomers **PA** and **PB**

The second strategy is based on the use of DPP dimers in the organic part (**Ar**) to decrease significantly the optical band gap. Hence, a narrow band gap metallooligomer **P2'** ( $E_g = 1.42$  eV) has been previously prepared in the team (Figure 162). The performances of BHJSCs showed PCE about 9.42 % with **P2'** as a donor and **PC<sub>71</sub>BM** as an acceptor. Our goal was to prepare a new low band gap metallooligomer, which can be prepared in larger scale with similar or better optical and optical properties. This requires a simplified synthetic route and increased stability of the deprotected ligand to improve the dehydrohalogenation step with formation of metallooligomers with higher chain lengths. In the first approach, the second thiophene was replaced by 3,4-ethylenedioxythiophene (EDOT), which is a stronger donor unit with increased push-pull effect with DPP moiety. Moreover, EDOT unit can increase the planarity of the conjugated backbone by S...O interactions, it increases the stabilization of quinoid structure, and it could be easily functionalized. The metallooligomer **PC** showed a twice higher average molar mass of  $12.4 \text{ Kg}\cdot\text{mol}^{-1}$  in respect of **P2'**. **PC** shows an optical band gap value of 1.48 eV close to **P2'** in agreement with  $E_g^{\text{elec}}$  of 1.42 eV with of  $\lambda_{\text{abs}}^{\text{(onset)}}$  of 840 nm and 875 nm for **PC** and **P2'**, respectively. Besides, **LC** discloses a higher molar extinction coefficient ( $\epsilon_\lambda$ ) ( $4.81 \times 10^4 \text{ mol}^{-1} \text{ L cm}^{-1}$ ,  $5.17 \times 10^4 \text{ mol}^{-1} \text{ L cm}^{-1}$ ) in comparison to **L2'** ( $1.39 \times 10^4 \text{ mol}^{-1} \text{ L cm}^{-1}$ ,  $1.42 \times 10^4 \text{ mol}^{-1} \text{ L cm}^{-1}$ ).

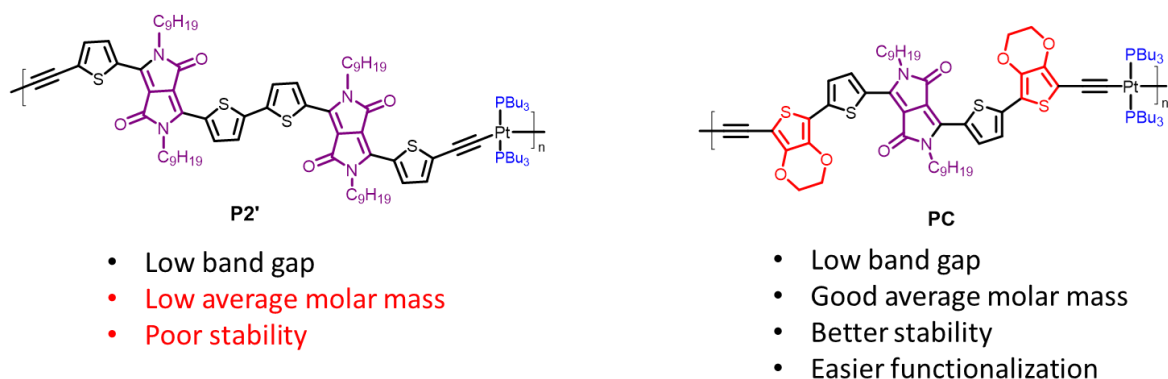
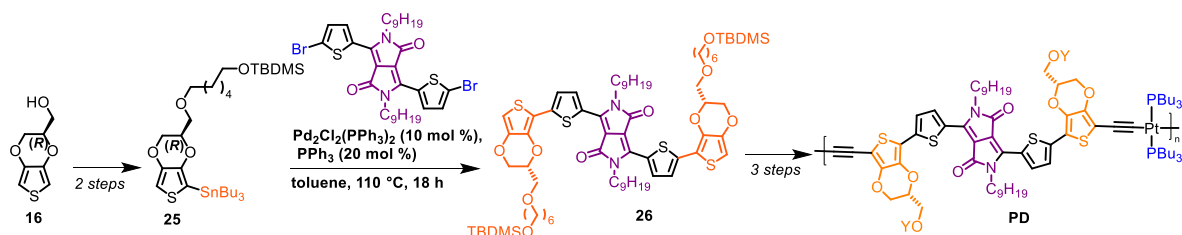


Figure 162: The structure of metallooligomers **P2'** and **PC**

From these promising results, the resynthesis of **PC** in larger quantities (to multiply by 10 the quantities) was performed, which required the optimization of some steps to improve the yields, like the dehydrohalogenation step to increase the purity and the average molar mass of **PC**. Using **PC** as a donor in a BHJSC led to PCE of 8.96 % with **PC<sub>71</sub>BM**, 11.94 % with **IT-4F** and a record of performances for [Pt]-metallooligomers with a PCE of 14.12 %, when associated to the acceptor **Y6**. As a perspective, **PC** could be resynthesized to be used in ternary systems (donor/ acceptor1/ acceptor2) to increase these performances.

The synthesis of **PC** also opened the opportunity for the preparation of metallooligomers with functionalized EDOT. The optoelectronic properties could be enhanced with the insertion of a side chain on the EDOT moiety. The presence of alkyl chains helps to increase the solubility, polar group can increase the exciton dissociation or siloxane group that can increase the donor/acceptor segregation, and the chain could be an organizing group as triphenylene. This family of metallooligomers requires the synthesis of two synthons (*R/S*)-**EDOT-MeOH** and (*R*)-**EDOT-MeOH**. The chiral EDOT (*R*)-**EDOT-MeOH** has been chosen to be functionalized due to the additional chiroptical properties. Different functionalized EDOT have been synthesized and characterized. Monostannic functionalized EDOT (**25**) has been prepared and integrated in Stille coupling reaction for the synthesis of intermediate **26**, which is a key step in obtaining a new ligand **LD** and consequently the metallooligomer **PD** (Scheme 37).



Scheme 37: The general synthetic route of **PD** using functionalized EDOT

Regarding n-type conjugated polymers, a previously prepared polymer (**DG90**) composed of benzo[1,2-b:4,5-b']-difurran-2,6-dione as an acceptor flanked with thiophene units as a donor unit functionalized with branched alkyl chain inspired from the work of Pie and *al*<sup>283</sup> displayed a low lying LUMO level of -4.52 eV. EDOT unit has been inserted to increase the planarity, to improve the rigidity of the conjugated polymer backbone by S...O interactions and to increase the quinoid stabilization. However, this polymer displayed rather low charge

mobilities ( $\mu_e = 6.8 \times 10^{-3} \text{ cm}^2 \text{ V}^{-1} \text{ s}^{-1}$  and  $\mu_h = 1.6 \times 10^{-3} \text{ cm}^2 \text{ V}^{-1} \text{ s}^{-1}$ ), which could be explained by an unfavorable orientation of the chains stacking and a low average molar mass of  $23.8 \text{ Kg.mol}^{-1}$ . We aimed to improve the electronic properties of this polymer. According to the literature, electronic properties of n-type conjugated polymer can be enhanced by improving its stability at ambient condition by lowering the LUMO level ( $E_{\text{LUMO}} < 4.00 \text{ eV}$ ) or by functionalizing the polymer with perfluoroalkyl chains. The increase of the average molar mass helps to improve charges transport as well as to favor better conductivity.

Consequently, our goal was to change the side chain carried on thiophene to trigger edge-on orientation and better aggregation, then to insert a solubilizing chain on the EDOT to improve the solubility of the polymer to increase the average molar mass (Figure 163).

The targets were prepared from a convergent synthesis with the use of synthons **A**, **B** and **C**. This strategy permits to change rapidly the type of side chain (R and R') when a lack of solubility or a wrong  $\pi$ - $\pi$ -stacking orientation is detected. The steps of this synthesis have been optimized to improve the global yield. A first polymer **T1** with linear chain (R) was synthesized to increase molecular organization. But **T1** was not pure enough and displayed a large molar mass dispersity, which prevented it from being analyzed. This could be explained by the lack of the solubility of the final intermediates which prevents obtaining larger quantities.

As a perspective to this work, extended branched chains could be used in the preparation of **T4** to increase the solubility of the final intermediates. The use of distinct synthons **C** functionalized with perfluoroalkyl chains and organizing groups to improve the stability and the molecular organization for the development of efficient and stable n-type OFET and n-type OTE at ambient conditions can also be reasonably targeted.

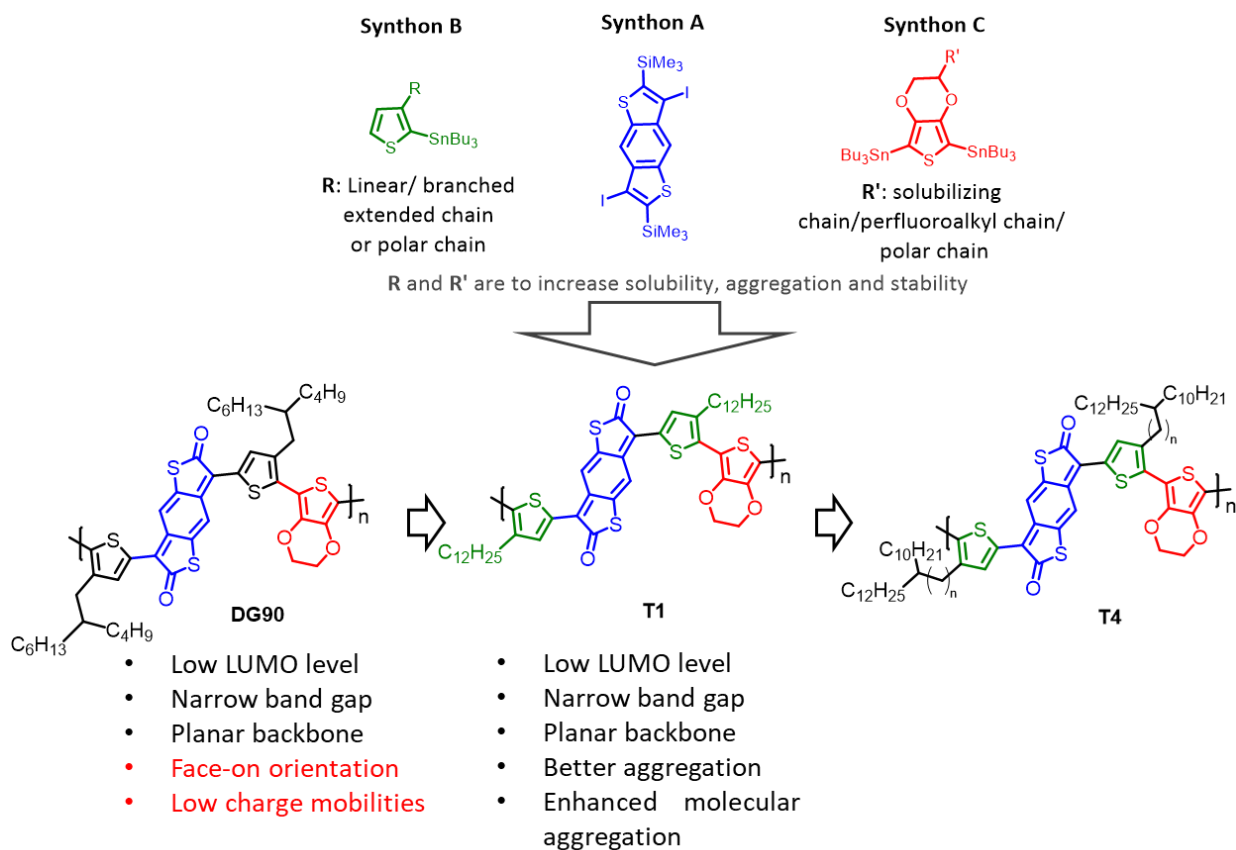


*Figure 163: The structure of conjugated polymers **DG90** and **T1***



# Supporting Information

## Materials and Methods

The Density functional theory (DFT) calculations were then performed to validate the targets **Ln** and **Pn**. by using the Gaussian09<sup>348</sup> at the Université de Sherbrooke with the Mammouth supercomputer supported by Le Réseau Québécois De Calculs Hautes Performances. The DFT geometry optimizations and Time dependent DFT (TD-DFT) calculations<sup>349</sup> were carried out using the B3LYP method. A 6-31g\* basis set was used for C, H, N atoms.<sup>350</sup> It is important to note that DFT calculations for all the molecules were made using a dichloromethane solvent field.

All the chemicals were purchased from commercial suppliers (Fischer Scientific, Sigma-Aldrich, Strem Chemicals, VWR chemicals) were used as received. The solvents (THF, CH<sub>2</sub>Cl<sub>2</sub>, CHCl<sub>3</sub>, trimethylamine,...) were dried and distilled before use.

Thin layer chromatography (TLC) was performed on Merck Silica gel 60 T254 (coated on aluminium sheet). Column chromatography was performed using silica gel 40-63 µm

NMR <sup>1</sup>H, <sup>13</sup>C and <sup>31</sup>P spectra were recorded on BRUKER Avance III400 and BRUKER Avance III500 in CDCl<sub>3</sub> and CH<sub>2</sub>Cl<sub>2</sub> using TMS as an internal standard. Chemical shifts are

---

<sup>348</sup> (a) Scattergood, P.A.; Delor, M.; Sazanovich, I.V.; Bouganov, O.V.; Tikhomirov, S.A., Stasheuski, A.S.; Parker, A.W.; Greetham, G.M.; Towrie, M.; Davies, E.S.; Meijer, A.J. Electron transfer dynamics and excited state branching in a charge-transfer platinum (II) donor-bridge-acceptor assembly. *Dalton Trans.*, **2014**, *43*, 17677-17693. (b) Ueda, M.; Ueno, T.; Suyama, Y.; 31 Ryu, I. Synthesis of 2, 3-disubstituted indenones by cobalt-catalyzed [3+2] annulation of o-methoxycarbonylphenylboronic acid with alkynes. *Chem. Commun.* **2016**, *52*, 13237-13240.

<sup>349</sup> (a) Bauernschmitt, R.; Ahlrichs, R. Treatment of electronic excitations within the adiabatic approximation of time dependent density functional theory. *Chem. Phys. Lett.* **1996**, *256*, 454-464. (b) Becke, A.D. Density-functional thermochemistry. III. The role of exact exchange. *J. Chem. Phys.* **1993**, *98*, 5648-5652. (c) Casida, M.E.; Jamorski, C.; Casida, K.C.; Salahub, D.R. Molecular excitation energies to high-lying bound states from time-dependent density-functional response theory: Characterization and correction of the time-dependent local density approximation ionization threshold. *J. Chem. Phys.* **1998**, *108*, 4439-4449.

<sup>350</sup> (a) Binkley, J.S.; Pople, J.A.; Hehre, W.J. Self-consistent molecular orbital methods. 21. Small split-valence basis sets for first-row elements. *J. Am. Chem. Soc.*, **1980**, *102*, 939-947. (b) Dobbs, K.D.; Hehre, W.J. Molecular orbital theory of the properties of inorganic and 32 organometallic compounds 4. Extended basis sets for third-and fourth-row, main-group elements. *J. Comput. Chem.*, **1986**, *7*, 359-378. (c) Dobbs, K.D.; Hehre, W.J. Molecular orbital theory of the properties of inorganic and organometallic compounds 5. Extended basis sets for first-row transition metals. *J. Comput. Chem.* **1987**, *8*, 861-879. (d) Dobbs, K.D.; Hehre, W.J. Molecular orbital theory of the properties of inorganic and organometallic compounds. 6. Extended basis sets for second-row transition metals. *J. Comput. Chem.*, **1987**, *8*, 880-893. (e) Gordon, M.S.; Binkley, J.S.; Pople, J.A.; Pietro, W.J.; Hehre, W.J. Self-consistent molecular-orbital methods. 22. Small split-valence basis sets for second-row elements. *J. Am. Chem. Soc.* **1982**, *104*, 2797-2803.

(f) Pietro, W.J.; Francl, M.M.; Hehre, W.J.; DeFrees, D.J.; Pople, J.A.; Binkley, J.S. Self-consistent molecular orbital methods. 24. Supplemented small split-valence basis sets for second-row elements. *J. Am. Chem. Soc.*, **1982**, *104*, 5039-5048.

reported in parts per million. The following notation are used to designate the NMR signals; s: singlet, d: doublet, t: triplet, m: multiplet, br: broad.

High-resolution ESI-MS (HR-MS). Samples were analyzed by ESI-MS on a high-resolution and high-accuracy mass spectrometer (LTQ-Orbitrap Elite, Thermo Scientific) in positive ion mode. Samples were dissolved in dichloromethane at a concentration between 1 and 5 pmol/ $\mu$ L according to the sample. They were infused at a flow rate of 3  $\mu$ L/min. The following experimental conditions were applied: spray high voltage, 3 kV; source temperature, 350°C; sheath gas flow rate, 10. External calibration was carried out using the Pierce LTQ Velos ESI positive ion calibration solution. The resolution was set at 240 000 at  $m/z$  400.

Gel permeation chromatography (GPC) were carried out on the GPC prominence Shimadzu with UV-visible detector SPD-20AV (Double wavelength), A metallooligomer concentration of 1 mg/mL were used and the solution were filtered through a 0.45 micron filter before injection. Average molecular weights ( $M_w$ ,  $M_n$ ) were determined by GPC against polystyrene standards. THF was used as eluents with a flow rate of 1ml/min.

Attenuated total reflection infrared (ATR IR) spectra were recorded on powders using Spectrum Two from PerkinElmer.

Matrix-assisted laser desorption/ionization time-of-flight mass spectrometry (MALDI-TOF/MS) Experiments were performed by MALDI-TOF/MS (Ultraflex, Bruker Daltonique) in positive ion mode and in reflectron or linear modes. The ion-accelerating voltage was 20 kV. One  $\mu$ L of sample was deposited on the target and was covered with the matrix. Dithranol and trans-2-[3-(4-tert-Butylphenyl)-2-methyl-2-propenylidene]malononitrile (DCTB) were chosen. External calibrations were carried out using the standard protein mixture (Peptide Calibration Standard kit, Bruker Daltonique). At least 150 laser shots were summed for each spectrum. Raw data were processed using Flex Analysis.

Thermogravimetric analysis (TGA) were conducted on Perkin Elmer TGA Pyris 1. The samples were measured into an aluminium pan and sealed before heating with rate of 10 °C/min under a nitrogen atmosphere

Metallooligomer thin films preparation. The solution of the metallooligomers (5mg.ml<sup>-1</sup>) in CH<sub>2</sub>Cl<sub>2</sub> were spin-coated using LabSpin6/8 from SÜSS MicroTec on glass and quartz substrates at 3000 rpm for 100 seconds at 600 rpm.s<sup>-1</sup> acceleration. The film thicknesses were determined using a KLA-Tencor D-120 stylus profilometer.

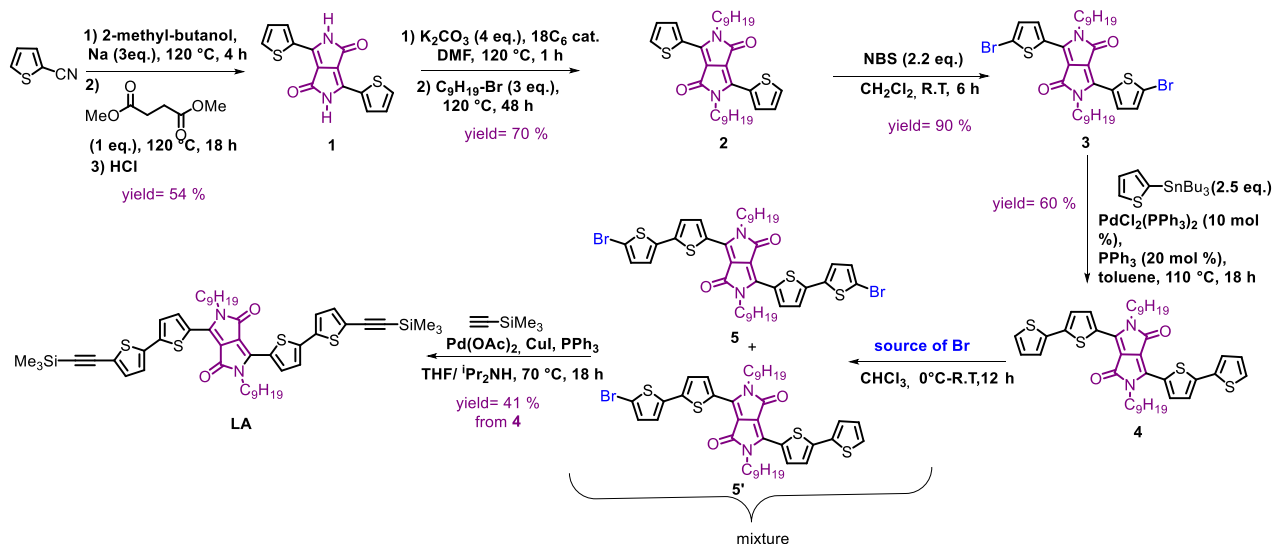
UV-Visible analysis in CH<sub>2</sub>Cl<sub>2</sub> were performed using the Perkin-Elmer (Lambda 35) UV-Vis Spectrometer (250-900 nm) in transmission mode. The UV-vis spectra (200 - 900 nm) of film coated on quartz substrates were recorded by a Cary 4000 spectrophotometer (Agilent Corporation) in transmission mode using the double-beam mode

Photoemission analysis. UV-visible spectroscopy was performed on a Varian Cary 50 spectrophotometer for solutions and films at 298 K and on a Hewlett-Packard 8452A diode array spectrometer for solutions at 77 K. Steady-state measurements, emission and excitation spectra, were made using a Edinburgh Instruments FLS980 Phosphorimeter equipped with single monochromator. Solutions for 298 K measurements were prepared in a glovebox to avoid excited state quenching by O<sub>2</sub> and sealed in an airtight 1 cm cell. Low temperature measurements were made in an NMR tube using a homemade sample holder. Films were made by spin-coating the polymers on 2.5 cm quartz discs. Measurements exceeding 800 nm were performed using a Photon Technology International QuantaMaster 400 phosphorimeter coupled with a NIR PMT-7-B detector. The fluorescence lifetime measurements were performed on the FLS980 using a 378 nm picosecond pulsed diode laser.

The electrochemical measurements were carried out using an BioLogic SP-300 apparatus, at room temperature, under an argon atmosphere, in a three-electrode cell containing anhydrous acetonitrile (MeCN, 10 mL) as solvent and tetrabutylammonium hexafluorophosphate (TBAPF<sub>6</sub>, 10<sup>-1</sup> mol.L<sup>-1</sup>) as supporting salt at a scan rate of 50 mV.s<sup>-1</sup>. The reference electrode was a saturated Hg/Hg<sub>2</sub>Cl<sub>2</sub> reference electrode (further noted SCE for Saturated Calomel Electrode) from Radiometer. It was separated from the cell solution by a

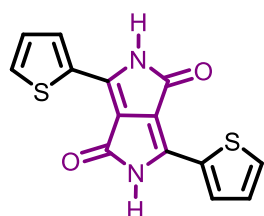
bridge compartment filled with the same solvent / supporting electrolyte solution as used in the cell. The counter electrode was a platinum wire. The working electrode was a disk obtained from a cross-section of a platinum wire (d = 5 mm) sealed in Teflon. Metallooligomer thin films were cast from dichloromethane solution on a platinum disc working electrode (d = 5 mm), and the cyclic voltammograms were recorded in acetonitrile solution containing TBAPF<sub>6</sub>, 10<sup>-1</sup> mol.L<sup>-1</sup> as supporting salt at a scan rate of 50 mV.s<sup>-1</sup>.

## Experimental part of chapter 2



Scheme S1: The synthetic route of metallooligomer LA

### 3,6-Bis(thiophen-2-yl)-2H,5H-pyrrolo[3,4-c]pyrrole-1,4-dione (1)<sup>222</sup>



The procedure was inspired from the literature, C. H. Woo, P. M. Beaujuge, T. W. Holcombe, O. P. Lee, J. M. J. Fréchet, *J. Am. Chem. Soc.* 2010, 132, 15547. In a flame-dried 250 mL bicol, sodium metal (Na (0)) (2.4 g, 104.39 mmol) was slowly added to the 2-methylbutan-2-ol (100 mL) at 120°C. The mixture was stirred at 120 °C until complete dissolution

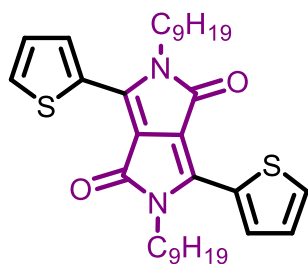
of Na (0). Then the temperature was decreased to 90 °C and the 2-thiophenecarbonitrile (8.5 g, 78.10 mmol) was added in one portion, affording a brown coloration of the reaction mixture. Afterwards, a solution of diethyl succinate (6.2 g, 35.48 mmol) was added dropwise and the mixture was stirred at 120 °C overnight. The solution turned progressively in dark

purple. After cooling to room temperature, the mixture was poured onto dilute HCl (1N, 100 mL) and was stirred vigorously for 1h at 0°C, the precipitated deep purple solid was collected by filtration under vacuum. Then the solid was washed several times with methanol and dried under vacuum to give a purple powder (5.7 g, 19.00 mmol, 54 % yield) and used without further purification.

**<sup>1</sup>H NMR (400 MHz, DMSO) δ (ppm):** 11.24 (s, 1H), 8.23 (s br., 1H), 7.96 (br., 1H), 7.30 (s br., 1H).

**<sup>13</sup>C NMR (400 MHz, DMSO) δ (ppm):** 161.61, 136.14, 132.63, 131.25, 130.78, 128.69, 108.54.

### 2,5-Dinonyl-3,6-bis(thiophen-2-yl)pyrrolo[3,4-c]pyrrole-1,4-dione (**2**)<sup>222</sup>



The procedure was inspired from the literature, S. Jung Park, J. E. Jung, M. K. Kang, Y. H. Na, H. H. Song, J. W. Kang, N. S. Baek, T.-D. Kim, *Synthetic Metals*, **2015**, 203, 221. In a 250 mL flame-dried schlenk, **1** (1.4 g, 4.67 mmol), anhydrous potassium carbonate (2.6 g, 18.81 mmol) and 18-crown-6 (cat., 5 mg) were added in freshly distilled

DMF (70 mL). The mixture was stirred at 100 °C for 1 h under argon atmosphere. Then, 1-bromononane (2.9 g, 14.00 mmol) was added dropwise and the reaction mixture was stirred at 100 °C for 36 h, monitored in TLC ( $R_f = 0.6$ , using  $\text{CHCl}_3$  as eluent). When the reaction was complete, the reaction mixture was cooled to room temperature and extracted with  $\text{CH}_2\text{Cl}_2$  (200 mL). The isolated organic layer was washed with brine (4 x 100 mL), dried over  $\text{MgSO}_4$ , filtered and evaporated under reduced pressure. The crude material was purified by chromatography using silica gel with  $\text{CHCl}_3$  as eluent to afford **2** as a purple solid (1.8 g, 3.26 mmol, 70 % yield).

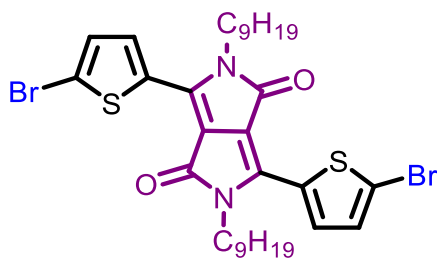
**<sup>1</sup>H NMR (500 MHz,  $\text{CDCl}_3$ ) δ (ppm):** 8.86 (dd, 2H,  $J = 4.0$  Hz,  $J = 1.0$  Hz), 7.57 (dd, 2H,  $J = 5.0$  Hz,  $J = 1.1$  Hz), 7.21 (t, 2H,  $J = 4.5$  Hz), 4.0 (t, 4H,  $J = 8.0$  Hz), 1.74-1.68 (m, 4H), 1.41-1.36 (m, 4H), 1.34-1.29 (m, 4H), 1.27-1.23 (m, 19H), 0.84 (m, 6H).

**<sup>13</sup>C NMR (500 MHz,  $\text{CDCl}_3$ ) δ (ppm):** 161.59, 140.42, 135.50, 130.90, 130.02, 128.84, 107.91, 42.48, 32.10, 30.22, 29.96, 29.74, 29.49, 27.13, 22.92, 14.37.

**IR ( $\text{cm}^{-1}$ ):**  $\nu = 3069$  (v, C-H aromatic), 2918 and 2848 (w, v (N- $\text{CH}_2$ )), 2145, 1655 (w, v(C=O)).

**MS-ASAP-TOF ( $m/z$ ):** calc. for  $C_{32}H_{44}N_2O_2S_2$  (**2**)  $[M+H]^+$ ,  $m/z = 553.28$  ; measured  $[M+H]^+$   $m/z = 553.29$ . **T**  $m.p$  ( $^{\circ}C$ ) = 154.

**3,6-bis-(5-bromothiophen-2-yl)-2,5-dinonyl-2,5-dihydropyrrolo[3,4-c]pyrrole-1,4-dione**  
**(3)**<sup>222</sup>



The procedure was inspired from the literature, C. Wang, Y. Qin, Y. Sun, Y-S. Guan, W. Xu, D. Zhu, *ACS Appl. Mater. Interfaces*, **2015**, 7, 15978. In a 100 mL round bottom flask wrapped with aluminium, **2** (735.0 mg, 1.33 mmol) was dissolved in methylene dichloride (50 mL) and *N*-

bromosuccinimide (521.0 mg, 2.93 mmol) was added in a single portion. Then the mixture was stirred at room temperature for 7 hours, monitored in TLC ( $R_f=0.5$  using  $CH_2Cl_2$ /pentane: 70/30). Afterwards, the product was precipitated after addition of methanol (50 mL) to the concentrated reaction mixture. The dark purple solid **3** (708.2 mg, 1.00 mmol, 90 % yield) was isolated after filtration, washed with cold methanol ( $2 \times 200$  mL) and dried under vacuum.

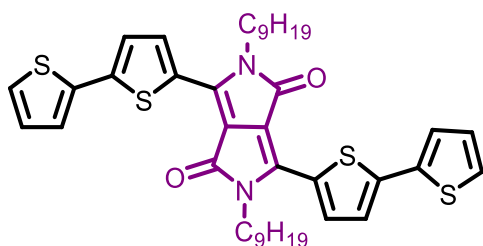
**$^1H$  NMR (400 MHz,  $CDCl_3$ )  $\delta$  (ppm):** 8.63 (d, 2H,  $J = 4.3$  Hz), 7.23 (d, 2H,  $J = 4.3$  Hz), 3.93 (t, 4H,  $J = 7.9$  Hz), 1.69 (m, 4H), 1.41-1.36 (m, 4H), 1.34-1.31 (m, 5 H), 1.28-1.24 (m, 20 H), 0.86 (m, 7H).

**$^{13}C$  NMR (500 MHz,  $CDCl_3$ )  $\delta$  (ppm):** 161.06, 139.00, 135.24, 131.62, 131.19, 119.05, 107.95, 31.81, 29.95, 29.40, 29.16, 26.80, 22.61, 14.01.

**IR ( $cm^{-1}$ ):**  $\nu = 3092$  (v, C-H aromatic), 2916 and 2.851 (w, v (N-CH<sub>2</sub>)), 1660 and 1558 (w, v(C=O)).

**MALDI-tof** (dithranol) calc. for  $C_{32}H_{42}Br_2N_2O_2S_2$  (**3**)  $[M^+]$ ,  $m/z = 708.11$ ; measured  $[M^+]$   $m/z = 708.10$ ; **T**  $m.p$  ( $^{\circ}C$ ) =175.

**3,6-di([2,2'-bithiophen]-5-yl)-2,5-dinonyl-2,5-dihydropyrrolo[3,4-c]pyrrole-1,4-dione** (**4**)



The procedure was inspired from the literature, Y. Zou, D. Gendron, R. Neagu-Plesu, and M. Leclerc, *Macromolecules*, **2009**, 42(17), 6361. In flamed-dried schlenk under argon atmosphere, **3** (170.4 mg, 0.240 mmol) was dissolved in 20 mL of anhydrous and

degassed toluene,  $Pd(PPh_3)_2Cl_2$  (16.84 mg, 24.0  $\mu$ mol, 10 mol%) and  $PPh_3$  (12.6 mg, 48.0  $\mu$ mol,

20 mol%) were added. Then 2-(tributylstannyl)thiophene (commercially available) (227.6 mg, 0.61 mmol, 2.5 eq.) was added. The mixture was refluxed overnight under argon atmosphere. After cooling, the solvent was evaporated under reduced pressure. The resulting solid was retaken in a mixture CH<sub>2</sub>Cl<sub>2</sub>/CH<sub>3</sub>OH: 30 mL/ 30mL, then filtered and washed with methanol several times to get compound **4** as dark-purple solid (104.8 mg, 0.15 mmol, 60 % yield).

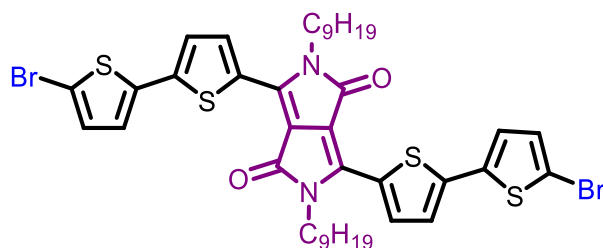
**<sup>1</sup>H NMR (500 MHz, CDCl<sub>3</sub>) δ (ppm):** 8.90 (d, 2H, *J* = 4.2 Hz), 7.31 (m, 6 H), 7.06 (t, 2H, *J* = 4.2 Hz), 4.07 (t, 4 H, *J* = 7.7 Hz), 1.79-1.72 (m, 4 H), 1.44-1.39 (m, 4 H), 1.36-1.32 (m, 6H), 1.29-1.21 (m, 24H), 0.84 (t, 6H).

**<sup>13</sup>C NMR (500 MHz, CDCl<sub>3</sub>) δ (ppm):** 160.25, 141.81, 138.11, 135.48, 135.15, 127.25, 127.11, 125.29, 124.23, 123.96, 107.16, 41.27, 30.82, 29.00, 28.68, 28.47, 28.22, 25.87, 21.65, 13.08.

**IR (cm<sup>-1</sup>):** ν = 3087 (v, C-H aromatic), 2921 and 2851 (w, v (N-CH<sub>2</sub>)), 1657 (w, v(C=O)).

**MALDI-tof** (dithranol) calc. for C<sub>40</sub>H<sub>48</sub>N<sub>2</sub>O<sub>2</sub>S<sub>4</sub> (**4**) [M<sup>+</sup>], *m/z* = 716.26; measured [M<sup>+</sup>]<sup>+</sup> *m/z* = 716.26 ; T<sub>m,p</sub> (°C) =233.

### 3,6-bis(5'-bromo-[2,2'-bithiophen]-5-yl)-2,5-dinonyl-2,5-dihydropyrrolo[3,4-c]pyrrole-1,4-dione (**5**)<sup>234</sup>



The procedure was inspired from the literature, Catherine Kanimozhi, Nir Yaacobi-Gross, Edmund K. Burnett, Alejandro L. Briseno, Thomas D. Anthopoulos, Ulrike Salznerd, Satish Patil, *Phys. Chem. Chem. Phys.*, 2014, 16,

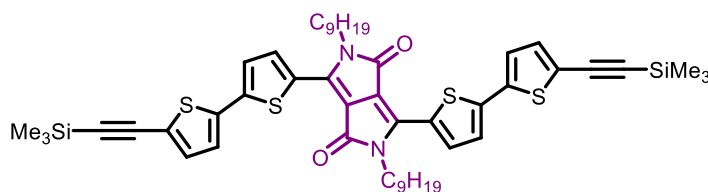
17253—17265. In a 50 mL round bottom flask wrapped with aluminum foil to prevent light, **2** (185.0 mg, 0.258 mmol) was dissolved in chloroform (20 mL). The solution was cooled to -5 °C with ice bath with NaCl. Keeping the temperature below 0°C, bromine (87 mg, 0.542 mmol) was added. Then, the mixture was stirred at a temperature below 0 °C for 3 hours. **Be cautious:** higher temperature causes degradation of the product with by-reactions and provides lower yields. The reaction was monitored by TLC (disappearance of the starting material *R<sub>f</sub>*=0.6 and formation of brominated compound, *R<sub>f</sub>*=0.7, using pentane/CH<sub>2</sub>Cl<sub>2</sub>:1/1 as eluent). The reaction mixture was quenched with sodium thiosulfate aqueous solution and extracted with methylene chloride. The organic layer was washed twice with water and evaporated under reduced pressure. The liquid residue was retaken several times with



toluene and evaporated to remove water traces. The crude product (m= 200 mg) was obtained as a dark purple solid, which is a mixture of **5** and **5'** evidenced by MALDI-TOF. Since the separation of those products was very difficult, the crude material was directly engaged in the next step. **Be cautious:** the brominated compounds are not very stable, they must be stored in the fridge and protected from light exposure, they must be rapidly engaged in the next step.

**MALDI-TOF** (dithranol) calc. for C<sub>40</sub>H<sub>46</sub>Br<sub>2</sub>N<sub>2</sub>O<sub>2</sub>S<sub>4</sub> (**5**) m/z = 872.08, measured [M+2]<sup>+</sup> m/z = 874.10  
calc. for C<sub>40</sub>H<sub>47</sub>BrN<sub>2</sub>O<sub>2</sub>S<sub>4</sub> (**5'**) m/z = 794.17, measured [M+2]<sup>+</sup> m/z = 796.19.

**2,5-dinonyl-3,6-bis(5'-((trimethylsilyl)ethynyl)-[2,2'-bithiophen]-5-yl)-2,5-dihydropyrrolo[3,4-c]pyrrole-1,4-dione (L)** <sup>234</sup>



The procedure was inspired from the literature, Yuping Yuan, Tsuyoshi Michinobu, Jun Oguma, Takehito Kato, Kunihiro Miyake, *Macromol. Chem. Phys.* **2013**, 214, 1465–1472. In flamed-dried Schlenk wrapped with aluminum foil to prevent light and under argon atmosphere, the crude product **5** and **5'** (200 mg) is dissolved in the mixture tetrahydrofuran/ diisopropylamine: 25mL/ 25mL. The solution was degassed with argon stream bubbling into the solution. Then CuI (6.0 mg, 31.5 μmol) and PdCl<sub>2</sub>(PPh<sub>3</sub>)<sub>2</sub> (33.0 mg, 47.0 μmol) were added. Then, trimethylsilylacetylene (TMSA), 98% purity (88.0 mg, 0.896 mmol) was added. The mixture was heated at 70 °C for 3 hours and monitored by TLC (eluent: CH<sub>2</sub>Cl<sub>2</sub>/pentane: 40/60, R<sub>f</sub>= 0.55). The solution was evaporated under reduced pressure and the crude product was purified by column chromatography on silica gel using pentane/CH<sub>2</sub>Cl<sub>2</sub> (60/40) as eluent to provide **L** as a dark blue solid (98 mg, 107.75 μmol, 41 % yield from **4**).

**<sup>1</sup>H NMR (500 MHz, CDCl<sub>3</sub>) δ (ppm):** 8.92 (d, 2H, J = 4.2 Hz), 7.30 (d, 2H, J = 4.2 Hz), 7.16 (m, 4H), 4.1 (t, 4H, J = 7.8 Hz), 1.75 (m, 5H\*), 1.44-1.19 (m, 65H\*), 0.84 (m, 18H\*) \*: *nonyl side chains on DPP + supplementary hydrogens from 1-bromononyl residue*, 0.24 (s, 18H), 0.07 (TMS residue).

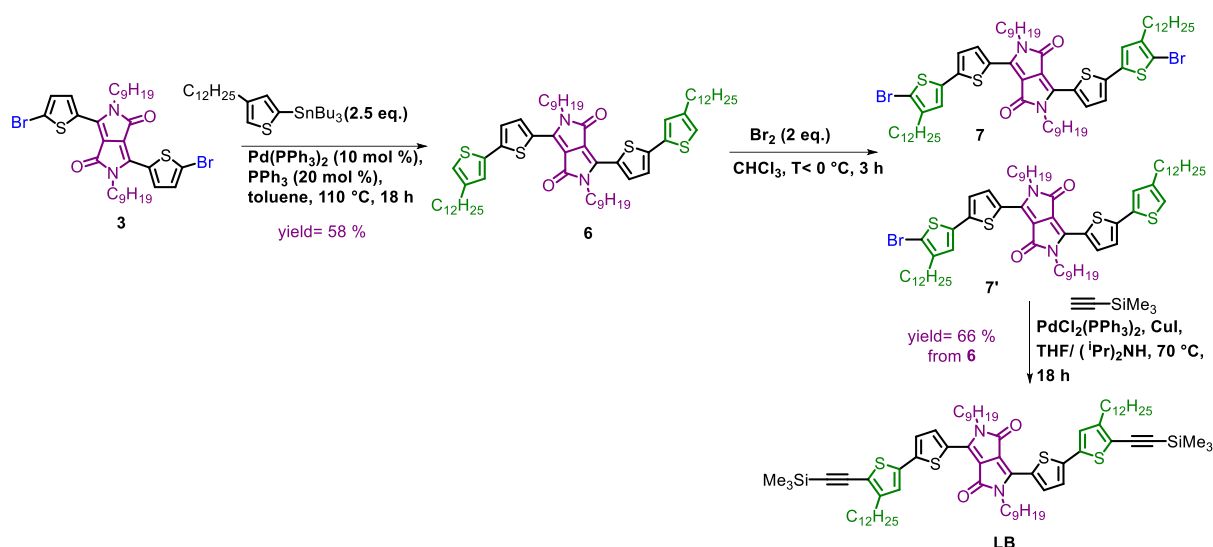
$^{13}\text{C}$  NMR (500 MHz,  $\text{CDCl}_3$ )  $\delta$  (ppm): 161.32, 142.02, 139.10, 137.41, 136.71, 133.81, 128.73, 125.55, 124.93, 123.99, 108.58, 101.74, 97.09, 42.44, 31.98, 31.10, 29.62, 29.39, 29.37, 27.10, 22.82, 14.27, 1.17, 0.07 (TMS residue).

IR ( $\text{cm}^{-1}$ ):  $\nu$  = 2920 and 2851 (w,  $\nu$  (N- $\text{CH}_2$ )), 2140 (w,  $\nu$ (C $\equiv$ C)), 1659 (w,  $\nu$ (C=O)).

HRMS (ESI) Calculated for (LA)  $\text{C}_{50}\text{H}_{64}\text{N}_2\text{O}_3\text{S}_4\text{Si}_2$  [ $\text{M}^{++}$ ]:  $m/z$  908.340. Found:  $m/z$  908.299;

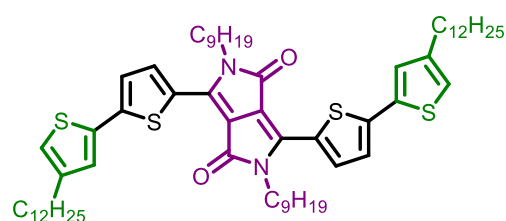
$T_{\text{m.p}}$  ( $^\circ\text{C}$ ) =258.

### Synthesis of LB



Scheme S2: the synthetic route of LB from compound 3

### 3,6-Bis(4'-dodecyl-[2,2'-bithiophen]-2-yl)-2,5-dinonyl-2,5-dihydropyrrolo[3,4-]pyrrole-1,4-dione (6)



The procedure was inspired from the literature, R.Y. Mahale et al, *Chem. Phys. Lett.* 2018, 696, 48-54 (10.1016/j.cplett.2018.02.021). In flamed-dried

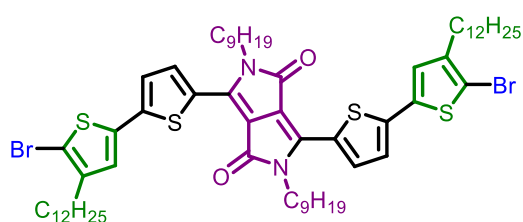
schlenk, to a solution of **5** (300 mg, 0.422 mmol) in 30 mL of anhydrous and degazed DMF, **T-Sn** freshly prepared (686 mg, 1.27 mmol) and  $\text{Pd}(\text{PPh}_3)_2\text{Cl}_2$  (30 mg, 0.042 mmol) were added. The mixture was heated at  $80^\circ\text{C}$  overnight under argon atmosphere. The reaction was monitored by TLC (eluent:  $\text{CH}_2\text{Cl}_2$ /pentane: 1/1,  $R_f$  (**6**) =0.6). After cooling, major part of DMF was evaporated under reduced pressure. To the residue, 10 mL of the solvent mixture ( $\text{CH}_3\text{OH}/\text{CH}_2\text{Cl}_2$ : 60/40) was added to precipitate the compound. The product **6** was collected after filtration and

washing with methanol three times. Compound **6** was isolated as dark-blue solid (260 mg, 0.246 mmol, 58 % yield).

$^1\text{H NMR}$  (500 MHz,  $\text{CDCl}_3$ )  $\delta$  (ppm): 8.90 (d, 2H,  $J = 4.2$  Hz), 7.29 (d, 2H,  $J = 4.2$  Hz), 7.16 (s, 2H), 6.92 (s, 2H), 4.09 (4H, m), 2.60 (4H, m), 1.82-1.20 (m, 78\*), 0.87 (m, 15H\*) alkyl side chains on DPP + supplementary hydrogens from 1-bromononyl residue.

HRMS (ESI) Calculated for (**6**)  $\text{C}_{64}\text{H}_{96}\text{N}_2\text{O}_2\text{S}_4$ :  $m/z$  1052.635. Found:  $m/z$  1053.635  $[\text{M}+\text{H}]^+$

### 3,6-Bis(5'-bromo-4'-dodecyl-[2,2'-bithiophen]-2-yl)-2,5-dinonyl-2,5-dihydropyrrolo[3,4-pyrrole-1,4-dione (**7**)

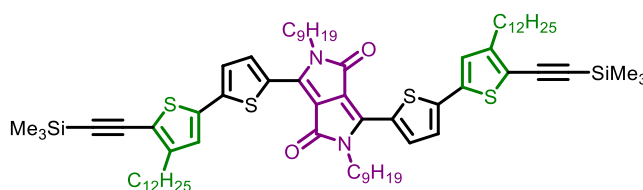


The procedure was inspired from the literature, Catherine Kanimozhi, Nir Yaacobi-Gross, Edmund K. Burnett, Alejandro L. Briseno, Thomas D. Anthopoulos, Ulrike Salzner, Satish Patil, *Phys. Chem. Chem. Phys.*, 2014, 16, 17253–17265. | In a 25

mL round bottom, **6** (100 mg, 0.095 mmol) was dissolved in  $\text{CH}_2\text{Cl}_2$  (20 mL) the solution was cooled to  $0^\circ\text{C}$  and bromine (32 mg, 0.199 mmol) was added slowly. The mixture was stirred at  $0^\circ\text{C}$  and the reaction was monitored by TLC (eluent:  $\text{CH}_2\text{Cl}_2/\text{pentane}$ : 1/1,  $R_f$  (**7**) = 0.8). The reaction mixture was quenched with sodium thiosulfate aqueous solution and extracted with  $\text{CH}_2\text{Cl}_2$ . The organic layer was washed with water and brine, then it was dried over  $\text{MgSO}_4$ , filtered and evaporated under reduced pressure. The crude product was isolated as a dark blue solid, 120 mg.

$^1\text{H NMR}$  spectrum has a poor resolution, and it was directly engaged in next step.

### 3,6-Bis(4'-dodecyl-5'-(trimethylsilyl)ethynyl)-[2,2'-bithiophen]-2-yl)-2,5-dinonyl-2,5-dihydropyrrolo[3,4-c]pyrrole-1,4-dione (**LB**)



In a flame-dried Schlenk, to a solution of the crude product **7** (100 mg) in a degassed solvent mixture  $i\text{Pr}_2\text{NH}/\text{THF}$ : 20 mL/20,  $\text{CuI}$  (2 mg, 10.5  $\mu\text{mol}$ ) and  $\text{PdCl}_2(\text{PPh}_3)_2$  (20 mg, 28.5  $\mu\text{mol}$ ) were added. Then trimethylsilylacetylene (TMSA) (69 mg, 0.704 mmol) was added.

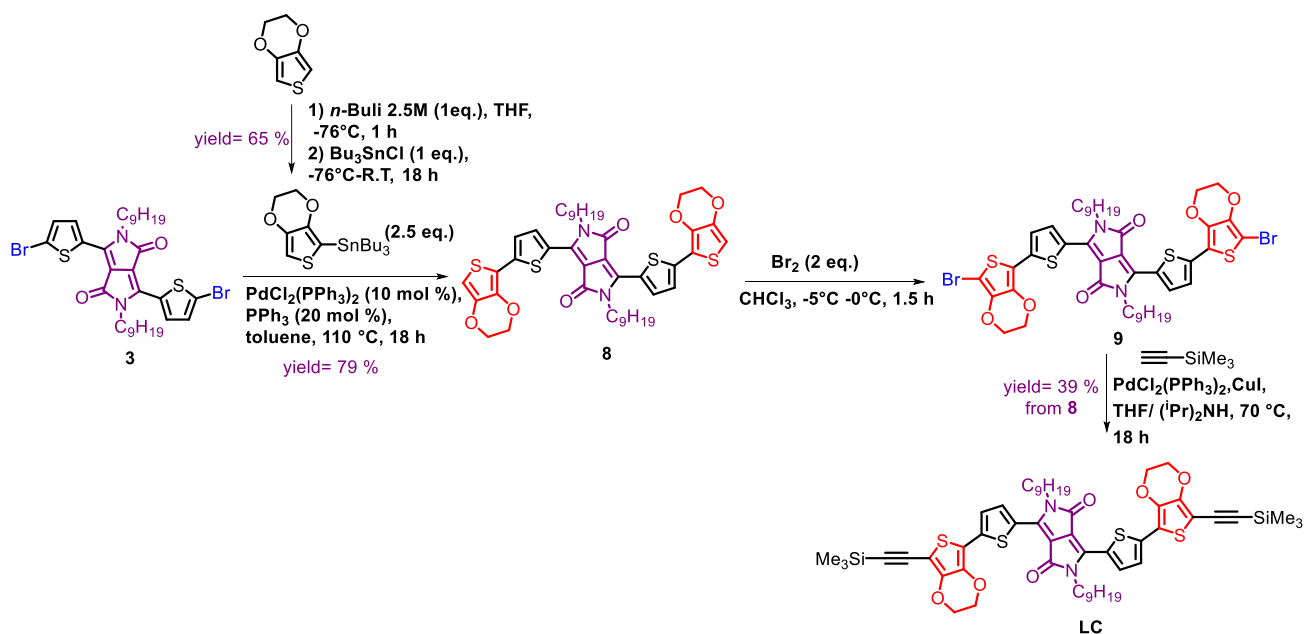
The mixture was refluxed at 70 °C overnight and monitored by TLC (eluent: CH<sub>2</sub>Cl<sub>2</sub>/pentane: 50/50, *R<sub>f</sub>* (**LB**) = 0.5). The solution was evaporated under reduced pressure and the crude product was purified by column chromatography on silica gel using pentane/CH<sub>2</sub>Cl<sub>2</sub>: 50/50 as eluent to provide **LB** as a dark blue solid (65 mg, 0.052 mmol, 66 % yield from **6**).

<sup>1</sup>H NMR (600 MHz, CDCl<sub>3</sub>) δ (ppm): 8.90 (d, 2H, J = 4.2 Hz), 7.29 (d, 2H, J = 4.2 Hz), 7.06 (s, 2H), 4.07 (4H, m), 2.67 (4H, m), 1.82-1.20 (m, 78\*), 0.87 (m, 15H\*) 0.26 (s, 18H), alkyl side chains on DPP + supplementary hydrogens from 1-bromononyle residue

<sup>13</sup>C NMR (600 MHz, CDCl<sub>3</sub>) δ (ppm): 161.31, 150.13, 142.40, 139.00, 136.49, 135.70, 128.49, 126.07, 125.25, 119.24, 108.46, 103.67, 96.99, 42.37, 32.02, 31.93, 30.96, 30.87, 30.14, 30.09, 29.79, 29.77, 29.76, 29.72, 29.58, 29.48, 29.46, 29.37, 29.34, 29.33, 28.72, 28.65, 28.40, 28.28, 26.97, 22.79, 22.76, 21.71, 14.22, 14.21, 13.16, 1.11, 0.05

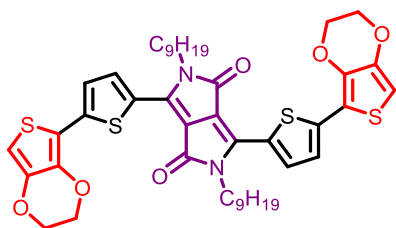
HRMS (ESI) Calculated for (**LB**) C<sub>74</sub>H<sub>112</sub>N<sub>2</sub>O<sub>2</sub>S<sub>4</sub>Si<sub>2</sub>: m/z 1244.715. Found: m/z 1245.833 [M+H]<sup>+</sup>

### Synthesis of LC



Scheme S3: The synthetic route of **LCC** from compound **3**

**3,6-Bis([2,2'-biEDOT]- thiophene-2-yl)- 2,5-dinonyl-2,5-dihydropyrrolo[3,4-]pyrrole-1,4-dione (8)**



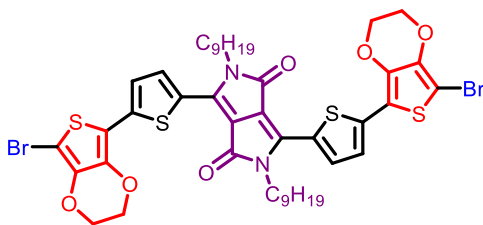
The procedure was inspired from the literature, R.Y. Mahale et al. / Chemical Physics Letters 696 (2018) 48–54 ([/doi.org/10.1016/j.cplett.2018.02.021](https://doi.org/10.1016/j.cplett.2018.02.021)). In a flask equipped with a magnetic stirrer and a nitrogen inlet, compound **3** (200 mg, 0.280 mmol) and EDOT-Sn freshly prepared<sup>227</sup> (341.58 mg, 1.12 mmol) in 20 mL of anhydrous and dry DMF, Pd(PPh<sub>3</sub>)<sub>2</sub>Cl<sub>2</sub> (20 mg, 28.5 μmol) were added. The mixture was refluxed overnight under argon atmosphere. After cooling, the solvent was evaporated under reduced pressure. The resulting solid was taken in a mixture CH<sub>2</sub>Cl<sub>2</sub>/CH<sub>3</sub>OH: 20 mL/20 mL, then filtered and washed with methanol several times to get compound **8** as dark-purple solid (185 mg, 0.222 mmol, 79 % yield).

<sup>1</sup>H NMR (500 MHz, CDCl<sub>3</sub>) δ (ppm): 8.98 (d, 2H, J = 4.19 Hz) 7.35 (d, 2H, J = 4.19 Hz), 6.35 (d, 2H), 4.39(dd, 4H), 4.28 (dd, 4H), 4.10(t, 4H), 1.2-1.20 (m, 28H), 0.86 (t, 6H)

<sup>13</sup>C NMR (500 MHz, CDCl<sub>3</sub>) δ (ppm): 161.48, 142.14, 140.80, 139.38, 139.27, 136.20, 127.67, 123.95, 11.82, 108.02, 99.48, 65.37, 64.67, 42.45, 32.01, 30.18, 29.85, 29.72, 29.40, 29.38, 27.05, 22.81, 14.26.

HRMS (ESI) Calculated for (**8**) C<sub>44</sub>H<sub>52</sub>N<sub>2</sub>O<sub>6</sub>S<sub>4</sub>: m/z 932.271. Found: m/z 933.30 [M+H]<sup>+</sup>

**3,6-Bis(7'-bromo-[2,2'-biEDOT]- thiophene-2-yl)- 2,5-dinonyl-2,5-dihydropyrrolo[3,4-]pyrrole-1,4-dione (9)**



The procedure was inspired from the literature, Catherine Kanimozhi, Nir Yaacobi-Gross, Edmund K. Burnett, Alejandro L. Briseno, Thomas D. Anthopoulos, Ulrike Salzner, Satish Patil, Phys. Chem. Chem. Phys., 2014, 16, 17253–17265. In a 25 mL round bottom flask, **8** (150 mg, 0.18 mmol) was dissolved in chloroform (15 mL), then bromine (57.54 mg, 0.36 mmol) was added slowly over 15 min at 0°C, then the mixture was stirred at -5°C-0°C for 90 minutes until the reaction was complete, it was monitored by TLC (eluent 100 % CH<sub>2</sub>Cl<sub>2</sub>,

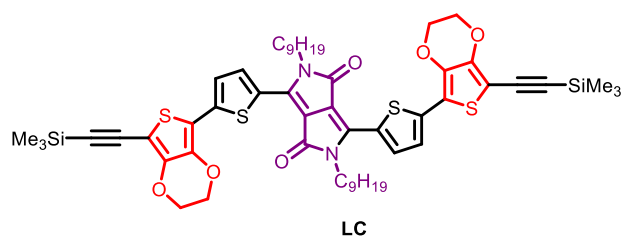
$R_f(\mathbf{9}) = 0.7$ ). The reaction mixture was quenched with sodium thiosulfate aqueous solution and extracted with methylene chloride. The organic layer was washed with brine, dried over magnesium sulfate and filtered. The solvent was evaporated under reduced pressure. The crude product was purified by chromatography on silica gel with 100 %  $\text{CH}_2\text{Cl}_2$  as eluent. The target product was isolated as dark purple solid (160 mg, 0.16 mmol, 89.7 % yield).

The resolution of  $^1\text{H}$  NMR spectrum was poor; only main signals were detected, but the compound was characterized by mass spectrometry and was engaged in next step without further purification.

$^1\text{H}$  NMR (500 MHz,  $\text{CDCl}_3$ )  $\delta$  (ppm): 8.99 (d, 2H  $J = 4.34$  Hz) 7.29 (d, 2H  $J = 4.34$  Hz), 4.40 (m, 4H), 4.36 (m, 4H), 4.26 (m, 4H)

HRMS (ESI) Calculated for ( $\mathbf{9}$ )  $\text{C}_{44}\text{H}_{50}\text{Br}_2\text{N}_2\text{O}_6\text{S}_4$ :  $m/z$  988.0918. Found:  $m/z$  988.0919 [ $^{79}\text{Br}$ ,  $\text{M}^+$ ], 990.0891 [ $^{81}\text{Br}$ ,  $\text{M}^+$ ].

### 3,6-Bis(5'-(trimethylsilyl)ethynyl)- [2,2'-biEDOT]- thiophene-2-yl)- 2,5-dinonyl-2,5-dihydropyrrolo[3,4-]pyrrole-1,4-dione (LC)



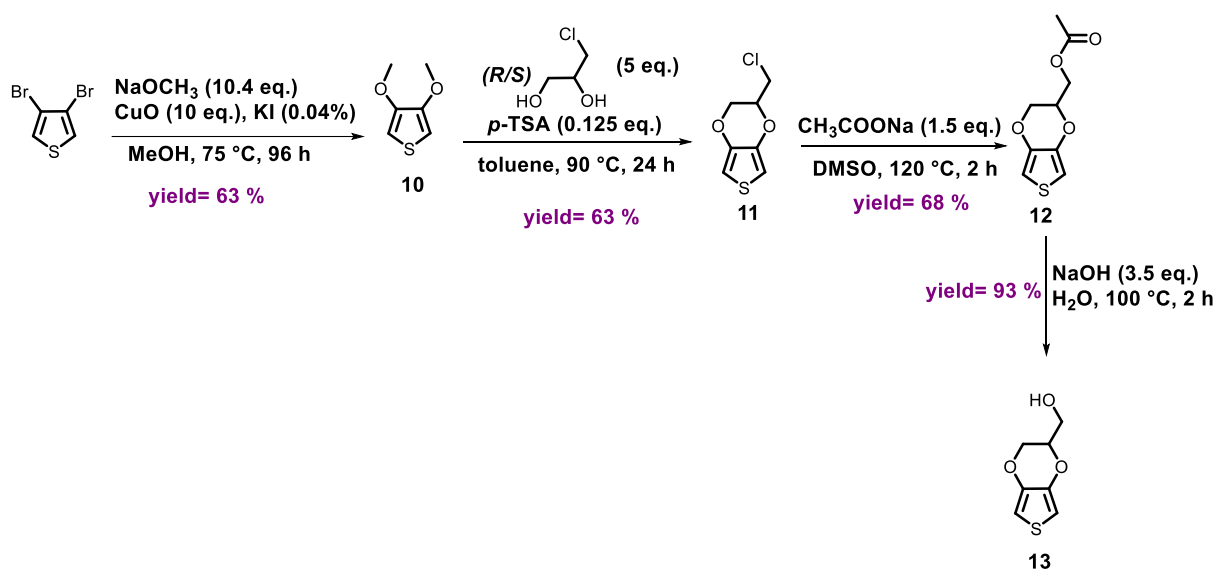
Product  $\mathbf{9}$  (150 mg) was dissolved in the mixture methylene tetrahydrofuran/  $i\text{Pr}_2\text{NH}$ : 30mL/ 30mL. The solution was degassed with argon stream passing in the solution warming at  $30^\circ\text{C}$ . Then,  $\text{CuI}$  (3 mg,  $15.7 \mu\text{mol}$ ) and  $\text{PdCl}_2(\text{PPh}_3)_2$  (30 mg,  $42.7 \mu\text{mol}$ ) were added under argon atmosphere. Then TMSA (0.3 mL, 207mg, 2.11 mmol) was added. The mixture was refluxed at  $70^\circ\text{C}$  overnight and monitored by TLC (eluent:  $\text{CH}_2\text{Cl}_2$ ,  $R_f(\text{LC}) = 0.9$ ). The reaction mixture was evaporated under reduced pressure and the crude product was purified by column chromatography on silica gel using pentane/ $\text{CH}_2\text{Cl}_2$  (60/40) as eluent to provide  $\text{LC}$  as a dark blue solid (45 mg,  $36.1 \mu\text{mol}$ , yield = 39 % from  $\mathbf{8}$ )

$^1\text{H}$  NMR (500 MHz,  $\text{CDCl}_3$ )  $\delta$  (ppm) 8.97 (d, 2H,  $J = 3.8$  Hz) 7.35 (d, 2H,  $J = 3.8$  Hz), 4.37(s, 8H), 4.08 (t, 4H), 1.27-1.20 (m, 28H), 0.86 (t, 6H), 0.26 (s, 18H)

$^{13}\text{C}$  NMR (500 MHz,  $\text{CDCl}_3$ )  $\delta$  (ppm): 161.32, 144.88, 139.65, 139.03, 138.11, 136.23, 128.31, 124.73, 112.80, 108.31, 104.95, 98.30, 94.38, 65.09, 65.05, 42.45, 32.00, 30.16, 29.72, 29.39, 29.36, 27.04, 22.81, 14.26, 0.06.

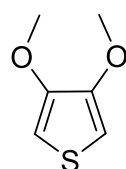
HRMS (ESI) Calculated for (LC)  $\text{C}_{54}\text{H}_{68}\text{N}_2\text{O}_6\text{S}_4\text{Si}_2$ :  $m/z$  1024.350. Found:  $m/z$  1025.364  $[\text{M}+\text{H}]^+$

### Synthesis of functionalized EDOT intermediate:



Scheme S4: The synthesis of the racemic mixture of EDOT-MeOH **13**

## 2- Chloromethyl-2,3-dihydroxythieno[3,4-b][1,4]dioxane (**10**)



The procedure was inspired from the literature,<sup>344</sup> but it was modified to increase the yield. To a three-necked flask equipped with an argon purge, 3,4-dibromothiophene (5.0 g, 20.8 mmol),  $\text{CH}_3\text{ONa}$  (21.8 g, 107.81 mmol),  $\text{CuO}$  (16.5 g, 207 mmol),  $\text{KI}$  (1.4 g, 8.43 mmol) and  $\text{CH}_3\text{OH}$  (20 mL) were added. The reaction mixture refluxed for three days. The reaction was regularly monitored by TLC. Adding 3.0 g of  $\text{CH}_3\text{ONa}$  each 3 hours was necessary in order to boost the reaction. After starting the reaction (21.8 g 107.81 mmol) additional grams of  $\text{CH}_3\text{ONa}$  and 11 mL of  $\text{CH}_3\text{OH}$  were added to the reaction mixture and the solution was refluxed for another one day. The reaction mixture was

cooled to room temperature and added in a few portions in Erlenmeyer flask in petroleum ether under stirring. Then, the product was filtered through celite. The resulting solution was then extracted with ether. The organic fractions were combined and dried over MgSO<sub>4</sub>. After removal of the solvent, the remaining crude product was isolated by flash chromatography (silica gel, petroleum ether) to give 3,4-dimethoxythiophene (2.45 g) as yellowish liquid in 63 % yield.

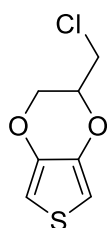
**<sup>1</sup>H NMR (500 MHz, CDCl<sub>3</sub>) δ (ppm):** 6.32 (s, 2H), 3.78 (s, 6H).

**<sup>13</sup>C NMR (500 MHz, CDCl<sub>3</sub>) δ (ppm):** 148.6, 117.9, 97.1, 57.6

**IR (neat, cm<sup>-1</sup>) λ** 3112 (C<sub>sp3</sub>-H), 3003-2822 (C<sub>sp3</sub>-H CH<sub>3</sub>, CH<sub>2</sub>), 1570 (aromatic C=C), 1502 (C-Oether), 900-700 (aromatic C-H).

**HR-MS (ESI+) m/z [M<sup>+</sup>]** calcd. for = C<sub>6</sub>H<sub>8</sub>O<sub>2</sub>S 144.0245, found = 144.0242.

### 2-(Chloromethyl)-2,3-dihydrothieno[3,4-b][1,4]dioxane (11)



To a three-necked flask equipped with an argon purge, product **10** 3,4-dimethoxythiophene (1.0 g, 7.0 mmol), racemic (R/S) 3-chloro-1,2-propanediol (3.87 g, 35 mmol), *p*-TSA (0.137 g, 0.875 mmol) and dry toluene (19 mL) were added. The reaction mixture was heated at 90 °C for 24 h. After 24 hours of reaction, the mixture was allowed to cool room temperature. The mixture was extracted with dichloromethane (2 x 15 mL). The organic fractions were combined, dried over MgSO<sub>4</sub> and concentrated under reduced pressure. The crude product was isolated by flash chromatography (silica gel, 100 % pentane to 8/2 pentane/ CH<sub>2</sub>Cl<sub>2</sub>) to afford the product **11** (842 mg) as a colorless oil in 63 % yield.

**<sup>1</sup>H NMR (500 MHz, CDCl<sub>3</sub>) δ (ppm):** 6.38 (1H, d, <sup>4</sup>J<sub>H-H</sub> = 3.8 Hz), 6.36 (d, 1H, <sup>4</sup>J<sub>H-H</sub> = 3.8 Hz) 4.38-4.34 (m, 1H), 4.27 (dd, 1H, <sup>2</sup>J<sub>H-H</sub> = 11.7 Hz, <sup>3</sup>J<sub>H-H</sub> = 2.2 Hz), 4.15 (dd, <sup>2</sup>J<sub>H-H</sub> = 11.7 Hz, <sup>3</sup>J<sub>H-H</sub> = 6.4 Hz), 3.72 (dd, 2H, <sup>2</sup>J<sub>H-H</sub> = 11.7 Hz, <sup>3</sup>J<sub>H-H</sub> = 5.1 Hz), 3.66 (dd, 2H, <sup>2</sup>J<sub>H-H</sub> = 11.7 Hz, <sup>3</sup>J<sub>H-H</sub> = 7.2 Hz)

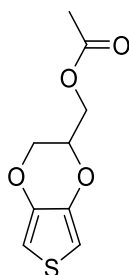
**<sup>13</sup>C NMR (500 MHz, CDCl<sub>3</sub>) δ (ppm):** 141.7, 140.7, 100.2, 72.9, 65.6, 41.4.

**IR (neat, cm<sup>-1</sup>) λ** 3113 (C<sub>sp3</sub>-H, CH<sub>3</sub>), 2919 (C<sub>sp3</sub>-H, CH<sub>2</sub>, CH), 1581 (aromatic C=C), 1184 (C-O), 900-700 (aromatic C-H).

**HR-MS (ESI+) m/z [M<sup>+</sup>]** calcd. for = C<sub>7</sub>H<sub>7</sub>O<sub>2</sub>S<sup>35</sup>Cl 189.9855, found= 189.9854, [<sup>35</sup>Cl]<sup>+</sup> = 190.9923, [<sup>37</sup>Cl]<sup>+</sup> = 192.9892.



### (2,3-Dihydrothieno[3,4-b][1,4]dioxin-2-yl)methyl Acetate (EDOT-MeOAc) (**12**)



To a 50 mL three-necked flask, 2-(Chloromethyl)-2,3-dihydrothieno[3,4-b][1,4]dioxane – (**11**) (0.83 g, 4.3 mmol), CH<sub>3</sub>COONa (0.549 g, 6.54 mmol), and DMSO (13 mL) were added. The solution was stirred for 2 h at 120 °C. The mixture was poured into distilled water (10 mL) and extracted with CH<sub>2</sub>Cl<sub>2</sub>. Then the solvent was removed under reduced pressure. The crude product was isolated by flash chromatography (aluminium oxide, neutral, 100 % pentane to 1/1 pentane/CH<sub>2</sub>Cl<sub>2</sub>) to afford the product **12** (0.629 g) as a yellow oil in 68 % yield.

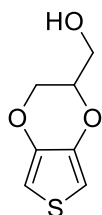
**<sup>1</sup>H NMR (500 MHz, CDCl<sub>3</sub>) δ (ppm):** 6.36 (d, 1H, <sup>4</sup>J<sub>H-H</sub> = 3.7 Hz), 6.34 (d, 1H, <sup>4</sup>J<sub>H-H</sub> = 3.7 Hz), 4.40-4.35 (m, 1H), 4.31-4.28 (m, 2H), 4.22 (dd, 3H, <sup>2</sup>J<sub>H-H</sub> = 11.7 Hz, <sup>3</sup>J<sub>H-H</sub> = 2.3 Hz), 4.04 (dd, 1H, <sup>2</sup>J<sub>H-H</sub> = 11.7 Hz, <sup>3</sup>J<sub>H-H</sub> = 7.3 Hz), 2.11 (s, 3H).

**<sup>13</sup>C NMR (500 MHz, CDCl<sub>3</sub>) δ (ppm):** 170.6, 141.2, 141.0, 71.5, 65.6, 62.4.

**IR (neat, cm<sup>-1</sup>)** λ 3113 (C<sub>sp3</sub>-H, CH<sub>3</sub>), 2921 (C<sub>sp3</sub>-H, CH<sub>2</sub>, CH), 1737 (C=O), 1582 (aromatic C=C), 1482 (C<sub>sp3</sub>-H), 1228-1184 (C-O<sub>ester</sub>, 2 bands), 900-700 (aromatic C-H).

**HR-MS (ESI+)** *m/z* [M + H]<sup>+</sup> calcd. for = C<sub>9</sub>H<sub>11</sub>O<sub>4</sub>S 215.0378, found = 215.0373.

### (2,3-Dihydrothieno[3,4-b][1,4]dioxin-2-yl)methanol (EDOT-MeOH) (**13**)



To a 50 mL three-necked flask, (2,3-Dihydrothieno[3,4-b][1,4]dioxin-2-yl)methyl Acetate – (**11**) (EDOT-MeOAc; 0.27 g, 1.26 mmol), was added to a solution of NaOH (0.17 g, 4.41 mmol) in distilled water (7.7 mL). The reaction mixture was refluxed for 2 h and then cooled to RT. The mixture was acidified with 8 mL 1M HCl and then extracted with CH<sub>2</sub>Cl<sub>2</sub>. The solvent was removed under reduced pressure and column chromatography (aluminum oxide, neutral, 100 % pentane to 1/1 pentane/CH<sub>2</sub>Cl<sub>2</sub>) was performed to give the product **13** (0.2 g) as a light brown oil in 93 % yield. Exact mass *m/z* 172.1980.

**<sup>1</sup>H NMR (500 MHz, CDCl<sub>3</sub>) δ (ppm):** 6.35 (d, 1H, <sup>4</sup>J<sub>H-H</sub> = 3.8 Hz), 6.34 (d, 1H, <sup>4</sup>J<sub>H-H</sub> = 3.8 Hz), 4.27-4.23 (m, 1H), 4.22 (dd, 1H, <sup>2</sup>J<sub>H-H</sub> = 6.2 Hz, <sup>3</sup>J<sub>H-H</sub> = 2.4 Hz), 4.09 (dd, 1H, <sup>2</sup>J<sub>H-H</sub> = 12.3 Hz, <sup>3</sup>J<sub>H-H</sub> = 8.4 Hz), 3.88 (dd, 1H, <sup>2</sup>J<sub>H-H</sub> = 12.3 Hz, <sup>3</sup>J<sub>H-H</sub> = 4.3 Hz), 3.82 (dd, 1H, <sup>2</sup>J<sub>H-H</sub> = 12.3 Hz, <sup>3</sup>J<sub>H-H</sub> = 5.1 Hz).

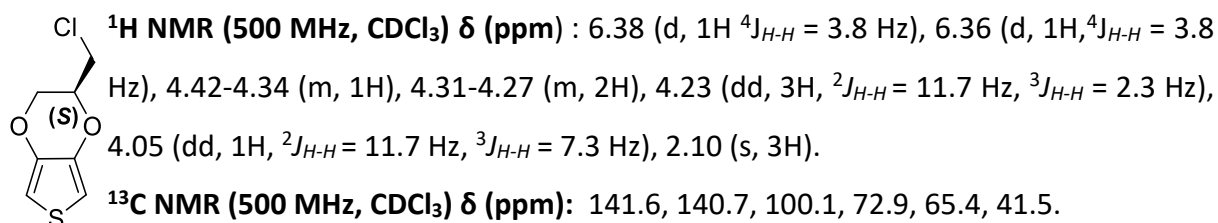
**<sup>13</sup>C NMR (500 MHz, CDCl<sub>3</sub>) δ (ppm):** 141.4, 99.8, 74.1, 65.7, 61.6.

**IR (neat, cm<sup>-1</sup>)** λ 3375 (OH), 3110 (C<sub>sp3</sub>-H, CH<sub>3</sub>), 2925 (C<sub>sp3</sub>-H CH<sub>2</sub>, CH), 1737 (C=O), 1580 (aromatic C=C), 1482 (C<sub>sp3</sub>-H), 1183 (C-O), 900-700 (aromatic C-H).

**HR-MS (ESI+)** *m/z* [M + H]<sup>+</sup> calcd. for = C<sub>9</sub>H<sub>9</sub>O<sub>3</sub>S 173.0273, found = 173.0267.

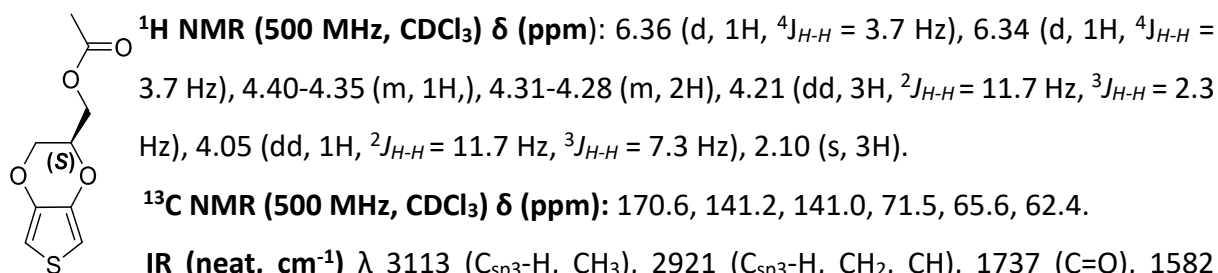
All the experimental procedures for the synthesis of the products **14**, **15** and **16** are the same as for the synthesis of the same products in racemic version.

**(S)-2-(chloromethyl)-2,3-dihydrothieno[3,4-b][1,4]dioxine (14)**

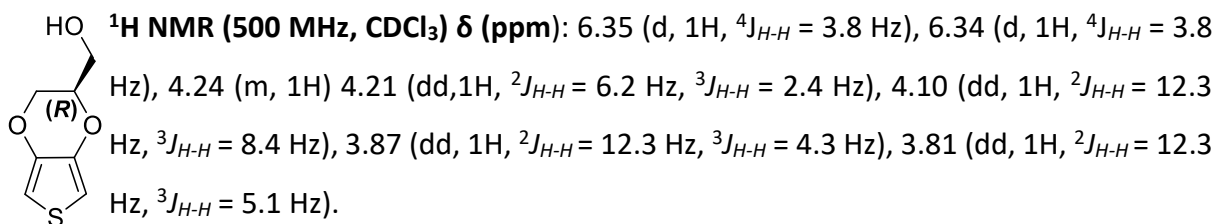


**IR (neat, cm<sup>-1</sup>)** λ 3113 (C<sub>sp3</sub>-H, CH<sub>3</sub>), 2919 (C<sub>sp3</sub>-H, CH<sub>2</sub>, CH), 1581 (aromatic C=C), 1184 (C-O), 900-700 (aromatic C-H).

**(S)-(2,3-dihydrothieno[3,4-b][1,4]dioxin-2-yl)methyl acetate (15)**



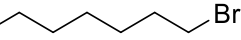
**(R)-(2,3-dihydrothieno[3,4-b][1,4]dioxin-2-yl)methanol (16)**



<sup>13</sup>C NMR (500 MHz, CDCl<sub>3</sub>) δ (ppm): 141.4, 99.8, 74.1, 65.7, 61.6.

IR (neat, cm<sup>-1</sup>) λ 3375 (OH), 3110 (C<sub>sp3</sub>-H, CH<sub>3</sub>), 2925 (C<sub>sp3</sub>-H CH<sub>2</sub>, CH), 1737 (C=O), 1580 (aromatic C=C), 1482 (C<sub>sp3</sub>-H), 1183 (C-O), 900-700 (aromatic C-H).

**(5-bromopentyl)oxy)(tert-butyl)dimethylsilane (17)**

TBDMSO  Br To a 100 mL two-necked flask equipped with Argon purge, 6-bromo-1-hexanol (1.0 g, 5.81 mmol) and imidazole (0.551 g, 8.1 mmol) in dry DCM (30 mL) were added. Then, *tert*-Butyldimethylsilyl solution in 50 % toluene (2.46 g, 8.15 mmol) was added to the solution. The reaction mixture was stirred at RT during 20 h. The mixture was poured into distilled water (25 mL) and extracted with CH<sub>2</sub>Cl<sub>2</sub> (2 x 20 mL). The organic phase was washed with brine, dried over MgSO<sub>4</sub> and concentrated under vacuum. The crude product was isolated by flash chromatography (silica gel, 100 % pentane to 8/2 pentane/ CH<sub>2</sub>Cl<sub>2</sub>), to afford the product **17** (1.7 g) as a colorless oil in 98 % yield.

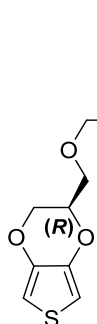
<sup>1</sup>H NMR (500 MHz, CDCl<sub>3</sub>) δ (ppm): 3.59 (t, <sup>3</sup>J = 6.45 Hz, 2H), 3.40 (t, <sup>3</sup>J = 6.9 Hz, 2H), 1.86 (quintet, <sup>3</sup>J = 6.9 Hz, 2H), 1.53 (quintet, <sup>3</sup>J = 6.8 Hz, 2H), 1.44 (quintet, <sup>3</sup>J = 7.1 Hz, 2H), 1.35 (quintet, <sup>3</sup>J = 7.15 Hz, 2H), 0.88 (s, 9H), 0.04 (s, 6H)

<sup>13</sup>C NMR (500 MHz, CDCl<sub>3</sub>) δ (ppm): 60.0, 33.9, 32.8, 32.6, 28.0, 25.9, 25.1, 18.4, -5.2.

IR (neat, cm<sup>-1</sup>) λ 2929 (C<sub>sp3</sub>-H, CH<sub>3</sub>, CH<sub>2</sub>), 2856 (C<sub>sp3</sub>-H, CH), 1500-800 (C-C), 1100 (C-O), 600-500 (C-Br).

HR-MS (ESI+) *m/z* [M+H]<sup>+</sup> calcd. for C<sub>12</sub>H<sub>28</sub>O<sub>2</sub>Si<sup>79</sup>Br = 296.1093, found = 296.1087, [<sup>79</sup>Br]<sup>+</sup> = 294.1087, [<sup>81</sup>Br]<sup>+</sup> = 298.1094.

**t-butyl((6-((2,3-dihydrothieno[3,4-b][1,4]dioxin-2-yl) methoxy) hexyl)oxy)dimethylsilane  
(18)<sup>247</sup>**



To a 50 mL three-necked flask equipped with Ar purge, EDOT-MeOH **13** (0.2 g, 1.16 mmol), NaH (60 %) (0.46 g, 11.6 mmol), 18-crown-6 (0.03 g, 0.16 mmol) and dry DMF (6 mL) were added. The mixture was stirred at RT for 1 h. Then, the product **17** (0.41 g, 1.4 mmol) was added dropwise in the mixture. After 20 h of reaction, the mixture was poured into a saturated solution of NH<sub>4</sub>Cl (15 mL) and extracted with CH<sub>2</sub>Cl<sub>2</sub> (2 x 15 mL). The organic phase was afterwards washed with distilled water (10 mL) and the solvent was removed under reduced pressure. The crude product was isolated by flash chromatography (puriFlash XS 520 Plus, 100 % pentane to 9/1 pentane/EtOAc), to afford the product **18** (0.32 g) as a colorless oil in 71 % yield.

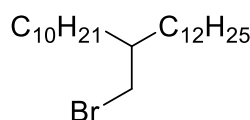
**<sup>1</sup>H NMR (500 MHz, CDCl<sub>3</sub>) δ (ppm):** 6.32 (m, 2H), 4.29 (m, 1H), 4.24 (dd, <sup>2</sup>J<sub>H-H</sub> = 11.6 Hz, <sup>3</sup>J<sub>H-H</sub> = 2.3 Hz, 1H), 4.0 (dd, <sup>2</sup>J<sub>H-H</sub> = 11.6 Hz, <sup>3</sup>J<sub>H-H</sub> = 7.6 Hz, 1H), 3.7 (dd, <sup>2</sup>J<sub>H-H</sub> = 10.4 Hz, <sup>3</sup>J<sub>H-H</sub> = 5.0 Hz, 1H), 3.59 (t, <sup>3</sup>J<sub>H-H</sub> = 6.6 Hz, 2H), 3.58 (dd, <sup>2</sup>J = 10.4 Hz, <sup>3</sup>J<sub>H-H</sub> = 5.9 Hz, 1H), 3.48 (t, <sup>3</sup>J<sub>H-H</sub> = 6.6 Hz, 2H), 1.58 (quint, <sup>3</sup>J<sub>H-H</sub> = 6.8 Hz, 2H) 1.51 (quint, <sup>3</sup>J<sub>H-H</sub> = 6.8 Hz, 2H), 1.34 (m, 4H), 0.89 (s, 9H), 0.04 (s, 6H).

**<sup>13</sup>C NMR (500 MHz, CDCl<sub>3</sub>) δ (ppm):** δ 141.6, 99.6, 72.6, 72.0, 69.1, 66.2, 63.2, 32.8, 29.6, 26.0, 25.9, 25.7, 18.4, -5.2.

**IR (neat, cm<sup>-1</sup>)** λ 2929 (C<sub>sp3</sub>-H, CH<sub>3</sub>, CH<sub>2</sub>), 2856 (C<sub>sp3</sub>-H, CH), 2922 (C<sub>sp3</sub>-H, CH<sub>3</sub>), 2855 (C<sub>sp3</sub>-H, CH<sub>2</sub>, CH). 1094 (C-O), 900-700 (C-H<sub>aromatic</sub>).

**HR-MS (ESI+)** *m/z* [M + H]<sup>+</sup> calcd. for C<sub>19</sub>H<sub>35</sub>O<sub>4</sub>SiS = 387.2025, found = 387.2033.

**11-(bromomethyl)tricosane (19)**



To a solution of triphenylphosphine (5.72 g, 20 mmol) in dichloromethane (15 mL) was added 2-decyl-1-tetradecanol **SM** (5.0 g, 14.1 mmol). Then, *N*-Bromosuccinimide (3.76 g, 20 mmol) was added to the mixture at 0 °C Cover 20 minutes. After the reaction mixture was stirred at room temperature for 20 h. The reaction mixture was quenched with distilled water (20 mL) and extracted with CH<sub>2</sub>Cl<sub>2</sub> (3 x 20 mL). The organic phase was dried over MgSO<sub>4</sub> and the solvent was removed by evaporation to

furnish the crude product. Purification by column chromatography (silica gel, 100 % pentane to 8/2 pentane/ CH<sub>2</sub>Cl<sub>2</sub>) gave pure brominated product as a colorless oil (5.288 g) in 90 % yield.

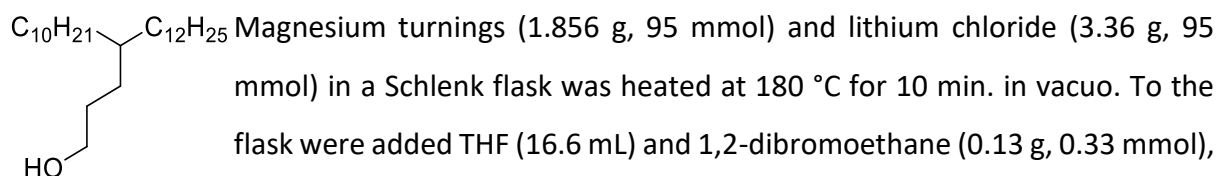
**<sup>1</sup>H NMR (500 MHz, CDCl<sub>3</sub>) δ (ppm):** 3.45 (d, <sup>3</sup>J<sub>H-H</sub> = 5Hz, 2H), 1.58 (m, 1H), 1.26 (s, 40H), 0.88 (t, <sup>3</sup>J<sub>H-H</sub> = 7Hz, 6H).

**<sup>13</sup>C NMR (500 MHz, CDCl<sub>3</sub>) δ (ppm):** 39.7, 39.5, 33.5, 32.1, 29.9, 29.5, 29.4, 29.3, 26.6, 22.5, 13.9– confirmation by DEPT135 et HSQC.

**IR (neat, cm<sup>-1</sup>)** λ 2921 (C<sub>sp3</sub>-H, CH<sub>3</sub>), 2852 (C<sub>sp3</sub>-H, CH<sub>2</sub>, CH).

**HR-MS (ESI+) m/z [M - H]<sup>+</sup> calcd. for C<sub>24</sub>H<sub>48</sub><sup>79</sup>Br = 415.2939, found = 415.2930, [<sup>79</sup>Br]<sup>+</sup> = 413.2930, [<sup>81</sup>Br]<sup>+</sup> = 417.2917.**

#### 4-decylhexadecan-1-ol (**21**)<sup>59</sup>



Magnesium turnings (1.856 g, 95 mmol) and lithium chloride (3.36 g, 95 mmol) in a Schlenk flask was heated at 180 °C for 10 min. in vacuo. To the flask were added THF (16.6 mL) and 1,2-dibromoethane (0.13 g, 0.33 mmol), and then the mixture was refluxed for 15 sec. by using a heat gun. After cooling to 15 °C, 11-(bromomethyl)tricosane **19** (4.8 g, 11.5 mmol) was added to the mixture. The mixture was then warmed to room temperature and stirred for 2 h. The Grignard reagent was then transferred to a three necked flask and diluted with THF (7.76 mL). To the solution was added dropwise a solution of ethylene oxide (1.2 M in THF) (0.4 g, 9.0 mmol) at 0 °C over 5 min. After the reaction mixture was stirred at 50 °C for 6 hours. The reaction was quenched with 1 M hydrochloric acid. The reaction mixture was extracted with pentane, and the organic layer was washed with water and dried over MgSO<sub>4</sub>. After removing the solvent by evaporation, the crude product was purified by column chromatography (silica gel, 100 % pentane to 75/35 pentane/EtOAc) to give the product **21** (0.5 g) in 30 % yield.

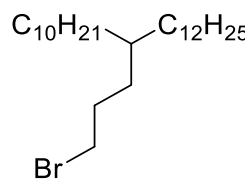
**<sup>1</sup>H NMR (500 MHz, CDCl<sub>3</sub>) δ (ppm):** 3.61 (t, <sup>3</sup>J<sub>H-H</sub> = 6.7 Hz, 2H), 1.53 (quintet, <sup>3</sup>J<sub>H-H</sub> = 7.1 Hz, 2H), 1.35 – 1.14 (m, 43H), 0.87 (t, <sup>3</sup>J<sub>H-H</sub> = 6.7 Hz, 6H).

**<sup>13</sup>C NMR (500 MHz, CDCl<sub>3</sub>) δ (ppm):** 63.6, 37.2, 33.6, 31.9, 30.1, 29.9, 29.7, 29.6, 29.5, 29.4, 26.6, 22.7, 14.1.

**IR (neat, cm<sup>-1</sup>)** λ 3316 (OH), 2920 (C<sub>sp3</sub>-H, CH<sub>3</sub>), 2852 (C<sub>sp3</sub>-H, CH<sub>2</sub>, CH).

**HR-MS (ESI+)**  $m/z$   $[M - H]^+$  calcd. for  $C_{28}H_{53}O = 381.4096$ , found = 381.4095. Exact mass measured on the ion  $m/z$  381 compatible with the ion  $[M - H]^+$  of the compound **21**.

### 11-(3-bromopropyl)tricosane (**22**)<sup>59</sup>

 To a solution of triphenylphosphine (0.21 g, 0.78 mmol) in dichloromethane (1.4 mL) was added bromine (0.13 g, 0.78 mmol) at 0 °C over 10 min. After the reaction mixture was stirred at 0 °C for 20 min, **21** (0.25 g, 0.65 mmol) was added dropwise over 5 min at 0 °C. After the reaction mixture was stirred at room temperature for 20 h. The reaction was quenched with distilled water (5 mL) and extracted with DCM (2 x 10 mL). The organic phase was dried over  $MgSO_4$ , filtered and the solvent was evaporated under reduced pressure. The crude product was purified by silica gel column chromatography (eluent: 100 % pentane) to give **22** (0.18 g) as colorless liquid in 62 % yield.

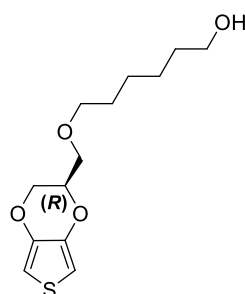
**$^1H$  NMR (500 MHz,  $CDCl_3$ )  $\delta$  (ppm):** 3.42 (t,  $^3J_{H-H} = 7.2$  Hz, 2H), 1.81 (quintet,  $^3J_{H-H} = 7.4$  Hz, 2H), 1.37 – 1.24 (m, 43H), 0.89 (t,  $^3J_{H-H} = 6.8$  Hz, 6H).

**$^{13}C$  NMR (500 MHz,  $CDCl_3$ )  $\delta$  (ppm):** 36.8, 34.5, 33.5, 32.2, 31.9, 30.2, 30.1, 29.7, 29.4, 26.6, 14.1.

**IR (neat,  $cm^{-1}$ )**  $\lambda$  2922 ( $C_{sp^3-H}$ ,  $CH_3$ ), 2855 ( $C_{sp^3-H}$ ,  $CH_2$ ,  $CH$ ).

**HR-MS (ESI+)**  $m/z$   $[M^{++}]$  calcd. for  $C_{26}H_{53}^{79}Br = 444.3331$ . found = 444.3319.  $[^{79}Br]^+ = 442.3329$ ,  $[^{81}Br]^+ = 446.3335$ .

### 6-((5-(tributylstannyl)-2,3-dihydrothieno[3,4-b][1,4]dioxin-2-yl)methoxy)hexan-1-ol (**23**)

 To a 25 mL two-necked flask equipped with Ar purge, the product **6** (0.12 g, 0.31 mmol) and dry THF (1.3 mL) were added. Then, 0.5 mL of TBAF (1M) were added to the mixture. The reaction took place at RT for 16 h. The reaction mixture was poured into water (10 mL) and extracted with ethyl acetate (2 x 15 mL). The combined organic extracts were washed with a saturated aqueous chloride solution (2 x 15 mL), brine (2 x 15 mL), dried over anhydrous magnesium sulfate, filtered and concentrated under reduced pressure to

furnish the crude product as a yellowish oil. Purification by flash column chromatography (silica gel, 100 % pentane to 1/1 pentane/EtOAc) furnished pure alcohol as a yellowish oil (0.065 g) in 81 % yield.

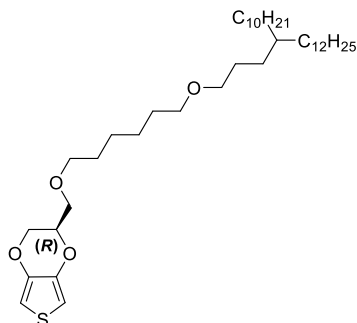
**<sup>1</sup>H NMR (500 MHz, CDCl<sub>3</sub>) δ (ppm):** 6.32 (m, 2H), 4.29 (m, 1H), 4.23 (dd, <sup>2</sup>J<sub>H-H</sub> = 11.7 Hz, <sup>3</sup>J<sub>H-H</sub> = 2.2 Hz, 1H), 4.0 (dd, <sup>2</sup>J<sub>H-H</sub> = 11.7 Hz, <sup>3</sup>J<sub>H-H</sub> = 7.7 Hz, 1H), 3.7 (dd, <sup>2</sup>J<sub>H-H</sub> = 10.4 Hz, <sup>3</sup>J<sub>H-H</sub> = 5.0 Hz, 1H), 3.63 (t, <sup>3</sup>J<sub>H-H</sub> = 6.6 Hz, 2H), 3.58 (dd, <sup>2</sup>J = 10.4 Hz, <sup>3</sup>J<sub>H-H</sub> = 6.0 Hz, 1H), 3.49 (t, <sup>3</sup>J<sub>H-H</sub> = 6.6 Hz, 2H), 1.58 (m, 4H), 1.37 (m, 4H).

**<sup>13</sup>C NMR (500 MHz, CDCl<sub>3</sub>) δ (ppm):** 141.6, 99.7, 72.7, 71.9, 69.1, 62.2, 62.9, 32.7, 29.5, 25.8, 25.6.

**IR (neat, cm<sup>-1</sup>)** λ 3361 (OH), 3111 (C<sub>sp3</sub>-H, CH<sub>3</sub>), 2930-2859 (C<sub>sp3</sub>-H, CH<sub>2</sub>, CH), 1484 (C-O<sub>ether</sub> aliphatic), 1089 (C-O), 900-700 (C-H<sub>aromatic</sub>).

**HR-MS (ESI+)** *m/z* [M+H]<sup>+</sup> calcd. for C<sub>13</sub>H<sub>21</sub>O<sub>4</sub>S = 273.1161, found = 273.1162.

**(R)-2-(((6-((4-decylhexadecyl)oxy)hexyl)oxy)methyl)-2,3-dihydrothieno[3,4-b][1,4]dioxine (24)**



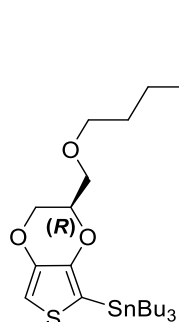
To a 10 mL two-necked flask equipped with Argon purge, the product **23** (0.065 g, 0.24 mmol), NaH (60 %) (0.1 g, 2.4 mmol), 18-crown-6 (0.03 g, 0.16 mmol) and dry DMF (2 mL) were added. The mixture was stirred at RT for 1 h. Then, **22** (0.11 g, 0.29 mmol) was added dropwise into the mixture. After 18 h of reaction, the mixture was poured into a saturated solution of NH<sub>4</sub>Cl (10 mL) and extracted with CH<sub>2</sub>Cl<sub>2</sub> (2 x 10 mL). The organic phase was afterwards washed with distilled water (8 mL) and the solvent was removed under reduced pressure. The crude product was isolated by flash chromatography (puriFlash XS 520 Plus, 100 % pentane to 9/1 pentane/DCM), to afford the product **24** (0.095 g) as a colorless oil in 63 % yield.

**<sup>1</sup>H NMR (500 MHz, CDCl<sub>3</sub>) δ (ppm):** 6.36 (d, <sup>4</sup>J<sub>H-H</sub> = 3.7 Hz, 1H), 6.34 (d, <sup>4</sup>J<sub>H-H</sub> = 3.7 Hz, 1H), 4.28 (m, 1H), 4.27 (dd, <sup>2</sup>J<sub>H-H</sub> = 11.6 Hz, <sup>3</sup>J<sub>H-H</sub> = 7.6 Hz, 1H), 4.04 (dd, <sup>2</sup>J<sub>H-H</sub> = 10.4 Hz, <sup>3</sup>J<sub>H-H</sub> = 6.2 Hz, 1H), 4.27 (dd, <sup>2</sup>J<sub>H-H</sub> = 11.7 Hz, <sup>3</sup>J<sub>H-H</sub> = 7.6 Hz, 1H), 3.64 (t, <sup>3</sup>J<sub>H-H</sub> = 7.4 Hz, 2H), 3.58 (dd, <sup>2</sup>J<sub>H-H</sub> = 10.4 Hz, <sup>3</sup>J<sub>H-H</sub> = 6.3 Hz, 1H), 3.39 (t, <sup>3</sup>J<sub>H-H</sub> = 6.8 Hz, 4H), 1.62-1.49 (m, 10H), 1.37-1.13 (m, 43H), 0.86 (t, <sup>3</sup>J<sub>H-H</sub> = 6.7 Hz, 6H).

$^{13}\text{C}$  NMR (500 MHz,  $\text{CDCl}_3$ )  $\delta$  (ppm): 146.3, 96.2, 76.4, 72.2, 70.9, 70.1, 39.3, 38.2, 32.1, 31.7, 30.9, 29.9, 29.6, 29.3, 29.0, 27.8, 24.8, 22.3, 14.4.

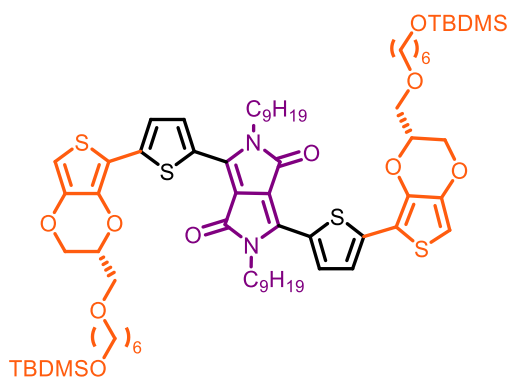
IR (neat,  $\text{cm}^{-1}$ )  $\lambda$  2922 ( $\text{C}_{\text{sp}^3}\text{-H}$ ,  $\text{CH}_3$ ), 2855 ( $\text{C}_{\text{sp}^3}\text{-H}$ ,  $\text{CH}_2$ ,  $\text{CH}$ ), 1484 ( $\text{C-O}_{\text{ether aliphatic}}$ ).

**(*R*)-tert-butyl dimethyl((6-((7-(tributylstannyl)-2,3-dihydrothieno[3,4-b][1,4]dioxin-2-yl)methoxy)hexyl)oxy)silane (25)**



To a small tube purged with argon, the compound **6** (0.2 g, 0.52 mmol) and dry THF (0.06 mL) were added. The mixture was cooled down to  $-75\text{ }^\circ\text{C}$  and *n*-BuLi [2.5] (0.04 mL, 0.46 mmol) was slowly added dropwise to the mixture. After one hour of deprotonation, the  $\text{Cl-Bu}_3\text{Sn}$  (0.13 mL, 0.46 mmol) was added dropwise at  $-75\text{ }^\circ\text{C}$ . The reaction mixture was then let cool down to rt and stirred for 18 h. The reaction mixture was quenched with distilled water and extracted with  $\text{CH}_2\text{Cl}_2$  (3 x 15 mL). The organic fraction was dried and filtered and the solvent was removed to give the pale brown colored product. This compound was used without further purification.

**3,6-bis(5-((*R*)-3-(((6-((tert-butyl dimethylsilyloxy)hexyl)oxy)methyl)-2,3-dihydrothieno[3,4-b][1,4]dioxin-5-yl)thiophen-2-yl)-2,5-dinonyl-2,5-dihydropyrrolo[3,4-c]pyrrole-1,4-dione (26)**



To a 10 mL tube, purged with Ar, the compound **25** (0.145 g, 0.066 mmol) and dry toluene (5 mL) were added. Then, the acceptor DPP (0.014 g, 0.02 mmol) was added to the solution. After bubbling the solvent under Ar, 10 mol% of the  $\text{PdCl}_2(\text{PPh}_3)_2$  and 20 mol% of the  $\text{PPh}_3$  were added to the reaction mixture. The reaction was stirred over night for about 18 h. The mixture was quenched with distilled water and extracted with DCM (3 x 10 mL). The organic phase was dried over  $\text{MgSO}_4$ , filtered and the solvent was evaporated under reduced pressure to furnish the crude product. Purification by Biobead<sup>®</sup> X1 by Size Exclusion Chromatography by 100%  $\text{CH}_2\text{Cl}_2$ . Then, a purification by column chromatography (silica gel, DCM/Toluene 9/1) was done. Alternatively,

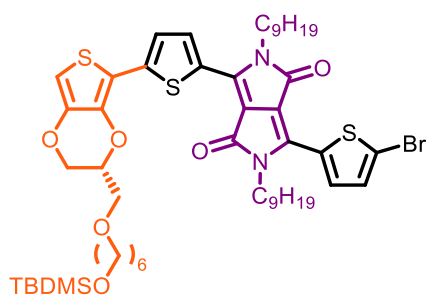


a precipitation was done in 7/3 DCM/MeOH, which after filtration gave the products **26** et **26'** with 75 % and 25 % conversion respectively.

**<sup>1</sup>H NMR (500 MHz, CDCl<sub>3</sub>) δ (ppm):** 8.99 (d, <sup>2</sup>J<sub>H-H</sub> = 4.5 Hz, 2H), 7.35 (d, <sup>2</sup>J<sub>H-H</sub> = 4.5 Hz, 2H), 6.35 (s, 2H), 4.46 (m, 2H), 4.39-4.12 (m, 4H), 4.10 (t, <sup>3</sup>J<sub>H-H</sub> = 7.4 Hz, 4H), 3.83-3.62 (m, 4H), 3.59 (q, <sup>3</sup>J<sub>H-H</sub> = 6.6 Hz, 4H), 3.52 (q, <sup>3</sup>J<sub>H-H</sub> = 7.1 Hz, 4H), 1.77 (m, 4H), 1.48-1.21 (m, 44H), 0.88 (s, 18H), 0.86 (t, <sup>3</sup>J<sub>H-H</sub> = 7.2 Hz, 6H) 0.06 (m, 12H).

**HR-MS (ESI+)** *m/z* [M - H]<sup>+</sup> calcd. for C<sub>70</sub>H<sub>108</sub>N<sub>2</sub>O<sub>10</sub>S<sub>4</sub>SI = 1320.6425, found = 1320.5425.

**(R)-3-(5-bromothiophen-2-yl)-6-(5-(3-(((6-((tert-butyl)dimethylsilyl)oxy)hexyl)oxy)methyl)-2,3-dihydrothieno[3,4-b][1,4]dioxin-5-yl)thiophen-2-yl)-2,5-dinonyl-2,5-dihydropyrrolo[3,4-c]pyrrole-1,4-dione (**26'**)**

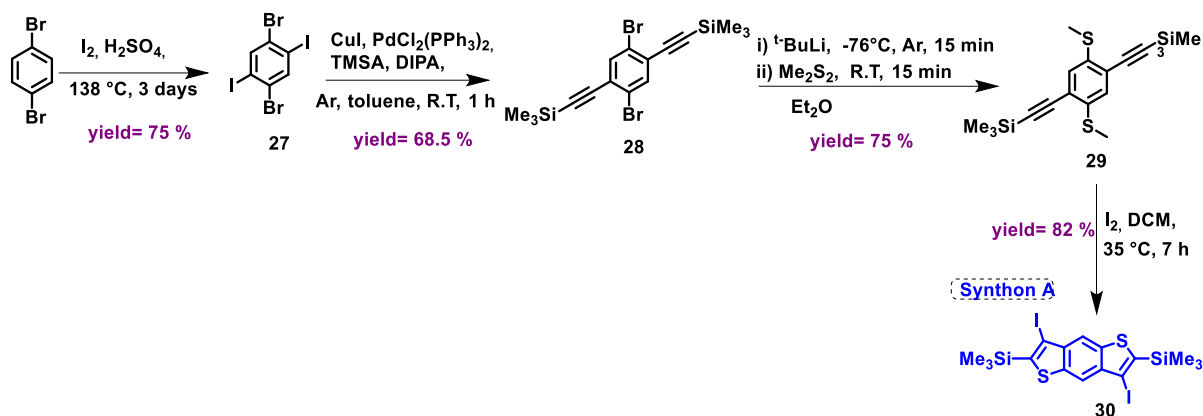


The product **26'** is issued from the same synthesis as the product **26**.

**<sup>1</sup>H NMR (500 MHz, CDCl<sub>3</sub>) δ (ppm):** 9.06 (d, <sup>2</sup>J<sub>H-H</sub> = 4.21 Hz, 1H), 8.62 (d, <sup>2</sup>J<sub>H-H</sub> = 4.21 Hz, 1H), 7.35 (d, <sup>2</sup>J<sub>H-H</sub> = 4.2 Hz, 1H), 7.22 (d, <sup>2</sup>J<sub>H-H</sub> = 4.2 Hz, 1H), 6.37 (s, 1H), 4.49-4.44 (m, 1H), 4.39-4.32 (m, 1H), 4.22 (dd, <sup>2</sup>J<sub>H-H</sub> = 11.5 Hz, <sup>3</sup>J<sub>H-H</sub> = 8.1 Hz, 1H), 4.08 (t, <sup>3</sup>J<sub>H-H</sub> = 4.1 Hz, 2H), 3.99 (t, <sup>3</sup>J<sub>H-H</sub> = 4.1 Hz, 2H), 3.83-3.62 (m, 2H), 3.59 (q, <sup>3</sup>J<sub>H-H</sub> = 6.3 Hz, 2H), 3.51 (q, <sup>3</sup>J<sub>H-H</sub> = 6.3 Hz, 2H), 1.18-1.66 (m, 4H), 1.48-1.2 (m, 28H), 0.88 (s, 18H), 0.86 (t, <sup>3</sup>J<sub>H-H</sub> = 7.6 Hz, 6H) 0.06 (m, 12H).

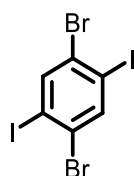
**HR-MS (ESI+)** *m/z* [M + H]<sup>+</sup> calcd. for C<sub>51</sub>H<sub>76</sub>N<sub>2</sub>O<sub>6</sub>S<sub>3</sub><sup>79</sup>Br = 1015.3818, found = 1015.3793

## Experimental part of chapter 3



Scheme S5: The general synthetic scheme of intermediate **30**

### 1,4-dibromo-2,5-diiodobenzene (**27**)



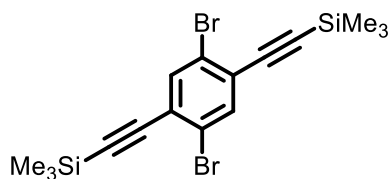
The procedure was inspired from the literature, Selma Duhović, Mircea Dincă Chem. Mater. 2015, 27, 16, 5487–5490. In 250ml flask, 1,4-dibromobenzene (10 g, 42.4 mmol, 1 eq.) and iodine (48g, 169.6mmol, 4eq.) were added to 100ml concentrated sulfuric acid and stirred at 125-135°C for 3 days. The obtained mixture was poured to ice (125g). A precipitate appeared in the solution. It was isolated after filtration, scratch and washed with pentane. The liquid part was extracted using  $\text{CH}_2\text{Cl}_2$ ,  $\text{Na}_2\text{S}_2\text{O}_3$ ,  $\text{NaHCO}_3$  and brine and dried by  $\text{MgSO}_4$ . The solvent was then evaporated under pressure; the obtained solid was washed with pentane and filtrated. Then all the powder was stirred in pentane overnight, this additional step is required to eliminate the maximum of iodine traces to prevent difficulties for the next step. 15.5g of compound **27** was isolated with 75% yield).

$^1\text{H NMR}$  (500 MHz,  $\text{CDCl}_3$ )  $\delta$  (ppm): 8.053 (s, 2H)

$^{13}\text{C NMR}$  (500 MHz,  $\text{CDCl}_3$ )  $\delta$  (ppm): 142.34, 129.23, 101.34

**MS (ESI)**: Calcd for  $\text{C}_{16}\text{H}_{20}\text{Br}_2\text{I}_2$  485.6615. Found: 485.6613  $[\text{M}]^+$

### 1,4-dibromo-2,5-bis(trimethylsilylacetylene)benzene (28)



The procedure was inspired from the literature, Selma Duhović, Mircea Dincă *Chem. Mater.* 2015, 27, 16, 5487–5490. In 100 ml Schlenk and under Ar, CuI (45.7mg, 0.24 mmol, 0.06eq.), PdCl<sub>2</sub>(PPh<sub>3</sub>)<sub>2</sub> (84.2mg, 0.12mol, 0.03eq.) and 1,4-

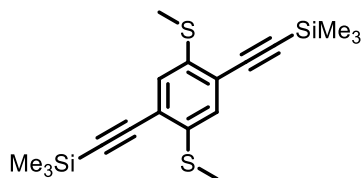
dibromo-2,6-diiodobenzene (2g, 4.1 mol, 1eq.) were added to the mixture of diisopropylamine (18 mL), trimethylsilylacetylene (1.1 mL, 7.94 mmol, 1.9 eq.) and toluene (30mL) were added. The reaction mixture was stirred at R.T for 1 hour. Then the reaction was quenched with water and the organic layer was washed with NH<sub>4</sub>Cl aqueous solution and brine and dried using MgSO<sub>4</sub>, then it was evaporated under reduced pressure. The obtained dark solid was purified by chromatography on silica gel with 100 % Pentane) to get a yellow product. Then, it was washed with ethanol until we get a white powder (1.2 g with 68.5 % yield).

<sup>1</sup>H NMR (500 MHz, CDCl<sub>3</sub>) δ (ppm): 7.678(H<sub>a</sub>, s, 2H), 0.278(H<sub>b</sub>, s, 18H)

<sup>13</sup>C NMR (500 MHz, CDCl<sub>3</sub>) δ (ppm): 136.73, 126.75, 124.02, 103.38, 101.67, 18.77

MS (ESI): Calcd for C<sub>16</sub>H<sub>20</sub>Si<sub>2</sub>Br<sub>2</sub> 425.9470. Found: 425.9474 [M]<sup>+</sup>

### 1,2-dimethylsulfide-2,5-bis(trimethylsillacetylene)benzene (29)



The procedure was inspired from the literature, Hideaki Ebata, Eigo Miyazaki, Tatsuya Yamamoto, and Kazuo Takimiya, *Org. Lett.* 2007, 9, 22, 4499–4502. In 50mL Schlenk and under argon, **28** (1.5g, 3.5mmol, 1eq.) were added in diethylether (15 mL).

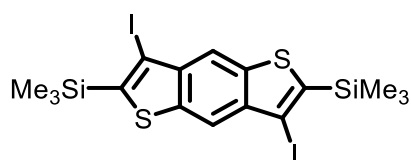
Then tert-Butyllithium 1.9 M in pentane (7.4 mL, 14.1 mmol, 4 eq.) were added at -78°C and stirred for 15 min at -78°C. Then the temperature was allowed to warm up to R.T gradually and dimethyldisulfide (0.62 mL, 7.0 mmol, 2 eq.) was added and the reaction medium was stirred for 15 min. The reaction was quenched with water and stirred for 1 hr. The mixture was extracted with chloroform. The organic layer was washed with NH<sub>4</sub>Cl aqueous solution and brine, then it was dried with MgSO<sub>4</sub>, filtered and evaporated evaporating under reduced pressure. The product was purified after its precipitaton in pentane/ethanol: 10 mL/ 10 mL and it was isolated as a green solid (1.07g, 84 %).

$^1\text{H NMR}$  (500 MHz,  $\text{CDCl}_3$ )  $\delta$  (ppm): 7.346 (s, 2H), 2.555 (s, 6H), 0.367 (s, 18H)

$^{13}\text{C NMR}$  (500 MHz,  $\text{CDCl}_3$ )  $\delta$  (ppm): 137.96, 128.26, 122.06, 103.56, 101.75, 17.74, 15.37

**MS (ESI):** Calcd for  $\text{C}_{18}\text{H}_{26}\text{S}_2\text{Si}_2$ ,  $[\text{M}^+]$ : 362.1014 found 363.1093  $[\text{M}+\text{H}]^+$

### 2,6-bistrimethylsilyl-3,7-diiodobenzo(1,2-b:4,5-b')dithiophene (30)



The procedure was inspired from the literature, Hideaki Ebata, Eigo Miyazaki, Tatsuya Yamamoto, and Kazuo Takimiya, *Org. Lett.* **2007**, 9, 22, 4499–4502. To a solution of

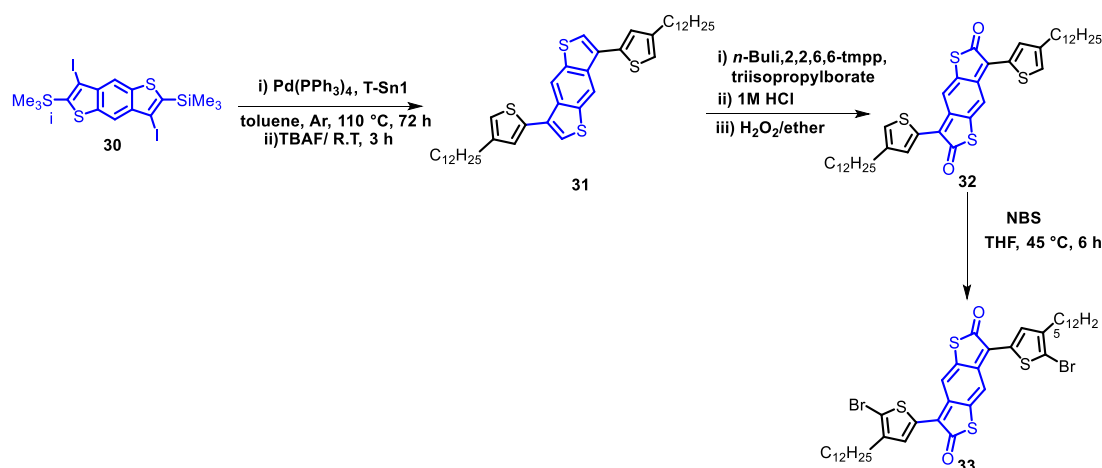
**29** (500 mg, 1.38 mmol) in 10 ml DCM, iodine (1.56 g, 5.5 mmol) was added. Then the mixture was heated at reflux for 7 hours under argon. After, an aqueous saturated  $\text{Na}_2\text{S}_2\text{O}_3$  was added to the reaction mixture, which was extracted with chloroform (15 mL). The organic layer was washed with brine and dried over  $\text{MgSO}_4$ , then filtered and concentrated under reduced pressure. The residue was purified by precipitation in  $\text{CH}_2\text{Cl}_2$  /methanol: 12 mL/12 mL to get pure compound (550 mg, 0.94 mmol, yield= 68 %).

$^1\text{H NMR}$  (500 MHz,  $\text{CDCl}_3$ )  $\delta$  (ppm): 8.237(s, 2H), 0.522(s, 18H)

$^{13}\text{C NMR}$  (500 MHz,  $\text{CDCl}_3$ )  $\delta$  (ppm): 144.11, 142.39, 139.74, 118.78, 86.23, 0.17

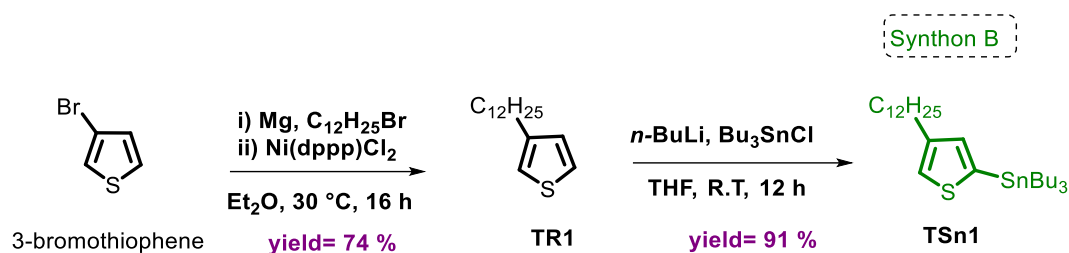
**IR** ( $\text{cm}^{-1}$ ):  $\nu$  = 1474 (w,  $\nu$  (C-H)), 1245 and 1216 (w,  $\nu$ (C-S)), 968 (w,  $\nu$ (C-Si)), 834 (w,  $\nu$  (C-I)).

**MS (ESI):** Calcd for  $\text{C}_{16}\text{H}_{20}\text{S}_2\text{Si}_2\text{I}_2$ , 585.8634 $[\text{M}^+]$ , found 586.8634



Scheme S6: The general synthetic scheme of last intermediate **33** from **30**

Applying the two routes requires the synthesis of the stannic thiophene functionalized with alkyl chain R1.



Scheme S7: The synthetic scheme of stannic thiophene **TSn1 (Synthon B)**

### 3-dodecylthiophene (TR1)

The procedure was inspired from the literature, Lanqi Huang, Guangjun Zhang, Kai Zhang, Qiang Peng, and Man Shing Wong, *macromolecule*, **2019**, 52, 12, 4447–4457.

To Magnesium tunings (3.06g, 0.126mol) in a Schlenk flask under Argon, 40 ml diethyl ether were added and 1-bromododecane (7.98g, 0.032mol), followed by reflux for 3 hours under Argon. After cooling to room temp the mixture were transferred to a solution of 3-bromothiophene (5 g, 0.0307mol), dichloro(1,3-bis(diphenylphosphino)propane)nickel(II) (57.7mg) in ether (10mL) at 0°C. after the reaction mixture was refluxed under Argon overnight. Then, the reaction mixture was poured into ice followed by extraction using diethyl ether and the organic layer was washed and dried over magnesium sulfate. After removing the solvent by evaporation, the crude product was purified by silica gel column chromatography and vacuum distillation, the product obtained as gel (74%)

$^1\text{H NMR}$  (500 MHz,  $\text{CDCl}_3$ )  $\delta$  (ppm): 7.24-4-7.23(dd,2H), 6.94-6.93 (d, 2H), 6.92-6.91(d, 2H)

$^{13}\text{C NMR}$  (500 MHz,  $\text{CDCl}_3$ )  $\delta$  (ppm): 143.30, 128.32, 125.04, 119.78, 31.98, 30.62, 30.34, 29.76, 29.73, 29.67, 29.53, 29.41, 22.75, 14.17

**MS (ESI): Calcd for  $\text{C}_{16}\text{H}_{29}\text{S}$  [M+]: 252.1912 found 253.1990**

### 2-tributylstannyl-4-dodecylthiophene (TSn1)

The procedure was inspired from the literature, Lanqi Huang, Guangjun Zhang, Kai Zhang, Qiang Peng, and Man Shing Wong, *macromolecule*, **2019**, 52, 12, 4447–4457. To a solution of 3-dodecylthiophene (TR1) (1.01 g, 4.00 mmol) in THF (30mL) cooled down to  $-78^\circ\text{C}$ , n-butyllithium 2.5M in hexane (1.76 mL, 4.4 mmol) was added and stirred for 90 min at  $-78^\circ\text{C}$

then tributyltin chloride (1.3 mL, 0.0048 mol) was added. The mixture was stirred for 3 hours, the temperature was allowed to raise to R.T. The reaction mixture was extracted with pentane. The organic layer was dried over magnesium sulfate and filtered. After evaporation of the solvent, the product **TSn1** was isolated as an oil. (1.96 g, 3.6 mmol, yield= 91%)

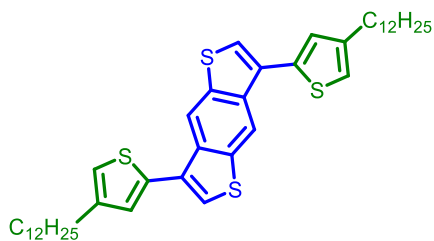
This compound was used in the next reaction without further purification.

**<sup>1</sup>H NMR (500 MHz, CDCl<sub>3</sub>) δ (ppm):** 7.92 (s, 1H), 7.06 (s, 1H), 2.56 (t, 2H, J = 7.57 Hz), 1.41 (m, 2H), 1.36-1.22 (m, 24H), 0.89 (t, 9H, J = 6.5 Hz), 0.86 (t, 3H, J = 7 Hz), 0.45 (t, 6H, J = 6.6 Hz)

**<sup>13</sup>C NMR (500 MHz, CDCl<sub>3</sub>) δ (ppm):** 136.1, 135.9, 123.8, 122.7, 31.75, 30.63, 29.4, 29.2, 28.1, 22.63, 20.9, 19.2, 14.02, 10.9

**MS (ESI): Calcd for C<sub>28</sub>H<sub>54</sub>SSn:** 542.2968 found 543.3046 [M+H]<sup>+</sup>

### 3,7-Bis[4-dodecyl]thiophene-2-yl]benzo[1,2-b:4,5-b']dithiophene (**31**)



The procedure was inspired from the literature, Kohsuke Kawabata, Masahiko Saito, Itaru Osaka, and Kazuo Takimiya, *J. Am. Chem. Soc.* **2016**, *138*, 772. In a schlenk under argon, to a solution of 2,6-bistrimethylsilyl-3,7-diiodobenzo[1,2-b:4,5-b']dithiophene **30** (1.00 g, 1.70

mmol) and tetrakis(triphenylphosphine)palladium(0) (196.45 mg, 0.17 mmol), in degassed and dry toluene (25 mL), TSn1 (3.33 g, 6.15 mmol) was added in four portions. **TSn1** (3.33 g, 6.36 mmol) was added in four portions. The reaction mixture was refluxed at 110°C for 3 days. The reaction was monitored by TLC (eluent: pentane, R<sub>f</sub> of compound before disilylation = 0.55). After cooling to room temperature, TBAF (12.75 mL, 1 M in THF, 12.75 mmol) was added, and the reaction mixture was stirred for 2 h at R.T. The reaction was monitored by TLC (eluent: pentane, R<sub>f</sub> (**31**) = 0.3). The reaction mixture was extracted with pentane, the organic layer was washed with water and dried over magnesium sulfate and filtered. After evaporation of the solvent under reduced pressure, the crude product was purified by silica gel column chromatography (eluent: 100% pentane). The product **31** was isolated as a white powder (480 g, 0.69 mmol, yield = 71%).

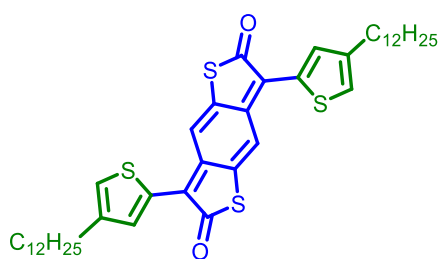
**<sup>1</sup>H NMR (500 MHz, CDCl<sub>3</sub>) δ (ppm):** 8.60 (s, 2H), 7.53 (s, 2H), 7.22 (d, 2H, J = 0.8 Hz), 6.98 (s, 2H), 2.68 (t, 4H, J = 7.4 Hz), 1.68 (m, 4H), 1.30-1.22 (m, 38H\*), 0.86 (t, 6H\*, J = 6.6 Hz) (supplementary H because of residual pentane).

**<sup>13</sup>C NMR (500 MHz, CDCl<sub>3</sub>) δ (ppm):** 144.00, 138.22, 136.77, 135.50, 129.89, 126.75, 124.86, 119.57, 116.87, 31.94, 30.67, 30.57, 29.71, 29.67, 29.53, 29.44, 29.38, 22.71, 14.14.

**MS (ESI):** Calcd for C<sub>42</sub>H<sub>58</sub>S<sub>4</sub> [M<sup>+</sup>]: 690.3421. Found: 691.3500 [M+H]<sup>+</sup>

The next two intermediates prepared from **31** for the synthesis of **33** are not stable in deuterated solvents. Therefore, they are not well characterized in <sup>13</sup>C NMR and due to the poor resolution only the signals from aromatic part were presiced in <sup>1</sup>H NMR. However, their formation was evidenced by ESI with exact mass determination by Karine Jarsale at LCMT-ENSICAEN.

### **3,7-Bis[(4-dodecyl) thiophen-2-yl] benzo[1,2-b:4,5-b']dithiophene-2,6-dione (**32**)**



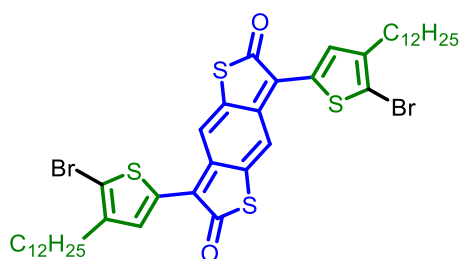
*The procedure was inspired from the literature, Kohsuke Kawabata, Masahiko Saito, Itaru Osaka, and Kazuo Takimiya, J. Am. Chem. Soc. **2016**, 138, 772.* 2,2,6,6-tetramethylpiperidine (58.56 μL, 0.347 mmol) was added dropwise into a solution of n-butyllithium (2.5M in

hexane) (0.14 mL, 0.347 mmol) in THF (2.5 mL) at -78°C to form lithium tetramethylpiperidine (LTMP). The mixture was stirred for 15 min at -78 °C. A solution of **31** (100 mg, 0.145 mmol) in THF (2.5 mL) was added dropwise over a period of 5 min. The mixture was stirred at -78°C for 3 hours. Then triisopropyl borate (219 μL, 0.95 mmol) was added. The reaction mixture was stirred overnight while gradually raising the temperature to RT. The temperature was raised gradually to R.T and the reaction mixture was stirred overnight. the reaction was monitored with TLC (eluent: pentane/ CH<sub>2</sub>Cl<sub>2</sub>, R<sub>f</sub>(**32**) = 0.6) and by <sup>1</sup>H NMR . The reaction was quenched with 1M HCL aqueous solution. The organic layer was extracted with ether and washed with water 3 times. The organic layer (4mL) was added to solution of 35% H<sub>2</sub>O<sub>2</sub> (7 ml) and ether (3ml) and stirred vigorously for 25 min. The reaction mixture was extracted with pentane and the organic layer was washed with water and dried over MgSO<sub>4</sub> and filtered. The solvent was evaporated under reduced pressure. The crude product was used for next step without further purification

**<sup>1</sup>H NMR (aromatic part) (CDCl<sub>3</sub>, 600 MHz) δ (ppm):** 7.67 (s, 2H), 7.66 (s, 2H), 7.27 (s, 2H)

**(ESI):** Calcd for C<sub>42</sub>H<sub>56</sub>O<sub>2</sub>S<sub>4</sub> [M<sup>+</sup>]: 720.3163 Found: 721.3241 [M+H]<sup>+</sup>

### 3,7-Bis[(5-bromo-4-dodecyl) thiophen-2-yl] benzo[1,2-b:4,5-b'] dithiophene-2,6-dione (**33**)



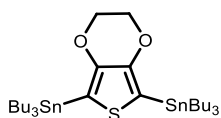
The procedure was inspired from the literature, Kohsuke Kawabata, Masahiko Saito, Itaru Osaka, and Kazuo Takimiya, *J. Am. Chem. Soc.* **2016**, 138, 772. To a solution of **32** (85 mg, 0.118 mmol) in THF (6 mL), NBS (46.15mg, 0.259 mmol) was added at 0°C, and the reaction was

gradually warmed to RT over a period of 20 min, and then stirred at 45°C for 6 hours. After cooling down to R.T, the solvent was evaporated and the crude mixture dissolved in pentane. After, the reaction mixture extracted with pentane, the organic layer washed with water and dried over MgSO<sub>4</sub> and filtered. The crude product was dried and used for next step without further purifications.

<sup>1</sup>H NMR (aromatic part) (CDCl<sub>3</sub>, 600 MHz) δ (ppm): 7.56 (s, 2H), 7.52 (s, 2H)

(ESI): Calcd for C<sub>42</sub>H<sub>54</sub>O<sub>2</sub>S<sub>4</sub><sup>79</sup>Br<sub>2</sub> [M<sup>+</sup>]: 876.1373 Found: 877.1452 [M+H]<sup>+</sup>

### Synthesis of 2,5-Bis(tributylstannyl)-3,4-ethylenedioxythiophene EDOT-Sn2 (Synthon C1) for T1 and T4 (**34**)



Rajashree Y.Mahale Satej S. Dharmapurikar Mrinmoy Kumar Chini, *Chemical Physics Letters*, **2018**, 696, 48-54. EDOT (0.71g, 0.005mol) was added to 20ml THF at -70°C and slowly add LDA (2 M, 7.5mL) and stir

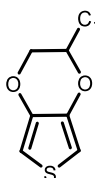
for 1 hour. Then tributyltin chloride (4.88 g, 4.06 mL) was added and stirred for additional hour at 0°C. then, water was added and the mixture was extracted with ethyl acetate. The organic layer was washed with brine, dried over MgSO<sub>4</sub> and filtered. The solvent was evaporated under reduced pressure. The obtained product was used in the next step without further purification.

<sup>1</sup>H NMR (500 MHz, CDCl<sub>3</sub>) δ (ppm): 4.11 (s, 4H), 7.15 (s, 2H), 1.52-1.58 (m, 12H), 1.30-1.36 (m, 12H), 1.06-1.10 (m, 12H), 0.87-0.91 (t, 18H, J = 7.2 Hz)

<sup>13</sup>C NMR (500 MHz, CDCl<sub>3</sub>) δ (ppm): 148.5, 116.1, 64.87, 29.25, 27.42, 13.89, 10.75

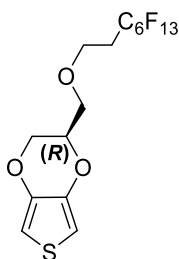


### (R)-2-dodecyl-2,3-dihydrothieno[3,4-b][1,4]dioxine (35)



The product **35** was prepared and characterized by Cyprien LEMOUCHI following the procedure *J mater Chem C* 7(46), 2019, 14745-51.

### (R)-2-(((3,3,4,4,5,5,6,6,7,7,8,8,8-tridecafluorooctyl)oxy)methyl)-2,3-dihydrothieno[3,4-b][1,4]dioxine (37)



To a 50 mL three-necked flask equipped with Argon purge, EDOT-MeOH **13** (0.1 g, 0.58 mmol), NaH (60 %) (0.46 g, 11.6 mmol), 18-crown-6 (0.03 g, 0.16 mmol) and dry DMF (21 mL) were added. The mixture was stirred at RT for 1 h. Then, the perfluorinated chain (0.55 g, 1.0 mmol) was added dropwise in the mixture. After 18 h of reaction, the mixture was poured into a saturated solution of NH<sub>4</sub>Cl (15 mL) and extracted with DCM (2 x 15 mL). The organic phase was afterwards washed with distilled water (10 mL) and the solvent was removed under reduced pressure. The crude product was isolated by flash chromatography (puriFlash XS 520 Plus, 100 % cyclohexane to 85/15 cyclohexane/EtOAc), to afford 40 % of the product **37** as a yellowish oil + 5 % elimination product.

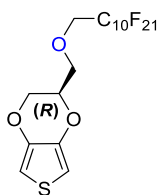
**<sup>1</sup>H NMR (500 MHz, CDCl<sub>3</sub>) δ (ppm):** 6.35 (d, <sup>4</sup>J<sub>H-H</sub> = 4.0 Hz), 6.33 (d, <sup>4</sup>J<sub>H-H</sub> = 4.0 Hz, 1H), 4.34-4.29 (m, 3H), 4.22 (dd, <sup>2</sup>J<sub>H-H</sub> = 11.7 Hz, <sup>3</sup>J<sub>H-H</sub> = 2.2 Hz, 1H), 4.06 (dd, <sup>2</sup>J<sub>H-H</sub> = 11.7 Hz, <sup>3</sup>J<sub>H-H</sub> = 7.4 Hz, 1H), 3.72 (dd, <sup>2</sup>J<sub>H-H</sub> = 10.5 Hz, <sup>3</sup>J<sub>H-H</sub> = 5.3 Hz, 1H), 3.66 (dd, <sup>2</sup>J<sub>H-H</sub> = 10.5 Hz, <sup>3</sup>J<sub>H-H</sub> = 5.3 Hz, 1H), 1.43 (t, <sup>3</sup>J<sub>H-H</sub> = 4.2 Hz, 2H).

**<sup>19</sup>F NMR (500 MHz, CDCl<sub>3</sub>) δ (ppm):** - 80.72, -119.60 (t, CF<sub>3</sub>), - 121.77, - 122.72, - 123.43.

**HR-MS (ASAP+) m/z [M<sup>+</sup>]** calcd. for C<sub>15</sub>H<sub>11</sub>O<sub>3</sub>F<sub>13</sub>S = 499.0237, found = 499.0237. Possibility of removal of one fluorine atom during the ionization.

- Mass corresponding on C<sub>15</sub>H<sub>11</sub>O<sub>3</sub>F<sub>12</sub>S

**(R)-2-(((2,2,3,3,4,4,5,5,6,6,7,7,8,8,9,9,10,10,11,11,11-henicosafluoroundecyl)oxy)methyl)-2,3-dihydrothieno[3,4-b][1,4]dioxine (38)**



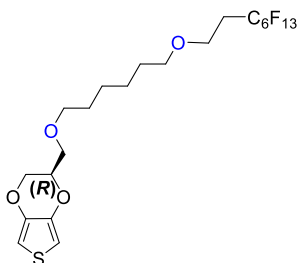
To a 10 mL three-necked flask equipped with Argon purge, perfluorinated chain-OH (0.31 g, 0.57 mmol), NaH (60 %) (0.21 g, 5.2 mmol), 18-crown-6 (0.03 g, 0.16 mmol) and dry DMF (4 mL) were added. The mixture was stirred at R.T for 1 h. Then, the compound **14** (0.1 g, 0.52 mmol) was added dropwise in the mixture. After 18 h of reaction, the mixture was poured into a saturated solution of NH<sub>4</sub>Cl (10 mL) and extracted with CH<sub>2</sub>Cl<sub>2</sub> (2 x 10 mL). The organic phase was afterwards washed with distilled water (10 mL) and the solvent was removed under reduced pressure. The crude product was isolated by flash chromatography (puriFlash XS 520 Plus, 100 % pentane to 6/4 pentane/EtOAc), to afford the product **38** (0.24 g) as a yellowish oil in 65 %.

**<sup>1</sup>H NMR (500 MHz, CDCl<sub>3</sub>) δ (ppm):** 6.34 (d, <sup>4</sup>J<sub>H-H</sub> = 4.0 Hz, 1H, H-4), 6.32 (d, <sup>4</sup>J<sub>H-H</sub> = 4.0 Hz, 1H), 4.34-4.29 (m, 3H), 4.20 (dd, <sup>2</sup>J<sub>H-H</sub> = 11.7 Hz, <sup>3</sup>J<sub>H-H</sub> = 2.2 Hz, 1H), 4.07 (dd, <sup>2</sup>J<sub>H-H</sub> = 11.7 Hz, <sup>3</sup>J<sub>H-H</sub> = 7.4 Hz, 1H), 3.71 (dd, <sup>2</sup>J<sub>H-H</sub> = 10.5 Hz, <sup>3</sup>J<sub>H-H</sub> = 5.3 Hz, 1H), 3.64 (dd, <sup>2</sup>J<sub>H-H</sub> = 10.5 Hz, <sup>3</sup>J<sub>H-H</sub> = 5.3 Hz, 1H), 3.7 (m, 2H)

**<sup>19</sup>F NMR (500 MHz, CDCl<sub>3</sub>) δ (ppm):** - 80.85, - 80.87, - 80.88, - 80.91, - 119.65 (t, CF<sub>3</sub>), - 121.85, - 122.10, -122.79, -123.49, -126.24.

**HR-MS (ASAP+) m/z [M + •]** calcd. for C<sub>18</sub>H<sub>9</sub>O<sub>3</sub>F<sub>21</sub>S = 703.9973, found = 703.9932.

**(R)-2-(((6-((3,3,4,4,5,5,6,6,7,7,8,8,8-tridecafluorooctyl)oxy)hexyl)oxy)methyl)-2,3-dihydrothieno[3,4-b][1,4]dioxine (39)**



To a 10 mL three-necked flask equipped with Argon purge, the product **23** (0.1 g, 0.37 mmol), NaH (60 %) (0.15 g, 3.7 mmol), 18-crown-6 (0.03 g, 0.16 mmol) and dry DMF (4 mL) were added. The mixture was stirred at R.T for 1 h. Then, perfluorinated compound (0.21 g, 0.45 mmol) was added dropwise in the mixture. After 18 h of reaction, the mixture was poured into a saturated solution of NH<sub>4</sub>Cl (10 mL) and extracted with DCM (2 x 10 mL). The organic phase was afterwards washed with distilled water (10 mL) and the solvent was

removed under reduced pressure. The crude product was isolated by flash chromatography (puriFlash XS 520 Plus, 100 % pentane to 6/4 pentane/EtOAc), to afford the product **39** (0.16 g) as a yellowish oil in 71 %.

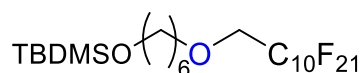
**<sup>1</sup>H NMR (500 MHz, CDCl<sub>3</sub>) δ (ppm):** 6.28(d, <sup>4</sup>J<sub>H-H</sub> = 3.8 Hz, 1H), 6.27 (d, <sup>4</sup>J<sub>H-H</sub> = 3.8 Hz, 1H), 4.28-4.23 (m, 1H), 4.25 (m, 2H), 4.19 (m, 1H), 4.01 (m, 1H), 3.55 (m, 1H), 3.35 (m, 2H), 1.64 (m, 2H), 1.51 (m, 2H), 1.44 (m, 2H), 1.32 (m, 4H) Pics not good resolved due to presence of DMSO.

**<sup>19</sup>F NMR (500 MHz, CDCl<sub>3</sub>) δ (ppm):** - 80.72, -119.60 (t, CF<sub>3</sub>), - 121.77, - 122.72, - 123.43.

**HR-MS (ASAP+) m/z [M + •]** calcd. for C<sub>12</sub>H<sub>22</sub>O<sub>4</sub>F<sub>12</sub>S = 598.1047, found = Possibility of removal of one fluorine atom during the ionization.

- Mass corresponding on C<sub>15</sub>H<sub>21</sub>O<sub>3</sub>F<sub>12</sub>S (M-HF)

**tert-butyl((6-((2,2,3,3,4,4,5,5,6,6,7,7,8,8,9,9,10,10,11,11,11-henicosafluoroundecyl)oxy)hexyl)oxy)dimethylsilane (40)**



To a 25 mL two-necked flask equipped with Argon purge, the perfluorinated chain (0.55 g, 0.99 mmol), NaH (60 %) (0.4 g, 9.9 mmol), 18-crown-6 (0.03 g, 0.16 mmol) and dry DMF (16.5 mL) were added. The mixture was stirred at RT for 1 h. Then, the product **17** (0.35 g, 1.18 mmol) was added dropwise into the mixture. After 18 h of reaction, the mixture was poured into a saturated solution of NH<sub>4</sub>Cl (20 mL) and extracted with CH<sub>2</sub>Cl<sub>2</sub> (2 x 20 mL). The organic phase was afterwards washed with distilled water (8 mL) and the solvent was removed under reduced pressure. The crude product was isolated by flash chromatography (silica gel, 100 % pentane to 6/4 pentane/ EtOAc), to afford the product **40** (0.57 g) as a colorless oil in 83 % yield.

**<sup>1</sup>H NMR (500 MHz, CDCl<sub>3</sub>) δ (ppm):** 3.89 (t, <sup>3</sup>J<sub>H-H</sub> = 13.8 Hz, 2H), 3.60-3.53 (m, 4H), 1.58 (quintet, <sup>3</sup>J<sub>H-H</sub> = 6.8 Hz, 2H), 1.49 (quintet, <sup>3</sup>J<sub>H-H</sub> = 6.8 Hz, 2H), 1.37-1.30 (m, 4H), 0.86 (s, 9H), 0.02 (s, 6H).

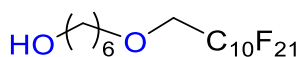
**<sup>13</sup>C NMR (500 MHz, CDCl<sub>3</sub>) δ (ppm):** 73.2 , 63.2, 32.7, 31.9, 29.7, 29.6, 29.5, 14.1, -5.3

**<sup>19</sup>F NMR (500 MHz, CDCl<sub>3</sub>) δ (ppm):** - 80.85, - 80.87, - 80.88, - 80.91, - 119.65 (t, CF<sub>3</sub>), - 121.85, - 122.10, -122.79, -123,49, -126.24.

**IR (neat, cm<sup>-1</sup>)**  $\lambda$  2927 (C<sub>sp3</sub>-H, CH<sub>3</sub>), 2857(C<sub>sp3</sub>-H, CH<sub>2</sub>, CH), 1213 (C-Oether *aliphatic*).

**HR-MS (ASAP+)** *m/z* [M + H]<sup>+</sup> calcd. for C<sub>23</sub>H<sub>29</sub>F<sub>21</sub>O<sub>2</sub>Si = 765.1680, found = 765.1686.

**6-((2,2,3,3,4,4,5,5,6,6,7,7,8,8,9,9,10,10,11,11,11-henicosafuoroundecyl)oxy)hexan-1-ol  
(41)**



To a 10 mL two-necked flask equipped with Ar purge, the product **40** (0.4 g, 0.52 mmol) and dry THF (4.4 mL) were added. Then, 0.88 mL (0.89 mmol) of TBAF (1M) were added to the mixture. The reaction took place at R.T for 16 h. The reaction mixture was poured into water (10 mL) and extracted with ethyl acetate (2 x 15 mL). The combined organic extracts were washed with a saturated aqueous chloride solution (2 x 15 mL), brine (2 x 15 mL), dried over anhydrous magnesium sulfate, filtered and concentrated under reduced pressure to furnish the crude product as a yellowish oil. Purification by flash column chromatography (silica gel, 100 % pentane to 6/4 pentane/EtOAc) furnished pure alcohol as a colorless oil (0.21 g) in 62 % yield.

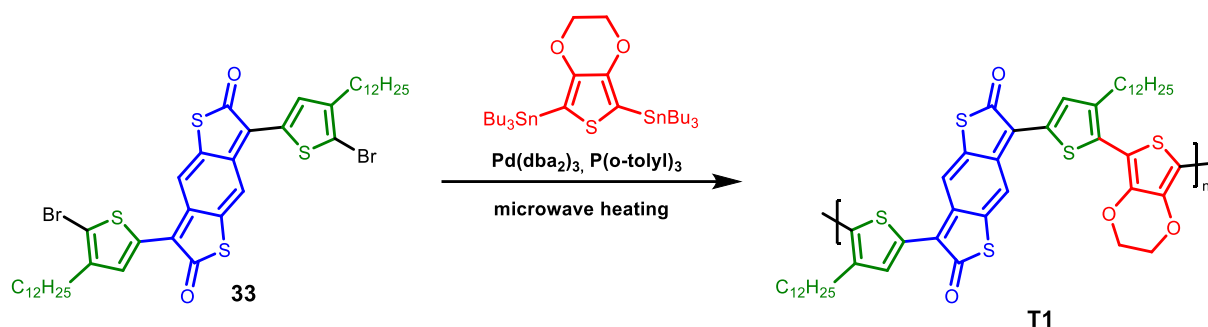
**<sup>1</sup>H NMR (500 MHz, CDCl<sub>3</sub>)  $\delta$  (ppm):** 3.90 (t, <sup>3</sup>J<sub>H-H</sub> = 14.0 Hz, 2H), 3.63 (t, <sup>3</sup>J<sub>H-H</sub> = 6.6 Hz, 2H), 3.58 (t, <sup>3</sup>J<sub>H-H</sub> = 6.6 Hz, 2H), 1.61 (quintet, <sup>3</sup>J<sub>H-H</sub> = 7.3 Hz, 2H), 1.56 (quintet, <sup>3</sup>J<sub>H-H</sub> = 7.3 Hz, 2H), 1.40-1.34 (m; 4H).

**<sup>13</sup>C NMR (500 MHz, CDCl<sub>3</sub>)  $\delta$  (ppm):** 70.6, 70.2, 62.2, 31.9, 29.8, 25.4, 25.1.

**<sup>19</sup>F NMR (500 MHz, CDCl<sub>3</sub>)  $\delta$  (ppm):** - 80.76, - 80.78, - 80.79, - 80.81, -119.60 (t, CF<sub>3</sub>), - 121.77, - 122.72, - 123.43, - 126.14, -126.17.

**IR (neat, cm<sup>-1</sup>)**  $\lambda$  2235 (OH), 2922 (C<sub>sp3</sub>-H, CH<sub>3</sub>), 2855(C<sub>sp3</sub>-H, CH<sub>2</sub>, CH), 1213 (C-Oether *aliphatic*).

## Synthesis of T1



Scheme S8: The synthesis of conjugated polymer **T1**

The procedure was inspired from the literature, Kohsuke Kawabata, Masahiko Saito, Itaru Osaka, and Kazuo Takimiya, *J. Am. Chem. Soc.* **2016**, *138*, 772. 3,7-Bis[(5-bromo-4-dodecyl)thiophen-2-yl]benzo[1,2-b:4,5-b']dithiophene-2,6-dione **33** (50 mg, 0.057 mmol),  $\text{Pd}_2(\text{dba})_3$  (1.6 mg), Tri(o-tolyl)phosphine (4 mg, 0.0114 mmol), and **EDOT-Sn2** (41 mg, 0.057 mmol), were added into Schlenk under Argon, then 4 mL of dry toluene were added. The reaction was carried using microwave for 30 min at 95°C under Argon. The reaction was monitored by TLC (eluent: pentane). After cooling to room temperature, the mixture was extracted with pentane, the organic layer was washed with water and dried over magnesium sulfate. After filtration and evaporation of the solvent by evaporation under reduced pressure, the crude product was purified on Biobead<sup>®</sup> X1 by Size Exclusion Chromatography by 100%  $\text{CH}_2\text{Cl}_2$  to isolate polymer **T1** as dark green product.

<sup>1</sup>H NMR (500 MHz,  $\text{CDCl}_3$ )  $\delta$  (ppm): 8.9ppm (broad peak),

## Résumé

Ce manuscrit se compose de deux parties. La première partie se concentre sur le développement de nouveaux métallooligomères à faible gap électronique utilisés comme donneurs dans les cellules solaires organiques à hétérojonction. Ils sont préparés par une réaction de déhydrohalogénéation entre un ligand L et le trans-PtCl<sub>2</sub>(PBU<sub>3</sub>)<sub>2</sub>. Ils sont constitués du métal platine avec les ligands phosphines et d'une partie organique composée de donneur (thiophènes) et d'accepteur avec le dicétopyrrolopyrrole (DPP). Pour réduire le gap électronique, la stratégie utilisée consiste à modifier la structure du ligand pour augmenter de la longueur de conjugaison, la planéité, la stabilisation de la forme quinonique ou renforcer l'effet « push-pull » en particulier avec l'insertion du 3,4-éthylènedioxythiophène (EDOT). Cette stratégie a permis de préparer de nouveaux donneurs qui ont permis d'atteindre de bonnes performances avec des PCE de 14-15 % lorsqu'ils sont associés avec des accepteurs non-fullerènes. Dans la deuxième partie, l'objectif est de synthétiser de nouveaux polymères conjugués électro-déficients pour développer des transistors à effet de champ organiques (OFETs) de type n avec de bonnes propriétés de transport de charges stables à l'air, ces composés pourront être dopés pour préparer des thermoélectriques (OTHEs) de type n. Les polymères conjugués ciblés doivent avoir des propriétés telles que : un faible gap électronique, une affinité électronique importante et donc un faible niveau de la LUMO, une bonne solubilité, une stabilité à l'ambient et une bonne  $\pi$ -agrégation avec une orientation « edge-on » de l'empilement des chaînes. La stratégie donneur-accepteur est appliquée pour obtenir une faible bande interdite avec l'unité benzo[1,2-b: 4,5-b']-dithiophène-2,6-dione (BDTD) comme accepteur associé à deux thiophènes fonctionnalisés par une chaîne alkyle. La synthèse convergente, qui utilise trois synthons, permet de changer le type de chaînes sur les unités aromatiques pour atteindre les propriétés ciblées, comme d'augmenter la solubilité, la stabilité ou l'organisation moléculaire. Un premier polymère fonctionnalisé avec des chaînes alkyles linéaires a été obtenu. Toutefois, le manque de solubilité et de stabilité ne permettent pas de l'isoler et de l'étudier. Ainsi, en perspective à ce travail, les chaînes branchées étendues seront utilisées pour augmenter la solubilité des intermédiaires et ainsi améliorer la synthèse et la pureté des polymères.

**Mots clés : polymères conjugués, métallooligomères, synthèse organique, thermoélectriques organiques, cellules solaires organiques, transistors à effet de champ organiques.**

## Abstract

This manuscript consists of two parts. The first part focuses on the development of new low band gap metallooligomers used as donors in organic heterojunction solar cells. They are prepared by a dehydrohalogenation reaction between a ligand **L** and trans-PtCl<sub>2</sub>(PBU<sub>3</sub>)<sub>2</sub>. They consist of the platinum metal with phosphine ligands and an organic part composed of donor (thiophenes) and acceptor (diketopyrrolopyrrole (DPP)). To reduce the electronic gap, the strategy used consists in modifying the structure of the ligand to increase the conjugation length, the planarity, the stabilization of the quinone form or to reinforce the "push-pull" effect in particular with the insertion of the 3,4-ethylenedioxythiophene (EDOT). This strategy allowed the preparation of new donors, which allowed to reach good performances with PCE of 14-15 % when they are associated with non-fullerene acceptors. In the second part, the objective is to synthesize new electro-deficient conjugated polymers to develop n-type organic field effect transistors (OFETs) with good air stability and high charge transport properties, these compounds can be doped to prepare n-type thermoelectrics (OTHEs). The targeted conjugated polymers should have properties such as: low band gap, high electron affinity and thus low LUMO level, good solubility, ambient stability, and good  $\pi$ -aggregation with an "edge-on" orientation of the chain stacking. The donor-acceptor strategy is applied to achieve a low band gap with benzo[1,2-b:4,5-b']-dithiophene-2,6-dione (BDTD) unit as the acceptor associated with two alkyl chain functionalized thiophenes. Convergent synthesis, using three synthons, allows changing the type of chains on the aromatic units to reach the targeted properties, such as increasing solubility, stability, and molecular organization. A first polymer functionalized with linear alkyl chains was obtained. However, the lack of solubility and stability did not allow isolating and studying it. Thus, in perspective to this work, extended branched alkyl chains will be used to increase the solubility of intermediates and thus improve the synthesis and the purity of polymers.

**Key words:** conjugated polymers, metallooligomers, organic synthesis, organic thermoelectrics, organic solar cells, organic field effect transistors

